Spring 1-1-2018

Deterioration of Multi-Functional Cementitious Materials in Nuclear Power Plants

Yuxiang Jing
University of Colorado at Boulder, jyxeng@gmail.com

DETERIORATION OF MULTI-FUNCTIONAL CEMENTITIOUS MATERIALS IN NUCLEAR POWER PLANTS

by

YUXIANG JING

B.S., Hohai University, 2010

M.S., University of Colorado Boulder, 2015

A thesis submitted to the

Faculty of the Graduate School of the

University of Colorado in partial fulfillment

of the requirement for the degree of

Doctor of Philosophy

Department of Civil, Environmental and Architectural Engineering

2018

This thesis entitled:

Deterioration of Multi-Functional Cementitious Materials in Nuclear Power Plants

written by Yuxiang Jing

has been approved for the Department of Civil, Environmental and Architectural Engineering

_____

Dr. Yunping Xi(Chair)

_____

Dr. Franck Vernerey

_____

Dr. Jeong-Hoon Song

_____

Dr. Mija H. Hubler

_____

Dr. Ross B. Corotis

Date_____

The final copy of this thesis has been examined by the signatories, and we find that both the content and the form meet acceptable presentation standards of scholarly work in the above mentioned discipline.

Jing, Yuxiang (Ph.D., Department of Civil, Environmental and Architectural Engineering)

Deterioration of Multi-Functional Cementitious Materials in Nuclear Power Plants

Thesis directed by Professor Yunping Xi

To ensure safe operation of nuclear power plants (NPPs) during their service life and enhance the performance of spent nuclear fuel (SNF) storage systems, comprehensive investigation on the behavior of concrete and their components under the long-term nuclear radiation is needed. A theoretical model was developed first to predict the deterioration of concrete under neutron radiation, taking into account both of the effects of neutron radiation and the radiation-induced heating on the mechanical property and volume change of concrete. It was shown that the volume change of concrete is dominated by the expanding characteristic of aggregates. Since neutron radiation can deteriorate mechanical properties of the concrete materials, it's critical to obtain the accurate neutron radiation levels in concrete structures during their service live. Neutron diffusion equations and heat conduction equation were used for prediction of neutron radiation and thermal field in concrete, respectively. The effects of potential variations of transport properties due to neutron radiation and elevated temperature on neutron diffusion in concrete were estimated. A simplified example of a typical concrete biological shielding wall was analyzed up to 80 years, and the results were discussed. The results show that neutron radiation and elevated temperature can result in considerable increases of neutron flux and fluence in the concrete. In order to understand the current state of knowledge about nuclear irradiated concrete, a collection of articles on neutron and gamma-ray radiation damage to concrete and/or its components was acquired. Information on testing conditions and concrete performance was extracted from the collected literature, and a database was developed. Data analysis of the effect of neutrons levels, water-cement ratio, aggregate fraction, and temperature on various properties of cementitious materials subjected to neutrons irradiation was conducted, and the results were presented. In order

to monitor the long-term deterioration process of concrete used in NPPs, the self-sensing capability of carbon fiber reinforced cementitious composites under mechanical loading and elevated temperature was experimentally studied, and the results were described. It has potential to become a sensor and can be used to monitor the long-term variation of strain in concrete of NPPs structures or SNF storage systems.

ACKNOWLEDGMENTS

First and foremost, I would like to sincerely thank my advisor, Professor Yunping Xi, who provided me guidance and support for both my research and life during the last 5 years. It has been a great honor and pleasure to work with him.

I would also like to thank my committee members, Prof. Jeong-Hoon Song, Prof. Mija H. Hubler, Prof. Ross B. Corotis, Prof. Franck Vernerey, for their valuable time, interest, and insightful recommendations. I would like to thank my fellows in Prof. Xi' group for their support, help and encouragement. I would specially thank Yao Wang and Linfei Li for their 6 years' support and friendship. Many thanks to Dr. Musiket Kamtornkiat, Dr. Zhilv Jiang, Mohamed Abdelrahman, Mohammed Zainy, Prof. Jiří Němeček, Prof. Shiping Yin, Prof. Hongqiang Chu, Xionghao Xu, Dr. Chao Jiang, and Christopher C. Frishcosy for all the help and joy they gave me. I would specially thank Prof. Ronald Y. S. Pak for mentoring my first year at CU boulder. Additionally, I would like to thank Derek Carpenter for his kind help in the lab. The support from CSC and Doctoral Assistantship for Completion of Dissertation from Department of Civil, Environmental and Architectural Engineering at the University of Colorado Boulder is also gratefully acknowledged.

Last but not least, I want to thank my parents and my brother for their endless love, support, and understanding. I would like to extend my deepest thanks to my wife, Yi Liu, for her companion, encouragement, and love.

CONTENTS

TABLES

FIGURES

CHAPTER 1

INTRODUCTION

1.1 Background

Concrete is widely used as a construction material for structures in nuclear power plants (NPPs) as well as dry casks in extended spent nuclear fuel (SNF) storage systems (William et al. 2013), due mainly to its good nuclear irradiation attenuation characteristics, long-term durability, and relatively low cost. Some of the concrete structures in NPPs , such as biological shield, support structures, and containment buildings, have been directly exposed to nuclear irradiation for a long time and many irradiation-induced deterioration phenomena have already been observed, such as reductions of mechanical and shielding properties (Field et al. 2015; Hilsdorf et al. 1978; William et al. 2013). In addition, in recent years, some NPPs in the United States have extended their service life to 60 years and the extension up to 80 years is being studied to fulfill energy demand in the future (Esselman and Bruck 2013; Remec et al. 2016), so higher radiation levels are expected. Therefore, the effects of nuclear irradiation on the properties of concrete need to be studied and taken into account in the long-term operation of NPPs (Pomaro 2016; Rosseel et al. 2016).

Various types of radiation could emit from nuclear reactions, concrete in a shielding wall is mainly subjected to two of them, namely neutron and gamma rays. The effects of nuclear irradiation on the properties of concrete primarily depend on radiation intensity and exposure time. Taking neutron irradiation as an example, when the irradiated neutrons accumulate in concrete to a critical value, mechanical properties of concrete such as compressive strength may be reduced to a level below the level of design requirement. The critical value of neutron irradiation was first

discussed in a paper by Hilsdorf et al. 1978, and 1×10^{19} n/cm^2 was suggested based on the experimental data collected in the paper. However, several scholars further analyzed the test data used in the paper and found some problems, for example, the experimental conditions used in some of the tests are unrepresentative and inconsistent with the service conditions in NPPs (Fujiwara et al. 2009; Kontani et al. 2014).

Extensive experimental studies (Field et al. 2015; Fujiwara et al. 2009; Maruyama et al. 2013, 2017) were conducted recently to investigate the effect of neutron radiation on different material characteristics of concrete, including strength, elastic modulus, water content and volume change. Based on the test results, possible deterioration mechanisms of concrete due to the nuclear radiation was discussed and summarized in detail (Field et al. 2015; Kontani et al. 2014). Numerical simulations have also been conducted to study the deterioration of concrete under nuclear irradiation (Pomaro et al. 2011a; b; Salomoni et al. 2014). A recently published paper Maruyama et al. 2016 proposed a numerical model for calculation of strength of nuclear irradiated concrete, which considered the effects of heat, moisture, and radiation. Furthermore, the radiation field as well as the heat field developed during the radiation attenuation process within the concrete structure were also calculated.

In addition to neutrons, Gamma ray is another type of nuclear irradiation that is important for the long-term performance of concrete. The interactions of Gamma rays with concrete and its components also have been studied by a number of studies (Kontani et al. 2013, 2014; Lowinska-Kluge and Piszora 2008; Vodák et al. 2005).

Comparing the effects of neutron and gamma ray, more deterioration phenomena of concrete are primarily due to neutron fluence (Field et al. 2015; Hilsdorf et al. 1978). Theoretical analyses also confirmed that neutron irradiation plays an important role in nuclear induced concrete degradations (Le Pape et al. 2015). Thus, neutron radiation in the concrete material is the

primary concern, and there is a lack of comprehensive investigation on the neutron irradiated concrete.

1.2 Neutron and gamma ray

Neutrons are electrically neutral particles and are a product of the nuclear fission reaction employed in commercial nuclear power reactors. Neutrons can be characterized into a number of different types by their energy. For example, three types of neutrons were defined by (Hilsdorf et al. 1978): thermal neutrons(Energy < 1eV), epithermal neutrons(1 eV < Energy < 0.1 MeV) and fast neutrons(Energy > 0.1 MeV). The measurement of neutron radiation is neutron fluence which quantifies the number of neutrons penetrating a unit area of media. The typical unit is cm^{-2}(Neutrons per centimeter squared). The rate of neutron radiation is called neutron flux. The typical unit is $cm^{-2}s^{-1}$(Neutrons per centimeter squared per second). Neutron radiation interacts with matter by the collisions between neutrons and the nuclei of atoms. The interaction can be either scattering or absorption partly depending on the kinetic energy of the neutron. There are two types of scattering: inelastic and elastic, as illustrated in Figure 1-1.

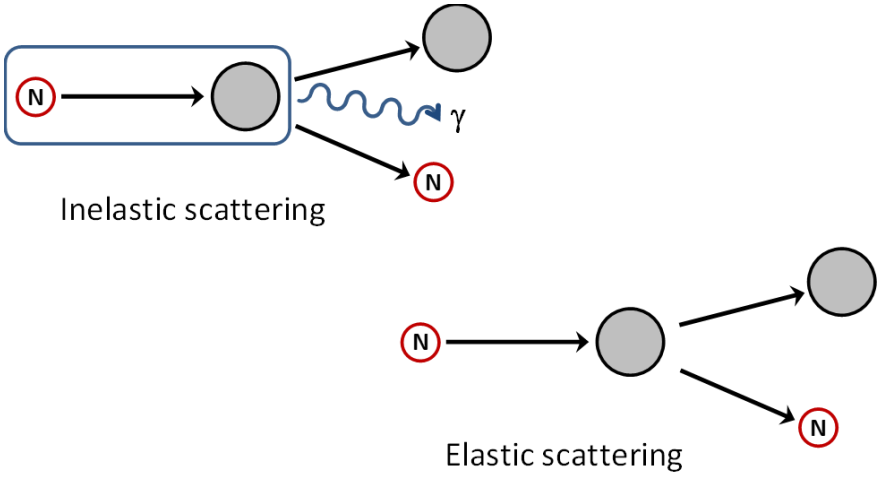

Figure 1-1 Inelastic and elastic scattering processes of neutron radiation

Gamma rays are energetic photons or light electromagnetic waves. Absorbed dose is usually used to measure the gamma-ray radiation. The unit is Gray(Gy) which is the absorption of one joule of ionizing radiation energy per kilogram of matter. Photons interact with matter in three primary ways: photoelectric effect, Compton scattering, and pair production. Each involves the ejection of an electron from the target atom as shown in Figure 1-2. Detailed mechanisms about these interactions between material and radiation will not be discussed further.

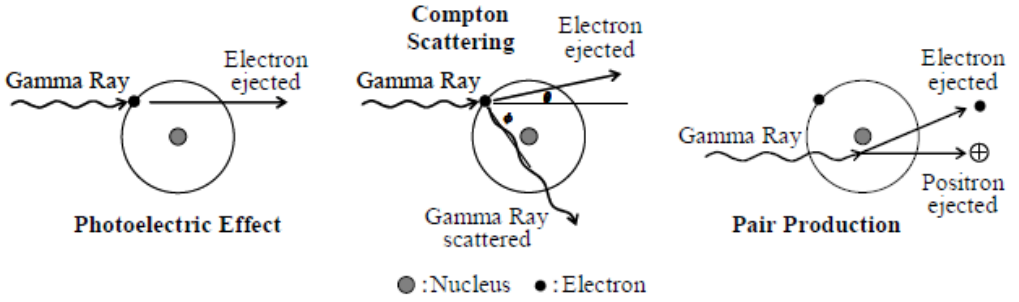

Figure 1-2 The photoelectric effect, Compton scattering, and pair production of gamma radiation(Kontani et al. 2014)

1.3 Objective and scope

The first objective of this research is to develop a theoretical model for mechanical properties of nuclear irradiated concrete taking into account the deterioration mechanisms at multiscale levels and a spatial distribution of the multi-phase constituents. Most of the studies about neutron effects on concrete are either experimental observations or qualitative description of the material properties with various degrees of irradiation-induced damage. There has been a lack of detailed analytical investigation on what happened in concrete and its components during the nuclear irradiation process. A composite model was used to characterize the multi-phase and multi-scale internal structure of concrete. The overall irradiation effect on concrete as a composite

material can be calculated by considering all of the irradiation effects on each constituent phase at each scale level.

The second objective is to obtain the accurate neutron radiation levels in concrete structures in NPPs during their service lives. Although neutron radiation can lead to the damage of concrete materials, the effect of damage in the internal structure of the concrete on the neutron shielding capacity has not been considered yet. The prediction model is based on one-speed neutron diffusion, heat conduction, cross-property relation theories, and available theoretical models. The neutron radiation distributions in a concrete biological shielding wall were predicted by taking into account the possible degradation of transport properties induced by neutron radiation and elevated temperatures

The third objective is to build a database about effects of nuclear radiation on concrete which almost include all experimental data about radiation damage to concrete and/or its components (i.e., rocks) so far. Information including the material used, material composition, mix design, physical properties, mechanical properties, testing conditions and concrete performance under nuclear radiation was stored. The effects of neutron radiation on the cementitious material were reviewed based on the collected data.

The last objective is to investigate the self-sensing capability of carbon fiber reinforced cementitious composites. Self-sensing concrete (Smart concrete) is concrete typically reinforced by conductive admixture (e.g., carbon fiber) and has very good potential to become a sensor which can be an alternative method for health monitoring of concrete structures, such as dry cask used in extended SNF storage systems. In order for the smart concrete to be used as a reliable sensor in real structures, tests were conducted for the material characterization under mechanical loadings and elevated temperature. The targets are to understand thermal and mechanical effects on the properties of smart concrete for material optimization.

1.4 Thesis organization

- Chapter 1 covers brief background information, thesis objective and scope, and organization.
- Chapter 2 presents the theoretical model for mechanical properties and deformations of nuclear irradiated concrete taking into account the deterioration mechanisms at multiscale levels and a spatial distribution of the multi-phase constituents.
- Chapter 3 presents the prediction models for long-term neutron radiation levels in distressed concrete biological shielding walls.
- Chapter 4 presents the review of effects of neutron radiation on various properties of cementitious materials based on the collected test data.
- Chapter 5 presents the experimental study of the self-sensing capability of carbon fiber reinforced cementitious material under mechanical loadings and elevated temperature.
- Chapter 6 consists of summary, conclusions and future work.

CHAPTER 2

THEORETICAL MODELING OF THE EFFECTS OF NEUTRON IRRADIATION ON PROPERTIES OF CONCRETE

2.1 Background

Most of the studies about neutron effects on concrete are either experimental observations or qualitative description of the material properties with various degrees of irradiation-induced damage. There has been a lack of detailed analytical investigation on what happened in concrete and its components during the nuclear irradiation process. Concrete is a multiphase heterogeneous material with constituent phases spanning several scale levels from C-S-H (calcium silicate hydrates) at the nanometer level to sand particles and gravels at the millimeter level. The constituent phases respond to nuclear irradiations differently and thus generate different types of damages. It is a challenging task to develop a comprehensive multiscale model including all damage mechanisms of the constituent phases. That is the primary reason why there is a lack of reliable prediction models based on multiscale nuclear irradiation-induced deterioration mechanisms. Recently, a micromechanical model (Le Pape et al. 2015) for neutron irradiated concrete was developed which provides a good approach to interpret available test data and to understand the behavior of concrete under neutron radiation. More work needs to be done along this direction.

This chapter focuses on the development of a theoretical model for mechanical properties of nuclear irradiated concrete taking into account the deterioration mechanisms at multiscale levels and a spatial distribution of the multi-phase constituents. A composite model was used in the

present study to characterize the multi-phase internal structure of concrete. Each constituent phase of concrete was further considered as a multiphase composite material that can be described by the same composite model at a lower scale level. The volume fraction of each constituent phase was calculated based on either concrete mix design or hydration reactions of Portland cement. As a result, the volume fractions of the constituent phases are functions of time and concrete mix design parameters. The scale levels considered in the theoretical model range from the nanometer to the meter scale level. The responses of the constituent phases to nuclear irradiation at different scale levels are quantitatively characterized based on available test data. The overall irradiation effect on concrete as a composite material can be calculated by considering all of the irradiation effects on each constituent phase at each scale level. The model predictions were then compared with experimental data available in the literature.

2.2 Multi-phase and multi-scale model

A multiphase composite model is introduced first in this section, and it will be followed by a description on how to use the multiphase composite model at different scale levels to deal with the heterogeneous internal structure of concrete. One of the objectives of this model is to include concrete design parameters in the model input so that the model can be used for various concrete materials with different mix designs. The input parameters are mechanical properties of aggregate and constituent phases in hardened cement paste, curing time, and mix proportions.

2.2.1 Generalized self-consistent model for multi-phase composite materials

In order to simplify the internal structure of composite materials and predict their behavior, many composite models have been proposed over the years. Generalized Self-Consistent (GSC) model is one of them. GSC model was first developed by (Christensen 1979) for transport

properties of composite materials. In this model, a heterogeneous composite material with multiple phases can be partitioned into different elements as shown in Figure 2-1(a). The scales of the elements are considered to be much smaller than that of the whole composite material. The sizes of the elements are different, but the volume fractions of the phases in each element are the same. This partitioning of the internal structure can be further simplified by making each element spherical shape of different sizes, and thus the internal structure of each element is a multilayered concentric sphere shown in Figure 2-1 (b). Since the volume fractions of the constituent phases are assumed to be the same, the ratios of the radius for the layers in each element are constants. Under the concentric spherical system, the displacement and stress components can be simplified from three dimensions to one dimension.

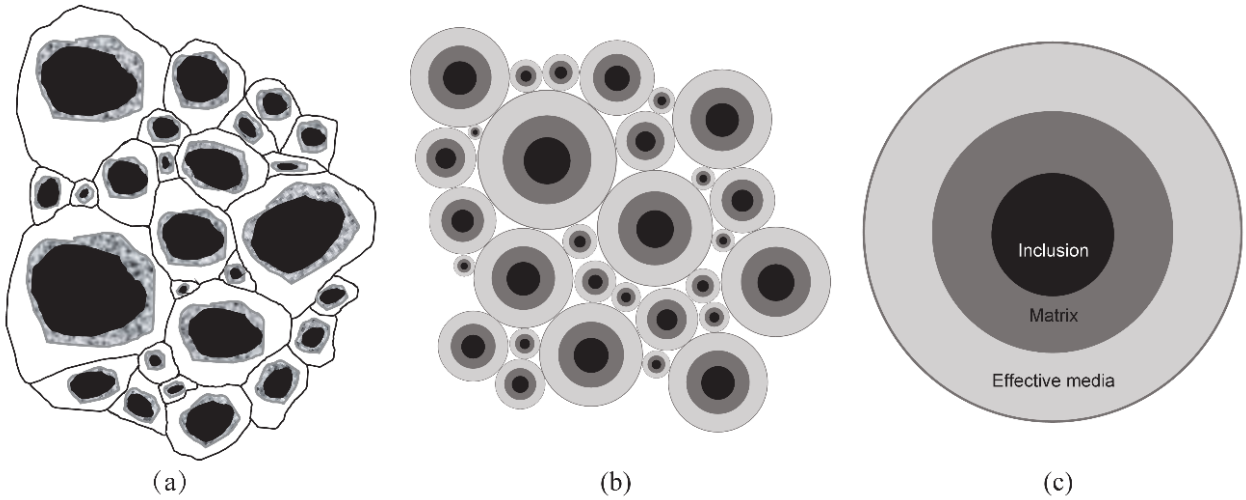

Figure 2-1 Multi-phase generalized self-consistent (GSC) model: (a) partitioning multi-phase composite into different elements; (b) partitioning multi-phase composite using spherical elements; (c) internal structure of each element

In the GSC model, first, a “three-phase model” (the GSC model) shown in Figure 2-1 (c) is solved, which is a basic element in the internal structure shown in Figure 2-1 (b). In Figure 2-1 (c), the inclusion and matrix are the two constituent phases, and the effective media (the outside

layer) is the composite material. So, the "three-phase" model is actually for a two-phase composite material.

Based on this theory, Xi and Jennings 1997 developed a model for the shrinkage of hardened cement paste and concrete as shown in Eq. (2-1) which can also be used to predict the expansion of any heterogeneous multi-phase medium. As shown later, the dominant damage mechanism of concrete is the mismatch between expansions of its components. So, the GSC model for volumetric expansion will be very useful in this study. The effective bulk modulus of a three-phase composite was also given as shown in Eq. (2-2), which will be used in later sections.

$$\varepsilon_{eff} = \frac{K_1\varepsilon_1 f_1(3K_2 + 4G_2) - K_2\varepsilon_2(1 - f_1)(3K_1 + 4G_2)}{K_2(3K_1 + 4G_2) - 4f_1G_2(K_2 - K_1)} \qquad (2\text{-}1)$$

$$K_{eff} = K_2 + \frac{f_1(K_1 - K_2)}{1 + (1 - f_1)\dfrac{K_1 - K_2}{K_2 + \frac{4}{3}G_2}} \qquad (2\text{-}2)$$

where K_i, G_i, ε_i, and f_i are bulk modulus, shear modulus, normal strain, and volume fraction of phase *i*, respectively; the subscripts *1*, *2*, and *eff* are for inclusion, matrix, and effective media, respectively. Furthermore, the "three-phase model" was generalized further and applied to composite materials composed of any number of phases. Figure 2-2 illustrates the basic idea of the generalization from three-phase to N-phase. A recursive method was developed for a multi-phase composite based on the multi-layered concentric spherical model. The general forms of effective bulk modulus and effective shrinkage (or expansion) of a composite material made of N constituent phases ($N \geq 2$) were given by Xi and Jennings 1997:

$$(K_{eff})_i = K_i + \frac{c_{i-1,i}\left[\left(K_{eff}\right)_{i-1} - K_i\right]}{1 + \left(1 - c_{i-1,i}\right)\dfrac{\left(K_{eff}\right)_{i-1} - K_i}{K_i + \frac{4}{3}G_i}} \qquad (2\text{-}3)$$

$$(\varepsilon_{eff})_i$$

$$= \frac{\left(K_{eff}\right)_{i-1}(\varepsilon_{eff})_{i-1}c_{i-1,i}(3K_i + 4G_i) - K_i\varepsilon_i(1 - c_{i-1,i})\left[3\left(K_{eff}\right)_{i-1} + 4G_i\right]}{K_i\left[3\left(K_{eff}\right)_{i-1} + 4G_i\right] - 4c_{i-1,i}G_i\left[K_i - \left(K_{eff}\right)_{i-1}\right]} \qquad (2\text{-}4)$$

$$c_{i-1,i} = \frac{\sum_{j=1}^{i-1} f_j}{\sum_{j=1}^{i} f_j} \; if \; i \neq N; \; c_{i-1,i} = 1 - f_i \; if \; i = N$$

where

$$(K_{eff})_1 = K_1; \; (\varepsilon_{eff})_1 = \varepsilon_1$$

For linear elastic materials, $K = E / [3(1-\mu)]$ *and* $G = E / [2(1+\mu)]$, in which, E is elastic modulus and μ is Poisson's ratio.

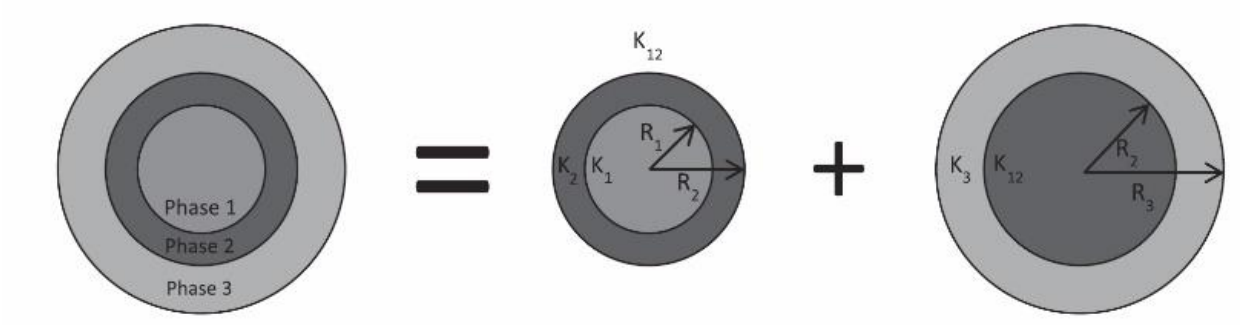

Figure 2-2 Generalization of the three-phase model to multi-phase model (e.g., cement paste)

2.2.2 Multi-scale model

Concrete is a multi-phase composite material, and the constituent phases, such as coarse aggregates, fine aggregates, hydration products and pores have different sizes which range from nanometer to decimeter scales. Thus, a multi-scale model is needed for characterizing the feature and behavior of the phases. In order to use GSC model to characterize the components of concrete

at different scales, five different scale levels were used in the present study, and they are shown in Figure 2-3.

Scale 1: Concrete (10^{-1} m and up). Concrete can be considered as a two-phase composite with coarse aggregates as inclusions embedded in a homogeneous mortar matrix.

Scale 2: Mortar (10^{-3}–10^{-1} m). Mortar can be considered as a two-phase composite with sand particles as inclusions embedded in a homogeneous cement paste matrix.

Scale 3: Cement paste (10^{-6}–10^{-3} m). Cement paste is a multi-phase composite including unreacted cement particles, hydration products, and capillary pores. Hydration products include calcium silicate hydrate (C-S-H), calcium hydroxide (CH), and other crystals such as ettringite. To better use GSC model simulating the internal structure of cement paste, three scale levels, Scale 3, 4, and 5 were used in this study for cement paste. In Scale 3, unreacted cement particles are considered as inclusions embedded in the matrix composed of hydration products and pores.

Scale 4: As shown in Figure 2-3, the capillary pores are considered as inclusions embedded in the matrix of hydration products.

Scale 5: As shown in Figure 2-3, the crystal phases (such as CH and ettringite) are considered as inclusions embedded in the matrix of C-S-H.

C-S-H(10^{-9}–10^{-6} m) exists in at least two forms with different layered structures (Constantinides and Ulm 2004). Gel pores are assumed to be an integral part of the C-S-H (Jennings and Tennis 1994; Lin and Meyer 2008). In the present study, C-S-H is not further decomposed into a multi-phase material. It should be also noted that this multi-scale model can only be used for ordinary Portland cement since other hydration products could exist when another type of cement is used.

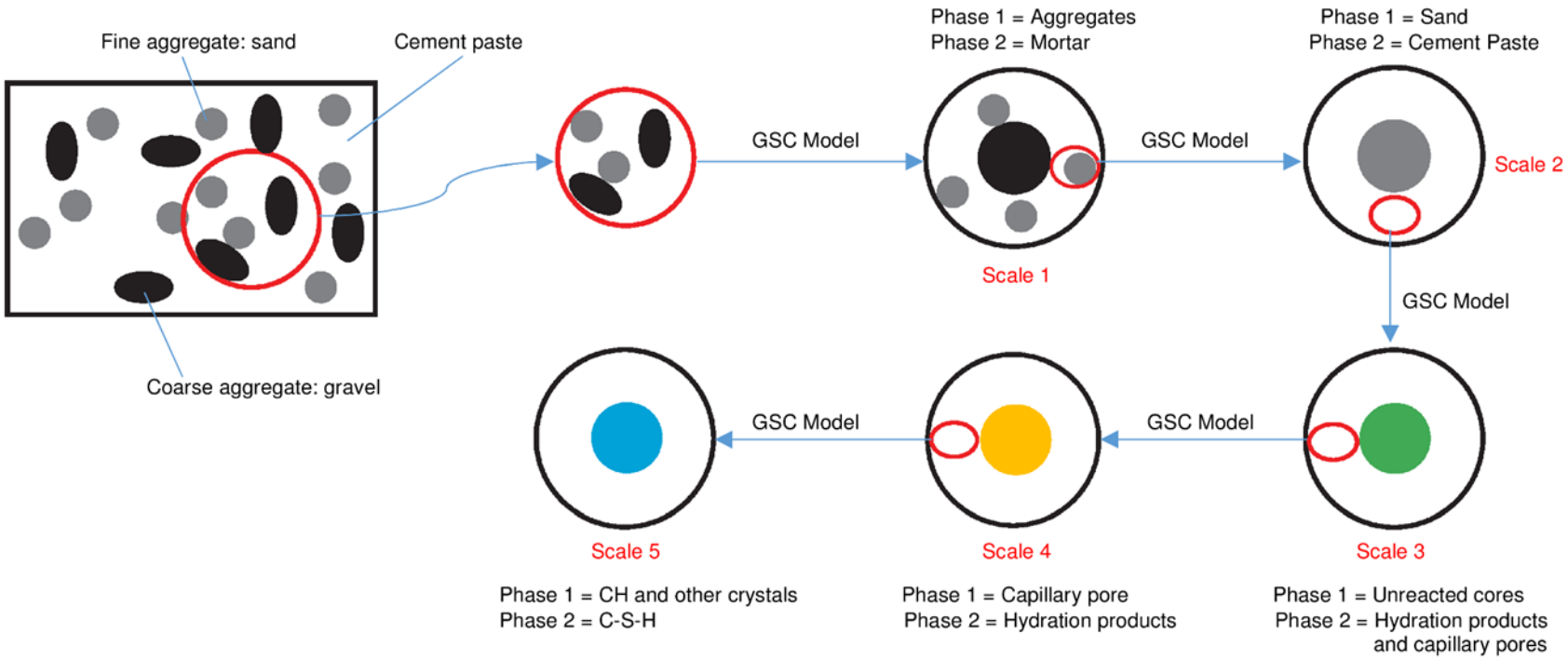

Figure 2-3 Schematic view of the multi-scale model for concrete

The effective elastic properties of concrete at Scale 1 can be evaluated using the equations listed above for the GSC model once the volume fractions and properties of the two constituent phases (aggregate and mortar) are available. The volume fractions and the properties of the matrix (mortar) need to be determined at the lower scale level, which is Scale 2. At Scale 2, the effective elastic properties of mortar can be evaluated using the same equations listed above for the GSC model. This process will be repeated at each scale until Scale 5. To use the GSC models at the multiple scale levels, it is important to calculate the volume fractions of the constituent phases.

2.2.3 Volume fractions

As noted, the volume fraction for each constituent phase (especially the hydration products) at each scale level must be obtained in the model. The total volume of the cement paste is the volumetric summation of unreacted cores, hydration products, and capillary pores

$$V_{cp} = V_{core} + V_{CH} + V_{AFm} + V_{CSH} + V_{cap} \qquad (2\text{-}5)$$

the subscripts *cp*, *core*, *CH*, *AFm*, *CSH*, and *cap* represent cement paste, unreacted core, CH crystals, AFm phases, C-S-H matrix, and capillary pores, respectively. The volume fractions of each phase can be evaluated as follows (Xi and Jennings 1997):

$$f_{core} = C\frac{(1-\alpha)}{\rho_c}p \qquad (2\text{-}6)$$

$$f_{CH} = C(0.189\alpha_{C_3S}W_{C_3S} + 0.058\alpha_{C_2S}W_{C_2S})p \qquad (2\text{-}7)$$

$$f_{AFm} = C\left(0.849\alpha_{C_3A}W_{C_3A} + 0.472\alpha_{C_4AF}W_{C_4AF}\right)p \qquad (2\text{-}8)$$

$$f_{cap} = (1 - C - C\Omega), \Omega$$
$$= 0.437\alpha_{C_3S}W_{C_3S} + 0.503\alpha_{C_2S}W_{C_2S} + 0.397\alpha_{C_3A}W_{C_3A} + 0.136\alpha_{C_4AF}W_{C_4AF} \quad (2\text{-}9)$$

$$f_{CSH} = 1 - \left(f_{core} + f_{CH} + f_{AFm} + f_{cap}\right) \quad (2\text{-}10)$$

$$C = \frac{1}{1 + w/c};\ p = \rho_c \frac{1 + \frac{w}{c}}{1 + w/c\,\frac{\rho_c}{\rho_w}} \quad (2\text{-}11)$$

where α is the degree of hydration for cement paste; α_i and W_i (i = C_3S, C_2S, C_3A, & C_4AF) are the degree of hydration and weight fraction for reacting compound i in Portland cement, respectively; w/c is water-to-cement ratio; ρ_c and ρ_w are density of cement and water in g/cm^3, respectively. Avrami equations (Taylor 1987) are employed to approximate the individual degree of hydration for each reacting compound

$$\alpha_i = 1 - exp[-a_i(t - b_i)^{c_i}] \quad (2\text{-}12)$$

where t is time in days. Coefficients a_i, b_i, and c_i are listed in Table 2-1. Based on the individual degrees of hydration for reacting compounds, the overall degree of hydration of the cement-based material can be obtained

$$\alpha = \frac{\sum_i W_i \alpha_i}{\sum_i W_i} \quad (2\text{-}13)$$

It should be noted that the service time of NPPs is very long for both biological shielding structures and waste storage facilities (usually 40 or 60 years), the effect of hydration period of cement is not significant. Compounds of Portland cement can be considered to be fully reacted,

and the degree of cement hydration can be considered as 100%, which means that the volume fraction of the anhydrous cores is zero.

Table 2-1 Coefficients a_i, b_i, and c_i

Compound	a_i	b_i	c_i
C_3S	0.25	0.90	0.70
C_2S	0.46	0.00	0.12
C_3A	0.28	0.90	0.77
C_3AF	0.26	0.90	0.55

At the mortar and concrete levels, the calculation of volume fractions of the constituent phases is straightforward based on mix design parameters. At the mortar level, volume fractions are

$$f_s = \frac{V_s}{V_s + V_c + V_w} = \frac{s/\rho_s}{s/\rho_s + c/\rho_c + w/\rho_w}; f_{cp} = 1 - f_s \qquad (2\text{-}14)$$

At the concrete level, volume fractions are

$$f_g = \frac{V_g}{V_s + V_c + V_w + V_g} = \frac{g/\rho_g}{s/\rho_s + c/\rho_c + w/\rho_w + g/\rho_g}; f_m = 1 - f_g \qquad (2\text{-}15)$$

where w, c, s, and g are the weights per unit volume of concrete for water, cement, sand (fine aggregates), and gravel (coarse aggregates), respectively; ρ_i ($i = w, c, s, \& g$) is the density of the corresponding constituent phase.

2.3 The effect of nuclear irradiation on constituents of concrete

As noted, only two types of nuclear radiations may have a significant effect on the properties of concrete: gamma-ray radiation and neutron radiation (Hilsdorf et al. 1978; Maruyama

et al. 2013; William et al. 2013). These two forms of nuclear irradiation attack concrete materials by very different mechanisms.

Gamma-ray irradiation can reduce the water content in a shielding material by radiolysis decomposition which generates hydrogen and hydrogen peroxide and by evaporation of water due to gamma-ray heating. It has a slight effect on the solid phases in concrete (Kontani et al. 2013). Since cement paste contains most of the water in concrete, the gamma rays have a more significant effect on cement paste than on aggregates. It was found that gamma rays can reduce the strength and pore surface area of concrete (Hilsdorf et al. 1978; Vodák et al. 2005). Scanning electron microscopy(SEM) images also show that a certain high dose of gamma rays can change the microstructure of cement paste dramatically, including generation of micro-cracking, separation of chemically bound water, and even complete disintegration of the solid framework (Lowinska-Kluge and Piszora 2008). However, recent test data from Kontani et al. 2014 suggested that the hydration products in cement paste are intact under gamma-ray irradiation since chemically bound water is almost unaffected during the exposure to gamma rays. Very different ranges of gamma ray doses were used in the previous studies, and their results are not consistent. Besides, it is still unclear how to distinguish the effect of gamma-ray heating from the effect of radiolysis, since these two phenomena always occur simultaneously during the tests.

Neutron irradiation can change the crystal lattice spacing due to collisions between neutrons and nuclei. Thus, neutron irradiation has a much more significant influence on dense and well-crystallized materials (e.g., typical aggregates used in concrete) than on amorphous materials with high porosity (e.g., cement paste) (Kontani et al. 2014). The integrated absorbed flux of fast neutrons during a long life span of operation of biological shielding could be quite closer to the critical values stated by American National Standard Institute (ANSI) than the integrated absorbed

dose of gamma rays (Fillmore 2004). A recent study pointed out that the neutron irradiation is primarily responsible for the damage of concrete (Le Pape et al. 2015).

Nuclear irradiations usually result in the localized temperature increase in irradiated materials. Although the design standards for NPPs in the U.S. and Japan state that the operating temperature is limited to 65 ºC (ASME 2015; Fujiwara et al. 2009), the temperatures of concrete samples collected in some experiments reached 250 ºC or higher (Fillmore 2004). Such an increase in temperature can lead to considerable thermal deterioration and strain of the concrete, so the thermal effect associated with nuclear radiations must be included in the present theoretical model.

In the theoretical model developed above, three material parameters are needed for each constituent phase: bulk modulus, shear modulus, and strain (expansion or shrinkage). The two mechanical properties, bulk modulus and shear modulus, and the deformation (strain) properties will be characterized in this section. In the present study, two major influential factors will be considered: neutron radiation and the heat of neutron radiation. Gamma-ray radiation will not be considered due to its less significant effect on concrete than neutron radiation and also due to a lack of available research results. The models for mechanical properties and deformations for different components in concrete will be combined together in the multiphase and multiscale model in the next section, in which a numerical example will be used to illustrate the capacity of the present model in predicting the effect of neutron irradiation on Portland cement concrete.

2.3.1 Degradation of mechanical properties

The mechanical properties of concrete such as the modulus of elasticity can be affected by neutron irradiation as well as the temperature rise caused by the neutron irradiation. In many experimental studies, control specimens are usually used to study the thermal effect. The temperature of the control specimens is controlled the same as in the irradiated specimens so that

the thermal effect can be distinguished from the irradiation effect. In the present study, the two effects are considered as two distinct influential factors and different models will be developed separately in the following sections. The degradation of modulus of elasticity and Poisson's ratio will be characterized first, and then the degradation of bulk modulus and shear modulus can be calculated based on the degraded modulus of elasticity and Poisson's ratio.

2.3.1.1 Degradation directly induced by neutron radiation

The experimental data reported by Hilsdorf et al. 1978 and Field et al. 2015 are the most comprehensive collections of test data about the effect of neutron irradiation on the modulus of elasticity of concrete so far. The latter one is shown in Figure 2-4. Both collections of test data show a gradual decay of elastic modulus of all kind of concrete under neutron irradiation. The decrease of elastic modulus is observed starting from a neutron fluence 1×10^{18} n/cm^2 approximately, and the reduction of elastic modulus finally reaches around 50% with the increase of neutron fluence regardless of the type of materials and environmental conditions used in the studies. The test data from Hilsdorf et al. were already used in some numerical simulations to take into account the impact of neutron irradiation (Pomaro et al. 2011a; Salomoni et al. 2014) and the middle trend line in Figure 2-4 can also be used to define the direct impact of irradiation on the modulus of elasticity of concrete. The following equation can be obtained to express the trend line in Figure 2-4:

$$\frac{E^{irr}}{E^{ref}} = -1.188 \times 10^{-8} N^{0.3711} + 1 \ \ (0 \le n \le 7 \times 10^{20}\ n/cm^2) \qquad (2\text{-}16)$$

where N is neutron fluence.

As mentioned earlier, concrete can be considered as a multiphase composite material, the effect of nuclear irradiation on each of the constituents needs to be studied separately and then combined together using the multiphase and multiscale model described in the next section.

Considering the modulus of elasticity of cement paste first. Literature review has shown that there are only two available studies on the modulus of elasticity of hardened cement paste exposed to neutron irradiation, and that the neutron irradiation has a negligible effect on elastic modulus of hardened cement paste compared to the effect on aggregates and concrete (as one can see in Figure 2-5 and Figure 2-7 later). The two studies will be discussed in detail later. Based on these test data, the modulus of elasticity of hardened cement paste can be assumed to be constant during neutron irradiation.

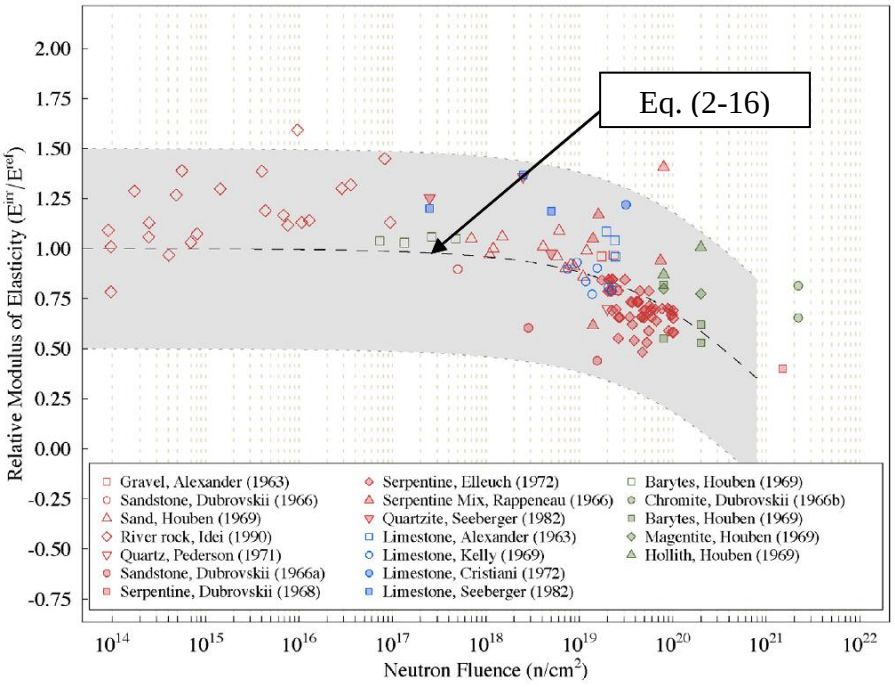

Figure 2-4 Relative moduli of elasticity of concrete and mortar specimens as a function of neutron radiation fluence (reprinted from Field et al. 2015)

Considering the effect of nuclear irradiation on the modulus of elasticity of aggregates. There has not been much test data available, so, the deterioration of aggregate under nuclear irradiation cannot be determined based on test data directly. In the multiphase GSC model shown earlier, the elastic modulus of concrete can be expressed in terms of elastic moduli of cement paste and aggregates. Therefore, the elastic modulus of aggregates can be determined from the multiphase model inversely and expressed by the properties of concrete and cement paste, and then calibrated based on the available test data. In this approach, the Poisson's ratio of concrete is assumed to be a constant due to the absence of experimental data.

2.3.1.2 Thermal deterioration

It has been confirmed by extensive studies that the elastic modulus of concrete decreases with increasing temperatures. Thus, both neutron irradiation and elevated temperature could cause the degradation of elastic modulus of concrete. The heat generated during nuclear irradiations affects the elastic modulus of concrete in two ways. The first one is that the high temperature could cause phase transformations of constituent phases, which can lead to the deterioration of the concrete because the newly formed phases are usually not as stiff as the original phases. The second one is the incompatibility between the thermal deformations of aggregates and cement paste. Under elevated temperatures, the expansions of aggregates and cement paste do not match with each other, and the volumetric mismatch could cause micro-cracking and debonding at the interface between the aggregate and cement paste. Both of the effects need to be analyzed and take into account in the model.

Considering the effect of phase transformation under elevated temperatures first, the degradation of mechanical properties of concrete has been well studied (Lee et al. 2009), and thermal degradation of concrete up to 800 ºC was obtained. According to the study, there is no

phase transformation in cement paste up to 120 ºC. Since the normal operating condition of biological shielding is ≤ 65 ºC, neutron irradiation has little effect on the elastic properties of cement paste. Therefore, the elastic properties of constituent phases of cement paste, e.g., clinker, C-S-H, and CH, can be considered as constants during the normal operating condition. The values of the elastic properties of the constituent phases are summarized in Table 2-2.

Table 2-2 Properties of constituent phases in hardened cement paste

Parameters	Mechanical			α (10^{-6} / ºC) (Lee 2006)
	E (GPa)	μ	Ref.	
Clinker	139	0.3	(Lin and Meyer 2008)	2.301
C-S-H matrix	23.8	0.24	(Constantinides and Ulm 2004)	7.222*
CH	38	0.31	(Constantinides and Ulm 2004)	11.11*
Pores	0	0	-	0

Note: α=coefficient of linear thermal expansion.
*Under 200 ºC.

In addition to the solid phases, the liquid phase, free water should also be considered. Free water evaporates under radiation heating, which means that the internal pores in cement paste can be considered as unsaturated and drained. For the sake of simplicity, it was assumed in this study that other crystalline phases in hydration products have the same elastic parameters as CH crystal.

Considering the effect of incompatibility between the thermal deformations of aggregates and hardened cement paste and considering the effect of thermal degradation of aggregates, the result in a previous study can be used (Lee et al. 2009) in the present model, in which a reduction factor was introduced to take into account the decreasing elastic modulus of concrete due to high temperature:

$$E = E_0(0.03921 + \exp(-0.002T)) \qquad (2\text{-}17)$$

where T is temperature in ºC. When T = 20 ºC (room temperature), $E = E_0$; and when T > 20 ºC, $E < E_0$.

Poisson's ratio is another parameter involved in the multiphase GSC model. The available experimental data about the effect of elevated temperature on Poisson's ratio of concrete are very limited and tend to be inconsistent (Naus 2006). Relationships between temperature and Poisson's ratio are only studied in a few papers (Bahr et al. 2013; Bamonte and Gambarova 2016; Marechal 1972). The general trend is that Poisson's ratio of concrete decreases with temperatures up to 300–600 ºC and then increases. An experimental study about fire-exposed ordinary concrete made of river sand as aggregates provided a degradation factor k_μ for Poisson's ratio of concrete:

$$k_\mu = e^{-0.002(T-20)} \qquad (2\text{-}18)$$

where 20 ºC ≤ T ≤ 500 ºC.

Further, the Poisson's effect of concrete comes from its two components, aggregate and cement paste. Experimental studies showed that the increase of temperature causes an insignificant increase in Poisson' ratio of rocks (Heuze 1983; Tarkov and Vavakin 1982). So, the Poisson's ratio of aggregates in concrete can be assumed as a constant. Then, the variation of Poisson's ratio as described by Eq. (2-18) can be attributed solely to the variation of Poisson's ratio of cement paste.

2.3.1.3 Calibration of the models

In order to calibrate the present multiphase and multiscale model, the experimental results from (Elleuch et al. 1972) on the effect of radiation heating were used. The concrete was made

from serpentine as aggregates and aluminous cement. The aluminous cement, usually called calcium aluminate cement (CAC), is cement which has quite different chemical compositions compared to ordinary Portland cement. It has much greater amount of alumina and a far less amount of silica. The mix proportions were w/c/g =0.38/1/3.85 for concrete and w/c=0.25 for cement paste by weight (note that the concrete and the cement paste have two different water-cement ratios). The propagation velocities of an ultrasonic wave in the irradiated concrete, aggregates, and pure cement paste samples were measured. According to ASTM C597-16, the dynamic modulus of elasticity (E) can be calculated in terms of pulse velocity (V), density (ρ) and Poisson's ratio (μ): $E = V^2\boldsymbol{\rho}(1+\mu)(1-2\mu)/(1-\mu)$. Specific Gravities (SG) for concrete, aggregates and pure cement paste were given as 2.51, 2.8 and 2.35, respectively. Their Poisson's ratios are assumed to be 0.15, 0.35 and 0.2, respectively, which are typical values.

The elastic modulus of cement paste usually reduces with the increase of water-cement ratio, so the elastic properties of pure cement paste and cement paste in concrete samples are different due to their different water-cement ratios (0.25 and 0.38). The present model for volume changes due to hydration reactions can only deal with ordinary Portland cement, as an approximation, the modulus ratio $E(w/c=0.38)/E(w/c=0.25) = 73.8\%$ for aluminous cement paste was assumed for the calibration. The value of 73.8% is based on the result of ASTM type I cement from (Haecker et al. 2005). A similar ratio was obtained from another study (Wittmann et al. 1987). Densities for all phases are assumed to be constants during nuclear irradiations.

The data points of elastic moduli for irradiated concrete, aggregates, and cement paste in concrete and their corresponding linear regressions are shown in Figure 2-5. In addition, all the pure cement paste and concrete samples in the test were heated to 250 ºC before irradiation; and temperatures for most samples during irradiation were lower than this value (only one pure cement paste sample exceeded it and reached 280 ºC). Since the deterioration under such high temperature

is irreversible, the temperature of all samples is assumed to be 250 ºC. It should be noted that the heat induced degradation of elastic properties of aggregates and cement paste was already included in the measured values. Based on the experimental data provided, the linear relationships between elastic moduli of aggregates and cement paste in concrete and neutron level were obtained as follows:

$$E_{agg} = 6.05 \times 10^{10} - 3.21 \times 10^{-10} N$$

$$E_{cp} = 2.21 \times 10^{10} - 2.38 \times 10^{-11} N$$

Using the mix proportions and the above equations as inputs, the elastic modulus of the concrete under irradiation can be predicted and compared with the measured data in Figure 2-5. As discussed in the previous section, the thermal degradation of elastic modulus of concrete can be calculated by incorporating Eqs. (2-17) and (2-18) into the multiphase and multiscale model. These two equations estimate the effect of mismatch between aggregates and cement paste interface and the variation of Poisson's ratio of cement paste, respectively. In Figure 2-5(a), as one can see, the model prediction for concrete including thermal degradation (solid line) agrees with the linear curve of measured concrete data very well. Elastic modulus for concrete without thermal degradation is also predicted (dashed line). It can be seen clearly that radiation heating caused elevated temperature has resulted in a significant additional reduction of elastic modulus of the neutron irradiated concrete, and the effect must be taken into account in the model.

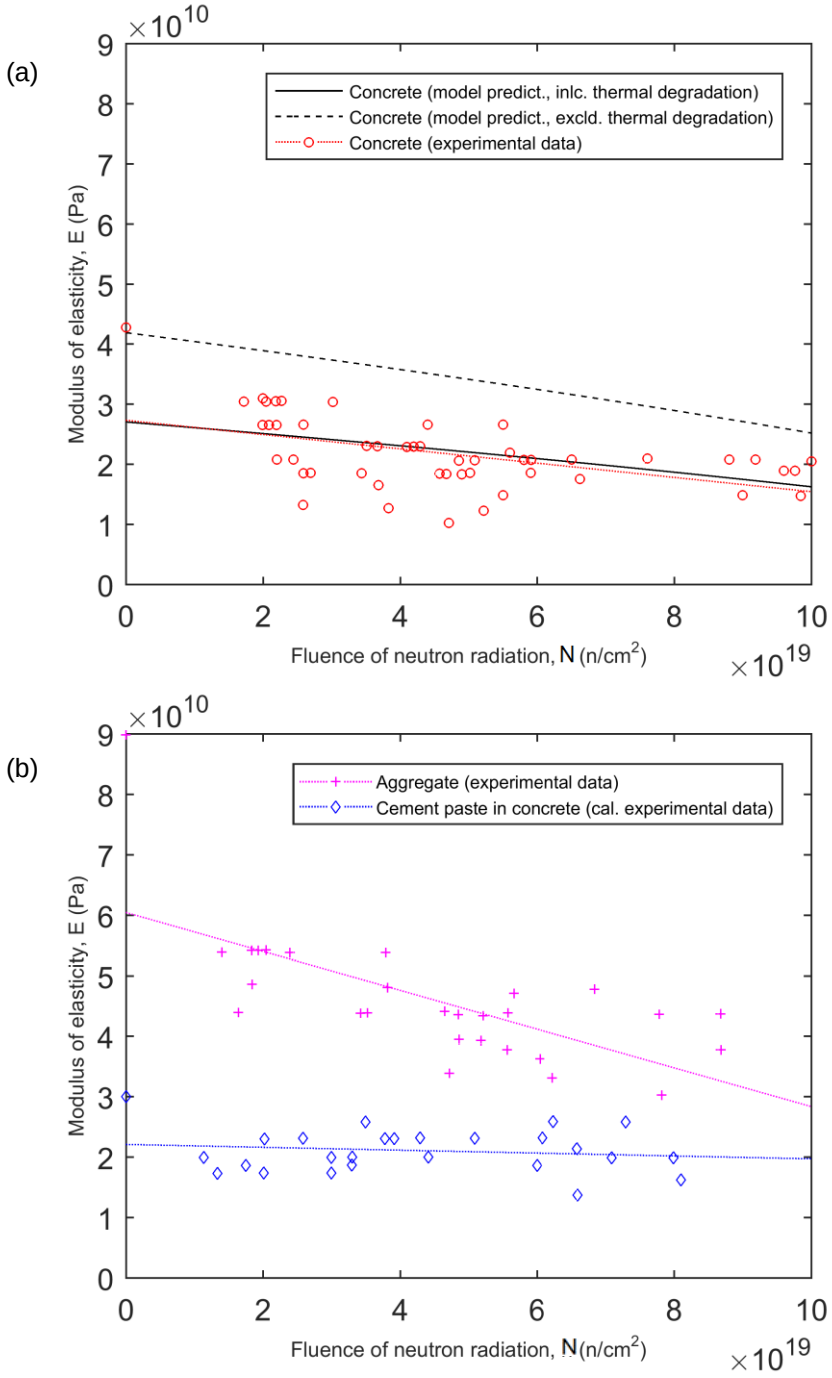

Figure 2-5 Modulus of elasticity as a function of neutron radiation fluence (data from Elleuch et al. 1972): (a) concrete; (b) aggregate and cement paste in concrete (Note: Energy > 1 MeV; dotted lines show linear regressions for different data sets; the color of each data set and its corresponding trend line is the same)

For aggregates, the control test in the same reference(Elleuch et al. 1972) indicated that the degradation of irradiated aggregates shown in Figure 2-5(b) was mainly due to neutron irradiation

itself and had nothing to do with the radiation heating. On the other hand, for cement paste in concrete, the high temperature caused by radiation was the major source of the reduction of elastic modulus and increasing neutron fluence cannot induce any further degradation as shown in Figure 2-5(b).

In summary, the degradation of elastic modulus of the neutron irradiated concrete mainly results from two different mechanisms for the aggregate and cement paste. For the aggregate, the degradation of elastic modulus is dominated by neutron irradiation and the effect of elevated temperature is relatively small. For the cement paste, the degradation of elastic modulus is dominated by radiation heating, and the effect of neutron irradiation is relatively small. The different responses of aggregate and cement paste can be explained by their different microstructures, which will not be listed further.

2.3.2 Volumetric strains of the constituent phases in concrete

Similarly, there are two mechanisms involved in the deformation analysis of concrete. One is neutron irradiation, and the other is the temperature rise caused by the neutron irradiation. Experimental results (as summarized in (William et al. 2013)) showed that there are basically three types of deformations in concrete under neutron irradiation: the expansion of aggregates, the shrinkage of cement paste, and the thermal expansion of the two phases under the heat due to neutron irradiation. They will be characterized separately in this section.

2.3.2.1 Expansion of aggregates directly induced by neutron irradiation

Quartz is the dominant crystalline form of SiO_2 which is one of the most abundant minerals in aggregates. The available experimental data on volume change of quartz at various neutron radiation fluence are plotted in Figure 2-6(a). The test data are determined by the relative change

in density. It has been demonstrated that the crystalline-to-amorphous transition is the main source of irradiation induced macroscopic expansion of several ceramic phases (quartz is one of them) and minerals (Weber et al. 1994, 1998). Thus, based on a model describing the accumulation of irradiation induced amorphous fraction (Wang et al. 2000), the following equation is developed and used to characterize the volume expansion of quartz due to neutron irradiation:

$$3\varepsilon_{ni} = \delta_{max}\left(1 - \frac{1}{\sqrt{A + (1-A)\exp(2B(1-A)N)}}\right) \qquad \textit{(2-19)}$$

where ε_{ni} is linear expansion induced by neutron radiation for i^{th} constituent phase in concrete; δ_{max} is the saturation value of volume change; $A \in [0, 1]$ is a dimensionless parameter called "crystallization efficiency parameter" and B is normalization factor for radiation dose. The result of curve fitting using this equation is shown in Figure 2-6(a). The least absolute residual method was used for the nonlinear regression analysis of the data, and the fitting process was conducted by using the curve fitting toolbox in MATLAB.

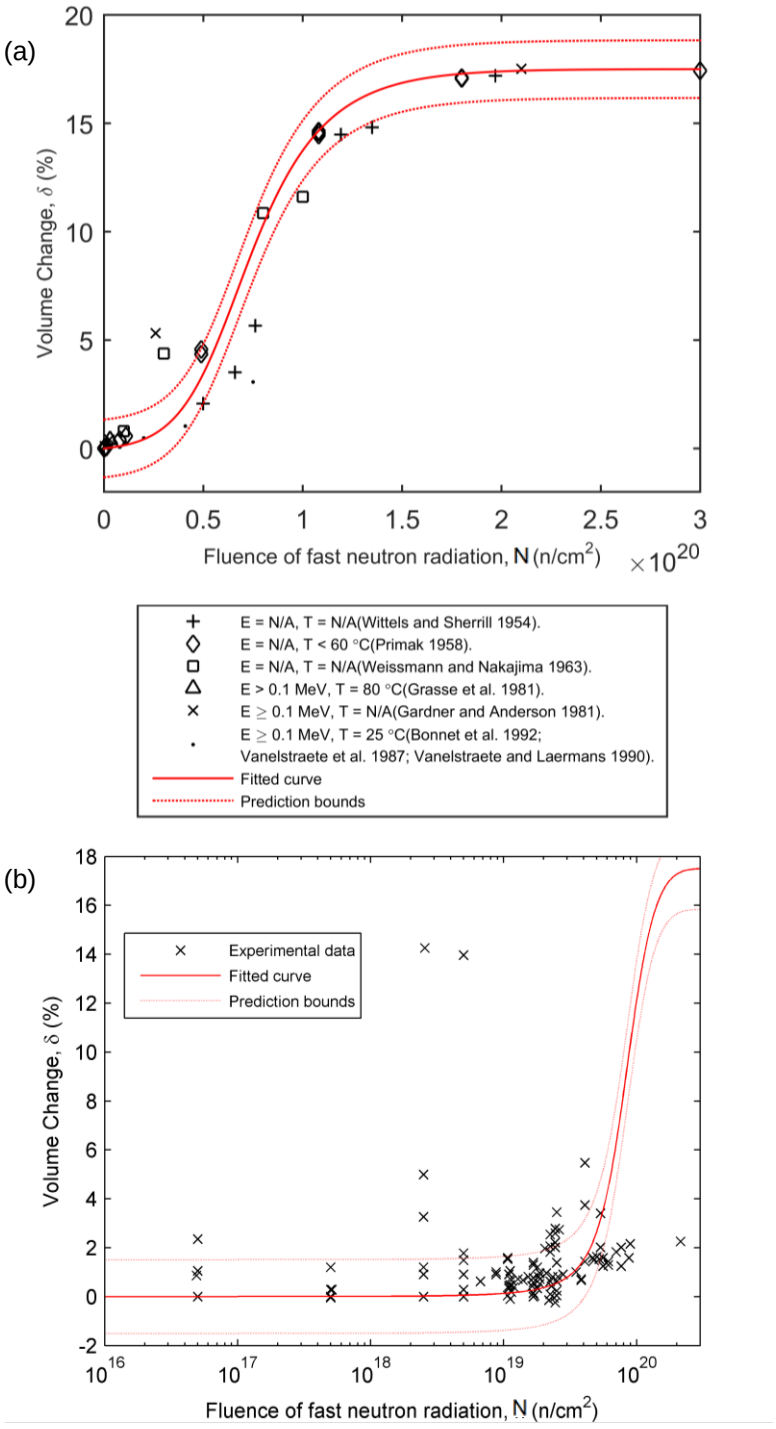

Figure 2-6 Measured volume change under fast neutron irradiation from literature: (a) quartz [the cut off energy (E) of measured fast neutron and temperature of the samples are marked; data are fitted using Eq. (2-19), where, δ_{max} = 17.5%, A = 0.9844, B = 2.051×10^{-18}; the prediction bounds define the 95% confidence interval of the fitting for the data]; (b) aggregates [curves shown in (a) are also plotted] (data from Field et al. 2015)

Besides quartz, some other crystalline oxides commonly found in aggregates also exhibit volume expansion behavior under fast neutron irradiation (Clinard Jr. et al. 1982; Wilks 1968). Because the internal structure of aggregates is nearly well-crystallized, both the coarse aggregates (gravel) and fine aggregates (sand) will expand when they are irradiated by neutron particles. Volume change data for different types of aggregates are shown in Figure 2-6(b). The expansion of aggregate primarily results from the phase transformations in the mineralogical structure of rocks. Under neutron irradiation, neutrons directly interact with nuclei of atoms and the damage of lattice structure of aggregates is reflected as a volume increase of the material. One of the detrimental effects during the process is the micro-cracking and debonding at aggregates and cement paste interface which will be considered in this study. Eq. (2-19) can be used to calculate the volume change of aggregate due to neutron irradiation. When experimental data are not available for a certain type of aggregate, as shown in Figure 2-6(b), quartz may be used as an estimation to consider the effect of neutron radiation on aggregates particles (up to 5×10^{19} n/cm^2). As one can see in Figure 2-6(a), a clear saturation of quartz expansion under neutron radiation can be observed. However, as shown in Figure 2-6(b), most of the experimental data of aggregates lay in the relatively low radiation level range, and there is no clear trend showing full development of the expansion of the aggregates. More test data of aggregate expansion at high fast neutron radiation level is needed.

2.3.2.2 Shrinkage of cement paste

It was observed that the shrinkage strains of neutron irradiated cement paste and the control sample subjected to the same thermal cycles are identical (Hilsdorf et al. 1978). Some other test results (Elleuch et al. 1972) also supported this observation. In fact, there is no strong evidence showing that neutron radiation has a direct impact on the shrinkage of cement paste. As mentioned

earlier, neutron irradiation leads to more distortion and damage to the internal structure of aggregates than to the structure of cement paste with high porosity and randomly layered internal structure. In general, the shrinkage of cement paste is mainly due to the loss of moisture during the heating process of irradiation. The moisture loss causes volumetric variation in the microstructure of cement paste, and there is usually no phase transformation involved. As discussed in the literature (Neubauer et al. 1996; Xi and Jennings 1997), the shrinkage of unreacted grain, CH, and other crystals can be considered as negligible, and the shrinking of C-S-H controls almost all the drying shrinkage of cement paste.

If the shrinkage test data are available, a curve fitting can be done based on the test data, and the fitted curve can be used in the model. Otherwise, as mentioned earlier, the present multiphase and multiscale model was originally developed for the shrinkage of concrete (Xi and Jennings 1997), so, the model can be used here for the shrinkage induced by the neutron irradiation. The control parameter for the shrinkage of concrete is the shrinkage of C-S-H, which can be considered as a constant value of -0.024. This value is measured in a micrometer level test for C_3S paste (Neubauer et al. 1997). The details can be found in Xi and Jennings 1997.

2.3.2.3 Thermal strain

During the heating process of irradiation, thermal expansion of concrete can be calculated

$$\varepsilon_{Ti} = \alpha_i \Delta T \qquad (2\text{-}20)$$

where α_i is coefficient of linear thermal expansion (CTE) for i^{th} constituent phase in concrete, and ΔT is the temperature increment. So, the problem of thermal expansion during neutron irradiation becomes the degradation of CTE under neutron irradiation. Again, the degradation of CTE must

be considered with the two mechanisms: direct neutron irradiation and the heat generated by neutron irradiation.

Consider the direct neutron irradiation first. The results of some experimental studies (Dubrovskii et al. 1966; Hilsdorf et al. 1978) show that the differences between the CTE of neutron irradiated concrete and that of temperature-exposed concrete are very small, which implies that the direct impact of neutron irradiation is not significant. Another experimental study (Kelly et al. 1971) also demonstrated that neutron radiation has little influence on CTEs of several types of aggregates. Various aggregates were used in these studies, and the neutron fluence was as high as 2.4×10^{21} n/cm^2. However, the result from another study (Dubrovskii et al. 1967) indicated that the CTE for irradiated concrete started to drop when neutron fluence is higher than 1.2×10^{20} n/cm^2. According to the given energy distribution profile, about 40-50% neutrons have energy higher than 0.1 MeV, so the threshold fast neutron fluence is (4.8-6) $\times$ 10^{19} n/cm^2. The aggregates used were river sand (mainly quartz) and sandstone (80-95% silicon oxide in the form of crystalline quartz). As one can see in Figure 2-6(a), quartz just begin to expand at this threshold value. A similar result can also be found in Kelly et al. 1971: CTEs of Magnesian Limestone begin to change when their volumes start to increase under fast neutron radiation. These test data imply that the neutron radiation may affect the nature of the thermal expansion of concrete. But, available test results are not sufficient to reach a conclusion. In the present model, α_i is assumed to be unaffected by neutron radiation.

Now, consider the effect of temperature rise due to neutron irradiation on CTE of concrete. Many test results showed that CTEs of concrete are temperature dependent (Lee et al. 2009). The CTE of cement paste and the CTE of aggregate behave differently under an elevated temperature and must to be considered separately.

For cement paste, above 120 ºC, phase transformations may be involved, and a stoichiometric model (Lee et al. 2009) may be used to calculate the volume fractions and the CTE. To simplify the model, for cement paste and its constituent phases, the values of CTE under 200 ºC may be considered as constants, and they are shown in Table 2-2.

Aggregates normally constitute 65-80% of the total volume of concrete. Therefore, the volumetric behavior of aggregates is very important for the volume changes of concrete. It has been reported that the CTEs of some types of aggregate increased with temperature above 100 ºC which is mainly due to the change of their mineralogical composition (Bažant and Kaplan 1996). CTE of aggregate also depends on whether the minerals are crystalline or amorphous. As mentioned earlier, neutron irradiation causes structural amorphization of crystalline phases which leads to the macroscopic expansion of the crystalline mineral.

The values and ranges of CTE for different groups of aggregates at normal temperature are available in the literature (Alexander and Mindess 2005). The behavior of CTEs of aggregates under elevated temperature can be found in available test data (Bažant and Kaplan 1996). It should be noticed that there is no consistency for values and the ranges for CTE of various types of aggregate, and the behavior within a particular rock group could vary considerably, since the chemical compositions of rocks are quite different, even if they share the same name.

For infinitesimal strain theory, the volumetric strain, i.e., volume change, is the trace of strain tensor:

$$\delta = \frac{\Delta V}{V} = \varepsilon_{xx} + \varepsilon_{yy} + \varepsilon_{zz} = 3\varepsilon_{eff} \qquad (2\text{-}21)$$

2.4 Numerical example for a neutron irradiated concrete

The combination of material models and the multiphase and multiscale model described in earlier sections can provide a comprehensive analytical model for predicting the effect of neutron irradiation on properties of concrete. This section presents a numerical example to show the prediction capacity of the comprehensive model. The experimental study by Kelly et al. 1971 was used in the numerical example because it has a relatively complete set of material parameters and experimental results for concrete, cement paste, and aggregate.

The concrete used in the study was made of limestone aggregates and ordinary Portland cement. The mineralogical compositions of cement were assumed as 63.2 % C_3S, 15.4 % C_2S, 9.9 % C_3A, and 8.1 % C_4AF by weight (Taylor 1987). The mix proportions and properties are listed in Table 2-3. The temperature measured during the irradiation test was 45±5 ºC. Curing time was not reported in the reference (Kelly et al. 1971), and it is assumed to be one week as an approximation. All these values are used as basic inputs in the comprehensive analytical model.

Table 2-3 Mix proportions and properties (w/c=0.36, a/Wtotal=0.67)

Compounds	Weight/cement weight	SG	E (GPa)	α (10^{-5} / ºC)
Ordinary Portland cement	1.0	3.15	-	-
Limestone	2.7	2.55	72.4	6.35[a]
Water	0.36	1	-	-

Note: a/W_{total} = weight ratio of coarse and fine aggregate and concrete.

[a]20-120 ºC.

2.4.1 Model predictions based on available test data of cement paste and aggregates

Since test data are available for the components of the concrete (cement paste and aggregate) in this example, these test data can be used first to obtain the material models for the responses of

cement paste and aggregate. The material models can then be used in the multiphase and multiscale comprehensive model to predict the response of concrete, and then compared with the available test data of concrete. In this way, the correctness of the model prediction can be examined.

The data points of modulus of elasticity for irradiated aggregates and cement paste in concrete are shown in Figure 2-7. Curve fitting was used to obtain linear relationships between the degraded moduli of elasticity for the aggregate and cement paste and neutron levels, respectively, and the linear relationships are plotted in Figure 2-7.

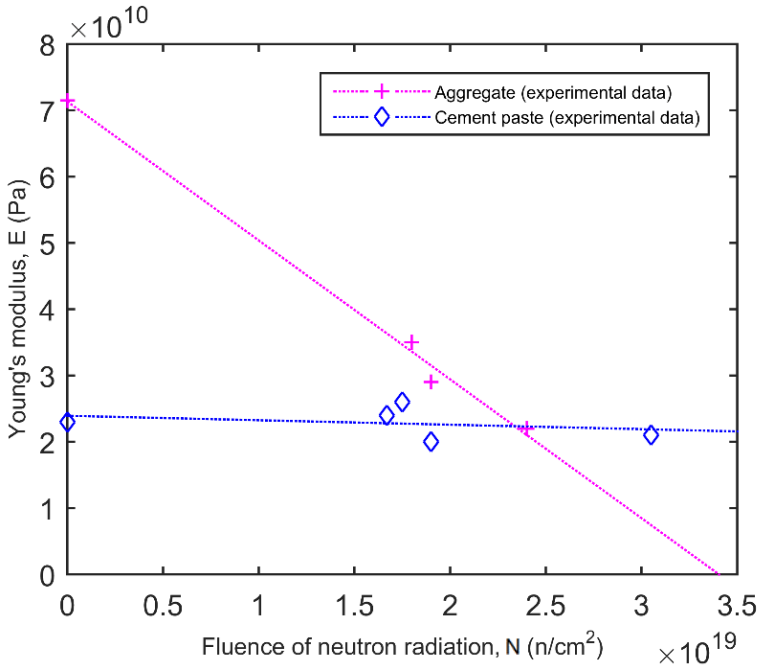

Figure 2-7 Measured Young's modulus of aggregates and cement paste in concrete as a function of fast neutron radiation fluence (dotted lines show linear regressions for different data sets)

For convenience, the linear relationships shown in Figure 2-7 are listed as Eqs. (2-22) and (2-23). They are the basic degradation models for modulus of elasticity of aggregate and cement paste in this example.

$$E_{agg} = 7.132 \times 10^{10} - 2.095 \times 10^{-9} N \quad (2\text{-}22)$$

$$E_{cp} = 2.393 \times 10^{10} - 6.746 \times 10^{-11} N \quad (2\text{-}23)$$

The above two equations obtained based on the test data shown in Figure 2-7 can be used as the lower scale level material models in the multiphase and multiscale model to predict the degradation of modulus of elasticity of concrete due to neutron irradiation. The model prediction and the comparison with test data are shown in Figure 2-8. As one can see in Figure 2-8, the predictions agree with test data quite well in the region of low neutron intensity, and less well with increasing intensity of neutron radiation. This is mainly because of the decreasing trend of experimental data about elastic modulus of aggregate described by Eq. (2-22), which may not be accurate.

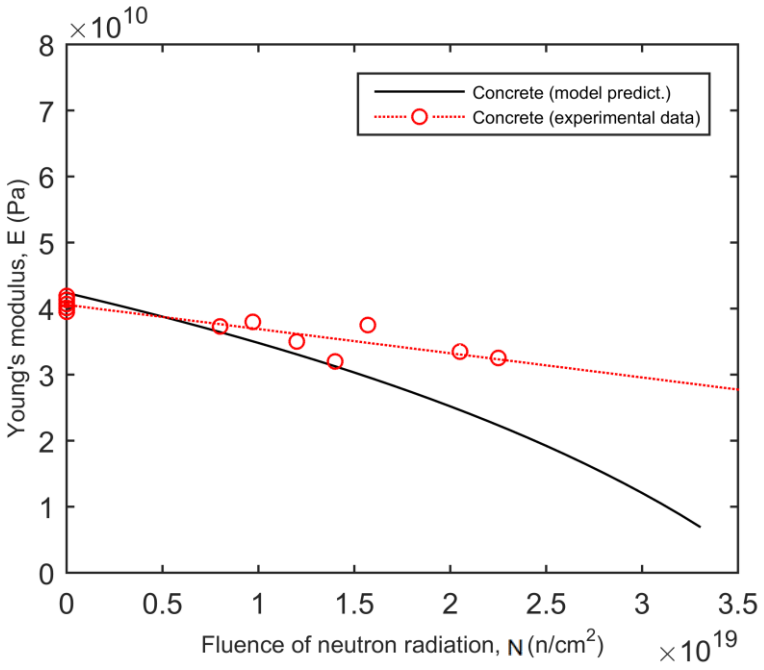

Figure 2-8 Model estimation of Young's modulus of concrete as a function of fast neutron radiation fluence (dotted line shows linear regression of the experimental data)

Among all the input parameters in this example, the degradation of modulus of elasticity of aggregates under neutron irradiation is the important one for predicting the degradation of irradiated concrete. This is because the modulus of elasticity of cement paste varies only slightly with increasing neutron intensity.

The present model can also predict the volume change of concrete under neutron irradiation. Figure 2-9 shows the available test data of volume change of aggregates and cement paste at various neutron radiation fluence. One can see that the aggregate showed volumetric expansion while the cement paste had volumetric shrinkage, which was discussed in previous sections. Curve fitting was used to obtain nonlinear relationships between the volume changes for the aggregate and cement paste and neutron intensity, respectively. Eq. (2-19) was used for the curve fitting and the resulting parameters are δ_{max} = 5.78%, A = 0.9997, B = 6.8×10^{-16} for aggregates and δ_{max} = -3.05%, A = 0.9979, B = 2.294×10^{-16} for cement paste. For convenience, the nonlinear relationships shown in Figure 2-9 are provided as Eqs. (2-24) and (2-25).

$$\delta_{agg} = 0.0578\left(1 - \frac{1}{\sqrt{0.9997 + (1-0.9997)\exp(13.6\times10^{-15}(1-0.9997)N)}}\right) \quad \textit{(2-24)}$$

$$\delta_{cp} = -0.0305\left(1 - \frac{1}{\sqrt{0.9979 + (1-0.9979)\exp(4.588\times10^{-16}(1-0.9979)N)}}\right) \quad \textit{(2-25)}$$

They are the basic degradation models for volume change of aggregate and cement paste in this example. The nonlinear equations are also plotted in Figure 2-9.

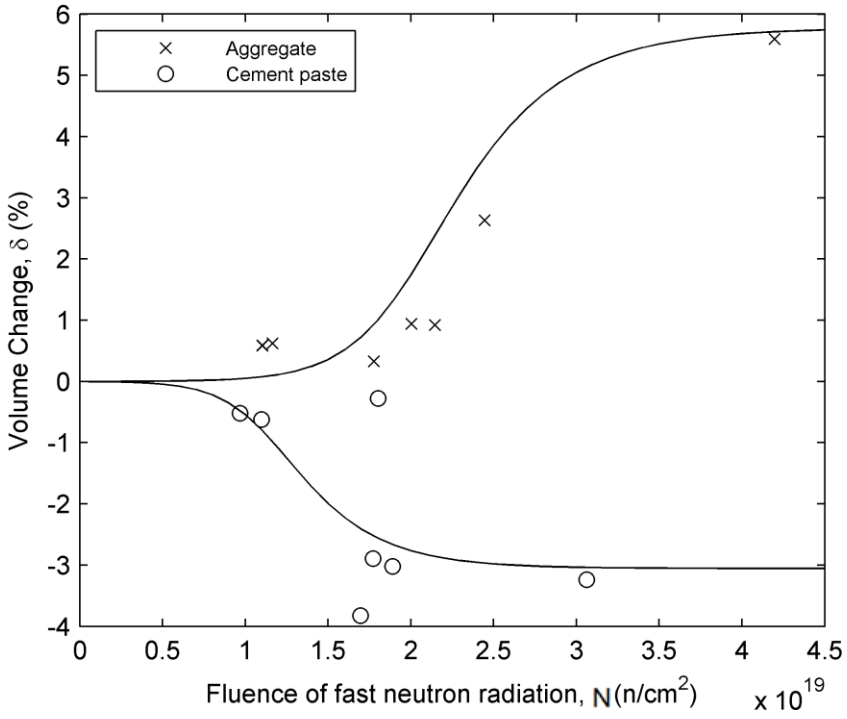

Figure 2-9 Measured volume changes of aggregates and cement paste under fast neutron irradiation

These two equations obtained based on available test data shown in Figure 2-9 can be used as the lower scale level material models in the multiphase and multiscale model to predict the volumetric change of concrete due to neutron irradiation. The model prediction and the comparison with test data are shown in Figure 2-10. A good agreement between model prediction and test data can be observed. The expansion of aggregates seems have a significant influence on the volume change of concrete.

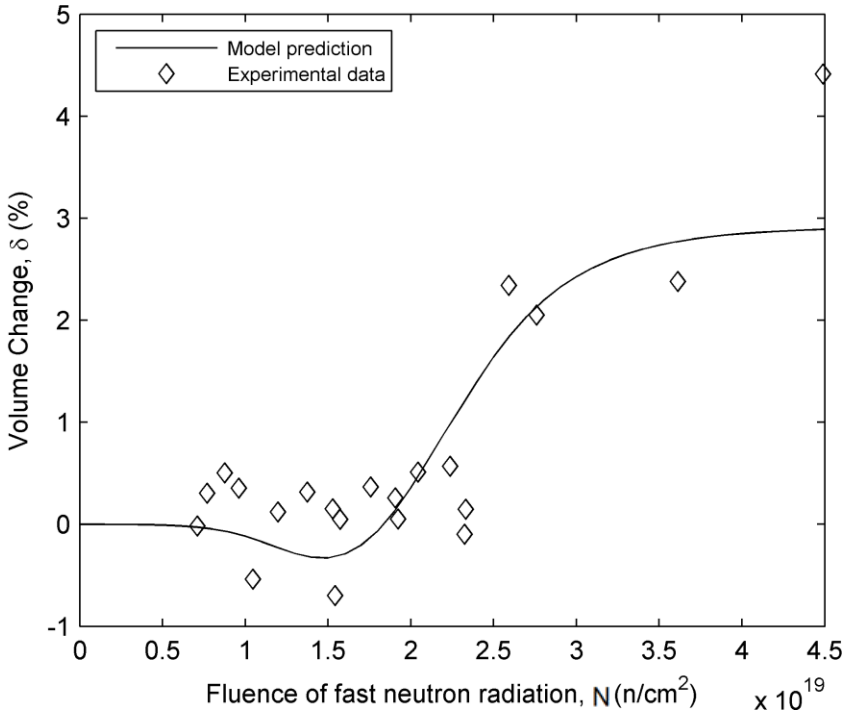

Figure 2-10 Volume change under fast neutron irradiation; the model prediction is based on available test data of cement paste and aggregate

2.4.2 Model predictions without using available test data of cement paste and aggregates

In general, there are no test data available for the effect of neutron irradiation on cement paste and aggregates. In this case, the present model can be used to give an estimation of the properties of concrete under neutron irradiation during the normal operating condition. Following the earlier discussion, the modulus of elasticity of hardened cement paste can be assumed to be a constant during neutron irradiation and be calculated by the multiphase and multiscale model based on the elastic properties of its constituent phases of cement paste, e.g. clinker, pores, C-S-H and CH, which are known and summarized in Table 2. The modulus of elasticity of aggregates can be determined from the multiphase model inversely based on Eq. (2-16) and the result of modulus of elasticity of hardened cement paste. The thermal degradation of elastic modulus of concrete can be calculated by using Eqs. (2-17) and (2-18). It should be noted that Eq. (2-16) is a general form

of the degradation curve for concrete. If test data are available for modulus of elasticity of concrete in a certain range of neutron intensity, Eq. (2-16) can be determined based on the available test data for the concrete under consideration; and if no test data are available, Eq. (2-16) should be determined based on test data in the literature with similar aggregate and concrete design parameters. Here, Eq. (2-16) was used assuming that no test data are available.

The expansion of aggregates particles under neutron radiation is estimated using the fitted curve and 95% confidence bounds on the prediction for the volume change of quartz shown in Figure 2-6(a). The model estimations and test data are plotted in Figure 2-11. The volume of concrete increases with increasing intensity of neutron radiation and the estimations are in a reasonable range.

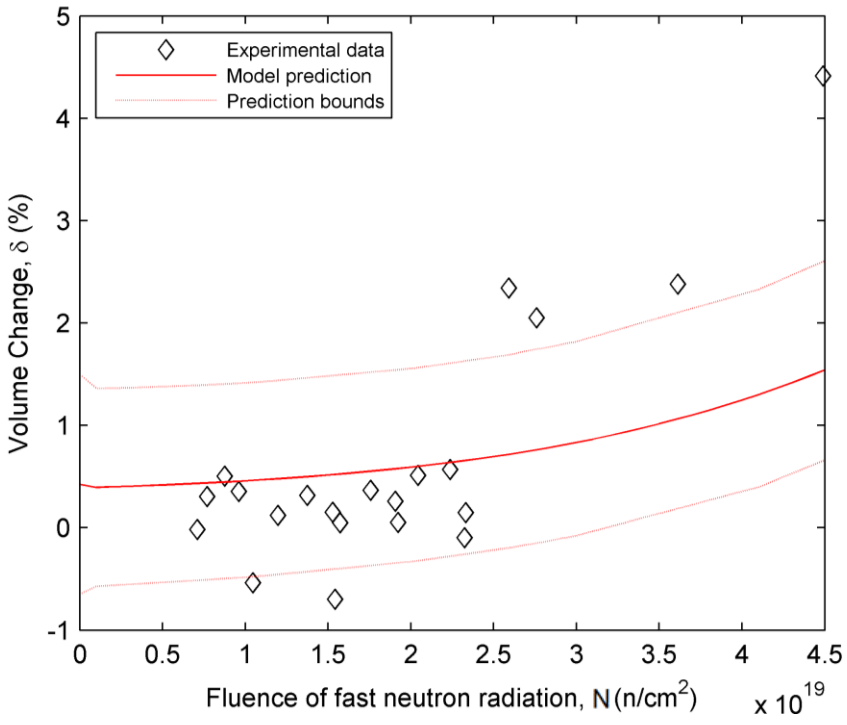

Figure 2-11 Volume change under fast neutron irradiation; the model prediction and prediction bounds are calculated based on the fitted curve and 95% confidence bounds for the volume change of quartz shown in Figure 2-6(a) , respectively

Comparison between the two model predictions shown in Figure 2-10 (using available test data of cement paste and aggregate) and Figure 2-11 (pure estimation without using available test data of cement paste and aggregate) indicates that the volume change of concrete is dominated by the expanding characteristics of aggregates in it. If the evaluation of the volume change of aggregate is more accurate, the estimation of the volume change of concrete will be more reliable.

From this numerical example, one can see that among all of the input parameters for the present model, the volumetric degradation of aggregates under neutron irradiation is the important one for predicting volume change of irradiated concrete.

2.5 Conclusions

- A theoretical model was developed to predict the deterioration of modulus of elasticity and volume change of neutron irradiated concrete. The heterogeneous internal structure of concrete was considered at five different scale levels with different constituent phases, and the volume fractions for each constituent phase were determined based on hydration reactions of Portland cement.
- During the service life of a concrete structure in a nuclear power plant, both neutron radiation and radiation-induced heating have considerable effects on mechanical properties and deformation of concrete. For the direct impact of neutron irradiation, a simple equation for the degradation of modulus of elasticity of concrete was developed (Eq.(2-16)) based on available test data. For the thermal effect, two degradation relations (Eq. (2-17) and Eq. (2-18)) for modulus of elasticity and Poisson' ratio were established based on available test data. The degradation of modulus of elasticity of a neutron irradiated concrete was used as a numerical

example to verify the model prediction, and the results of model prediction agreed with the test data quite well.

- Based on available test data, it was concluded that neutron radiation can directly lead to degradation of elastic modulus of aggregates but has less effect on the elastic properties of hardened cement paste. On the other hand, the elevated temperature has a more significant effect on hardened cement paste than on aggregates.
- There are three different types of volumetric strains in concrete under neutron irradiation: the expansion of aggregates, the shrinkage of cement paste and the thermal expansions of the two phases under the heat of neutron irradiation. It was shown that the volume change of concrete is dominated by the expanding characteristic of aggregates. A model (Eq. (2-19)) was introduced to characterize the volume change of aggregates directly induced by neutron irradiation. Due to crystallization characteristics of aggregates, the expansion of quartz could be used as an estimation to consider the direct effect of neutron radiation on aggregates particles in a certain neutron radiation fluence range. For now, the shrinkage of cement paste under neutron radiation was considered only due to the loss of moisture during the heating process of radiation. The thermal strain due to radiation heating was also included in the proposed model.
- The model can be used for two different scenarios. One is that the knowledge on irradiation effects of cement paste and aggregates are available, in this case, the model can be used to predict the degradation of the specific concrete based on the knowledge of the two components. The other one is that the knowledge on irradiation effect of the cement paste and aggregates are not available, in this case, the model can be used to estimate the degradation of the concrete based on its mix design parameters and environmental conditions. An example was provided to show the applications of the model for the two scenarios.

CHAPTER 3

LONG-TERM NEUTRON RADIATION LEVELS IN DISTRESSED CONCRETE BIOLOGICAL SHIELDING WALLS

3.1 Introduction

Most safety-related concrete structures in a typical NPP are listed in a report (Naus 2009). Among these concrete structures, the biological shielding wall is usually of the primary concern. It is typically a concrete structure placed around the reactor pressure vessel (RPV) as shown in Figure 3-1 and usually suffers the highest radiation level during the operation of NPPs. The thickness of the biological shield wall varies, usually ranging between 1.5 and 2.2 m (4.9–7.2 ft.) for pressurized water reactors(PWRs) and 0.60 to 1.20 m (2–4 ft.) for boiling water reactors (BWRs) (Le Pape 2015). Reliable performance of biological shielding walls is very important to ensure the effective safety protection of workers working in NPPs and general public living near NPPs. When the neutron fluence in a concrete sample reaches a threshold value, mechanical properties of the concrete such as compressive strength and modulus of elasticity will start to decrease with the increase of neutron fluence. The threshold value of neutron irradiation was first discussed by Hilsdorf et al. 1978, and 1×10^{19} n/cm^2 was suggested as the threshold value, and another value 1×10^{20} n/cm^2 was used in Japan (Maruyama et al. 2013) for fast neutrons. Besides, degradation of neutron irradiated concrete is mainly due to the expansion of aggregate which leads to microcracking at the aggregate-cement paste interface (Maruyama et al. 2017). The extent of expansion is thus neutron fluence dependent. Therefore, it's critical to obtain the accurate neutron

radiation levels in concrete structures in NPPs during their service lives. The neutron level varies with time and depth from the exposed surface of biological shielding walls.

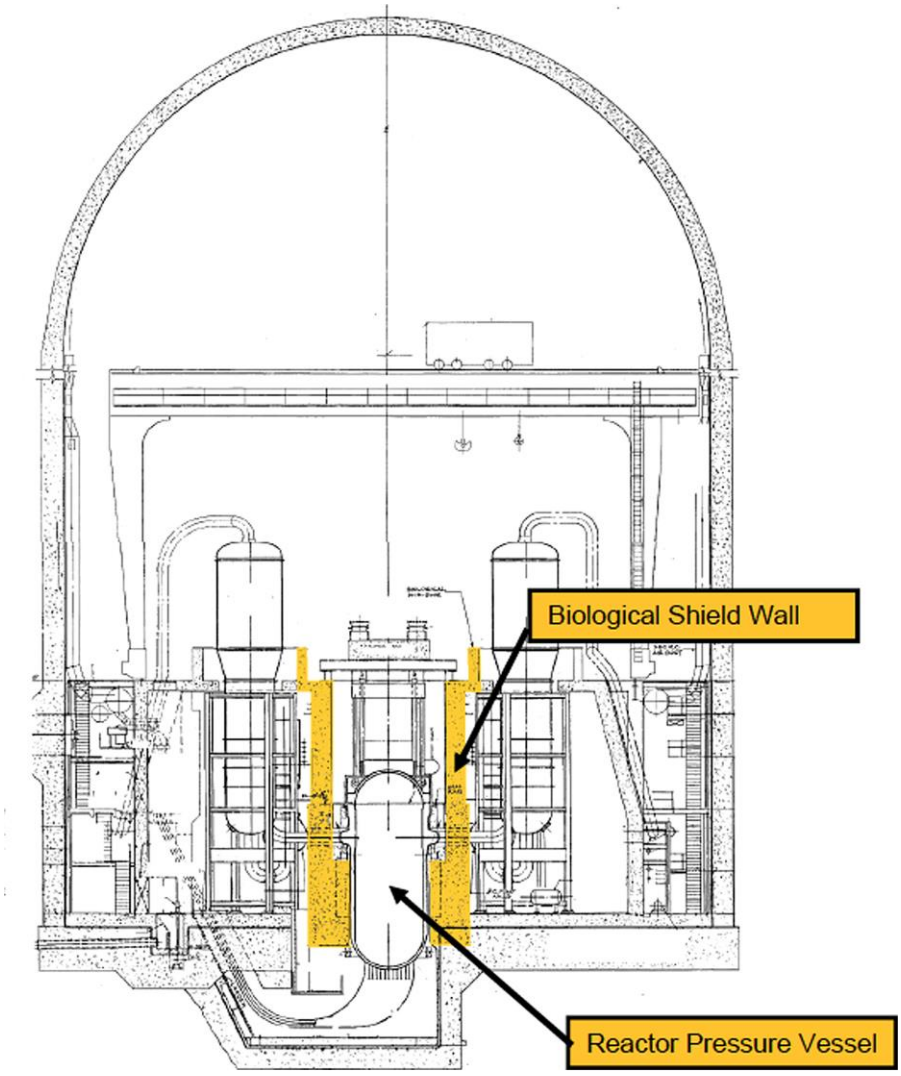

Figure 3-1 Typical configuration of concrete containment. Yellow highlighted areas indicate the location of the biological shield wall (Esselman and Bruck 2013)

Although neutron radiation can lead to the damage of concrete materials, the effect of damage in the internal structure of the concrete on the neutron shielding capacity has not been considered yet, and the neutron flux profile in biological shielding wall has been considered to be unchanged with time (Field et al. 2015; Maruyama et al. 2016; Pomaro et al. 2011a; b). Since

mechanical properties of concrete will degrade under nuclear radiations, and elevated temperatures, the neutron transport properties of concrete may degrade too, during the life span of biological shielding wall. The neutron radiation distributions in a concrete biological shielding wall are predicted by taking into account the possible degradation of transport properties induced by neutron radiation and elevated temperatures. The prediction model is based on one-speed neutron diffusion, heat conduction, cross-property relation theories, and available theoretical models.

3.2 Neutron transport and heat conduction

3.2.1 Neutron transport

Neutron radiation is the emission of neutrons which are electrically neutral particles. The motion of neutrons in a medium is called neutron transport process during which they are either scattered in, attenuated or absorbed by the medium. There are two commonly used methods for neutron transport calculation: Monte Carlo simulation and deterministic transport theory (Shultis and Faw 1996). The former one is to use Monte Carlo technique to simulate neutron particle migration in a medium, and the latter one is to rigorously describe neutron radiation distribution in a medium by using an equation whose solution provides the expected neutron flux. The latter one is the approach adopted in this chapter. The governing equation is known as the neutron transport equation (Duderstadt and Hamilton 1976).

$$\frac{\partial n}{\partial t} + v\hat{\boldsymbol{\Omega}} \cdot \boldsymbol{\nabla} n + v\Sigma_t n(\boldsymbol{r}, \mathcal{E}, \hat{\boldsymbol{\Omega}}, t) = \int_{4\pi} d\hat{\boldsymbol{\Omega}}' \int_{\mathbf{0}}^{\infty} \boldsymbol{d}\mathcal{E}' v' \, \Sigma_s(\mathcal{E}' \to \mathcal{E}, \hat{\boldsymbol{\Omega}}' \to \hat{\boldsymbol{\Omega}}) n(\boldsymbol{r}, \mathcal{E}', \hat{\boldsymbol{\Omega}}', t) + s(\boldsymbol{r}, \mathcal{E}, \hat{\boldsymbol{\Omega}}, t) \quad (3\text{-}1)$$

where n is angular neutron density; v is neutron speed; Σ_t is total macroscopic cross section and Σ_s is macroscopic scattering cross section; s is internal neutron source term; $\boldsymbol{r}$ is position vector, $\mathcal{E}$ is neutron energy, $\hat{\boldsymbol{\Omega}}$ is unit vector describing the direction of neutron motion and t is time. This

equation contains seven independent variables ($\boldsymbol{r} = x, y, z$; $\mathcal{E}$; $\widehat{\boldsymbol{\Omega}} = \theta, \varphi$; t) and is very complex and difficult to be solved. Some details in the equation are also not necessary for many practical cases. Therefore, several approaches have been developed to simplify the equation and the simplified equation requires much less effort to obtain the solution. One of the simplification approaches is called diffusion approximation which will be used here.

For diffusion approximation, neutron energy dependence could be eliminated, and one-speed diffusion could be assumed. "One-speed" means one neutron energy level is considered in the analysis and it does not change during a scattering collision. It was found that one-speed neutron diffusion equation is sufficiently simple to solve either numerically or analytically, and gives reasonable estimates for shielding problems if the cross sections involved are appropriately chosen (Duderstadt and Hamilton 1976; Shultis and Faw 1996). The governing equation for one-speed neutron diffusion is shown below.

$$\frac{1}{v}\frac{\partial \phi(x,t)}{\partial t} - \boldsymbol{\nabla} \cdot D(x)\boldsymbol{\nabla}\phi(x,t) + \Sigma_a(x)\phi(x,t) = S(x,t) \qquad (3\text{-}2)$$

where ϕ is scalar neutron flux in n/(cm^2·sec); v is neutron speed in cm/sec; D is neutron diffusion coefficient in cm; Σ_a is macroscopic absorption cross section in cm^{-1}; S is internal neutron source term in n/(cm^3·sec); x and t are position and time in cm and sec, respectively. Suitable initial conditions and boundary conditions need to be used along with the above equation to obtain the solution of neutron flux.

In many cases, the neutron diffusion medium can be assumed to be homogeneous so that D and Σ_a are constants instead of being position dependent. For a shielding wall of width L suffering neutron radiation from an external source with initial conditions: $\phi(x, 0) = 0$ and boundary conditions: $\phi(0, t) = A$ (a constant value), $\phi(L, t) = 0$, the linear one-dimensional solution for neutron flux profile is obtained by using separation of variables,

$$\phi(x,t) = -\frac{A}{L}(x-L) + \sum_{n=1}^{\infty} T_n(t)\sin\frac{n\pi x}{L} \qquad (3\text{-}3)$$

where

$$T_n(t) = e^{-(\lambda_n^2+b)t}\left(-\frac{2A}{n\pi}\right) + \frac{w_n}{\lambda_n^2+b}\left(1\text{-}e^{-(\lambda_n^2+b)t}\right)$$

$$w_n = -\frac{2bA}{n\pi},\ \lambda_n = \frac{na\pi}{L},\ a = Dv, b = \Sigma_a v$$

However, as mentioned earlier, the neutron transport properties of a concrete wall could be changed by the damage induced by neutron radiation and elevated temperatures, the parameters shown in Eq. (3-2), especially, D, cannot be simply treated as constants. Actually, the parameters are not only position dependent but also time dependent variables, since deterioration of the concrete keeps evolving during the long radiation exposure time. Thus, the straightforward linear solution as shown in Eq. (3-3) is not accurate enough to describe the neutron radiation field in a concrete biological shielding wall.

3.2.2 Heat conduction

The biological shielding wall in a NPP is usually surrounded by an environment whose temperature is above ambient temperature. Nuclear radiation can further lead to localized temperature increases in the irradiated concrete, and the heat of radiation can change the temperature distribution in the wall. Besides, thermal deterioration of concrete could also possibly change its neutron transport properties. Thus, the temperature profile of the neutron irradiated concrete is needed. Classical with internal source term is used

$$c_p\rho\frac{\partial T(x,t)}{\partial t} = \boldsymbol{\nabla}\cdot k\boldsymbol{\nabla}T(x,t) + Q(x,t) \qquad (3\text{-}4)$$

where c_p is specific heat capacity in J/(kg·K); ρ is mass density in kg/cm^3; T is temperature in K; k is thermal conductivity in W/(cm·K); Q is volumetric heat source in W/cm^3.

Neutron radiation generates heat in the material through three primary interactions: capture, elastic scattering and inelastic scattering (Yevick 1966). For thermal neutrons, they heat the material mainly by the binding energy released when they are captured in the material, and their kinetic energy can be ignored. For non-thermal neutrons (neutrons with energy above thermal), they must first be attenuated by being scattering before they can be captured eventually in the material. However, the heat generated during the attenuation is quite small compared to the heat caused during the capture process (Price et al. 1957). Therefore, the volumetric heating rate caused by neutron radiation can be estimated by only considering the heat generation due to neutron capture (El-Sayed Abdo and Amin 2001; William et al. 2013; Yevick 1966)

$$Q(x,t) \approx 1.6 \times 10^{-13} \Sigma_c \mathcal{E}_b \phi(x,t) \qquad (3\text{-}5)$$

where Σ_c is the macroscopic capture cross section of the transport media for neutrons in cm^{-1}; $\mathcal{E}_b$ is the binding energy for capture reaction in MeV. It is assumed that gamma, beta or alpha radiation emitted during neutron capture is absorbed at once, and the heat is released immediately.

Like neutron transport problem, the parameters in Eq. (3-4), especially, ρ and k, could possibly be affected by radiation and elevated temperature, so these two parameters should also be position and time dependent variables. How to handle the variation of the parameters involved in neutron and heat transport processes in concrete will be discussed in details in the next section.

3.3 Damage evaluations in concrete biological shielding walls

As noted, neutron radiation and heat will result in deterioration of concrete material which highly depends on radiation intensity and exposure time, and the effect of the deterioration on the neutron shielding capacity of concrete has not been properly considered yet. If neutron transport properties are constants, then the time derivative term in Eq. (3-2) can be dropped and a

stra1ightforward exponential solution can be obtained for the one-dimensional problem. However, the neutron transport properties are not constants, and they are affected by many parameters, especially the voids (the pathway for neutron movement) in concrete. Studies (Seshadri et al. 1988; Shin 1989) about radiation streaming already confirmed that the ducts in the shielding facilities could result in the leakage of radiation and the distribution of neutron flux in a concrete wall could be significantly altered by the ducts in it. Similarly, the cracks in concrete, especially those on the surface, could be pathways for neutron streaming and could promote the penetration of neutron radiation. The neutron radiation and high temperatures result in cracks and subsequently, neutron flux profiles change in the distressed concrete materials is far more significant than the changes in an intact concrete. Since radiation time of a biological shield wall is very long (up to 80 years), it is important to take into account the change in radiation field due to neutron damage.

Correspondingly, the thermal field in concrete could also be changed by internal damage and heat transport properties which cannot be treated as constants as well. Unlike the neutron transport in distressed concrete, the process of heat conduction should be slowed down by the damage, and this is because cracks in the distressed phase are filled by air whose thermal conductivity is much lower than the concrete's.

No research about the degradation of neutron and heat transport properties of concrete (i.e., D and k) under neutron radiation and elevated temperature is available yet, and it's quite challengeable to directly study neutron radiation effects on these properties by analyzing the actual mechanisms. However, experimental data and theoretical studies of mechanical properties of neutron irradiated and heated concrete are available, so a cross-property correlation between transport and mechanical properties coupled with damage theory could be used to handle this problem.

3.3.1 Cross-property correlation for distressed materials

The cross-property correlations for distressed materials were developed based on both composite mechanics and damage mechanics for two-phase composite materials (Eskandari-Ghadi et al. 2014). This method provides an approach that transport properties of a distressed material can be evaluated by using the available mechanical test data. The approach is mainly based on GSC model (Christensen 1979) which was originally developed for composite materials without any damage. In GSC model, a heterogeneous composite material (e.g., concrete) can be partitioned into simplified spherical elements whose scales are relatively small compared to the representative volume element (RVE) of the composite, as shown in Figure 3-2 (a) and (b). Each spherical element has two constituent phases: the inclusion and matrix, as shown in Figure 3-2 (c). The sizes of these spherical elements could be different as shown in Figure 3-2 (b), but the volume fractions of the two constituent phases within each spherical element are the same.

By using this GSC model, the effective elastic modulus can be written in terms of the elastic moduli of the inclusion and matrix (Xi et al. 2006)

$$E_{eff} = E_m \left(1 + \frac{d}{\frac{1-d}{3} + \frac{1}{\frac{E_i}{E_m} - 1}} \right) \qquad (3\text{-}6)$$

where E with different subscripts are elastic moduli of different phases and d is volume fraction of the inclusion; and subscripts i, m, and eff = inclusion, matrix, and effective media, respectively.

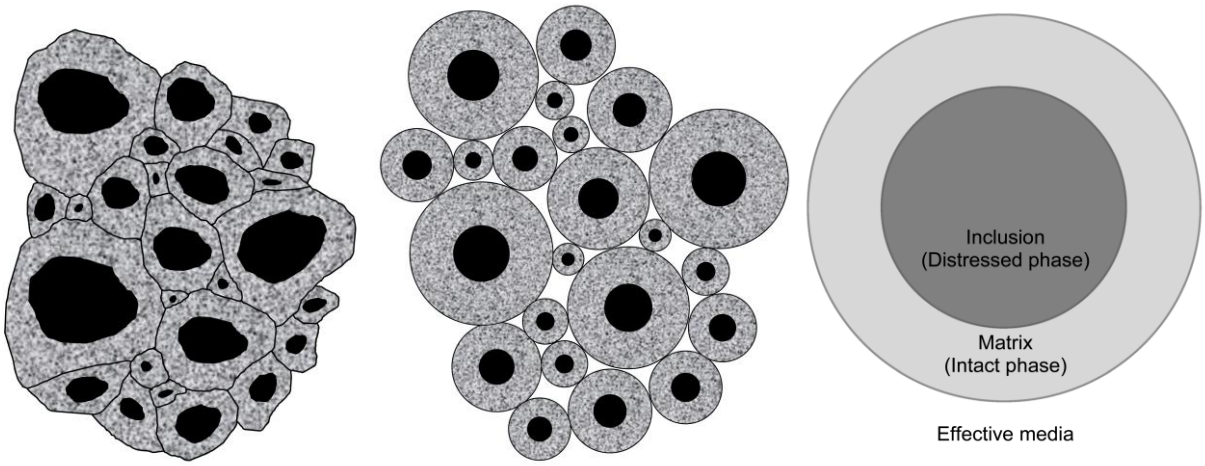

Figure 3-2 GSC model for composite and distressed materials: (a) RVE of the composite material; (b) simplified spherical element in the RVE; and (c) An individual spherical element and the constituent phases.

The composite model can be further applied to estimate the stiffness of distressed materials and the theory is called *composite damage mechanics* (Eskandari-Ghadi et al. 2013; Xi et al. 2006). As one can see in Figure 3-2 (c), the inclusion is the distressed phase, and the matrix is the intact phase. The distressed phase has smaller stiffness than the intact one when damage appears. The distressed material is treated as a two-phase composite material. The volume fraction of the inclusion, *d*, is the variable parameter which describes the development of internal damage in the material and can be derived from Eq. (3-6)

$$d = \frac{\left(\frac{E_{eff}}{E_m} - 1\right)\left(1 + \frac{3}{\frac{E_i}{E_m} - 1}\right)}{\frac{E_{eff}}{E_m} + 2} \tag{3-7}$$

It needs to be noticed that in the composite damage mechanics, both the matrix and inclusion can carry loads and have their own non-zero elastic modulus, which is different from the conventional scalar damage mechanics that the damaged phase has a zero modulus. Apparently,

the internal damage of the material reduces the stiffness of the distressed phase, thus, $0 \le d \le 1, 0 < \frac{E_i}{E_m} \le 1, 0 < \frac{E_{eff}}{E_m} \le 1$.

By using above equation, the damage in a material can be characterized based on its known mechanical performance. In order to model the transport problem in a distressed media, expressions of transport properties need to be obtained first. For concrete, heat conduction problem is one of the most common transport problems encountered, and the equation for effective thermal conductivity based on the same GSC model shown in Figure 3-2 (b) has already been derived (Eskandari-Ghadi et al. 2014; Meshgin and Xi 2013)

$$k_{eff} = k_m \left(1 + \frac{d}{\frac{1-d}{3} + \frac{1}{\frac{k_i}{k_m} - 1}} \right) \tag{3-8}$$

Then, substitute Eq. (3-7) in to Eq. (3-8)

$$k_{eff} = k_m \left(1 + \frac{(\frac{E_{eff}}{E_m} - 1)(\frac{E_i}{E_m} + 2)}{\frac{E_i}{E_m} - \frac{E_{eff}}{E_m} + \frac{(\frac{E_{eff}}{E_m} + 2)(b-1)}{\frac{k_i}{k_m} - 1}} \right) = f_k \left(k_m, \frac{E_i}{E_m}, \frac{k_i}{k_m}, \frac{E_{eff}}{E_m} \right) \tag{3-9}$$

The distressed phase has a higher porosity (voids and cracks developed during the damage process), so its thermal conductivity should be lower than the intact phase's ($0 < \frac{k_i}{k_m} \le 1$).

Due to the mathematical analogy, the formulation of effective neutron diffusion coefficient can share the same form of Eq. (3-8), then

$$D_{eff} = D_m \left(1 + \frac{(\frac{E_{eff}}{E_m} - 1)(\frac{E_i}{E_m} + 2)}{\frac{E_i}{E_m} - \frac{E_{eff}}{E_m} + \frac{(\frac{E_{eff}}{E_m} + 2)(b-1)}{\frac{D_i}{D_m} - 1}} \right) = f_D \left(D_m, \frac{E_i}{E_m}, \frac{D_i}{D_m}, \frac{E_{eff}}{E_m} \right) \quad (3\text{-}10)$$

Since the damage in the material provides more accessible pathways for neutron transport, the diffusion coefficient of the distressed phase should be higher than that of the intact phase ($\frac{D_i}{D_m} \geq 1$).

The application of the method developed above for distressed materials requires that the damage evolution in the material is a random nucleation process. Since neutron radiation and high temperature induced damage in concrete material fulfills this requirement, the method is capable of calculating the variations of neutron and heat transport properties of concrete by analyzing degradation of the elastic modulus of concrete under neutron radiation and heat which has been investigated by many experimental and theoretical studies. The present method can consider the effects of neutron radiation and elevated temperature on the modulus of elasticity of concrete to be two distinct influential factors, and two different models will be developed and used in the governing equations Eq. (3-2) and Eq. (3-4).

3.3.2 Neutron radiation induced degradation

The experimental data collected by Hilsdorf et al. 1978 and Field et al. 2015 are the most comprehensive database about the degradation of the elastic modulus of neutron irradiated concrete so far. The former one has already been used by some numerical studies concerning concrete performance under nuclear radiation to consider the effect of neutron radiation on mechanical properties (Pomaro et al. 2011a; b; Salomoni et al. 2014). The middle trend line of the

data reported in the latter one was used, and the expression has been obtained in Chapter 2 about neutron radiation effects on concrete

$$\mathcal{F}_r(N) = \frac{E_{eff}}{E_m} = -1.188 \times 10^{-8} N^{0.3711} + 1 \ \ (0 \le N \le 7 \times 10^{20}\ n/cm^2) \qquad (3\text{-}11)$$

where N is neutron fluence which is the integration of neutron flux over time, $N = \int_0^t \phi$. According to above equation, the elastic modulus of concrete starts to show a clear reduction from about 1×10^{18} n/cm^2 neutron fluence and reaches 35.37% of the original value eventually which could be used for the value of $\frac{E_i}{E_m}$ .in Eq.(3-9) and Eq. (3-10).

It should be aware that the data used to obtain Eq. (3-11) comes from different studies and different types of materials and test conditions were used, so this equation only provides a general trend of the variation of elastic modulus of neutron irradiated concrete and was used here assuming no test data is available. If experimental data is available for a certain case, the elastic modulus of concrete can be predicted using the model developed in Chapter 2.

3.3.3 Thermal deterioration

There are quite a lot studies about the thermal degradation of the elastic modulus of concrete. The heat during the neutron radiation could reduce the elastic modulus of concrete by two mechanisms: the phase transformation of constituent phases and the volumetric mismatch between aggregates and cement pastes due to their different thermal deformation (Lee et al. 2009). The former one can generate new phases with lower stiffnesses than that of the original phases, and the latter one usually results in microcracking and debonding at the aggregate-cement paste interface.

The prediction model for the thermal degradation of the elastic modulus of concrete up to 800 ºC has already been developed(Lee et al. 2009). Under 120 ºC, there is no phase transformation involved in the cement paste, and the degradation of concrete mainly comes from the incompatibility between the thermal expansions of aggregates and cement paste, as well as thermal degradation of aggregates. Since NPPs design codes of the United States and Japan require the normal operating temperature within the containment structures be less than 65 ºC (ASME 2015; Fujiwara et al. 2009), so usually, only the equation for low temperature range is needed (Lee et al. 2009)

$$\mathcal{F}_t(T) = \frac{E_{eff}}{E_m} = 0.03921 + exp(-0.002T)\ (20℃ \le T \le 120℃) \qquad (3\text{-}12)$$

When T=20 ºC , $F_t(T)$=1 and T=120 ºC , $F_t(T)$=82.58% which could also be used for the value of $\frac{E_i}{E_m}$ in Eq.(3-9) and Eq. (3-10).

Neutron irradiated concrete usually suffers from neutron radiation, and resultant temperature rises simultaneously, so the degradation of the elastic modulus of concrete should include both the degradation induced by neutron radiation and thermal degradation

$$\frac{E_{eff}}{E_m} = \mathcal{F}_r(N)\mathcal{F}_t\ (T) \qquad (3\text{-}13)$$

Therefore, effective thermal conductivity and effective neutron diffusion coefficient are functions of time, neutron flux and temperature and Eq.(3-9) and Eq. (3-10) turn to be

$$k_{eff} = f_k\left(k_m, \frac{E_i}{E_m}, \frac{k_i}{k_m}, \int_0^t \phi\ , T\right), D_{eff} = f_D\left(D_m, \frac{E_i}{E_m}, \frac{D_i}{D_m}, \int_0^t \phi\ , T\right) \qquad (3\text{-}14)$$

where $k_m, D_m, \frac{E_i}{E_m}, \frac{k_i}{k_m}, \frac{D_i}{D_m}$ are constant values and ϕ and T are time and position dependent variables.

3.3.4 Other variable parameters

In addition to *k* and *D,* other parameters in Eq. (3-2) and Eq. (3-4), including neutron speed v, macroscopic cross sections Σ_a and Σ_c, specific heat capacity c_p, and mass density ρ, could potentially be affected by neutron radiation and temperature.

Generally, neutron speed indicates a neutron' kinetic energy and is temperature dependent. For example, v_T, the most probable velocity of thermal neutrons at temperature *T*, can be calculated based on v_0, the most probable velocity at room temperature T_0: $v_T = v_0\sqrt{\frac{T}{T_0}}$ (DOE Fundamentals Handbook 1993). The temperature used here is absolute the temperature of the media. Since the temperature considered for concrete biological shield remains at low range, the variation of *v* caused by temperature rise is not significant., So neutron speed *v* can be assumed to be unchanged during the neutron radiation process. Furthermore, one neutron energy level is used for neutron diffusion calculation and it is assumed that neutron energy does change during a scattering collision.

Neutron macroscopic cross section (Σ) of a medium is derived from atomic number density and neutron microscopic cross section of each element in it and both of them can be changed by radiation and temperature. For instance, loss of hydrogen and oxide due to the dehydration in concrete will lead to the change of atomic number density of these two elements and neutron microscopic cross section is also temperature dependent (DOE Fundamentals Handbook 1993). However, determination of neutron macroscopic cross section of a heterogeneous material like concrete is quite complicated and is not the major concern in this work. Thus, all the neutron macroscopic cross sections encountered in this work are considered to be constants.

The specific heat capacity of concrete will vary with temperature (Kodur V. K. R. and Sultan M. A. 2003; Pan et al. 2016), but there is no research about the nuclear radiation effects on it. Actually, for the composite material with two phases, the effective specific heat capacity can be determined based on the temperature and two phase's specific heat capacities, coefficients of thermal expansion and bulk moduli (Rosen and Hashin 1970). For simplicity, specific heat capacity is assumed to be a constant in the present study.

Mass density is the ratio of mass to volume. It has been confirmed that concrete will expand under neutron radiation (Field et al. 2015; Hilsdorf et al. 1978). The volumetric change of concrete under neutron irradiation mainly results from a combination of expansion of aggregates, shrinkage of cement paste and thermal expansions of these two phases. The theoretical model in Chapter 2 used here to predict the volume change of concrete under neutron radiation. This model also takes into account the effects of neutron radiation and radiation-induced heating on the mechanical properties. Experimental data shows that the maximum weight loss of neutron irradiated concrete is less than 5% and the average value of the weight loss is around 2% (Field et al. 2015). No clear trend was observed. Weight loss of concrete under the normal operating temperature of NPPs is also negligible (Kodur 2014; Kodur V. K. R. and Sultan M. A. 2003; Sancak et al. 2008). Weight loss induced by both neutron radiation and temperature rise is very likely mainly due to the dehydration of the cement paste. Constant 2% weight loss can be assumed in the calculation.

3.4 Numerical analyses

3.4.1 Coupled Radio-Thermo analysis

As discussed in the previous sections, neutron speed v, neutron macroscopic cross sections Σ_a and Σ_c, and specific heat capacity c_p can be considered as constants and heat conductivity k, neutron diffusion coefficient D, and mass density ρ are time and position dependent parameters.

Coupled Radio-Thermo analysis of radiation and thermal field within neutron irradiated concrete can be performed based on the neutron diffusion and heat conduction equations. The effects of neutron radiation induced degradation and thermal deterioration on concrete can be taken into account by the composite damage mechanics and cross-property correlation theory discussed in above sections. The two governing equations are

$$\frac{1}{v}\frac{\partial \phi(x,t)}{\partial t} - \nabla \cdot D(x,t)\nabla\phi(x,t) + \Sigma_a \phi(x,t) = 0 \qquad (3\text{-}15)$$

$$c_p \rho(x,t)\frac{\partial T(x,t)}{\partial t} = \nabla \cdot k(x,t)\nabla T(x,t) + 1.6 \times 10^{-13}\Sigma_c \mathcal{E}_b \phi(x,t) \qquad (3\text{-}16)$$

These coupled nonlinear transient equations are too complex to solve analytically. Thus, an implicit finite differential approach was used to solve them numerically. Proper initial conditions, boundary conditions, and time step should be defined, which are shown in a case study. Bisection method was used for root-finding iteration in each time step, and the speed of convergence is very good. The calculation flow chart is shown in Figure 3-3.

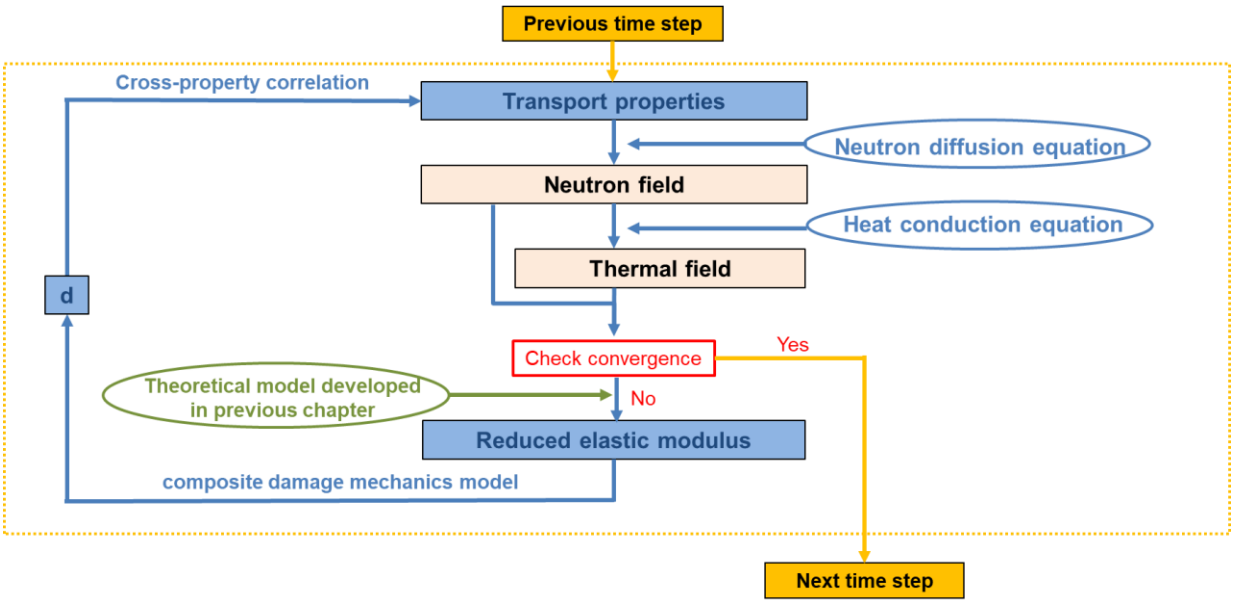

Figure 3-3 Calculation flow chart for one-speed neutron diffusion

3.4.2 A case study

While there is usually no routine monitoring of the radiation levels in concrete biological shields in NPPs, and thus it's quite difficult to find experimental studies with comprehensive parameters and results to validate the model developed above. A case study was developed to show the capability of the model, to compare the neutron distributions in a concrete wall with and without the effect of damage due to high neutron and temperatures, and to analysis the neutron radiation and temperature fields in a concrete biological shield during 80 years of operation.

A wall made of Portland cement concrete without rebar embedment was analyzed as a simplified example of a typical concrete biological shield in NPPs. The thickness of the wall is 1.8 meter. It usually can be assumed that the neutron flux and temperature are uniformly distributed on the inner surface of the wall. Thus the neutron and heat conduction can be considered to be a one-dimensional problem along the depth of the concrete wall. The outer surface of the wall is the ambient environment. The configuration of the concrete wall is shown in.

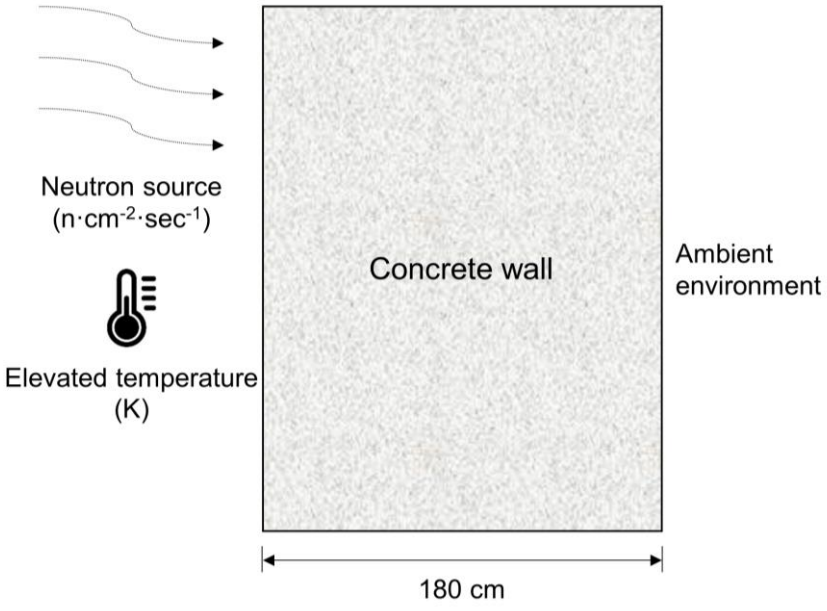

Figure 3-4 The configuration of the concrete wall for numerical analysis.

A constant neutron flux density of 3.5×10^{10} n/(cm^2·sec) is assumed at the inner surface of the wall for neutrons with 0.1 MeV energy level, and the neutron flux at the outer surface of the wall is approximately 10^{-6} of the neutron flux at the inner surface (Esselman and Bruck 2013). The use of 0.1 MeV neutron energy is consistent with the energy used by other studies (Esselman and Bruck 2013; Fujiwara et al. 2009; Maruyama et al. 2017). The temperature is 65 ºC at the inner surface and 20 ºC at the outer surface. The main parameters of concrete used in the analysis are listed in Table 3-1. All of them are typical values for ordinary concrete. It should be noticed that the value of Σ_c given by El-Sayed Abdo and Amin 2001 is too large to be true since Σ_c is part of Σ_a and should be a much smaller number. Thus, the value of Σ_a is used as an approximation of Σ_c. The water-cement ratio of the concrete is 0.36, and the aggregate to cement ratio is 2.7. The expansion of aggregate particles under neutron radiation is estimated by the volume expansion of neutron irradiated quartz since no test data available here. As mentioned earlier, either 35.37% and 82.58% can be used for $\frac{E_i}{E_m}$. For the combined effect of neutron radiation and temperature, usually lowest value is used. It is assumed that $\frac{k_i}{k_m}$=0.1 and $\frac{D_i}{D_m}$=10.

Table 3-1 Assumed parameters used in the numerical analysis of the analyzed ordinary concrete.

Parameters	Values	Reference
Concrete		
D[cm]	0.65	(Shultis and Faw 1996)
Σ_a[cm^{-1}]	0.0094	(Shultis and Faw 1996)
v[cm/sec]	4.37×10^{8}*	–
c_p[J/(kg·K)]	650	(Ursu 1985)
ρ[kg/cm^3]	2.3×10^{-3}	(Ursu 1985)
k[W/(cm·K)]	8.7×10^{-3}	(Ursu 1985)
Σ_c[cm^{-1}]	0.0094†	–
E_b[MeV]	5.5	(Price et al. 1957)
Cement		
ρ[kg/cm^3]	3.15×10^{-3}	(Xi and Jennings 1997)
Aggregates		
ρ[kg/m^3]	2.55×10^{-3}	(Kelly et al. 1969)
E [GPa]	72.4	(Kelly et al. 1969)
α ‡ [10^{-5} / ºC]	6.35§	(Kelly et al. 1969)

* Calculated based on classical kinetic energy equation for 0.1 MeV neutron.

† Use the value of Σ_a as an approximation.

‡ α is coefficient of linear thermal expansion.

§ 20-120 ºC.

3.4.3 Numerical results

Figure 3-5 shows the variation of the damage parameter, *d*, due to neutron radiation and temperature. As mentioned earlier, *d* can be calculated from Eq. (3-7); and $d = 0$ means no damage and $d = 1$ means complete damage. The profiles of damage parameter, *d*, of the concrete up to 80 years are reported in Figure 3-5. Damage of the concrete due to neutron radiation and the temperature continues to develop with increasing time, especially for the concrete close to the neutron source (with small depth in the wall). The concrete near ambient environment (large depth) has quite smaller damages. As one can see, on the surface, even after one month of exposure, the concrete already shows some damage; and on the other side of the wall (large depth), *d* shows little variation along time for up to 80 years.

The reason for the short-term damage (e.g., after one month) is that the elevated temperature, even though is not very high, can solely lead to the degradation of the modulus of elasticity which is considered as the indicator of damage in the present model. Since the heat conduction is a much faster transport process than the neutron diffusion in concrete, the temperature induced damage is relatively large compared to the damage due to neutron radiation for the concrete with large depth. This conclusion can be further confirmed by Figure 3-6. If thermal degradation of concrete is not considered and only neutron radiation induced degradation is included, *d* will be quite smaller compared to the case that both of them are considered. Therefore, the temperature effect on distressed concrete under nuclear radiation must be considered, especially for the concrete with large depth from the radiation source.

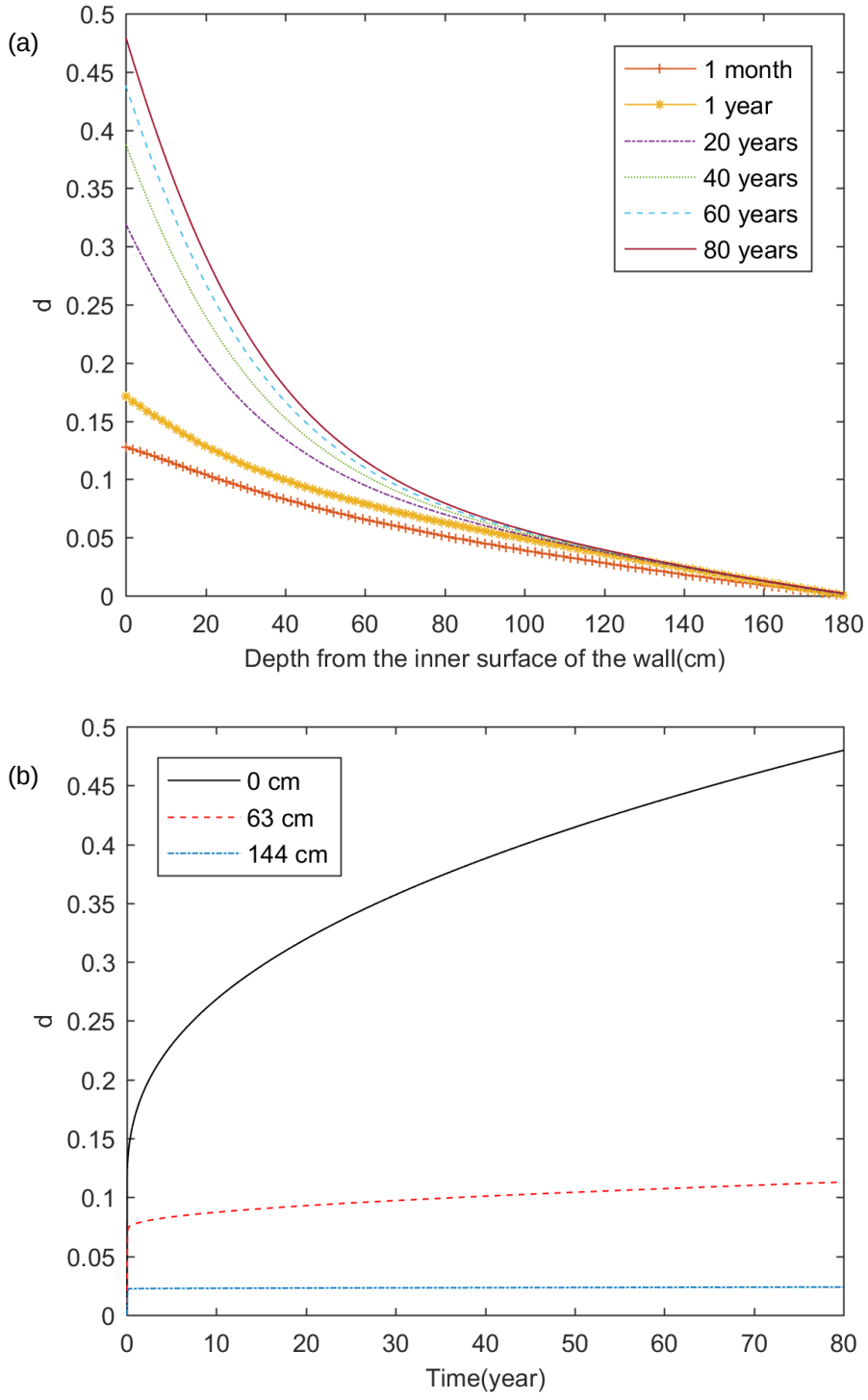

Figure 3-5 Damage progression due to neutron radiation and the temperature: (a) with the depth of concrete at difference time; (b) with time at different depths.

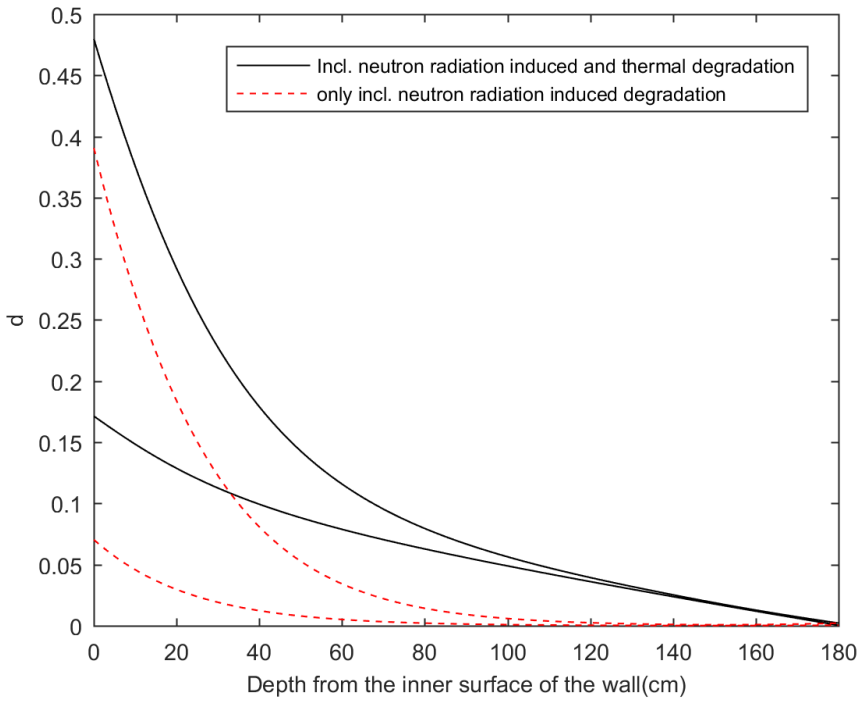

Figure 3-6 The effect of thermal degradation on radiation damage progression at different depths after 10 years and 80 years of exposure.

The effect of temperature and neutron radiation on thermal conductivity of concrete, *k*, is shown in Figure 3-7. The value of *k* gradually decreases with time. Concrete close to the neutron source shows larger variations of *k* than the concrete near ambient environment since the damage in that area is more significant.

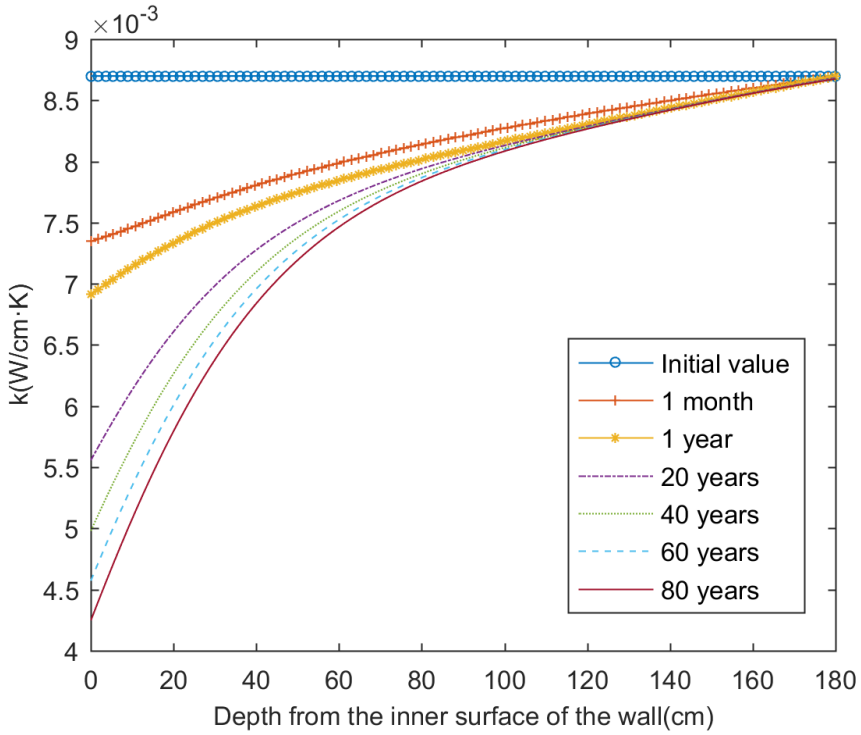

Figure 3-7 Thermal conductivity profiles along the depth at different times.

Figure 3-8(a) shows the temperature profiles in the concrete with and without the effects of radiation and thermal damage after 1 month, 40 years and 80 years of exposure. If no damage is considered, the temperature profile will not change over time. As one can see from Figure 3-8(b), the damage of radiation and temperature in concrete leads to minor changes of the temperature profile in the concrete (maximum change is less than 4 ºC) which is consistent with results reported in (El-Sayed Abdo and Amin 2001; Esselman and Bruck 2013). Since radiation heating is flux dependent and neutron flux is increasing over time as one can see later on in Figure 3-10(a), the temperature profile should always keep increasing correspondingly. However, the temperature at 1 month for the concrete with a depth greater than 35cm dropped as shown in Figure 3-8(b). Actually, the damage induced by neutron radiation and elevated temperature neutralizes some of

the temperature increase in concrete caused by radiation heating, since the developing damage keeps reducing the thermal conductivity of concrete as shown in Figure 3-7.

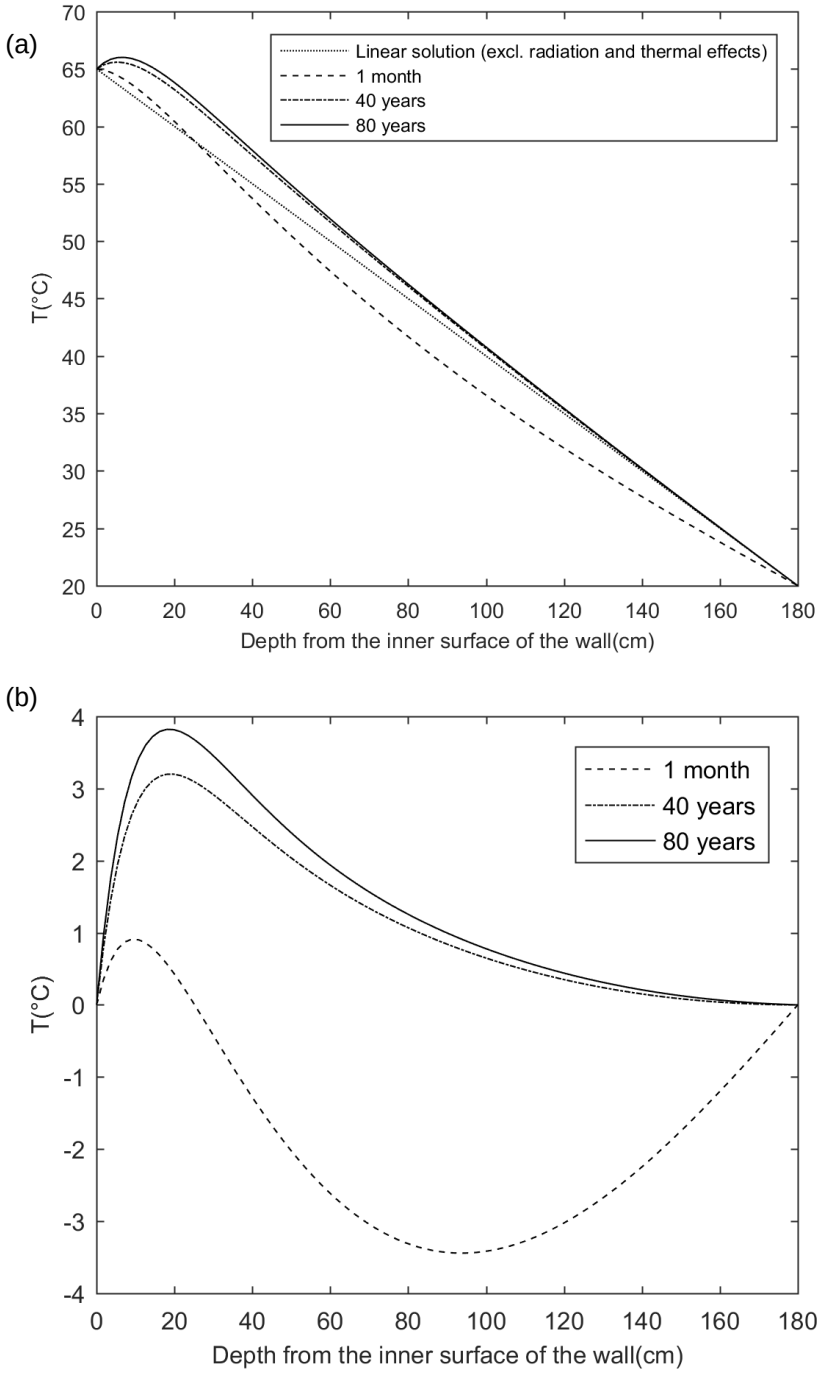

Figure 3-8 Temperature profiles along the concrete depth: (a) Absolute values without radiation and thermal effects considered and with these effects considered at 1 year, 80 years; (b) Temperature changes compared to the initial values.

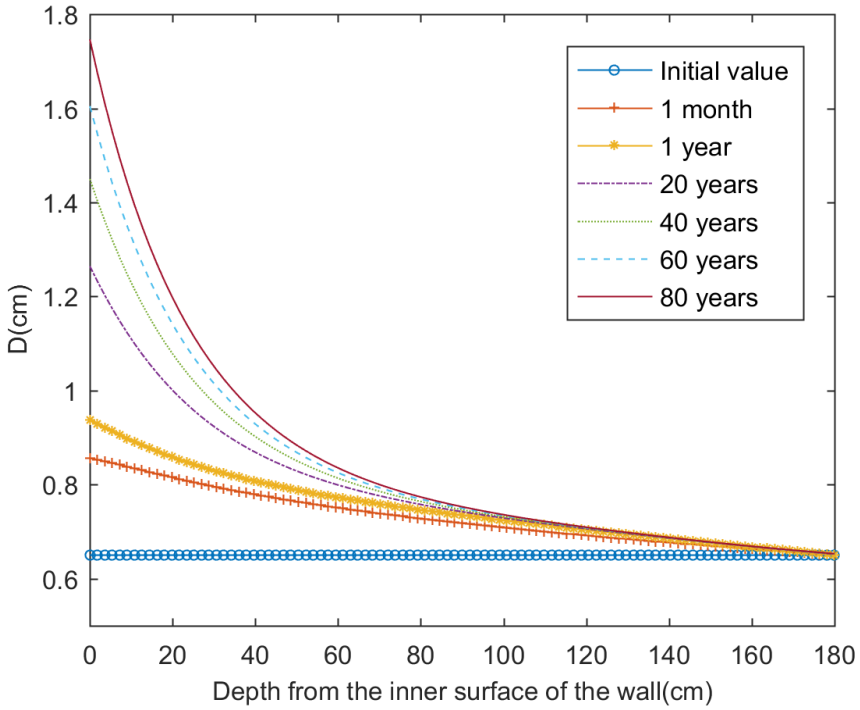

Figure 3-9 Neutron diffusion coefficient profiles along the concrete depth at different times.

The profiles of neutron diffusion coefficient, *D*, are shown in Figure 3-9. The value of *D* gradually increases with time, and the change is quite large comparing to its initial value. In the surface layer, the value of *D* is almost tripled. Similar to the behavior of thermal conductivity discussed earlier, *D* of the concrete close to the neutron source shows larger variation than *D* of the concrete near ambient environment, and this is because the damage of concrete near the neutron source is more severe.

After the determination of the material parameters as functions of time and location (depth), the nonlinear solutions of neutron flux profiles in the concrete up to 80 years are obtained which includes the effects of radiation and temperature, as shown in Figure 3-10(a). The linear one-dimensional solution, Eq. (3-3), which excludes these effects is also plotted in Figure 3-10 (a). The differences between the nonlinear solutions and linear solution at different times are calculated

and plotted in Figure 3-10 (b). Figure 3-10 (b) indicates that the maximum neutron flux increase in the concrete at 80 years is 6.3×10^{9} n/(cm^2·sec) which is about 18% of the largest neutron flux at the boundary. Clearly, neutron radiation and elevated temperature can result in considerable degradation of concrete as a shielding material, and thus can lead to a large increase of neutron flux in concrete. The neutron flux increases with time significantly, especially for the concrete near the radiation source. The peak occurs at about 10 cm depth from the surface. This is mainly caused by the increase of neutron diffusion coefficient of concrete as shown in Figure 3-9.

Neutron fluence is responsible for the degradation of concrete. Neutron fluence can be obtained by integrating neutron flux with time. Neutron fluence profiles at different times can be obtained for both linear solution and nonlinear solutions (without and with the radiation and thermal effect). Capacity factor 0.92 is assumed to be the estimated effective full power years of a NPP which considers the actual time when the neutron radiation is present (Esselman and Bruck 2013). Neutron fluence profiles in the concrete wall at 60 years and 80 years are plotted in Figure 3-11. Similar to the neutron flux profiles, considerable increases of neutron fluence from the linear solution without considering the radiation and thermal effects are observed for the concrete near the radiation source. The maximum neutron fluence increases in the concrete are 7.9×10^{18} n/cm^2 and 1.14×10^{19} n/cm^2 for 60 years and 80 years, respectively. These values are very high for concrete. It is worthwhile to compare these values with the critical neutron fluence for concrete recommended by Hilsdorf et al. 1978, which is in the order of magnitude of 10^{19} n/cm^2. This means that the neutron radiation and thermal effects could be in the same range of the critical neutron fluence. Evidently, the damage induced by neutron radiation and elevated temperature can effectively accelerate the penetration of neutron radiation into the concrete.

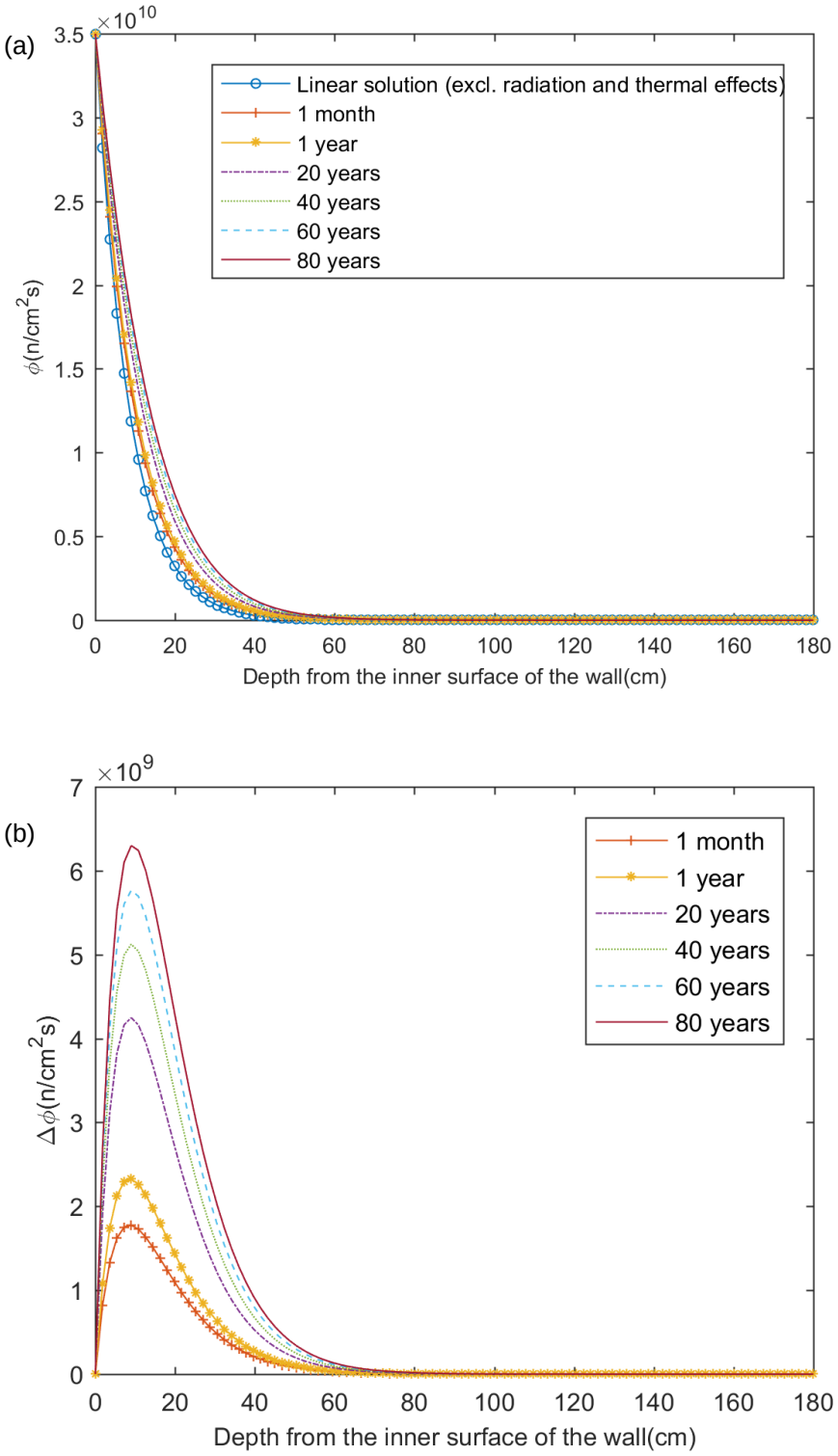

Figure 3-10 Neutron flux profiles along the concrete depth (energy = 0.1MeV): (a) Absolute values with and without the radiation and thermal effects after different periods of exposure; (b) Neutron flux increases compared to the case without the radiation and thermal effects.

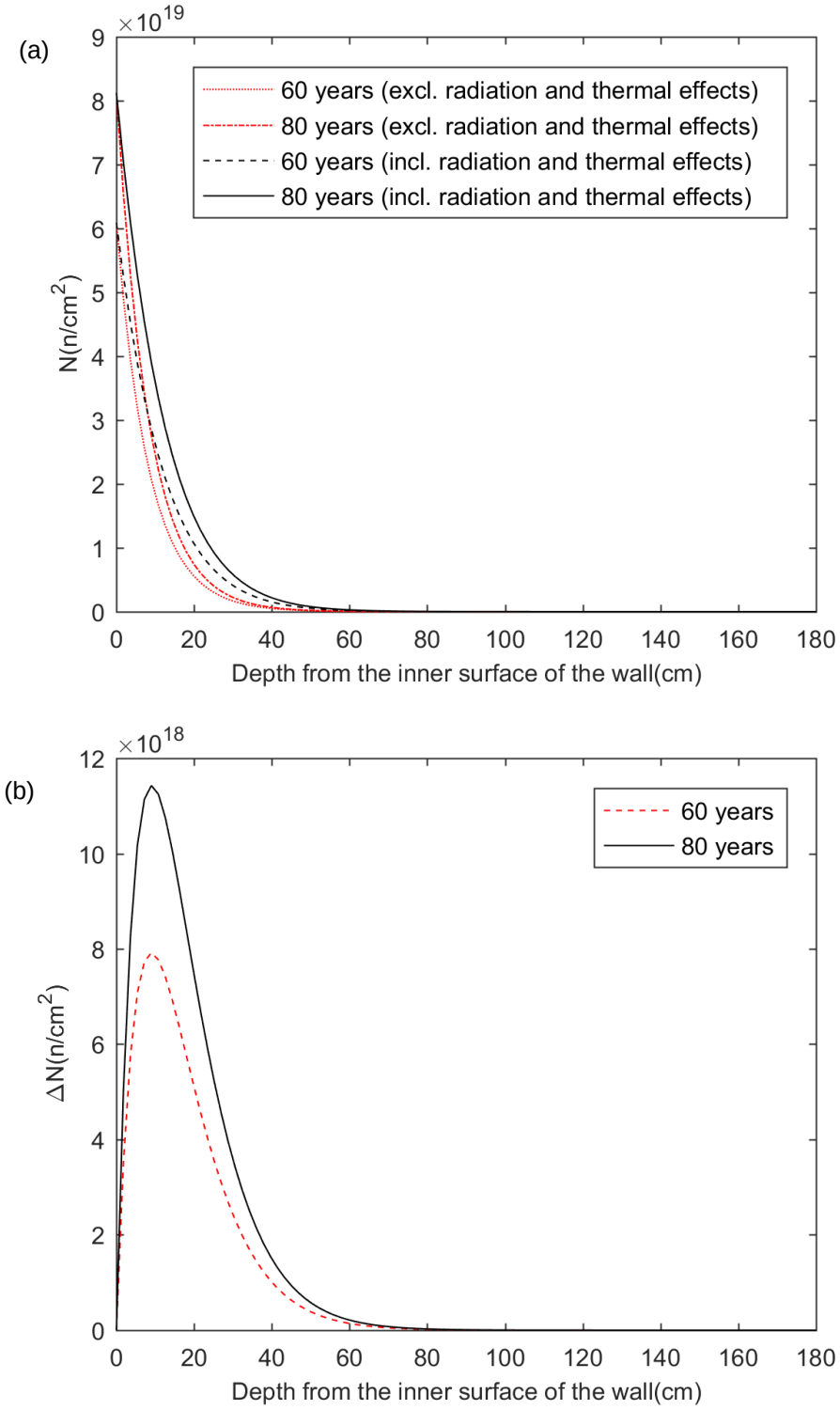

Figure 3-11 Neutron fluence profiles along the concrete depth at 60 years and 80 years (energy=0.1MeV): (a) Absolute values with and without considering the radiation and thermal effects; (b) Neutron fluence increase compared to the case without these effects considered.

3.5 Multigroup neutron diffusion method

As stated earlier, one very important assumption that neutrons are characterized by only one single energy level and do not change during a scattering collision, was made for one-speed neutron diffusion model. However, the neutrons escaped from the reactors usually have very wide energy spectrum ranging from 10 MeV down to less than 0.01 eV(Duderstadt and Hamilton 1976). and neutron cross sections are also energy dependent, thus, a more realistic consideration of the neutron energy dependence is needed.

Instead of treating the neutron energy as a continuous variable, the energy domain of neutrons can be divided into a set of energy groups. The neutrons inside each group were assumed to behave as one-speed particles, and the neutron source in one group included the secondary neutrons from scattering reactions in the other groups with higher energy. Usually, no up-scattering from one group with lower energy to one group with higher energy is considered.

3.5.1 Two-group neutron diffusion model

Sufficient accuracy can be achieved by using only a few energy groups, but the group averaged parameters must be carefully determined. The case of two energy groups(two energy levels) could be used for the analysis of neutron irradiated concrete, one was to characterize fast neutrons(1 eV~10 MeV) and the other one thermal neutrons(0 eV~1 eV) as shown in Figure 3-12. The neutron source in the thermal group included the production of secondary neutrons from scattering reactions of fast neutrons. As mentioned earlier, thermal neutrons could never gain energy in a scattering collision and become fast neutrons. Fast neutrons only slow down. The governing equations are listed below for fast and thermal neutrons, respectively.

$$\frac{1}{v_1}\frac{\partial \phi_1(x,t)}{\partial t} - \nabla \cdot D_1(x,t)\nabla\phi_1(x,t) + \Sigma_{R1}\phi_1(x,t) = 0 \qquad (3\text{-}17)$$

$$\frac{1}{v_2}\frac{\partial \phi_2(x,t)}{\partial t} - \nabla \cdot D_2(x,t)\nabla\phi_2(x,t) + \Sigma_{a2}\phi_2(x,t) = \Sigma_{s12}\phi_1(x,t) \qquad (3\text{-}18)$$

where Σ_R is macroscopic removal cross section in cm^{-1}; Σ_{s12} is macroscopic fast to thermal group-transfer cross section; subscripts 1 and 2 = fast group and thermal group, respectively.

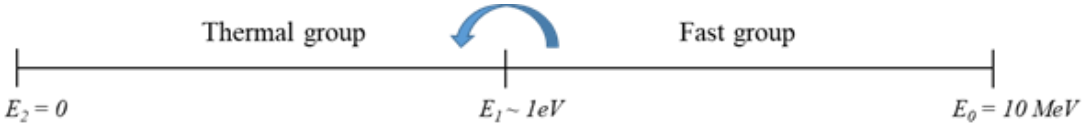

Figure 3-12 The group structure of two-group neutron diffusion model

The same classical heat conduction equation with internal source term is used as described in Eq. (3-4). The only difference for two-group neutron diffusion model here is that the volumetric heating generation should only due to thermal neutron radiation. This is because the heat generated during the attenuation of fast neutron kinetic energy is quite small comparing to the heat generated during the capture process of thermal neutrons. Thus, Eq. (3-5) turns to be

$$Q(x,t) \approx 1.6 \times 10^{-13}\Sigma_c \mathcal{E}_b \phi_2(x,t) \qquad (3\text{-}19)$$

For damage evaluations, cross-property correlation method for distressed materials described in Section 3.3 is still used. However, when evaluating the neutron radiation induced degradation, only the fast neutron effect is considered, and the thermal neutron damage is ignored:

$$\mathcal{F}_r(N) = \frac{E_{eff}}{E_m} = -1.188 \times 10^{-8} {N_1}^{0.3711} + 1 \ \ (0 \le N \le 7 \times 10^{20}\ n/cm^2) \qquad (3\text{-}20)$$

Therefore, effective thermal conductivity and effective fast/thermal neutron diffusion coefficients are functions of time, fast neutron flux, thermal neutron flux and temperature:

$$k_{eff} = f_k\left(k_m, \frac{E_i}{E_m}, \frac{k_i}{k_m}, \int_0^t \phi_1, \phi_2, T\right), D_{eff} = f_D\left(D_m, \frac{E_i}{E_m}, \frac{D_i}{D_m}, \int_0^t \phi_1, \phi_2, T\right) \quad (3\text{-}21)$$

where $k_m, D_m, \frac{E_i}{E_m}, \frac{k_i}{k_m}, \frac{D_i}{D_m}$ are constant values and ϕ_1, ϕ_2 and T are time and position dependent variables.

3.5.2 Numerical analyses

Coupled Radio-Thermo analysis of fast neutron, thermal neutron and thermal fields within neutron irradiated concrete can be performed based on two-group neutron diffusion model and the heat conduction equation. The effects of neutron radiation induced degradation and thermal deterioration on concrete can be taken into account. The three governing equations are

$$\frac{1}{v_1}\frac{\partial \phi_1(x,t)}{\partial t} - \nabla \cdot D_1(x,t)\nabla\phi_1(x,t) + \Sigma_{R1}\phi_1(x,t) = 0 \quad (3\text{-}22)$$

$$\frac{1}{v_2}\frac{\partial \phi_2(x,t)}{\partial t} - \nabla \cdot D_2(x,t)\nabla\phi_2(x,t) + \Sigma_{a2}\phi_2(x,t) = \Sigma_{s12}\phi_1(x,t) \quad (3\text{-}23)$$

$$c_p\rho(x,t)\frac{\partial T(x,t)}{\partial t} = \nabla \cdot k(x,t)\nabla T(x,t) + 1.6 \times 10^{-13}\Sigma_c\mathcal{E}_b\phi_2(x,t) \quad (3\text{-}24)$$

The same concrete wall shown in Figure 3-4 is used here as a study case to show the capability of the model. The fast and thermal neutron distribution as well as temperature field in a concrete biological shield during 80 years of operation are obtained. The calculation flow chart is shown in Figure 3-13.

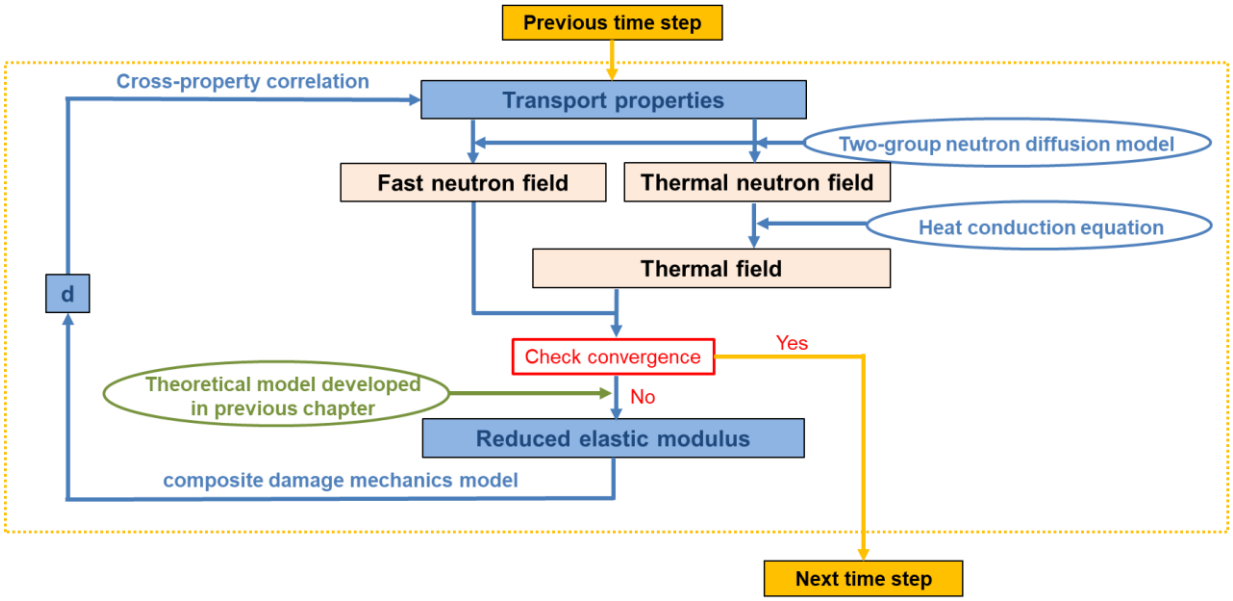

Figure 3-13 Calculation flow chart for two-group neutron diffusion

A constant neutron flux density of 3.5×10^{10} n/(cm^2·sec) is assumed at the inner surface of the wall for fast neutrons with 0.1 MeV energy level and a neutron flux density of 2×10^{10} n/(cm^2·sec) is assumed for thermal neutrons with 0.0253 MeV energy level. The neutron flux at the outer surface of the wall is approximately 10^{-6} of the neutron flux at the inner surface (Esselman and Bruck 2013). The temperature is 65 ºC at the inner surface and 20 ºC at the outer surface. Ordinary concrete 02-a from *REACTOR PHYSICS CONSTANTS* 1963 is used since major parameters are provided. The mix proportion is water/cement/aggregate= 260/318/3300 lb/yd^3. All other parameters of concrete are assumed and listed in Table 3-2. All of them are typical values for ordinary concrete. The expansion of aggregate particles under neutron radiation is still estimated by the volume expansion of neutron irradiated quartz since no test data available here. $\frac{E_i}{E_m}$=0.3537, $\frac{k_i}{k_m}$=0.1, $\frac{D_{1i}}{D_{1m}}$=10 and $\frac{D_{2i}}{D_{2m}}$=10 are used. The coupled equation was numerically solved using the approach described in Section 3.4.

Table 3-2 Assumed parameters used in the numerical analysis of the analyzed ordinary concrete.

Parameters	Values	Reference
Concrete		
D_1[cm]	1.14	(*REACTOR PHYSICS CONSTANTS* 1963)
D_2[cm]	0.484	(*REACTOR PHYSICS CONSTANTS* 1963)
Σ_{R1}[cm^{-1}]	0.085	(*REACTOR PHYSICS CONSTANTS* 1963)
Σ_{S12}[cm^{-1}]	0.08*	–
Σ_{a2}[cm^{-1}]	0.0094	(*REACTOR PHYSICS CONSTANTS* 1963)
v_1[cm/sec]	4.37×10^{8}†	–
v_2[cm/sec]	2.2×10^{5}†	–
c_p[J/(kg·K)]	650	(Ursu 1985)
ρ[kg/cm^3]	2.3×10^{-3}	(*REACTOR PHYSICS CONSTANTS* 1963)
k[W/(cm·K)]	8.7×10^{-3}	(Ursu 1985)
Σ_c[cm^{-1}]	0.0094‡	–
E_b[MeV]	5.5	(Price et al. 1957)
Cement		
ρ[kg/cm^3]	3.15×10^{-3}	(Xi and Jennings 1997)
Aggregates		
ρ[kg/m^3]	2.55×10^{-3}	(Kelly et al. 1969)
E [GPa]	72.4	(Kelly et al. 1969)
α[10^{-5} / ºC]	6.35§	(Kelly et al. 1969)

* Assumed value

† Calculated based on classical kinetic energy equation for 0.1 MeV and 0.0253 eV neutrons.

‡ Use the value of Σ_{a2} as an approximation.

§ 20-120 ºC.

3.5.3 Numerical results

The Figure 3-14 through Figure 3-22 show the results of numerical analyses. Most of them are very similar to the corresponding results using one-speed neutron diffusion equation in Section 3.4.3, including the profiles of damage parameter, thermal conductivity profiles, fast/thermal neutron diffusion coefficient profiles, and fast neutron flux and fluence profiles. However, there are also some different points need to be noticed.

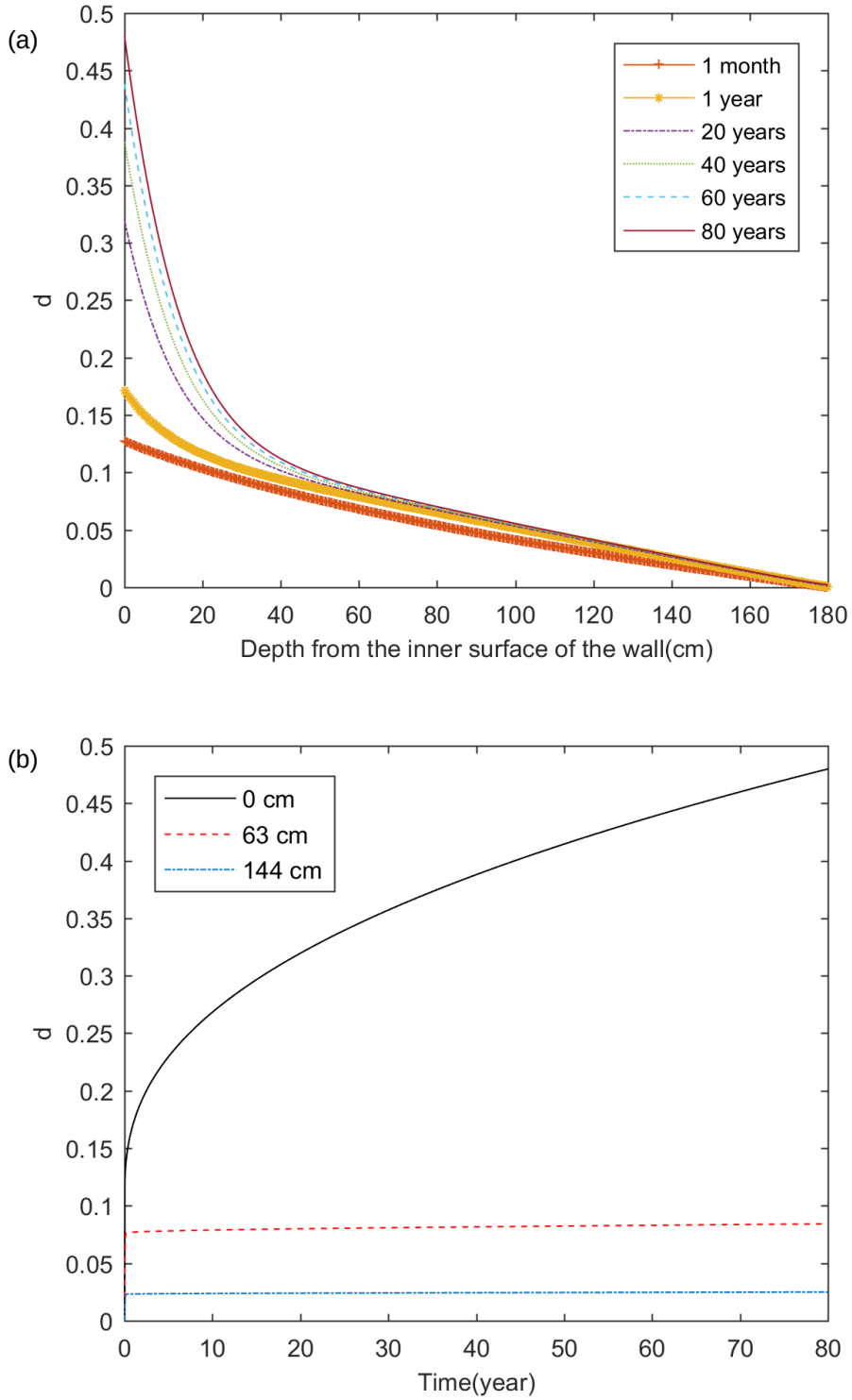

Figure 3-14 Damage progression due to neutron radiation and the temperature: (a) with the depth of concrete at difference time; (b) with time at different depths.

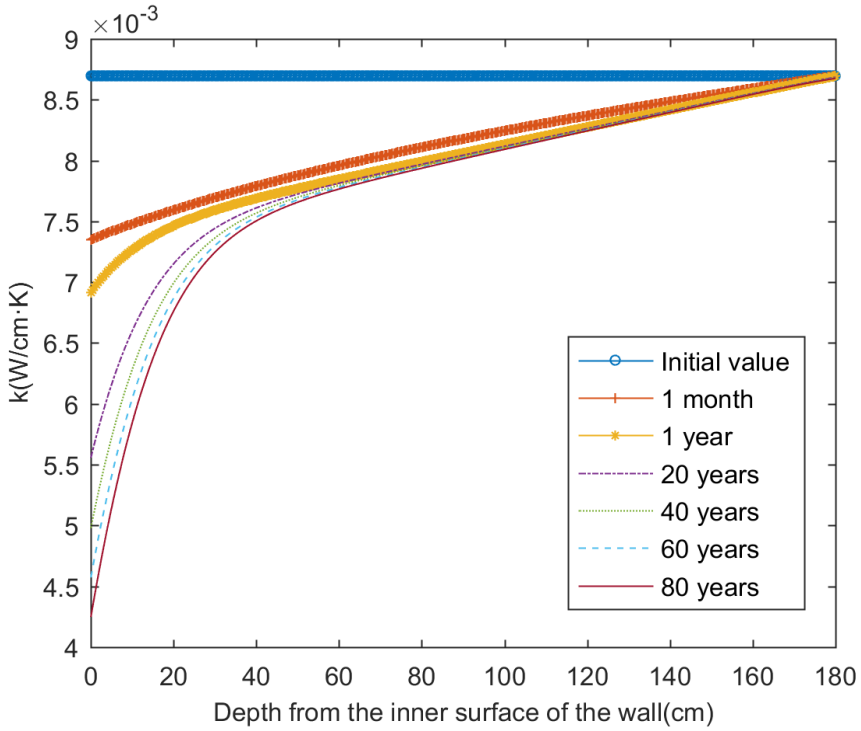

Figure 3-15 Thermal conductivity profiles along the depth at different times.

Figure 3-16 shows the temperature profiles in the concrete with and without the effects of radiation and thermal damage after 1 month, 40 years and 80 years of exposure. Although the change of the temperature profile is still very small(maximum change is around 9 ºC), the rise of temperature in the concrete increases compared to Figure 3-8(b) (maximum change is less than 4 ºC). Since radiation heating is thermal neutron flux dependent, the peaks of thermal neutron flux profiles as one can observe later on in Figure 3-21(a) will lead to the increase of temperature rise.

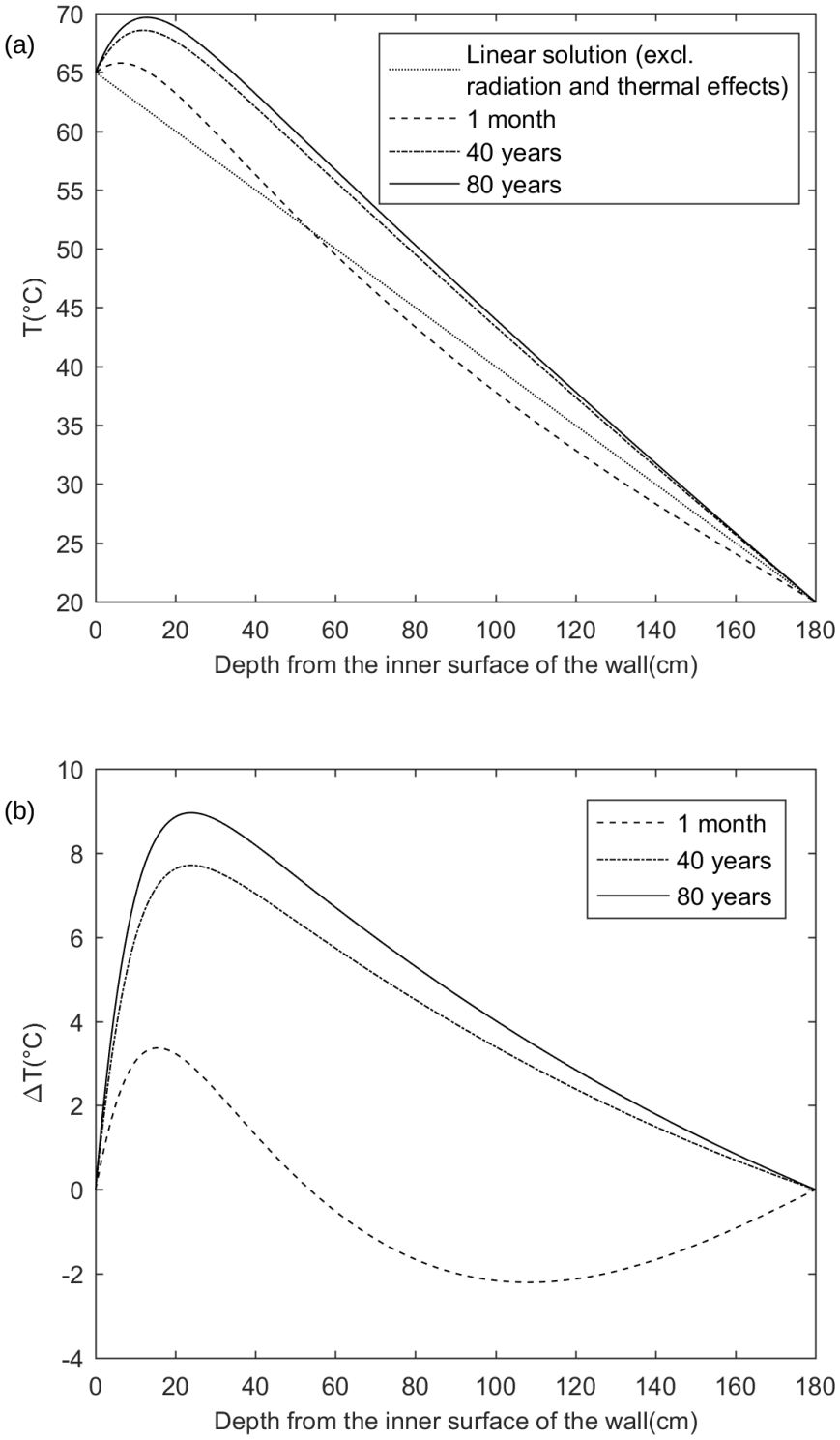

Figure 3-16 Temperature profiles along the concrete depth: (a) Absolute values without radiation and thermal effects considered and with these effects considered at 1 year, 80 years; (b) Temperature changes compared to the initial values.

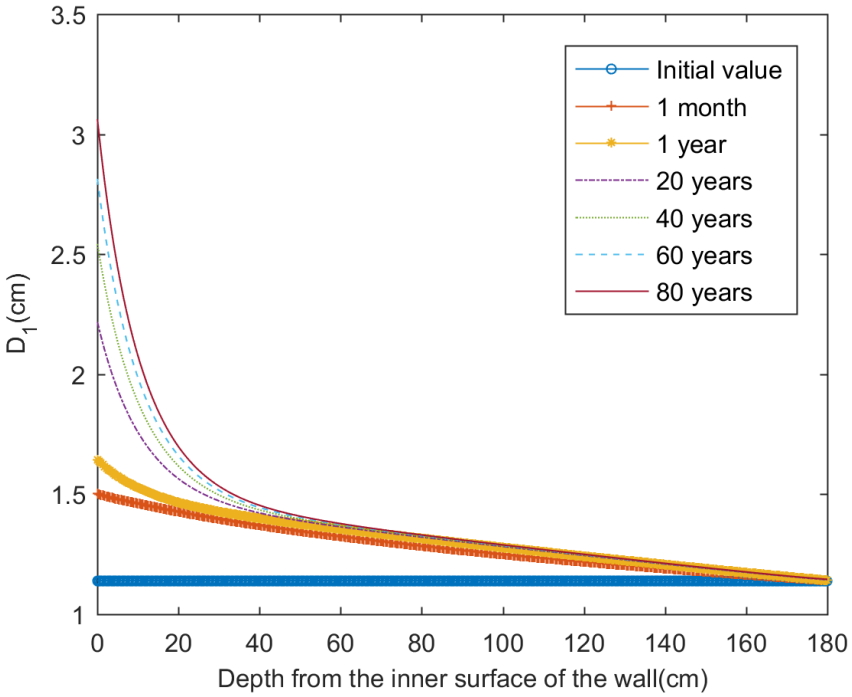

Figure 3-17 Fast neutron diffusion coefficient profiles along the concrete depth at different times.

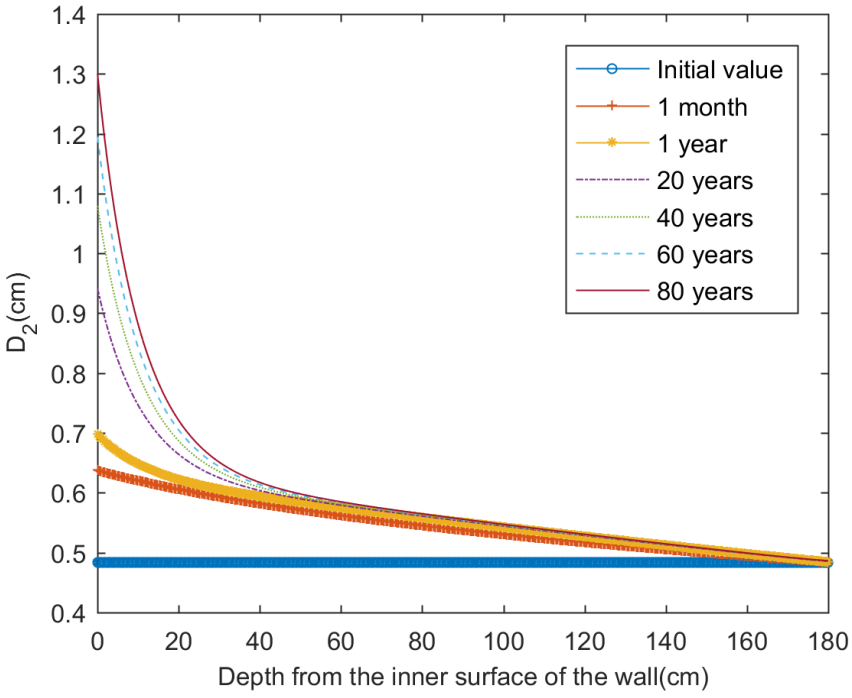

Figure 3-18 Thermal neutron diffusion coefficient profiles along the concrete depth at different times.

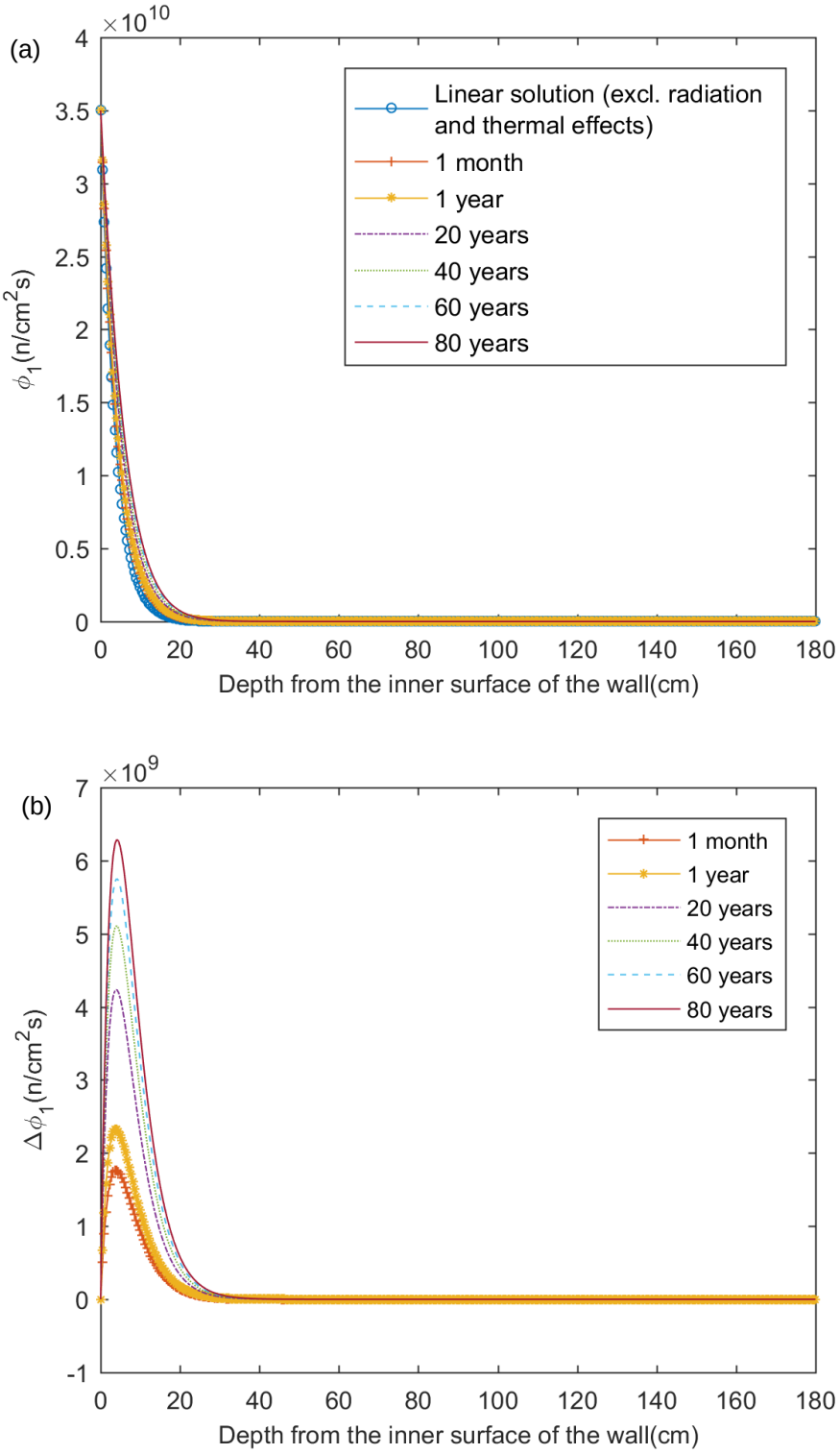

Figure 3-19 Fast neutron flux profiles along the concrete depth (energy = 0.1MeV): (a) Absolute values with and without the radiation and thermal effects after different periods of exposure; (b) Neutron flux increases compared to the case without the radiation and thermal effects.

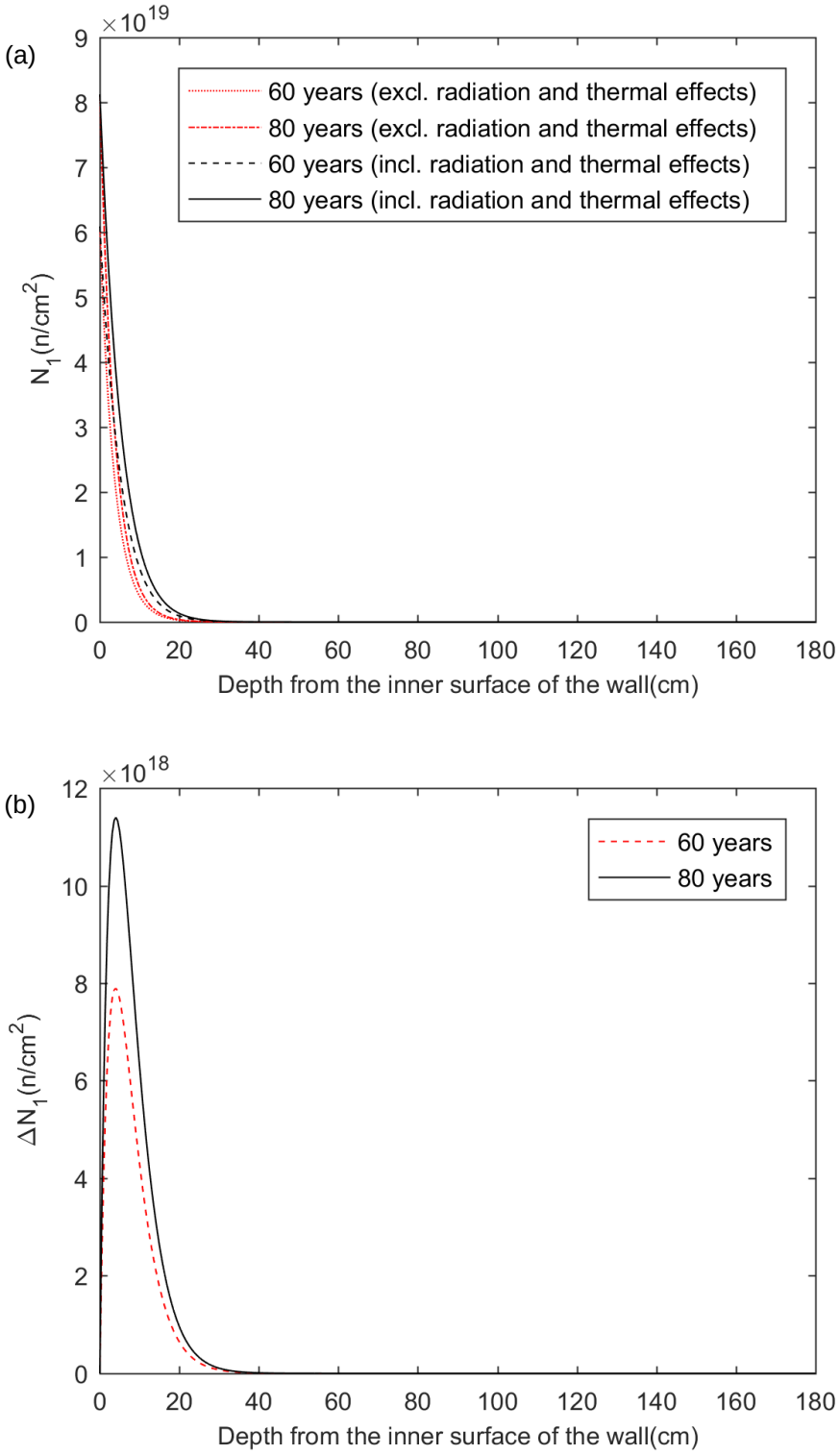

Figure 3-20 Fast neutron fluence profiles along the concrete depth at 60 years and 80 years (energy=0.1MeV): (a) Absolute values with and without considering the radiation and thermal effects; (b) Neutron fluence increase compared to the case without these effects considered.

The nonlinear solutions of thermal neutron flux profiles in the concrete up to 80 years are obtained, as shown in Figure 3-21(a). The profiles are very different from the profiles of fast neutrons shown in Figure 3-19(a), and peaks near the inner surface of the wall are observed. This is due to the production of secondary thermal neutrons from the fast neutron group. The differences between the nonlinear solutions and linear solution at different times are calculated and plotted in Figure 3-21 (b). Figure 3-21 (b) indicates that the maximum neutron flux increase in the concrete at 80 years is around 1.1×10^{10} n/(cm^2·sec) which is much larger than the increase shown in Figure 3-19 (b) for fast neutrons. Besides, the reduction of thermal neutron flux in the concrete near the inner surface is observed, and the reduction increases with time. The reason is that the reduction of thermal neutron number due to absorption is larger than the increase of thermal neutron number due to the production of secondary thermal neutrons from the fast neutron group.

Neutron fluence profiles in the concrete wall at 60 years and 80 years are plotted in Figure 3-22. The maximum neutron fluence increases in the concrete are 1.4×10^{19} n/cm^2 and 2.1×10^{19} n/cm^2 for 60 years and 80 years, respectively. Similar to the neutron flux profiles, peaks and reductions of the neutron fluence near the inner surface of the wall are observed.

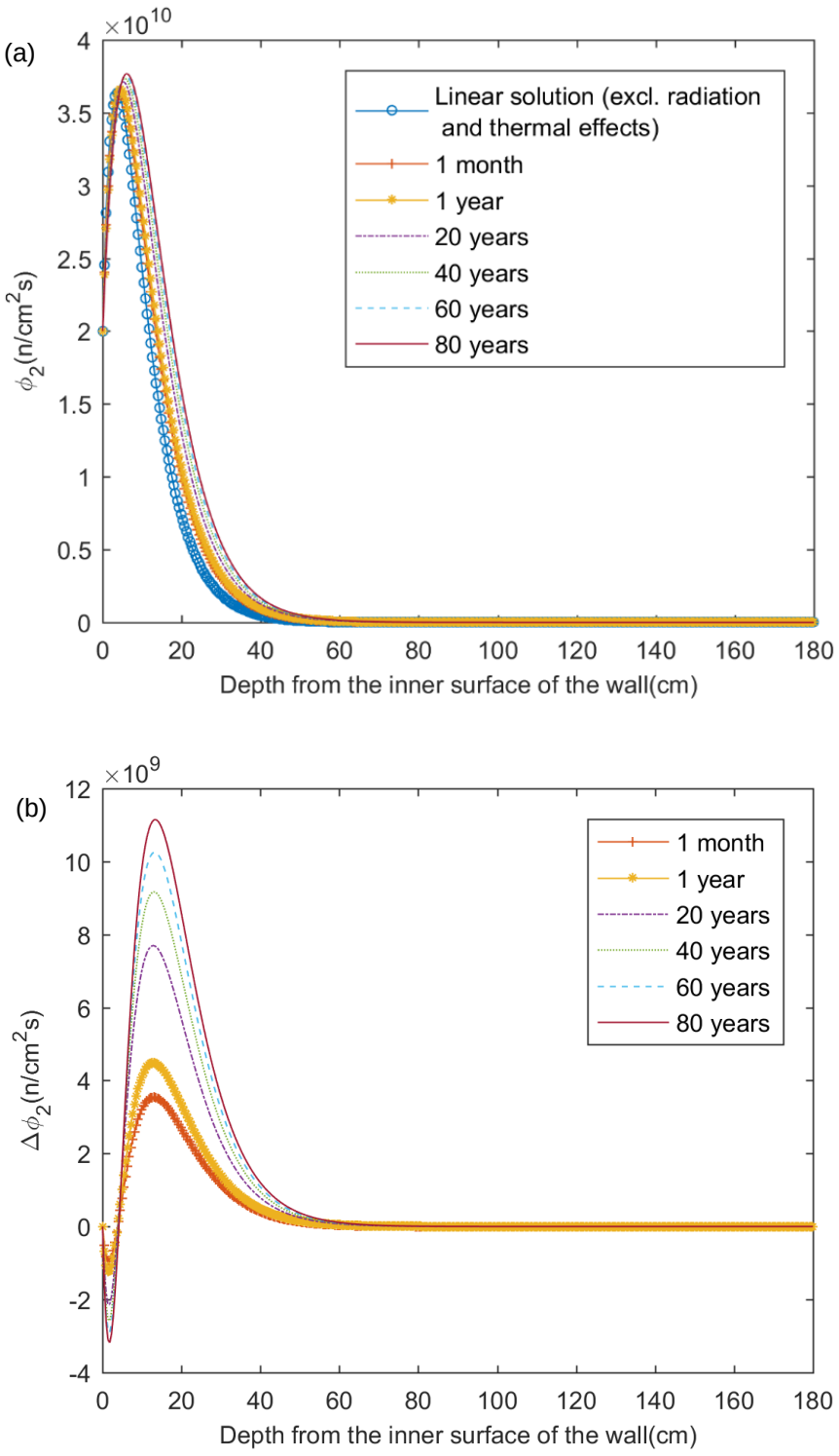

Figure 3-21 Thermal neutron flux profiles along the concrete depth (energy = 0.1MeV): (a) Absolute values with and without the radiation and thermal effects after different periods of exposure; (b) Neutron flux increases compared to the case without the radiation and thermal effects.

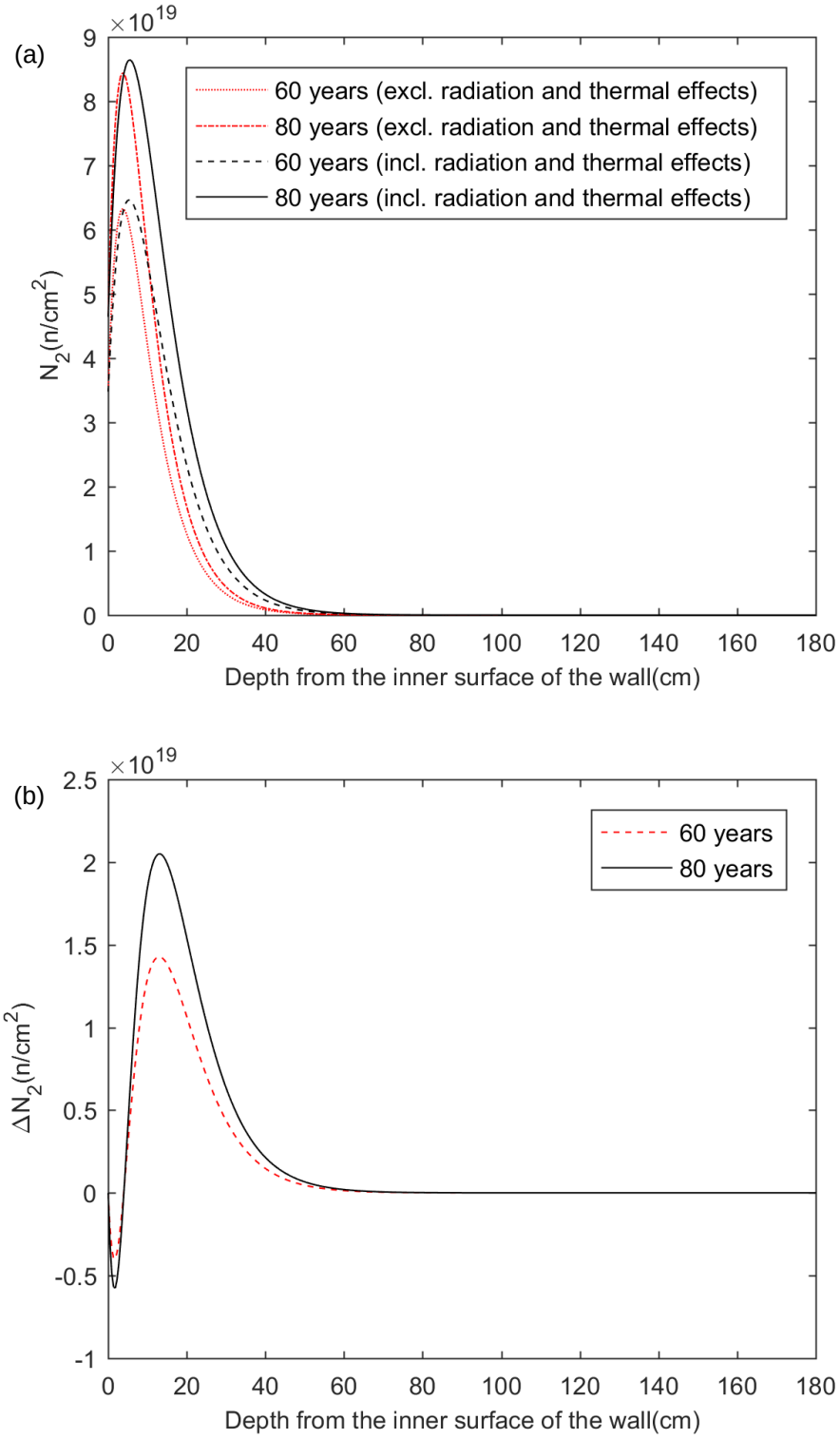

Figure 3-22 Thermal neutron fluence profiles along the concrete depth at 60 years and 80 years (energy=0.1MeV): (a) Absolute values with and without considering the radiation and thermal effects; (b) Neutron fluence increase compared to the case without these effects considered.

3.6 Conclusions

- It is well known that neutron radiation can lead to the damage of concrete materials which reduces its mechanical properties, and thus it is questionable to assume that transport properties of concrete are unchanged during the life span of biological shielding wall.
- One-dimensional and one-speed neutron diffusion equation and the heat conduction equation were used as governing equations for prediction of neutron radiation and thermal field in concrete, respectively. In the diffusion equations, the transport parameters were considered not as constants but as functions of time and location so that the neutron radiation and thermal effects can be taken into account. As a result, the diffusion equations became nonlinear equations.

  The potential variations of transport properties of a composite material can be estimated by cross-property correlation theories which can convert the variation in mechanical properties into the corresponding variation in transport properties of the material. A cross-property correlation theory was used together with a composite damage theory and neutron irradiation test data on the modulus of elasticity of concrete to estimate the change of neutron diffusion coefficient due to neutron radiation and thermal effect. This work is the first attempt to deal with the degradation of neutron and heat transport properties of concrete biological shielding walls and provides a possible way to determine the long-term neutron and thermal fields in concrete biological shielding walls. An ordinary concrete wall was analyzed up to 80 years of operation as a simplified example of a typical concrete biological shield in NPPs. Proper boundary and initial conditions and material parameters were assumed. Both the case which included the effects of radiation and temperature and the case which excluded these effects were analyzed. Some preliminary findings were obtained.

- Elevated temperature has considerable effects on the damage parameter of concrete. The effect of elevated temperature on distressed concrete under nuclear radiation must be considered, especially for concrete with large depth from the radiation source. The thermal conductivity of concrete under neutron radiation gradually decreases with time, and the damage and radiation heating lead to minor changes of the temperature profile in the concrete. Actually, the damage induced by neutron radiation and elevated temperature neutralizes some of the temperature increase in the concrete caused by radiation heating.
- The neutron diffusion coefficient of neutron irradiated concrete gradually increases with time. Neutron radiation and elevated temperature can result in considerable increases of neutron flux in the concrete, and the neutron flux increases with time quite a lot, especially for the concrete near the radiation source. Similarly, considerable increases of neutron fluence are observed. Evidently, the damage of concrete induced by neutron radiation and elevated temperature can effectively accelerate the penetration of neutron radiation into the concrete. For a reliable evaluation of the long-term performance of concrete biological shields in NPPs, effects of neutron radiation and elevated temperature on the neutron and thermal fields must be taken into consideration.
- Two-group neutron diffusion model was introduced to treat the neutron energy dependence more realistically. The fast and thermal neutron fields as well as the thermal field in concrete were solved. Heat generated during the radiation should only result from thermal neutron radiation. When evaluating the neutron radiation induced degradation, only the fast neutron effect is considered, and the thermal neutron damage is ignored. The same concrete wall was analyzed up to 80 years of operation. Some findings were obtained.
- The rise of temperature in the concrete increases compared to the results using one-speed diffusion equation. The profiles of thermal neutron flux/fluence are very different from the

profiles of fast neutron flux/fluence and peaks near the inner surface of the wall are observed. Besides, the reductions of thermal neutron flux/fluence in the concrete near the inner surface are observed, and the reductions increase with time. In order to predict long-term neutron radiation level in concrete biological shields accurately, a proper treatment of the neutron energy dependence is needed.

CHAPTER 4

EFFECTS OF NEUTRON RADIATION ON CONCRETE

4.1 Introduction

As one can see in previous chapters, experimental data about the effects of radiation on concrete is very important. In order to understand the current state of knowledge about nuclear irradiated concrete, 59 articles which almost include all experimental data about radiation damage to concrete and/or its components (i.e., rocks) so far was acquired. Information including the material used, material composition, mix design, physical properties, mechanical properties, testing conditions and concrete performance under nuclear radiation was extracted from the collected literature. A database storing all the information collected was developed based on Microsoft Access. The citations for these documents are presented in a bibliography presented in the Appendix. In this chapter, the effects of neutron radiation on the cementitious material will be reviewed based on the collected data, including the effects on weight loss, volume change, and mechanical properties. These mechanical properties will be examined from several different perspectives where the effects of the temperature, the water-cement ratio, and the aggregate content are considered in conjunction with neutron fluence.

4.2 Volume change and weight loss

4.2.1 Cement paste

As shown in Figure 2-3, cement paste is a multi-phase porous and amorphous composite with small crystallites. It is composed of unreacted cement particles, hydration products, and

water. There are several types of water in cement paste: chemically combined water, capillary water, and interlayer water between the solid layers of C-S-H. The amorphous nature of the cement paste and its water content are important to the effect of neutron radiation on concrete.

Neutrons can directly interact with nuclei of atoms in the cement paste and change its structure, but that interaction does not change the original amorphous nature of the cement paste. However, neutron irradiation may lead to dehydration of cement paste caused by 1) a high hydrogen cross-section, 2) evaporation of water due to radiation heating, and 3) radiolysis decomposition due to the secondary gamma-ray formation. Thus, the shrinkage of cement paste is expected as shown in Figure 4-1. The results from a recent study also indicated that neutron radiation would lead to the shrinkage of cement paste(Maruyama et al. 2017).

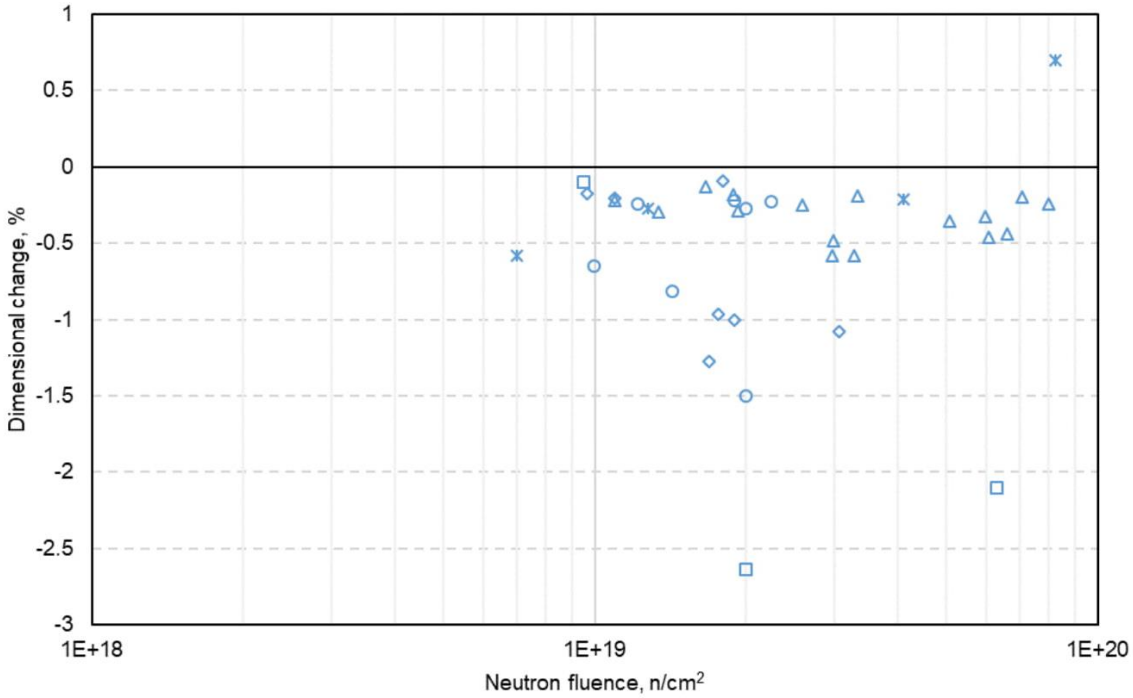

	w/c	T_{max} (°C)	E(MeV)	Cement used	Reference
□	0.3	150-450	0.8	Portland cement	Dubrovskii 1970
△	0.25	280	1	Aluminous cement	Elleuch 1972
◇	0.36	50	Fast	Portland cement	Kelly 1969, Gray 1971
○	0.36	55	Fast	Cement grout	Kelly 1969, Gray 1971
✳	0.55	53.3	0.1	White cement	Maruyama 2017

Figure 4-1 Dimensional change of cement paste induced by neutron irradiation

In Figure 4-2 shows the weight loss due to irradiation for cement paste. The weight loss for hardened cement paste is about 10% or less. There is no clear trend for the effect of neutron radiation on weight loss of hardened cement paste. In Figure 4-2, the solid markers are the test data for the "control group" which are the available control test data obtained under the same temperature history as the irradiated specimens. Test data for the "control group" and the "irradiated group" share the same color if they come from the same test and the same materials are used. No obvious difference can be observed between the control group and the irradiated group. Weight loss is mainly due to dehydration of the cement paste under high temperatures which also leads to shrinkage. Negative values from (Maruyama et al. 2017) are not reliable due to insufficient drying during the measurement.

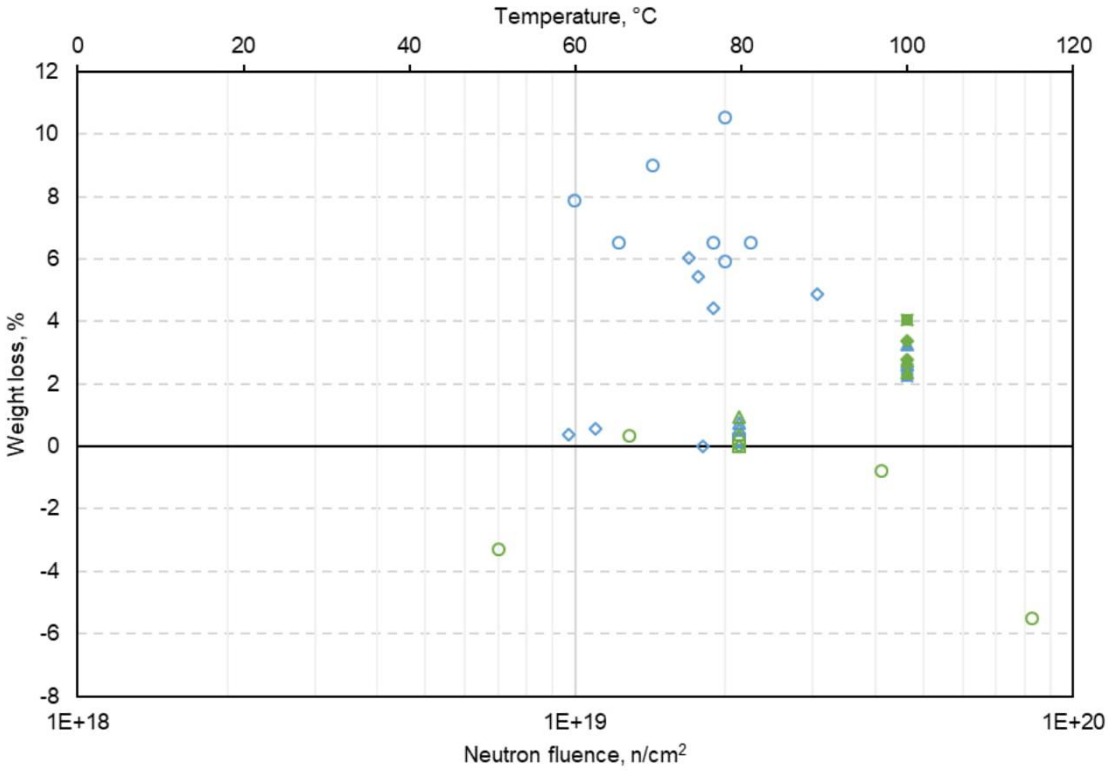

w/c	T_{max} (°C)	E(MeV)	Cement used	Reference
0.36	50	Fast	Portland cement	Kelly 1969, Gray 1971
NA	100	Thermal	Portland cement	Alexander 1963
NA	100	Thermal	High-alumina cement paste	Alexander 1963
0.36	55	Fast	Cement grout	Kelly 1969, Gray 1971
NA	100	Thermal	Low-heat-slag cement paste	Alexander 1963
NA	100	Thermal	Supersulphate cement	Alexander 1963
NA	100	Thermal	Portland cement & Pulverised fuel ash paste	Alexander 1963
0.55	53.3	0.1	White cement	Maruyama 2017

Note: Solid markers represent unirradiated reference samples on the temperature axis. Open markers of same shape and color represent corresponding irradiated test samples on the neutron fluence axis.

Figure 4-2 Weight loss of cement paste induced by neutron irradiation

4.2.2 Aggregate

For ordinary concrete, aggregates can be categorized into two groups by mineralogical composition: siliceous aggregates such as quartzite, gravel, granite and flint; and calcareous aggregates such as limestone, dolomite, and anorthosite. Under irradiation, neutrons directly

interact with nuclei of atoms and the damage of lattice structure of aggregates is reflected as a volume increase of the material. Siliceous aggregates with covalent bonding(Si-O) are more likely to affected by neutron radiation than calcareous aggregates which contain weaker ionic bonds(William et al. 2013).

As discussed earlier, quartz is one of the most abundant minerals in aggregates and the primary constituent in siliceous aggregates. Studies about neutron irradiated quartz indicate that fast neutron fluence larger than 1×10^{19} n/cm^2 leads to significant expansion of quartz. The macroscopic expansion is due to the crystalline-to-amorphous transition. The available experimental data collected is plotted in Figure 4-3. A clear saturation of quartz expansion under neutron radiation (just under 6%) can be observed. The dimensional change of quartz is also temperature dependent leading to the shift in dimensional change with neutron fluence as a function of temperature in Figure 4-3. It can be explained by the partial annealing of irradiation amorphization of quartz by the temperature (Pape et al. 2016). The annealing caused by temperature reduces the neutron induced expansion and occurs even at low radiation level.

The dimensional changes of other aggregates are shown in Figure 4-4. A noticeable increase in volume can be observed at a neutron fluence of 1×10^{19} n/cm^2 or higher. Aggregates such as flint and the dolerites are silicates, and expansion is observed. There is also some dimensional increase observed for calcareous aggregates such as limestone.

Maruyama et al. 2017 further confirmed that quartz-based aggregate has poor neutron resistance and will expand. This kind of aggregate expanded more with increasing quartz content. The neutron induced quartz expansion behavior in aggregates is highly temperature dependent. No significant expansion of neutron irradiated limestone（ionic bonded mineral）was observed.

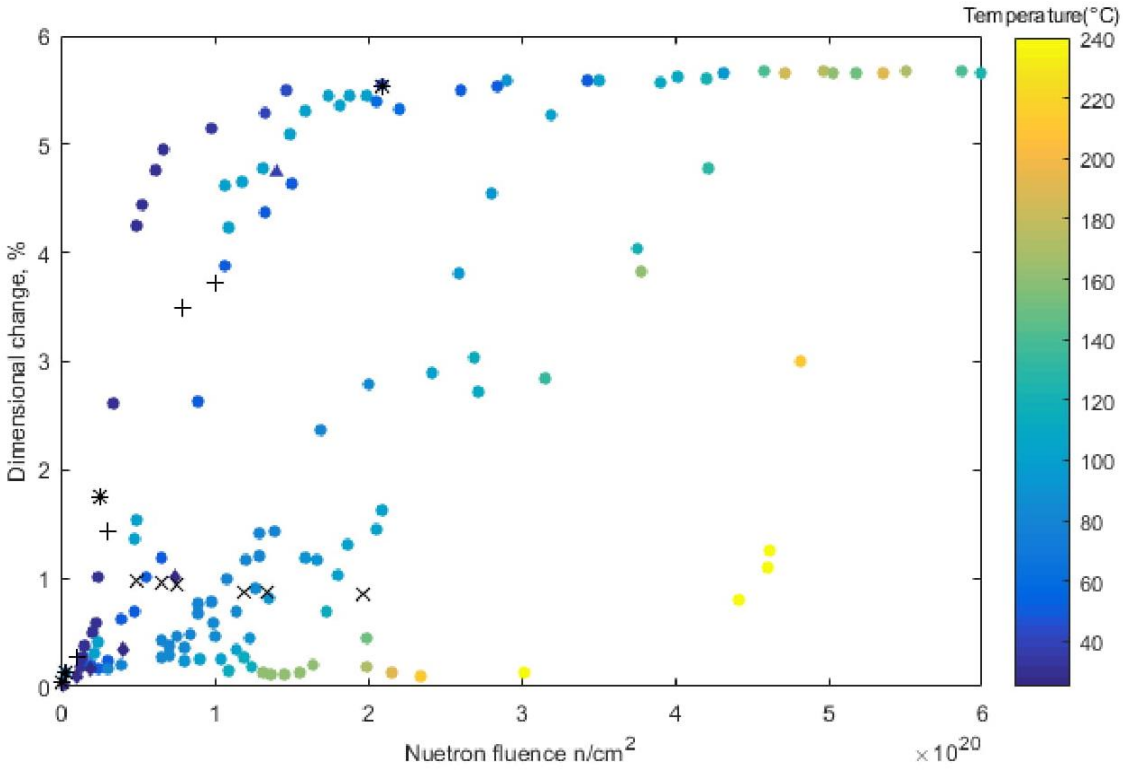

E(MeV)	Reference
0.01	Bykov 1981, Wittels 1957, Primak1958, Primak 1953, Primak 1955
0.1	Vanelstraete1987, Bonnet 1992, Vanelstraete 1990
0.1	Grasse 1981
Fast	Simon 1957, Simon 1956
Fast	Weissmann 1963
Fast	Wittels 1954, Wittels1953,
0.1	Gardner 1981

Note: black markers are test data without information about the temperature during the experiment.

Figure 4-3 Dimensional change of quartz with fast neutron irradiation

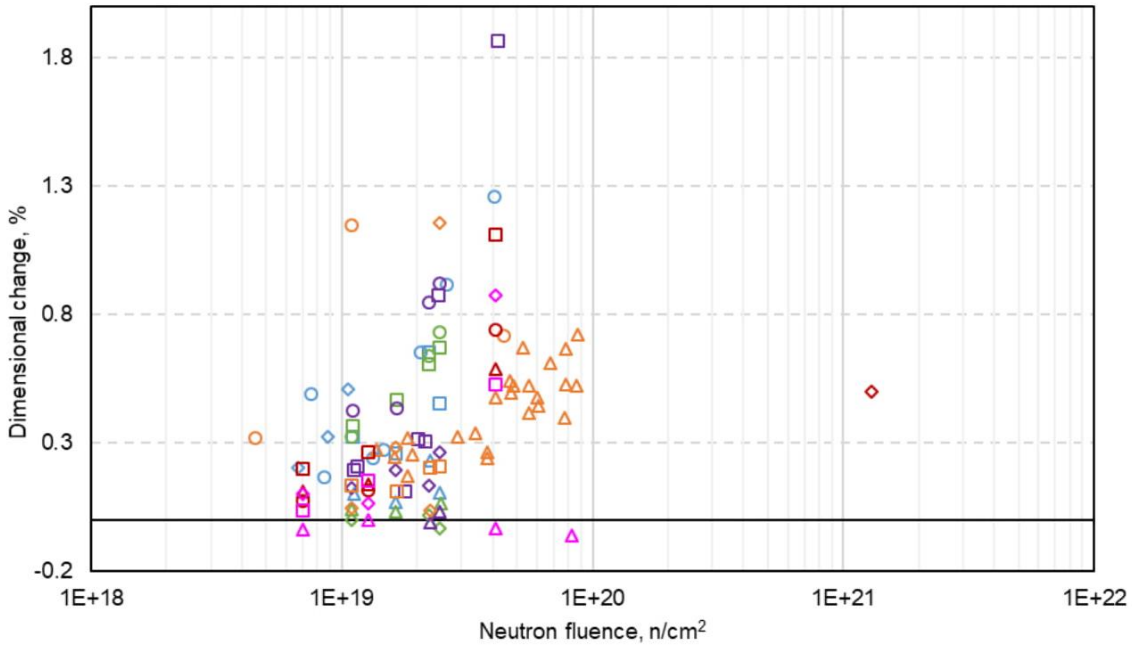

T_{max} (°C)	E(MeV)	Rock type	Reference
50	Fast	Basalt	Kelly 1969, Gray 1971
50	Fast	Creywacke	Kelly 1969, Gray 1971
50	Fast	Cromhall limestone	Kelly 1969, Gray 1971
50	Fast	Flint	Kelly 1969, Gray 1971
50	Fast	Foster Yeoman Limestone	Kelly 1969, Gray 1971
50	Fast	High E. Dolerite	Kelly 1969, Gray 1971
50	Fast	High Mag. Limestone	Kelly 1969, Gray 1971
50	Fast	Hillhouse Whinstone	Kelly 1969, Gray 1971
50	Fast	Hornfels	Kelly 1969, Gray 1971
50	Fast	Limestone	Kelly 1969, Gray 1971
50	Fast	Limestone(Esperstone)	Kelly 1969, Gray 1971
50	Fast	Low E. Dolerite	Kelly 1969, Gray 1971
50	Fast	Low Mag. Limestone	Kelly 1969, Gray 1971
50	Fast	Trachy Andersite	Kelly 1969, Gray 1971
240	1	Serpentine	Elleuch 1972
100-400	0.8	Hematite	Dubrovski 1970
NA	0.01	Serpentine	Dubrovski 1968
53.3	0.1	Thermally altered tuff	Maruyama 2017
53.3	0.1	Felsic sandstone	Maruyama 2017
53.3	0.1	Felsic sandstone	Maruyama 2017
53.3	0.1	Felsic sandstone	Maruyama 2017
53.3	0.1	Felsic sandstone	Maruyama 2017
53.3	0.1	Limestone	Maruyama 2017

Figure 4-4 Dimensional change of aggregates (absent quartz) induced by neutron irradiation

No obvious weight loss is observed for aggregates. Only two sets of test data are available: it showed no change in weight for serpentine(Elleuch et al. 1972) and slight weight increase of aggregates was observed in (Maruyama et al. 2017) up to a fast neutron fluence $8.25*10^{19}n/cm^2$.

4.2.3 Concrete

Concrete expands with increasing fast neutron radiation as shown in Figure 4-5. Whereas the cement paste in concrete contracts, the increase in volume for concrete is driven by aggregate expansion. Similar to the behavior of aggregates, a noticeable increase in volume can be observed at a neutron fluence of 1×10^{19} n/cm^2 or higher. Neutron irradiation is associated with temperature rise, which results in thermal expansion. The volume expansion of concrete is very likely to be induced mainly by the expansion of aggregates under neutron irradiation.

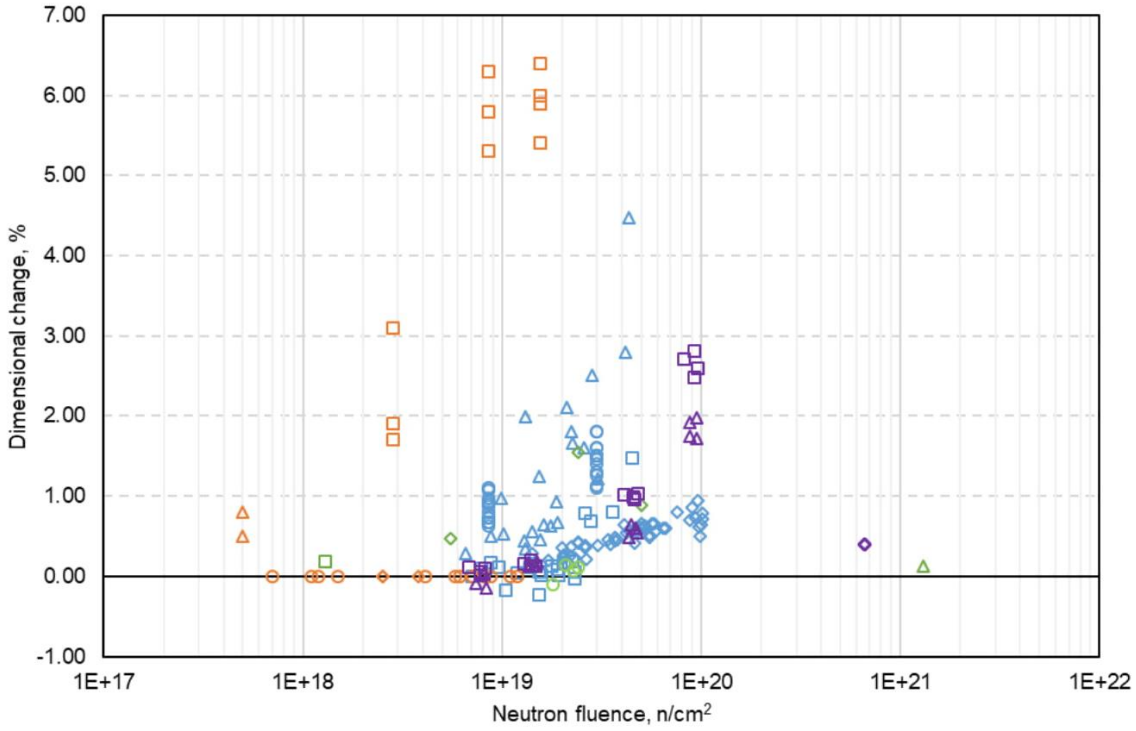

w/c	Agg. Frac.	T_{max} (°C)	E(MeV)	Agg. used	Reference
0.38	0.74	240	1	Serpentine	Elleuch 1972
0.36	0.67	50	Fast	Limestone	Kelly 1969, Gray 1971
0.36	0.67	50	Fast	Flint	Kelly 1969, Gray 1971
0.4	0.68	80	Fast	Quartz	Pedersen 1971
0.5	0.67	100-125	Fast	Limestone	Cristiani 1971, Granata 1972, Crispino 1972
0.5	0.76	150-350	0.8	Riversand & sandstone	Dubrovskii 1967
0.5	0.76	50	0.8	Riversand & sandstone	Dubrovskii 1967
0.55	0.79	50-56	0.1	Sand & gravel	Fujiwara 2009
1.01	0.8	100-400	0.8	Hematite	Dubrovskii 1970
NA	NA	120	Thermal	NA	Dickeman 1951
NA	NA	350	0.01	Serpentine	Dubrovskii 1968
NA	NA	50	Fast	Sand & light weight agg.	Kelly 1969, Gray 1971
NA	NA	550	0.7	Chromite	Dubrovskii 1966
0.5	0.77	57.6-72.6	0.1	Sandstone & thermally altered tuff	Maruyama 2017
0.5	0.77	57.6-72.6	0.1	Sandstone & telsic sandstone	Maruyama 2017

Figure 4-5 Dimensional change of concrete and mortar induced by neutron irradiation

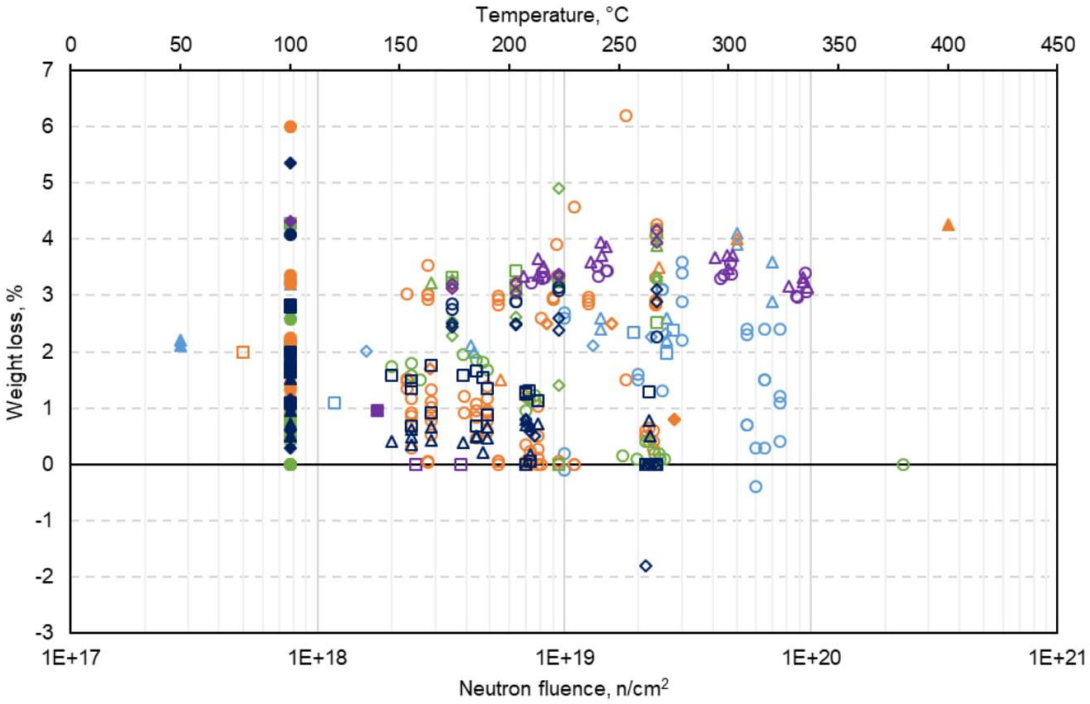

	w/c	Agg. Frac.	T_{max} (°C)	E(MeV)	Agg. used	Reference
◇	0.36	0.67	50	Fast	Flint	Kelly 1969, Gray 1971
□	0.36	0.67	50	Fast	Limestone	Kelly 1969, Gray 1971
△	0.45	0.67	50	Thermal	Riversand	Batten 1960, Price 1957
○	0.5	0.84	50	Thermal	Riversand	Batten 1960, Price 1957
□	0.5	0.67	100-125	Fast	Limestone	Cristiani 1971, Granata 1972, Crispino 1972
◇	0.5	0.76	150-350	0.8	Riversand & sandstone	Dubrovskii 1967
□	0.5	0.76	50	0.8	Riversand & sandstone	Dubrovskii 1967
△	1.01	0.8	100-400	0.8	Hematite	Dubrovskii 1970
○	NA	NA	100	Thermal	Heston sand	Alexander 1963
◇	NA	NA	100	Thermal	Barytes	Alexander 1963
□	NA	NA	100	Thermal	Crushed firebrick	Alexander 1963
△	NA	NA	100	Thermal	Granite	Alexander 1963
○	NA	NA	100	Thermal	Heston gravel	Alexander 1963
◇	NA	NA	100	Thermal	Ilmenite	Alexander 1963
□	NA	NA	100	Thermal	Limestone	Alexander 1963
△	NA	NA	100	Thermal	Magnetite	Alexander 1963
○	NA	NA	100	Thermal	Slag	Alexander 1963
◇	NA	NA	100	Thermal	Whinstone	Alexander 1963
△	0.5	0.77	57.6-72.6	0.1	Sandstone & thermally altered tuff	Maruyama 2017
○	0.5	0.77	57.6-72.6	0.1	Sandstone & felsic sandstone	Maruyama 2017

Note: Solid markers represent unirradiated reference samples on the temperature axis. Open markers of same shape and color represent corresponding irradiated test samples on the neutron fluence axis.

Figure 4-6 Weight loss of concrete and mortar induced by neutron irradiation

Figure 4-6 shows the weight loss due to irradiation for concrete and mortar. The weight loss for concrete and mortar is less than 5%. As with the hardened cement paste, there is no clear trend for the effect of neutron radiation on weight loss of concrete. No obvious difference can be observed between the control group and the irradiated group. Weight loss is mainly due to dehydration of the cement paste in concrete under high temperatures.

4.3 Mechanical properties

The effects of neutron radiation on the mechanical properties of cementitious materials were reviewed based on the collected test data. The mechanical properties included compressive strength and tensile strength. The effect of neutron irradiation on the modulus of elasticity was also reviewed. These mechanical properties are examined from several different perspectives where the effects of the water-cement ratio (w/c) and the aggregate content are considered in conjunction with neutron fluence.

4.3.1 Compressive strength

Figure 4-7 shows the significant reduction of the compressive strength of concrete and mortar by neutron irradiation and potential thermal effects, which is consistent with the general trends shown in the literature. In the figure, normalized compressive strength was used, so the value of 1.0 means that there is no strength reduction. As shown in the figure, with increasing neutron level, the normalized strength decreased to 0.4, which is 40% of the original value. On the other hand, there are no general trends for significant reductions of compressive strength of cement paste and aggregate, which are shown in Figure 4-8 for cement paste and Figure 4-9 for aggregate. Different types of cement were used for the concrete and mortar specimens, including slag cement, aluminous cement, and regular Portland cement.

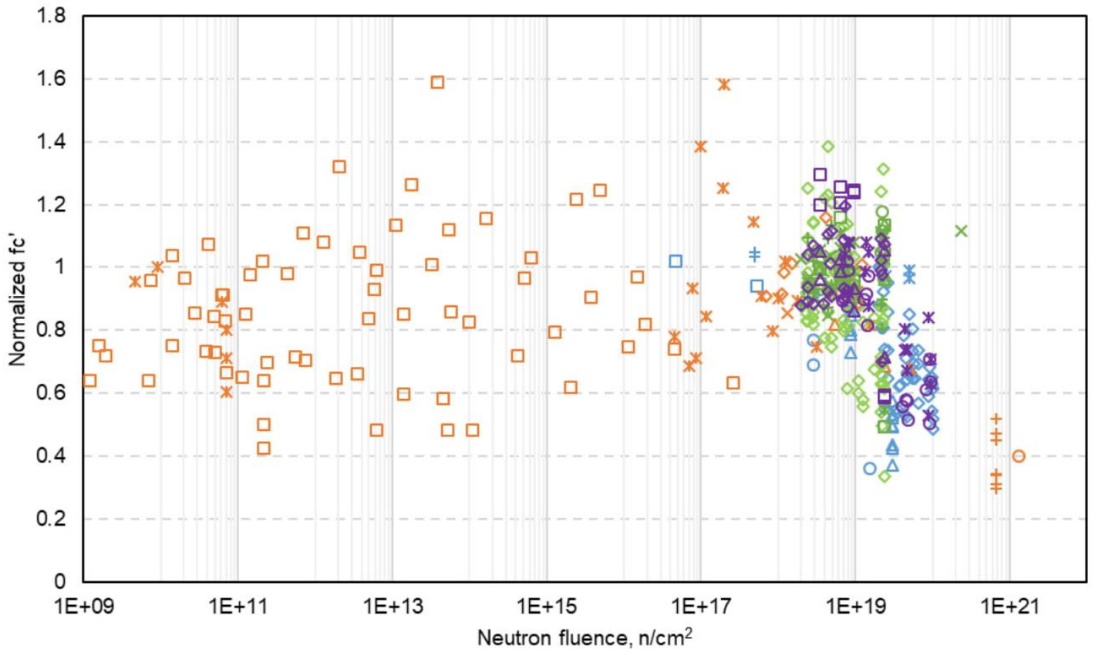

	w/c	Agg. Frac.	T_{max} (°C)	E(MeV)	Agg. used	Reference
◇	0.38	0.74	240	1	Serpentine	Elleuch 1972
□	0.35	0.73	80	1	Sand & Crushed stone	Stoces 1970
△	0.4	0.68	80	Fast	Quartz	Pedersen 1971
✱	0.45	0.67	50	Thermal	Riversand	Batten 1960, Price 1957
×	0.5	0.84	50	Thermal	Riversand	Batten 1960, Price 1957
○	0.5	0.76	150-350	0.8	Riversand & sandstone	Dubrovskii 1967
+	0.5	0.76	50	0.8	Riversand & sandstone	Dubrovskii 1967
◇	0.55	0.79	50-56	0.1	Sand & Gravel	Fujiwara 2009
□	0.61	0.74	21-37	Thermal	Haydite&Barytes	Blosser 1958, Rockwell 1948, Grantham 1960
△	1.01	0.8	100-400	0.8	Hematite	Dubrovskii 1970
✱	NA	NA	20-75	Thermal	Haydite&Barytes	Blosser 1958, Rockwell 1948, Grantham 1960
×	NA	NA	120	Thermal	NA	Dickman 1951
○	NA	NA	350	0.01	Serpentine	Dubrovskii 1968
+	NA	NA	550	0.7	Chromite	Dubrovskii 1966
◇	NA	NA	100	Thermal	Heston sand	Alexander 1963
□	NA	NA	100	Thermal	Barytes	Alexander 1963
△	NA	NA	100	Thermal	Crushed firebrick	Alexander 1963
✱	NA	NA	100	Thermal	Granite	Alexander 1963
×	NA	NA	100	Thermal	Heston gravel	Alexander 1963
○	NA	NA	100	Thermal	Ilmenite	Alexander 1963
+	NA	NA	100	Thermal	Limestone	Alexander 1963
◇	NA	NA	100	Thermal	Magnetite	Alexander 1963
□	NA	NA	100	Thermal	Slag	Alexander 1963
△	NA	NA	100	Thermal	Whinstone	Alexander 1963
○	0.5	0.77	57.6-72.6	0.1	Sandstone & thermally altered tuff	Maruyama 2017
✱	0.5	0.77	57.6-72.6	0.1	Sandstone & felsic sandstone	Maruyama 2017

Figure 4-7 Significant reduction of the compressive strength of concrete and mortar by neutron irradiation

In Figure 4-8, the scattering of test data is very large, and there is a reduction in the compressive strength, but it is not as significant as shown in Figure 4-7 for concrete. However, Vickers hardness test data from Maruyama et al. 2017 shows that cement paste was not reduced in strength when exposed to fast neutron fluence up to 8.09 x 10^{19} n/cm^2. The test data on the compressive strength of aggregates shown in Figure 4-9 are from one experimental study of serpentine specimens(Elleuch et al. 1972). Serpentine is found to be very good at neutron radiation shielding and is used in several NPPs. The scattering of test data in Figure 4-9 is also very large. There is no obvious decrease in strength. In fact, in this figure, there is an obvious increase in the compressive strength. This increase is because both neutron radiation and high temperature (in this case, the environmental temperature is 150-240 °C) result in the expansion of the minerals in the aggregates which may increase the compactness of the components and thus leads to the increase in compressive strength.

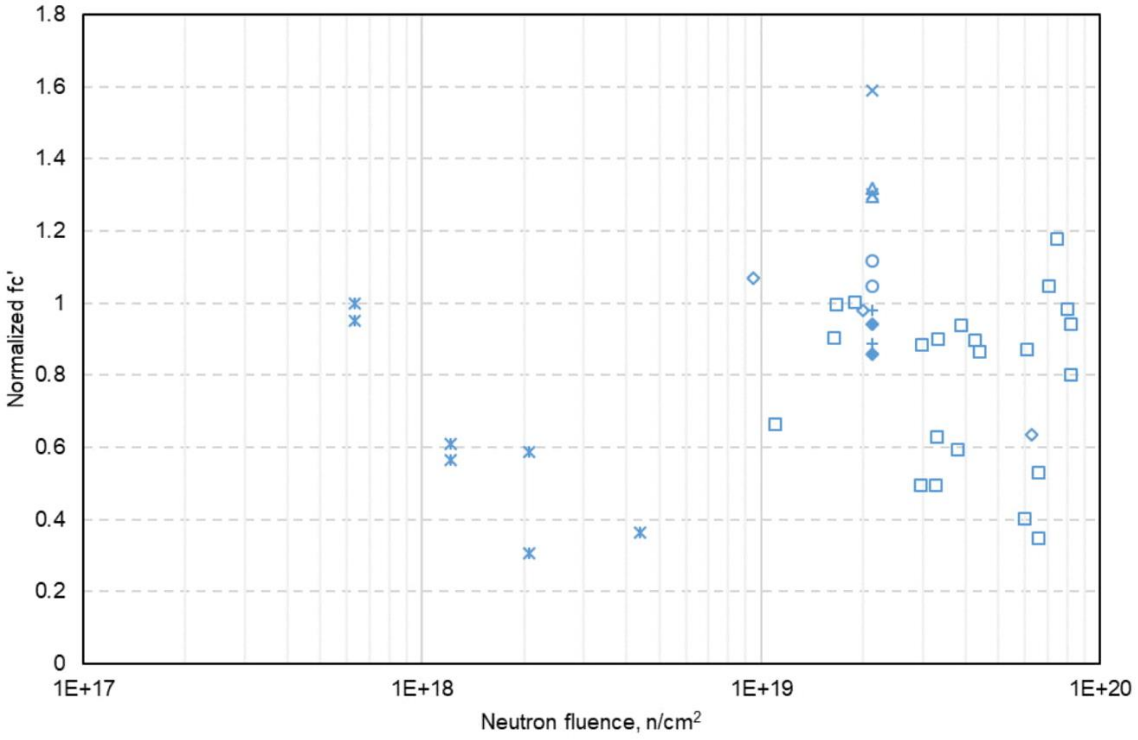

	w/c	T_{max} (°C)	E(MeV)	Cement used	Reference
◇	0.3	150-450	0.8	Portland cement	Dubrovskii 1970
□	0.25	280	1	Aluminous cement	Elleuch 1972
✱	NA	NA	Thermal	Magnesium oxychloride cement	Lyon 1960
△	NA	100	Thermal	Portland cement	Alexander 1963
×	NA	100	Thermal	High-alumina cement paste	Alexander 1963
○	NA	100	Thermal	Low-heat-slag cement paste	Alexander 1963
+	NA	100	Thermal	Supersulphate cement	Alexander 1963
◆	NA	100	Thermal	Portland cement & Pulverised fuel ash paste	Alexander 1963

Figure 4-8 No significant reduction of the compressive strength of cement paste by neutron irradiation

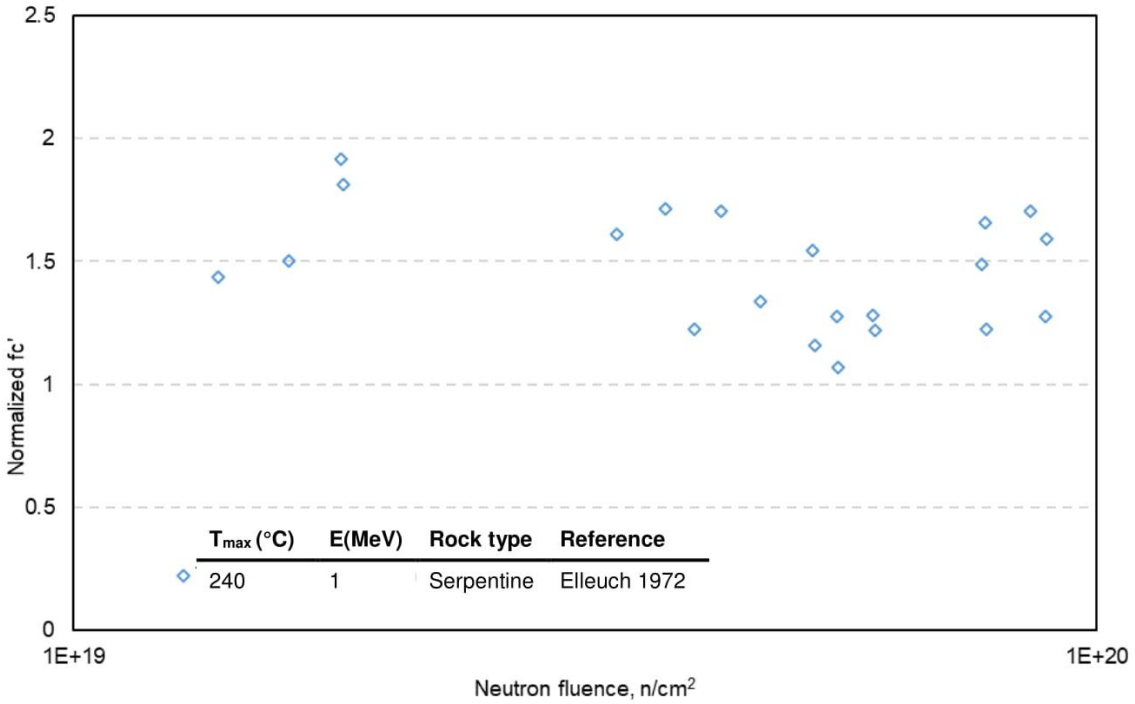

Figure 4-9 No significant reduction of the compressive strength of aggregates by neutron irradiation

Since concrete can be considered as a composite material with the aggregate as inclusions and cement paste as matrix, the general trends shown in Figure 4-7 through Figure 4-9 suggest that the strength reduction of concrete is not due to the strength degradation of its components but due to the increased volumetric mismatches in the two constituent phases during the long-term neutron irradiation. To confirm this conclusion, more data on the compressive strength changes for concrete and individually for its cement paste and aggregate components is needed as this conclusion is based on only one set of experiments about aggregate and was conducted around 240^{o}C, well outside the expected temperature in a reactor cavity.

As one can see in Figure 4-10, compressive strength decreases with the expansion of the specimen. The volumetric mismatch is the critical mechanism that results in the degradation of the compressive strength. This result is different from the conventional long-term durability problems

of concrete. For example, during a sulfate attack, the mechanical properties of aggregate remain intact and those of cement paste decrease, resulting in the degradation of concrete. Therefore, for evaluating the effect of neutron irradiation on concrete, the volumetric properties of the aggregate and the cement paste are very important, such as the coefficient of thermal expansion and the coefficient of drying shrinkage. Furthermore, the volumetric properties depend on the type and amount of aggregate and the water-cement ratio used in the concrete.

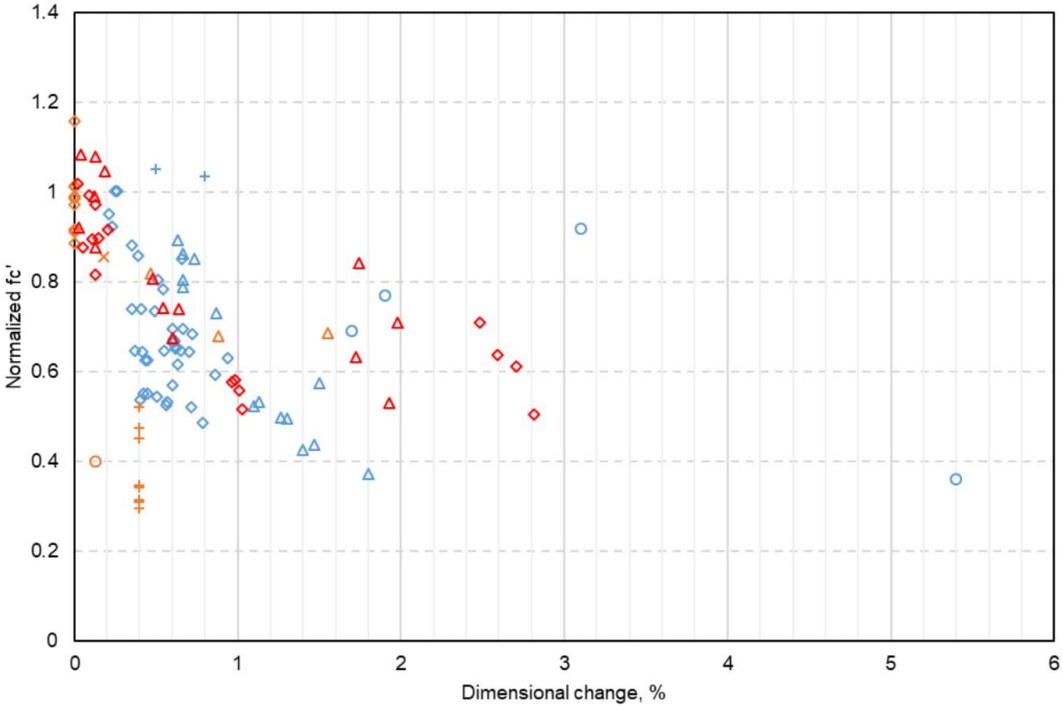

	w/c	Agg. Frac.	T_{max} (°C)	E(MeV)	Agg. used	Reference
◇	0.32	0.74	240	1	Serpentine	Elleuch 1972
△	0.4	0.68	80	Fast	Quartz	Pedersen 1971
○	0.5	0.76	150-350	0.8	Riversand & sandstone	Dubrovskii 1967
+	0.5	0.76	50	0.8	Riversand & sandstone	Dubrovskii 1967
◇	0.55	0.79	50-56	0.1	Sand & gravel	Fujiwara 2009
△	1.01	0.8	100-400	0.8	Hematite	Dubrovskii 1970
×	NA	NA	120	Thermal	NA	Dickeman 1951
○	NA	NA	350	0.01	Serpentine	Dubrovskii 1968
+	NA	NA	550	0.7	Chromite	Dubrovskii 1966
◇	0.5	0.77	57.6-72.6	0.1	Sandstone & thermally altered tuff	Maruyama 2017
△	0.5	0.77	57.6-72.6	0.1	Sandstone & telsic sandstone	Maruyama 2017

Figure 4-10 Relationship between the normalized compressive strength of neutron irradiated concrete samples and their dimensional change

4.3.1.1 Water-cement ratio

The water-cement ratio is the most important parameter among all concrete mix design parameters. In theory, the strength reduction of samples with higher w/c should be smaller, since a higher w/c ratio results in a larger discrepancy in terms of volumetric deformation between cement paste and aggregate (such as the higher drying shrinkage of cement paste). The larger discrepancy results in higher degree of damage in the interface between the cement paste and the aggregate. However, the data plot shown in Figure 4-11 does not show a very clear trend. There may be a considerable effect due to high temperature.

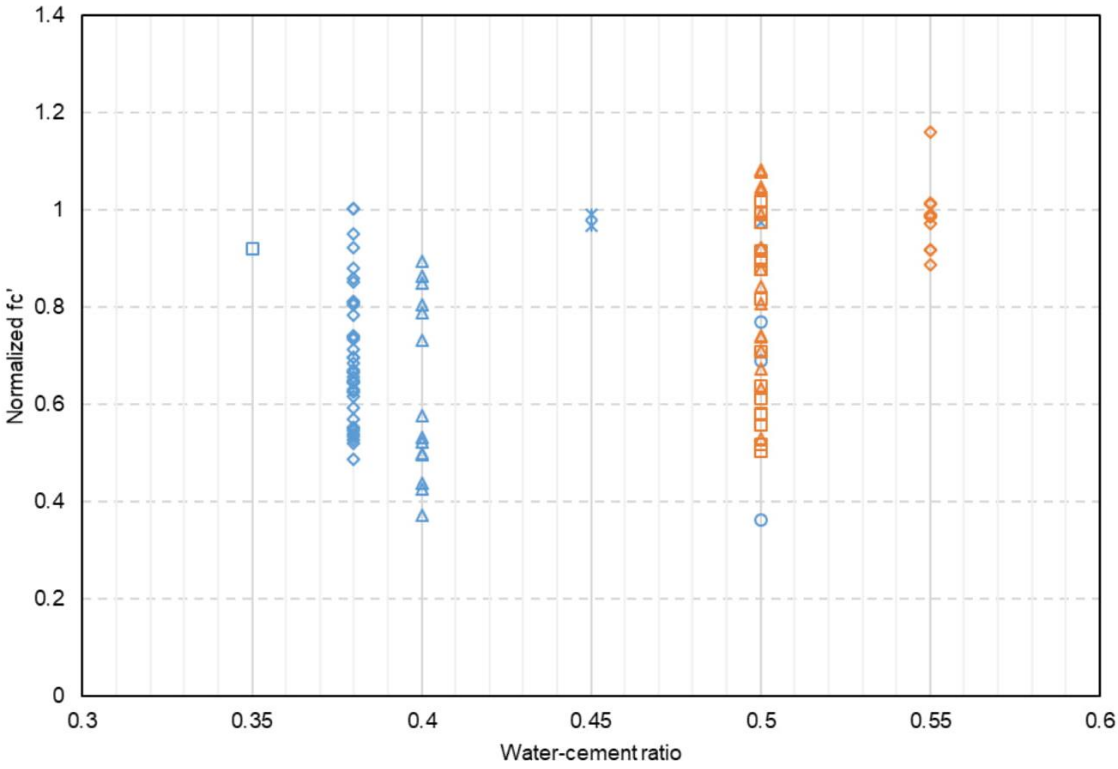

	w/c	Agg. Frac.	T_{max} (°C)	E(MeV)	Agg. used	Reference
◇	0.38	0.74	240	1	Serpentine	Elleuch 1972
□	0.35	0.73	80	1	Sand & Crushed stone	Stoces 1970
△	0.4	0.68	80	Fast	Quartz	Pedersen 1971
✳	0.45	0.67	50	Thermal	Riversand	Batten 1960, Price 1957
×	0.5	0.84	50	Thermal	Riversand	Batten 1960, Price 1957
○	0.5	0.76	150-350	0.8	Riversand & sandstone	Dubrovskii 1967
◇	0.55	0.79	50-56	0.1	Sand & Gravel	Fujiwara 2009
□	0.5	0.77	57.6-72.6	0.1	Sandstone & thermally altered tuff	Maruyama 2017
△	0.5	0.77	57.6-72.6	0.1	Sandstone & felsic sandstone	Maruyama 2017

Figure 4-11 The effect of the w/c ratio on the normalized compressive strength of concrete and mortar (neutron fluence >1 x10^{18} n/cm^2)

4.3.1.2 Aggregate content

Figure 4-12 shows that the compressive strength reduction of high-level neutron irradiated concrete samples. One can see that the strength reduction is higher when the aggregate volume fraction is lower. The effect is quite significant. The mechanisms behind this trend are unknown.

The same effect was also noted by (Naus 2006) for unirradiated concrete, but there was no discussion about the mechanism as well.

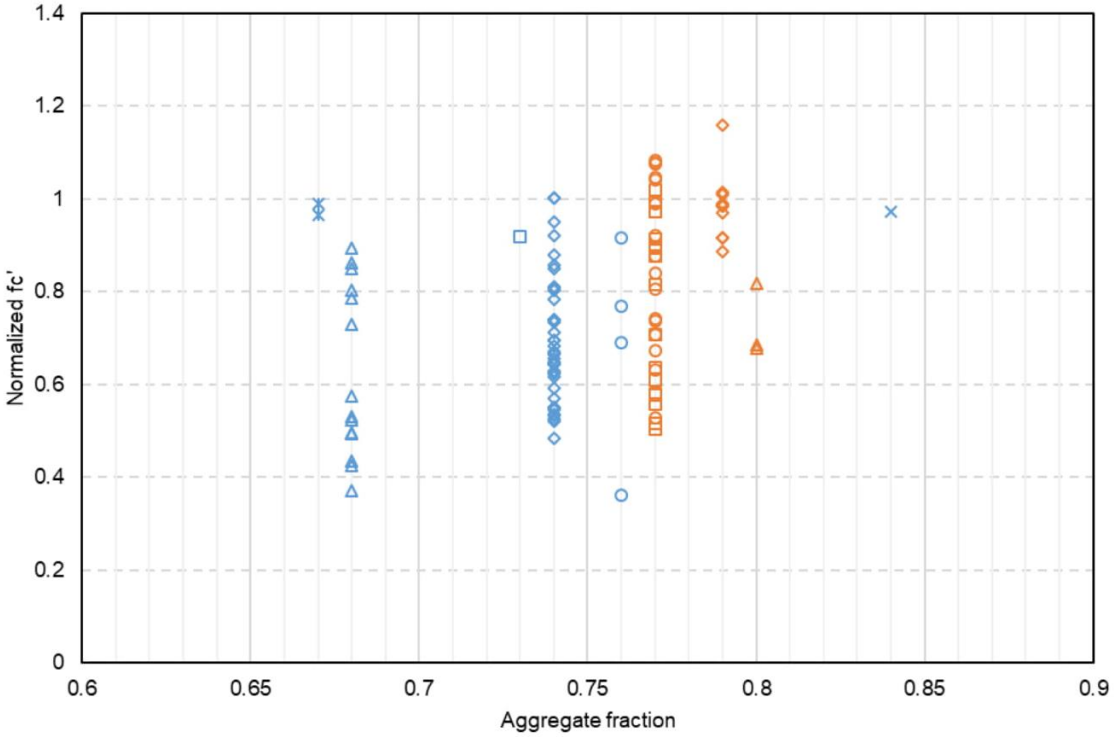

	w/c	Agg. Frac.	T_{max} (°C)	E(MeV)	Agg. used	Reference
◇	0.38	0.74	240	1	Serpentine	Elleuch 1972
□	0.35	0.73	80	1	Sand & Crushed stone	Stoces 1970
△	0.4	0.68	80	Fast	Quartz	Pedersen 1971
✱	0.45	0.67	50	Thermal	Riversand	Batten 1960, Price 1957
×	0.5	0.84	50	Thermal	Riversand	Batten 1960, Price 1957
○	0.5	0.76	150-350	0.8	Riversand & sandstone	Dubrovskii 1967
◇	0.55	0.79	50-56	0.1	Sand & Gravel	Fujiwara 2009
△	1.01	0.8	100-400	0.8	Hematite	Dubrovskii 1970
□	0.5	0.77	57.6-72.6	0.1	Sandstone & thermally altered tuff	Maruyama 2017
○	0.5	0.77	57.6-72.6	0.1	Sandstone & felsic sandstone	Maruyama 2017

Figure 4-12 The effect of aggregate fraction on the compressive strength of concrete and mortar (neutron fluence >1 x10^{18} n/cm^2)

4.3.2 Tensile strength

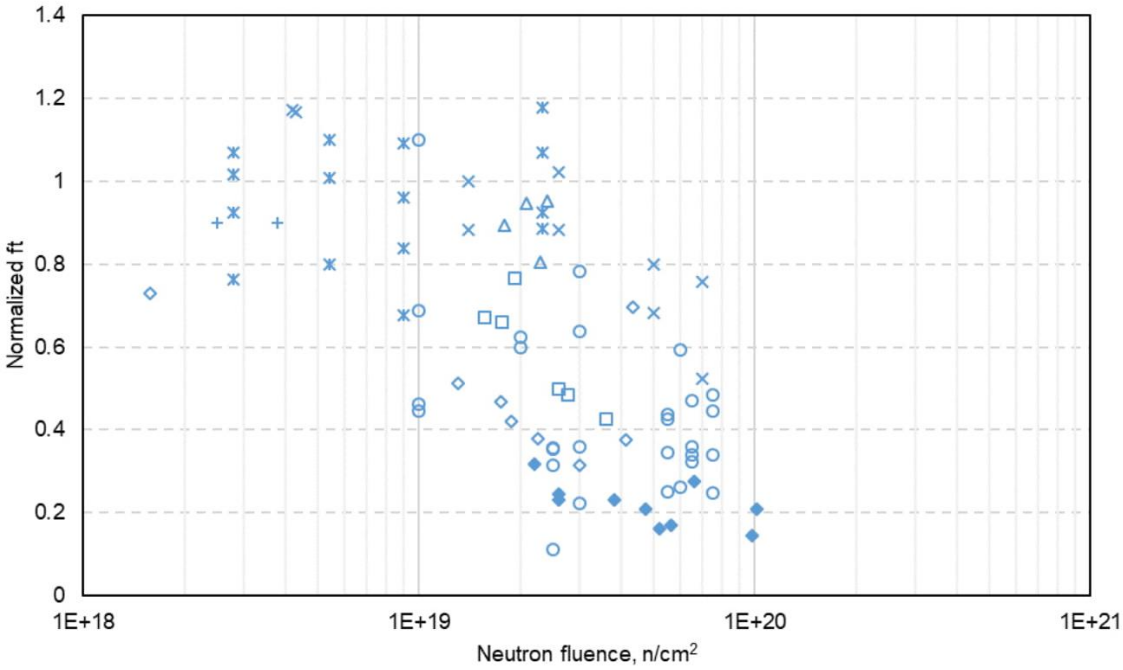

	w/c	Agg. Frac.	T_{max} (°C)	E(MeV)	Agg. used	Reference
◇	0.36	0.67	50	Fast	Flint	Kelly 1969, Gray 1971
□	0.36	0.67	50	Fast	Limestone	Kelly 1969, Gray 1971
△	NA	NA	50	Fast	Sand & light weight agg.	Kelly 1969, Gray 1971
✱	NA	NA	100	Thermal	Heston sand	Alexander 1963
×	0.45	0.67	50	Thermal	Riversand	Batten 1960, Price 1957
○	0.5	0.84	50	Thermal	Riversand	Batten 1960, Price 1957
+	0.5	0.67	100-125	Fast	Limestone	Cristiani 1971, Granata 1972, Crispino 1972
◆	0.38	0.74	240	1	Serpentine	Elleuch 1972

Figure 4-13 Significant tensile strength reduction of concrete and mortar by neutron irradiation

Figure 4-13 shows a significant reduction of tensile strength of concrete and mortar by neutron irradiation, which is consistent with the general trends noted in the literature. In the figure, the normalized compressive strength was used. As shown in Figure 4-13, with increasing neutron level, the normalized strength decreased to 0.2, which is 20% of the original value. Different from the compressive strength, there are very clear trends for significant reduction of tensile strength of

both cement paste and aggregate, which are shown in Figure 4-14 for cement paste and Figure 4-15 for aggregate. As evident in the two figures, the available data for the tensile strength of pure cement paste and aggregates are very limited.

Since concrete can be considered as a composite material with the aggregate as inclusions and the cement paste as the matrix, the general trends shown in Figure 4-13 through Figure 4-15 mean that the tensile strength reduction of concrete is due to the strength degradation of its components. The volumetric mismatches between the two constituent phases during the long-term neutron irradiation are additional factors. This effect is totally different from the strength reduction in compressive strength.

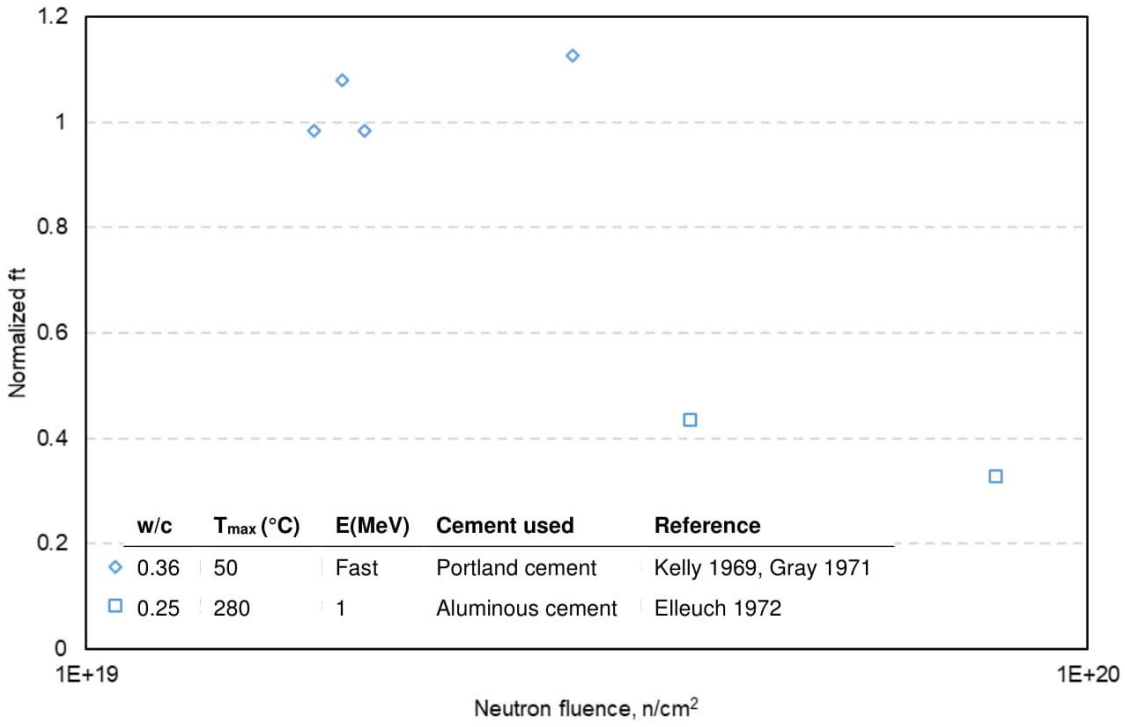

Figure 4-14 Significant tensile strength reduction of cement paste by neutron irradiation

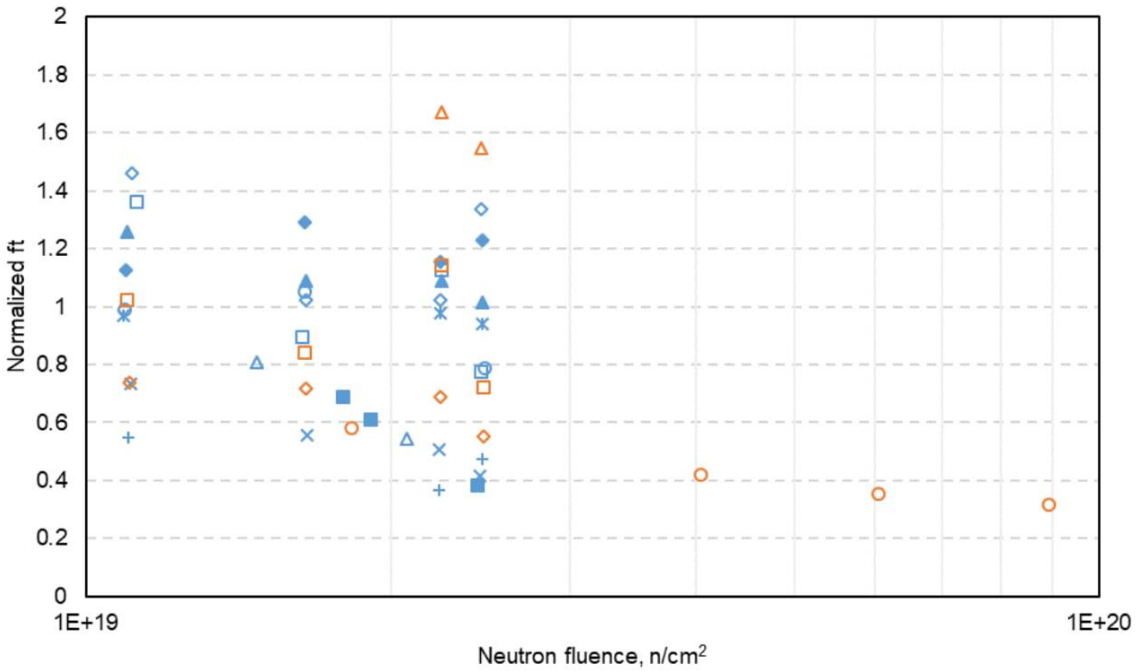

T_{max} (°C)	E(MeV)	Rock type	Reference
50	Fast	Creywacke	Kelly 1969, Gray 1971
50	Fast	Cromhall limestone	Kelly 1969, Gray 1971
50	Fast	Flint	Kelly 1969, Gray 1971
50	Fast	Foster Yeoman Limestone	Kelly 1969, Gray 1971
50	Fast	High E. Dolerite	Kelly 1969, Gray 1971
50	Fast	High Mag. Limestone	Kelly 1969, Gray 1971
50	Fast	Hillhouse Whinstone	Kelly 1969, Gray 1971
50	Fast	Hornfels	Kelly 1969, Gray 1971
50	Fast	Limestone	Kelly 1969, Gray 1971
50	Fast	Limestone(Esperstone)	Kelly 1969, Gray 1971
50	Fast	Low E. Dolerite	Kelly 1969, Gray 1971
50	Fast	Low Mag. Limestone	Kelly 1969, Gray 1971
50	Fast	Trachy Andersite	Kelly 1969, Gray 1971
240	1	Serpentine	Elleuch 1972

Figure 4-15 Significant tensile strength reduction of aggregates by neutron irradiation

4.3.2.1 Water-cement ratio

The effect of the w/c ratio on the tensile strength is shown in Figure 4-16. The general trend is different from Figure 4-11 for compressive strength. The strength reduction of samples is getting smaller with the increase of w/c ratio. As mentioned earlier, tensile strength reduction of concrete under neutron radiation is due to the strength degradation of its components: cement paste

and aggregates. Thus, the trend showed in Figure 4-16 indicates that cement paste with lower w/c and aggregate with less moisture have more tensile strength reductions. The reason may be that there is more water in cement paste with higher w/c ratio which makes the cement paste and aggregate become more resistant to neutron radiation since the hydrogen in water is very efficient to moderate neutrons

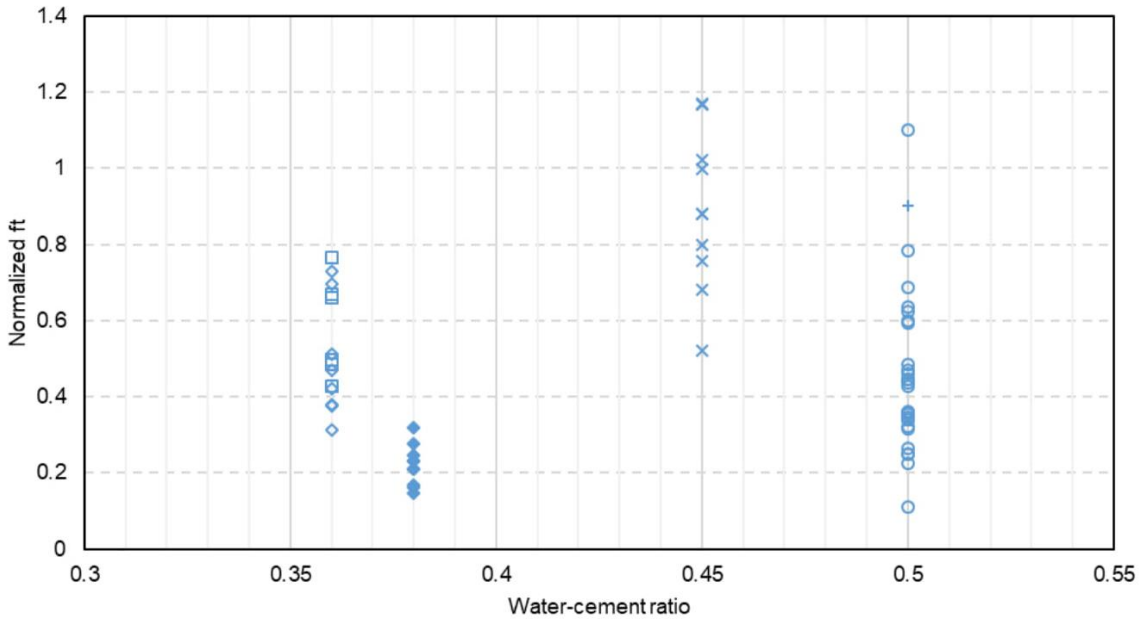

w/c	Agg. Frac.	T_{max} (°C)	E(MeV)	Agg. used	Reference
◇ 0.36	0.67	50	Fast	Flint	Kelly 1969, Gray 1971
□ 0.36	0.67	50	Fast	Limestone	Kelly 1969, Gray 1971
× 0.45	0.67	50	Thermal	Riversand	Batten 1960, Price 1957
○ 0.5	0.84	50	Thermal	Riversand	Batten 1960, Price 1957
+ 0.5	0.67	100-125	Fast	Limestone	Cristiani 1971, Granata 1972, Crispino 1972
◆ 0.38	0.74	240	1	Serpentine	Elleuch 1972

Figure 4-16 The effect of w/c on the tensile strength of concrete and mortar (neutron fluence >1 $x10^{18}$ n/cm^2)

4.3.2.2 Aggregate content

Figure 4-17 shows the effect of aggregate fraction on the tensile strength of concrete and mortar. It is very clear to see that with more aggregate in the concrete, the tensile strength reduction is higher. This trend is because the tensile strength of aggregate is decreased by the neutron irradiation (See Figure 4-15). Thus, with more distressed aggregate in the composite, the effective strength of the composite (the irradiated concrete) is lower.

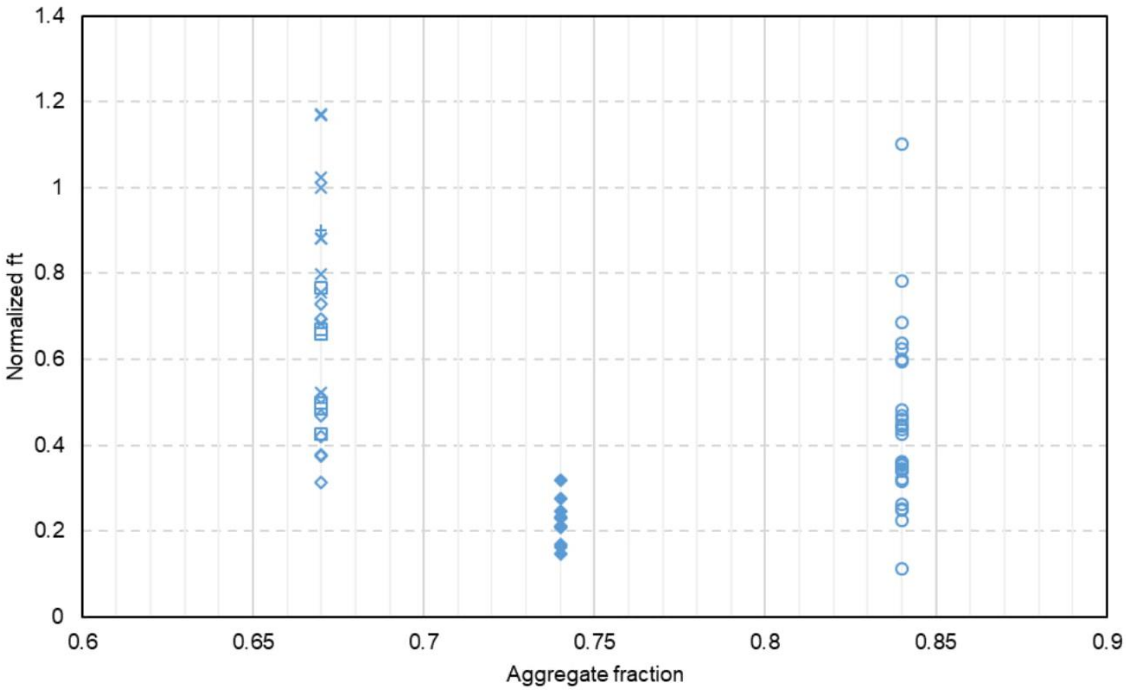

w/c	Agg. Frac.	T_{max} (°C)	E(MeV)	Agg. used	Reference
◇ 0.36	0.67	50	Fast	Flint	Kelly 1969, Gray 1971
□ 0.36	0.67	50	Fast	Limestone	Kelly 1969, Gray 1971
× 0.45	0.67	50	Thermal	Riversand	Batten 1960, Price 1957
○ 0.5	0.84	50	Thermal	Riversand	Batten 1960, Price 1957
+ 0.5	0.67	100-125	Fast	Limestone	Cristiani 1971, Granata 1972, Crispino 1972
◆ 0.38	0.74	240	1	Serpentine	Elleuch 1972

Figure 4-17 The effect of aggregate fraction on the tensile strength of concrete and mortar (neutron fluence >1 x10^{18} n/cm^2)

4.3.3 Modulus of elasticity

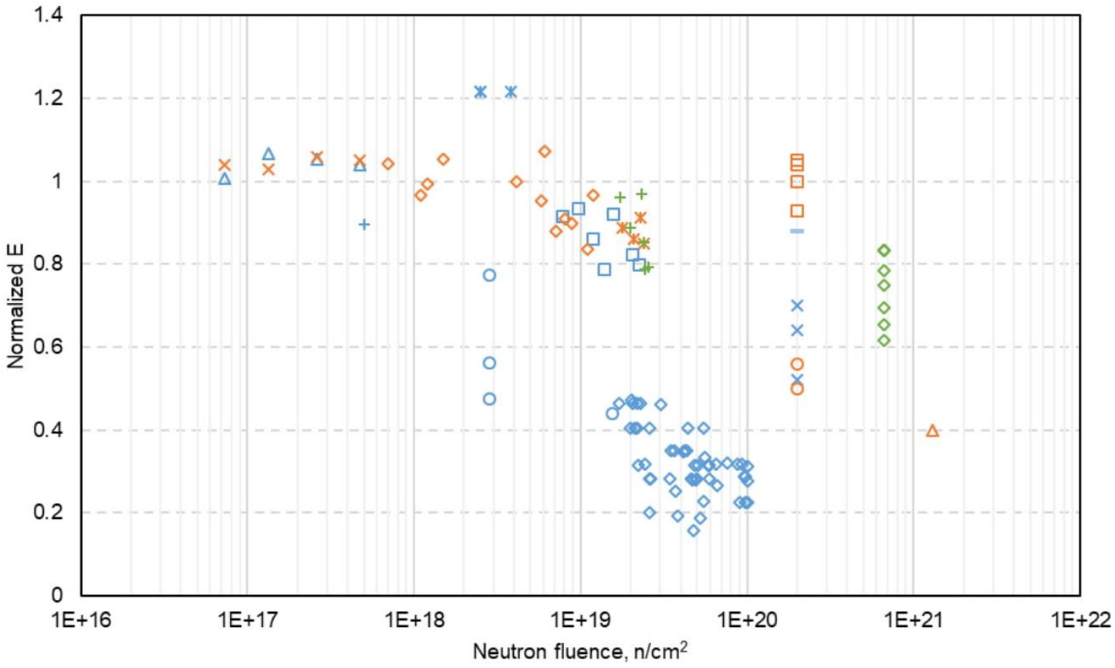

	w/c	Agg. Frac.	T_{max} (°C)	E(MeV)	Agg. used	Reference
◇	0.38	0.74	240	1	Serpentine	Elleuch 1972
□	0.36	0.67	50	Fast	Limestone	Kelly 1969, Gray 1971
△	0.45	NA	60	Fast	Sand	Van der Schaaf 1967, Van der Schaaf 1969, Houben 1969
✱	0.5	0.67	100-125	Fast	Limestone	Cristiani 1971, Granata 1972, Crispino 1972
×	0.5	NA	200	Fast	Barite	Van der Schaaf 1967, Van der Schaaf 1969, Houben 1969
−	0.5	NA	200	Fast	Magnetite	Van der Schaaf 1967, Van der Schaaf 1969, Houben 1969
○	0.5	0.76	150-350	0.8	Riversand & sandstone	Dubrovskii 1967
+	0.5	0.76	50	0.8	Riversand & sandstone	Dubrovskii 1967
◇	0.55	0.79	50-56	0.1	Sand & Gravel	Fujiwara 2009
□	1	NA	200	Fast	Sintered shale	Van der Schaaf 1967, Van der Schaaf 1969, Houben 1969
△	NA	NA	350	0.01	Serpentine	Dubrovskii 1968
✱	NA	NA	50	Fast	Sand & light weight agg.	Kelly 1969, Gray 1971
×	NA	NA	60	Fast	Barite	Van der Schaaf 1967, Van der Schaaf 1969, Houben 1969
○	NA	NA	200	Fast	Barite	Van der Schaaf 1967, Van der Schaaf 1969, Houben 1969
+	NA	NA	100	Thermal	Heston gravel	Alexander 1963
◇	NA	NA	550	0.7	Chromite	Dubrovskii 1966

Figure 4-18 Potential reduction of the elastic modulus of concrete and mortar by neutron irradiation

The effect of neutron irradiation on the modulus of elasticity, E of concrete and mortar, cement paste, and aggregate are shown in Figure 4-18 through Figure 4-20. The general trends shown by the test data are that there is a significant reduction of the elastic modulus of concrete and mortar by neutron irradiation; there is a less significant reduction of the elastic modulus of cement paste by neutron irradiation; and there is a significant reduction of the elastic modulus of aggregates by neutron irradiation. Therefore, the reduction of the stiffness of concrete as indicated by the reduction of E is mainly due to the reduction of E of the aggregate. However, the reduction in E may also be due to some contribution from high temperature which has already been confirmed in Chapter 2.

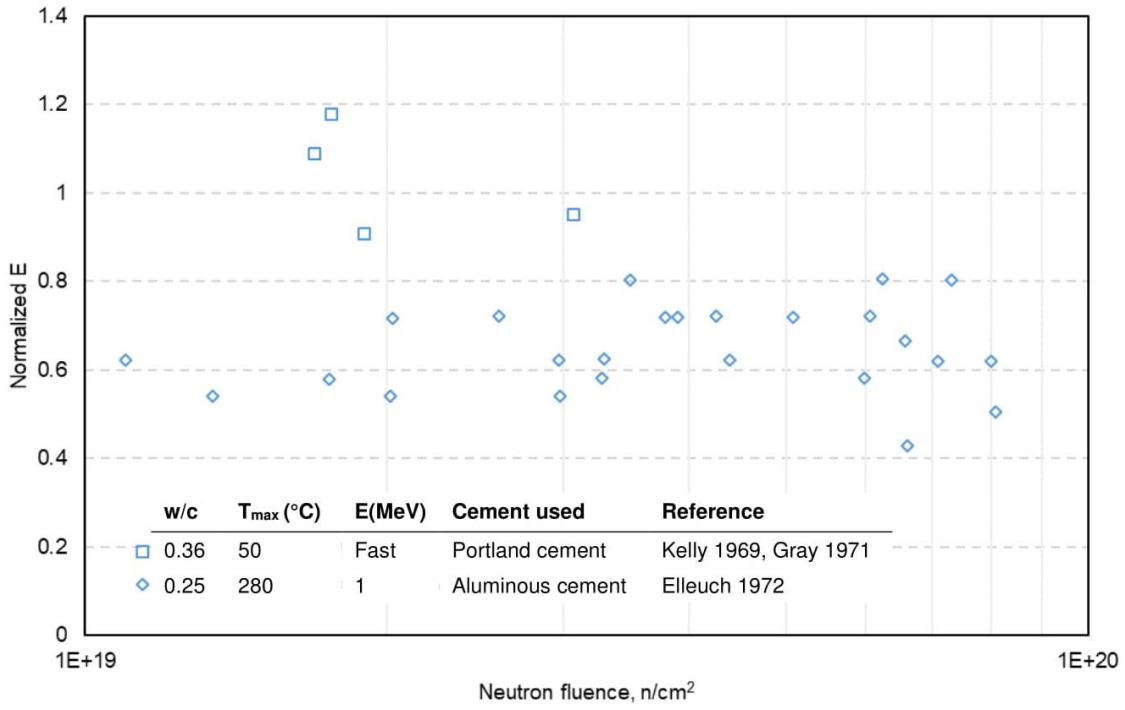

Figure 4-19 Less significant reduction of the elastic modulus of cement paste by neutron irradiation

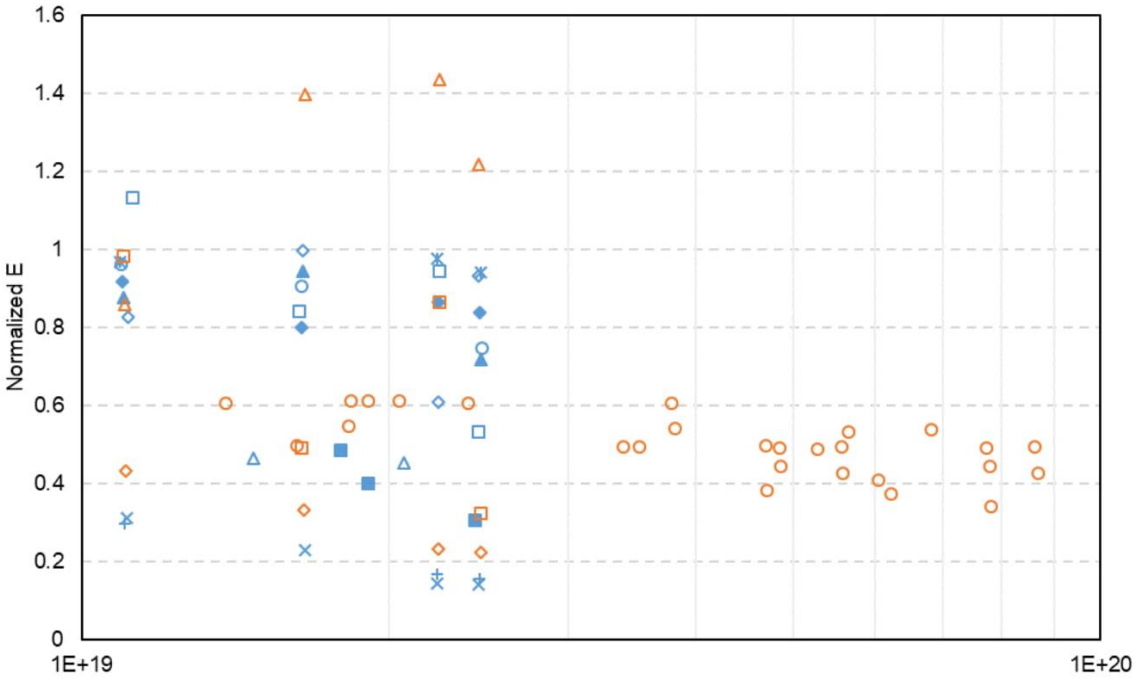

T_{max} (°C)	E(MeV)	Rock type	Reference
50	Fast	Creywacke	Kelly 1969, Gray 1971
50	Fast	Cromhall limestone	Kelly 1969, Gray 1971
50	Fast	Flint	Kelly 1969, Gray 1971
50	Fast	Foster Yeoman Limestone	Kelly 1969, Gray 1971
50	Fast	High E. Dolerite	Kelly 1969, Gray 1971
50	Fast	High Mag. Limestone	Kelly 1969, Gray 1971
50	Fast	Hillhouse Whinstone	Kelly 1969, Gray 1971
50	Fast	Hornfels	Kelly 1969, Gray 1971
50	Fast	Limestone	Kelly 1969, Gray 1971
50	Fast	Limestone(Esperstone)	Kelly 1969, Gray 1971
50	Fast	Low E. Dolerite	Kelly 1969, Gray 1971
50	Fast	Low Mag. Limestone	Kelly 1969, Gray 1971
50	Fast	Trachy Andersite	Kelly 1969, Gray 1971
240	1	Serpentine	Elleuch 1972

Figure 4-20 Significant reduction of the elastic modulus of aggregates by neutron irradiation

4.3.3.1 Water-cement ratio

Concrete design parameters are important. The effect of w/c is very consistent. A lower w/c appears to lead to a higher reduction of E as shown in Figure 4-21. This result is because a lower w/c results in a more densified concrete framework in which it is more difficult to

accommodate the volume change of aggregate, and thus results in more damage in the concrete. On the other hand, those data showing a reduction of E are from experiments with elevated temperatures that could also be responsible for the reduction in E.

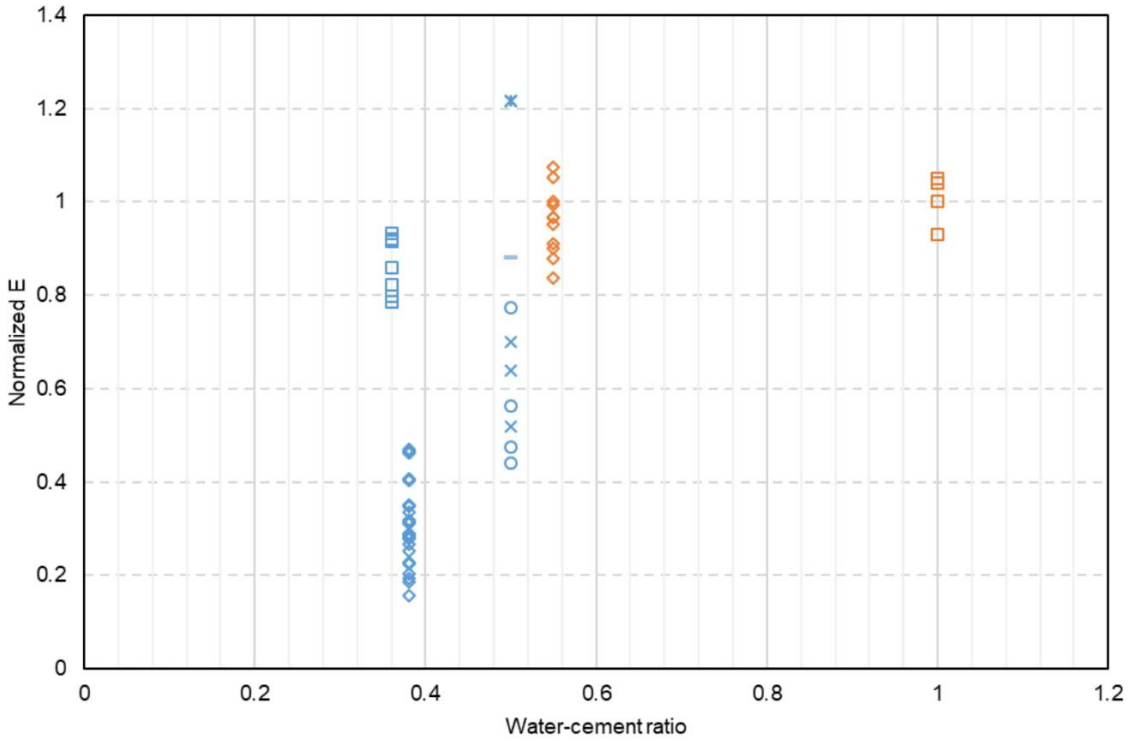

w/c	Agg. Frac.	T_{max} (°C)	E(MeV)	Agg. used	Reference
0.38	0.74	240	1	Serpentine	Elleuch 1972
0.36	0.67	50	Fast	Limestone	Kelly 1969, Gray 1971
0.5	0.67	100-125	Fast	Limestone	Cristiani 1971, Granata 1972, Crispino 1972
0.5	NA	200	Fast	Barite	Van der Schaaf 1967, Van der Schaaf 1969, Houben 1969
0.5	NA	200	Fast	Magnetite	Van der Schaaf 1967, Van der Schaaf 1969, Houben 1969
0.5	0.76	150-350	0.8	Riversand & sandstone	Dubrovskii 1967
0.55	0.79	50-56	0.1	Sand & Gravel	Fujiwara 2009
1	NA	200	Fast	Sintered shale	Van der Schaaf 1967, Van der Schaaf 1969, Houben 1969

Figure 4-21 The effect of w/c on the elastic modulus of concrete and mortar (neutron fluence >1 x10^{18} n/cm^2)

4.3.3.2 Aggregate content

The effect of the aggregate volume fraction on E is shown in Figure 4-22. With increasing aggregate volume fraction, the reduction increases and then decreases. The effect is quite significant, reaching about 80% reduction at the aggregate volume fraction of 74%, and then reverting back to the original value at the aggregate volume fraction of 79%. This trend is difficult to explain, but it could be due to temperature effects.

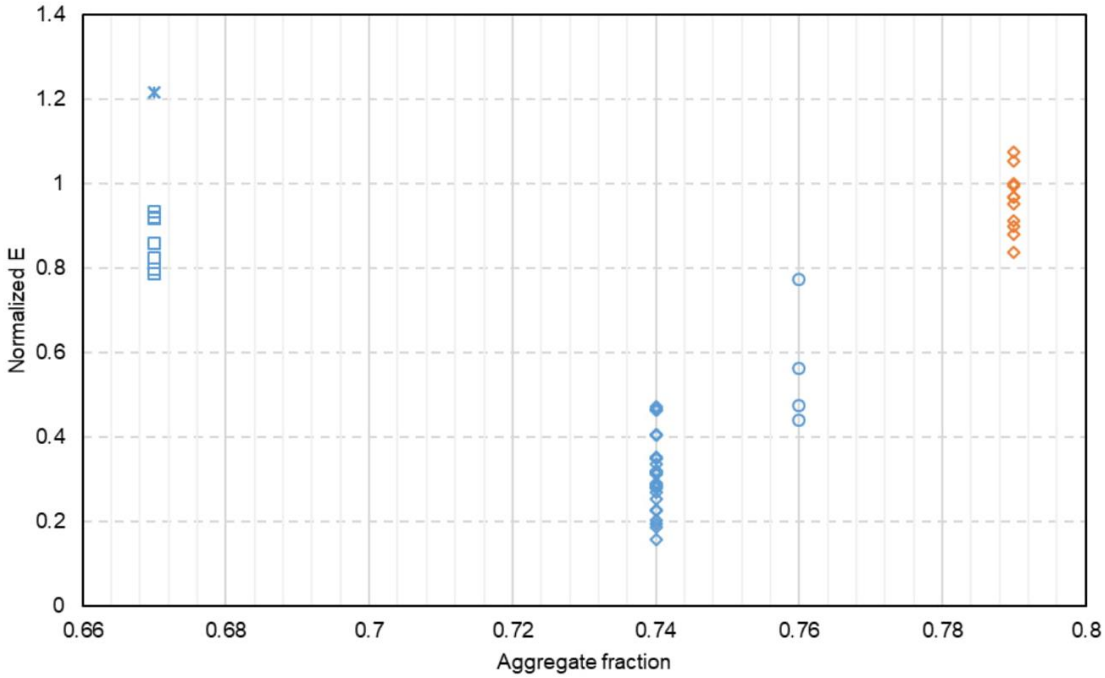

w/c	Agg. Frac.	T_{max} (°C)	E(MeV)	Agg. used	Reference
◇ 0.38	0.74	240	1	Serpentine	Elleuch 1972
□ 0.36	0.67	50	Fast	Limestone	Kelly 1969, Gray 1971
✳ 0.5	0.67	100-125	Fast	Limestone	Cristiani 1971, Granata 1972, Crispino 1972
○ 0.5	0.76	150-350	0.8	Riversand & sandstone	Dubrovskii 1967
◇ 0.55	0.79	50-56	0.1	Sand & Gravel	Fujiwara 2009

Figure 4-22 The effect of aggregate fraction on the elastic modulus of concrete and mortar (neutron fluence >1 x10^{18} n/cm^2)

4.4 Thermal impacts

As discussed in Chapter 2 and Chapter 3, temperature rise could potentially occur in the reactor cavity and is associated with nuclear irradiation. The properties of concrete can be changed.

4.4.1 Compressive strength

Figure 4-23 shows the effect of thermal expansion on the compressive strength of neutron irradiated concrete. One can see a very clear relationship between temperature and the mechanical properties of concrete and mortar: high environmental temperature can result in significant reductions of mechanical properties at a high neutron irradiation level. The normalized compressive strength is around 0.4 when 500^{o}C is reached. It should be mentioned that the compressive strength reduction observed in Figure 4-23 is due to the combined effect of neutron radiation and elevated temperature. It is difficult to distinguish between the two effects because many experimental radiation studies in the literature did not have a control group for the temperature effect. In order to be consistent, the original properties for all samples (before irradiation testing) listed in our data collection were measured under normal ambient temperature instead of the testing temperatures. Observation of Figure 4-7 through Figure 4-9 indicates that the trend shown in Figure 4-23 is mainly due to the difference in the coefficients of thermal expansion of aggregate and cement paste. At a higher temperature, the difference in the thermal strains of the two phases becomes larger, which leads to higher long-term damage.

This decreasing trend in neutron irradiated concrete compressive strength with an increase in temperature is consistent with these studies on the effect of temperature on the mechanical properties of concrete in the absence of radiation(Naus 2010, 2006). Thus, while increasing temperature is expected to result in a reduced compressive strength for concrete as a whole, the results in Chapter 2 show that the reduction is due to the aggregate-cement paste mismatch at a

temperature of 240^{o}C as discussed above. For lower temperatures (<100 ^{o}C), there is no phase transformation involved, and the decrease of the compressive strength should mainly be due to the mismatch between the deformations of hardened cement paste and the aggregate and the subsequent damage. When concretes are exposed to elevated temperatures (>100^{o}C), the change of concrete properties results from the mismatch as well as the phase transformations in hardened cement paste and the possible deterioration aggregate(Graves et al., 2014; Lee et al., 2009).

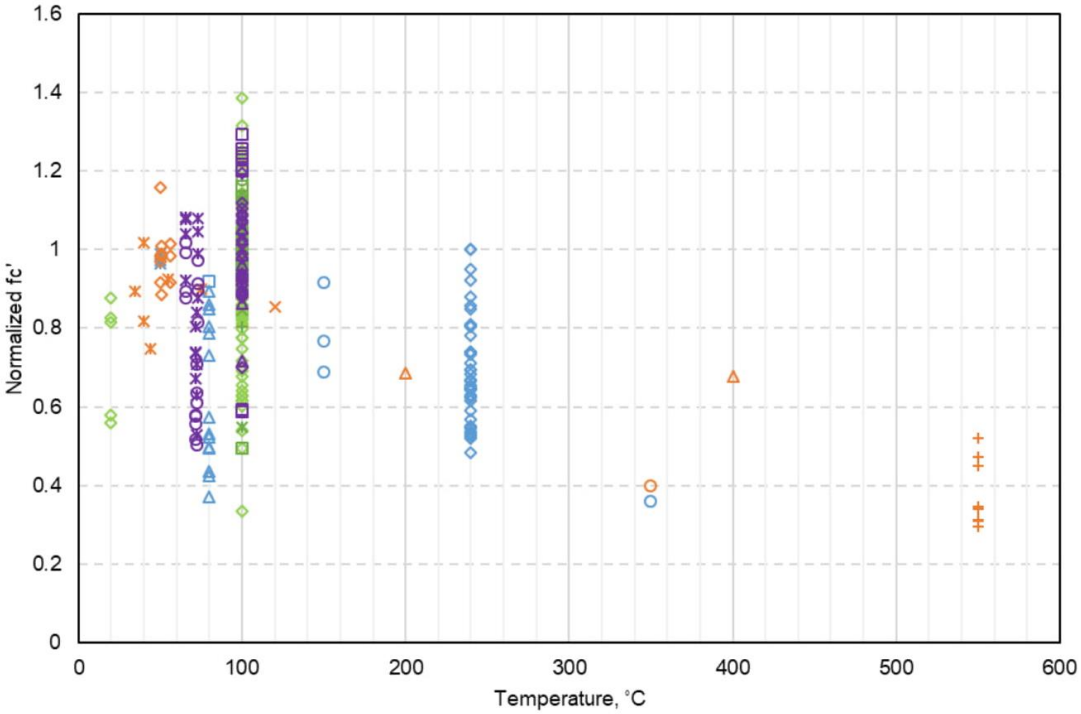

w/c	Agg. Frac.	T_{max} (°C)	E(MeV)	Agg. used	Reference
0.38	0.74	240	1	Serpentine	Elleuch 1972
0.35	0.73	80	1	Sand & Crushed stone	Stoces 1970
0.4	0.68	80	Fast	Quartz	Pedersen 1971
0.45	0.67	50	Thermal	Riversand	Batten 1960, Price 1957
0.5	0.84	50	Thermal	Riversand	Batten 1960, Price 1957
0.5	0.76	150-350	0.8	Riversand & sandstone	Dubrovskii 1967
0.55	0.79	50-56	0.1	Sand & Gravel	Fujiwara 2009
1.01	0.8	100-400	0.8	Hematite	Dubrovskii 1970
NA	NA	20-75	Thermal	Haydite&Barytes	Blosser 1958, Rockwell 1948, Grantham 1960
NA	NA	120	Thermal	NA	Dickman 1951
NA	NA	350	0.01	Serpentine	Dubrovskii 1968
NA	NA	550	0.7	Chromite	Dubrovskii 1966
NA	NA	100	Thermal	Heston sand	Alexander 1963
NA	NA	100	Thermal	Barytes	Alexander 1963
NA	NA	100	Thermal	Crushed firebrick	Alexander 1963
NA	NA	100	Thermal	Granite	Alexander 1963
NA	NA	100	Thermal	Heston gravel	Alexander 1963
NA	NA	100	Thermal	Ilmenite	Alexander 1963
NA	NA	100	Thermal	Limestone	Alexander 1963
NA	NA	100	Thermal	Magnetite	Alexander 1963
NA	NA	100	Thermal	Slag	Alexander 1963
NA	NA	100	Thermal	Whinstone	Alexander 1963
0.5	0.77	57.6-72.6	0.1	Sandstone & thermally altered tuff	Maruyama 2017
0.5	0.77	57.6-72.6	0.1	Sandstone & felsic sandstone	Maruyama 2017

Figure 4-23 The effect of temperature and neutron irradiation on the compressive strength of concrete and mortar (neutron fluence >1 x10^{18} n/cm^2)

4.4.2 Tensile strength

Figure 4-24 shows the effect of temperature on the tensile strength of concrete and mortar, which is similar to the trend shown in Figure 4-23 for compressive strength. One can see a very clear relationship between temperature and the tensile strength of concrete and mortar. The trend shown in Figure 4-24 is due to the difference in the coefficients of thermal expansion (CTE) of aggregate and cement paste. At a higher temperature, the difference in the thermal strains of the two phases becomes larger, which leads to higher long-term damage. Similar to compressive strength, the tensile strength reduction observed in the figures is due to the combined effect of neutron radiation and elevated temperature. Combining the results shown in Figure 4-23 and Figure 4-24, we can conclude that high environmental temperatures can result in significant reduction of concrete strength at a high neutron irradiation level.

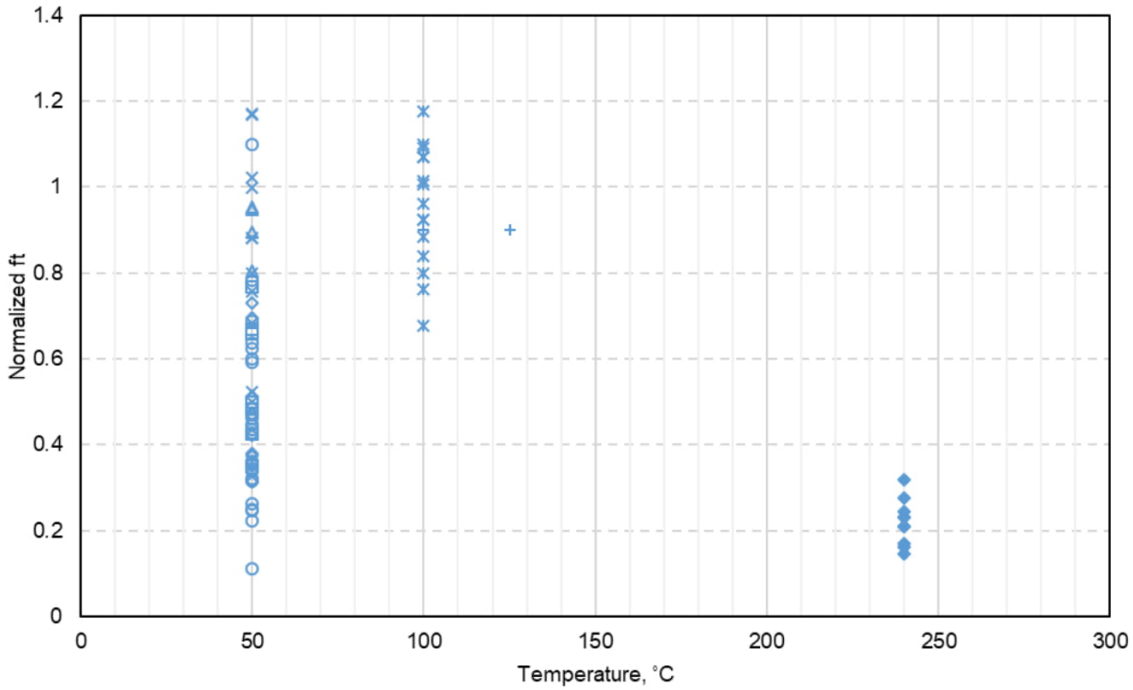

	w/c	Agg. Frac.	T_{max} (°C)	E(MeV)	Agg. used	Reference
◇	0.36	0.67	50	Fast	Flint	Kelly 1969, Gray 1971
□	0.36	0.67	50	Fast	Limestone	Kelly 1969, Gray 1971
△	NA	NA	50	Fast	Sand & light weight agg.	Kelly 1969, Gray 1971
✳	NA	NA	100	Thermal	Heston sand	Alexander 1963
×	0.45	0.67	50	Thermal	Riversand	Batten 1960, Price 1957
○	0.5	0.84	50	Thermal	Riversand	Batten 1960, Price 1957
+	0.5	0.67	100-125	Fast	Limestone	Cristiani 1971, Granata 1972, Crispino 1972
◆	0.38	0.74	240	1	Serpentine	Elleuch 1972

Figure 4-24 The effect of temperature and neutron irradiation on the tensile strength of concrete and mortar (neutron fluence >1 x10^{18} n/cm^2)

4.4.3 Modulus of elasticity

The effect of temperature on E of irradiated concrete and mortar is shown in Figure 4-25. The general trends shown by the test data are that there is a significant reduction of the elastic modulus of concrete and mortar by temperature under a high level of neutron irradiation. The rate of reduction is almost linearly related with the temperature. However, there are a few data above 300 ˚C showing a different trend.

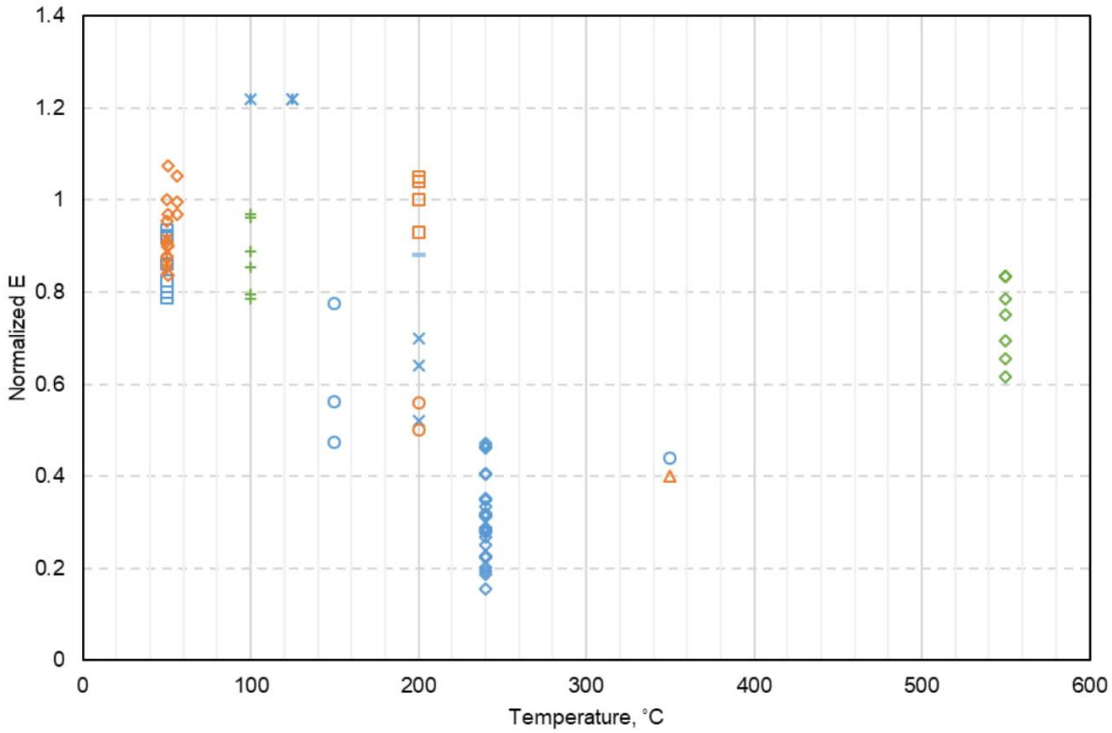

w/c	Agg. Frac.	T_{max} (°C)	E(MeV)	Agg. used	Reference
0.38	0.74	240	1	Serpentine	Elleuch 1972
0.36	0.67	50	Fast	Limestone	Kelly 1969, Gray 1971
0.5	0.67	100-125	Fast	Limestone	Cristiani 1971, Granata 1972, Crispino 1972
0.5	NA	200	Fast	Barite	Van der Schaaf 1967, Van der Schaaf 1969, Houben 1969
0.5	NA	200	Fast	Magnetite	Van der Schaaf 1967, Van der Schaaf 1969, Houben 1969
0.5	0.76	150-350	0.8	Riversand & sandstone	Dubrovskii 1967
0.55	0.79	50-56	0.1	Sand & Gravel	Fujiwara 2009
1	NA	200	Fast	Sintered shale	Van der Schaaf 1967, Van der Schaaf 1969, Houben 1969
NA	NA	350	0.01	Serpentine	Dubrovskii 1968
NA	NA	50	Fast	Sand & light weight agg.	Kelly 1969, Gray 1971
NA	NA	200	Fast	Barite	Van der Schaaf 1967, Van der Schaaf 1969, Houben 1969
NA	NA	100	Thermal	Heston gravel	Alexander 1963
NA	NA	550	0.7	Chromite	Dubrovskii 1966

Figure 4-25 The effect of temperature and neutron irradiation on the elastic modulus of concrete and mortar (neutron fluence >1 x10^{18} n/cm^2)

4.5 Other effects

4.5.1 Alkali-Silica Reaction(ASR)

There is no direct experimental data on the combined synergistic effects of ASR and neutron on concrete performance. Experimental studies(Ichikawa and Koizumi 2002; Pignatelli et al. 2016) showed that the reactivity of quartz towards alkali was significantly increased by nuclear radiation. In the study conducted by Ichikawa and Koizumi 2002, a part of the crystalline and amorphous quartz plates was irradiated with 200 keV Ar ions to different dosages, and the plates were then immersed in the NaOH solution to simulate the alkali environment in concrete. The critical fast neutron fluence and beta and gamma-ray dose for both aggregates containing crystalline quartz and aggregates containing amorphous quartz were obtained. The follow up experimental research (Ichikawa and Kimura 2007) showed a reactivity change of plagioclase to alkali under electron beam-irradiation. Critical values were also obtained. The test results from the above studies suggest that the distorted structure of aggregate caused by neutron irradiation would also increase its reactivity towards alkali, i.e., leading to additional ASR in the presence of sufficient alkali. Thus, aggregates not typically prone to the ASR could be vulnerable to ASR through neutron irradiation.

In addition, environmental conditions such as the temperature and moisture could affect ASR in concrete. In the reactor cavity, radiation can generate additional heat in concrete and moisture content in concrete could be reduced by radiolysis decomposition and by evaporation of water due to heating. Therefore, radiation can affect the ASR in concrete by several different mechanisms.

4.5.2 Carbonation

Carbonation is the conversion of calcium hydroxide (in the form of portlandite) in the cement paste to calcium carbonate (in the form of calcite) through interaction with carbon dioxide (CO_2) and water. Carbonation is normally associated with diffusion of CO_2 from the atmosphere through open pores in the cement paste, and, thus, carbonation is generally relegated to relatively small depths at the surface of the concrete. There are no experimental studies concerning the combined effect of carbonation and neutron irradiation on cementitious materials. Only a couple of studies have simultaneously investigated carbonation and gamma-ray irradiation effects.

One study (Vodák et al. 2011) about carbonation of hydrated cement paste indicated that carbonation in the material was accelerated by gamma-ray irradiation and average pore diameter reduced, more importantly, carbonation can result directly from gamma rays, in addition to the "natural" carbonation. The same conclusion was also reached by an earlier study about concrete under gamma-ray radiation (Vodák et al. 2005).

Another experimental study (Bar-Nes et al. 2008) also investigated the combined effect of carbonation and gamma-ray radiation on cement pastes. Two different water-cement ratios were used in the study and carbonation depths of all samples were measured. A gamma-ray exposure of 10^7 Gy over 6 months resulted in carbonation depths approximately 5 to 10 times deeper than reference samples under atmospheric conditions. This indicates that gamma-ray irradiation can accelerate the carbonation process of concrete.

Similar to ASR in concrete, temperature and moisture changes induced by neutron and gamma-ray irradiation can affect the carbonation of concrete.

4.5.3 Creep

There are not many studies concerning concrete creep under irradiation. An experimental study was conducted about the creep properties of a limestone aggregate concrete which was used in the pressure vessel of the Oldbury Nuclear Power Station(McDowall 1972). The shrinkage and creep of the samples under an average gamma-ray dose rate of 11.4×10^3 rad/h for 10 months was obtained and compared with the results of control samples. As one can see in Figure 4-26, the creep of irradiated concrete decreases under gamma-ray radiation. However, since the elastic modulus of irradiated concrete is smaller than that of unirradiated concrete, the creep of concrete would be expected to increase under irradiation, and the trend shown in Figure 4-26 should be opposite. One possible explanation is that the irradiated concrete samples were drier than the control samples due to radiolysis decomposition of water in them. Besides, increased viscosity caused by hindered water movement and high internal gas pressures under radiation could also affect concrete creep properties (Giorla et al. 2017; McDowall 1972; Pomaro 2016).

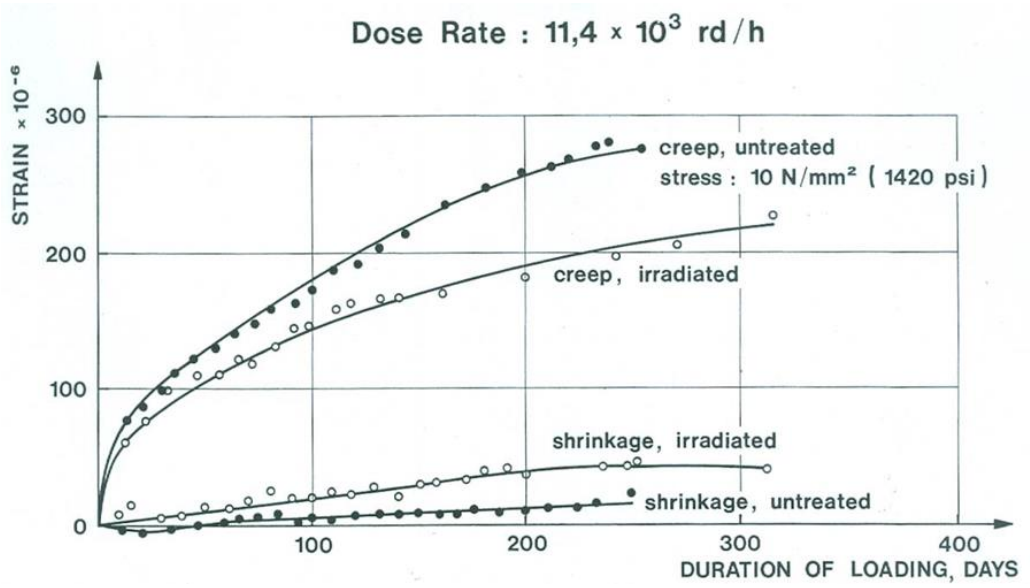

Figure 4-26 The effect of gamma-ray radiation on creep and shrinkage of concrete(McDowall 1972)

Creep of Portland cement grout specimens under concurrent neutron and gamma-ray irradiation were obtained by Gray 1972. Figure 4-27 presents shrinkage and creep results obtained from the original paper. The irradiation test was done in Herald test reactor in the U.K., and the fast neutron fluence is about 0.75×10^{19}n/cm^2. The creep of specimens under irradiation is much higher than that before and after irradiation which is very different from the results from McDowall 1972. The mechanisms are unknown.

A recent numerical simulation of concrete specimens subject to irradiation-induced expansion and degradation concluded that "creep can play a favorable role in terms of LWRs long-term operation by delaying the initiation of damage to a higher fluence exposure" (Giorla et al. 2017).

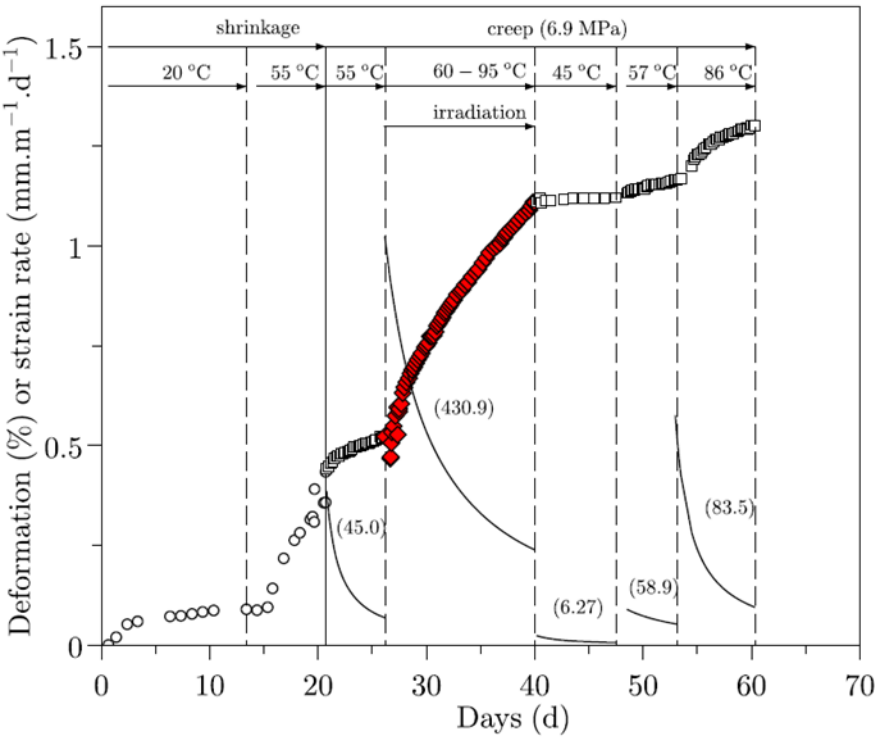

Figure 4-27 Measured shrinkage and creep strain of portland cement grout(Giorla et al. 2017) (reconstructed from data in (Gray 1972))

CHAPTER 5

EXPERIMENTAL STUDY OF SELF-SENSING CAPABILITY OF CARBON FIBER REINFORCED CEMENTITIOUS COMPOSITES

5.1 Introduction

Self-sensing concrete (Smart concrete) is concrete typically reinforced by conductive admixture (e.g., carbon fiber). The results of numerous studies (Chen and Chung 1993, 1996; Chung 2000b; Fu and Chung 1998; Huang 2012) show that mechanical properties and durability of the concrete can be improved by various admixture and fibers. Moreover, a lot of research (Azhari and Banthia 2012; Chen and Chung 1996; Chung 2000a; b; Fu and Chung 1998; Huang 2012) found that the electrical resistivity of smart concrete can response according to different strains and stresses experienced by the material, which makes it feasible to be used as a sensor in concrete structures. Compared to the conventional sensors used in structures, the expense of smart concrete is significantly cheaper (Chen and Chung 1996), and the monitoring capability of the concrete can be high and reliable (Huang 2012). Thus, smart concrete has very good potential to become a sensor and can be used to monitor the strain state of concrete, such as dry cask used in extended SNF storage systems. However, in order for the smart concrete to be used as a reliable sensor in real structures, its behavior under practical environmental conditions must be studied. The impacts of environmental loadings, such as temperature changes, moisture fluctuations, and attaches of chemicals are critical for the sensor calibration and application and will be systematically examined.

5.2 Literature review

5.2.1 Piezoresistivity effect

All materials have electrical properties, and most of them can be classified as conductors or resistors. Materials that are electrically resistive are typically labeled as resistors. The resistance of a resistor (R) is typically determined by the bulk resistivity (ρ) as well as the length (L) and cross section (A). The equation is given as:

$$R = \frac{V}{I} = \rho \frac{L}{A} \tag{5-1}$$

Piezoresistivity effect is the electrical resistance change of a material when a mechanical load is applied to it. The fractional change in resistance (FCR) of an intact specimen without damage is usually due to the strain and the piezoresistive effect caused by resistivity changes (Du et al. 2013):

$$\frac{dR}{R} = (1 + 2\upsilon)\varepsilon + \frac{d\rho}{\rho} \tag{5-2}$$

in which υ is Poisson's ratio. If a material shows negligible piezoresistive effect, the above equation becomes

$$\frac{d\,R/R}{\varepsilon} = 1 + 2\upsilon \tag{5-3}$$

The FCR per unit strain shown in the left side of the above equation is usually known as Gauge Factor (GF). The upper bound of GF is 2 (if the Poisson ratio of the material is 0.5).

5.2.2 Conductive admixtures

Concrete is intrinsically a material with very poor conductivity, but reinforcing the concrete by conductive admixtures will significantly improve its electrical properties and provides it self-sensing capability. Carbon-based admixtures, such as carbon fibers and carbon nanotubes, are the

most widely used conductive admixture in previous studies to develop multifunctional cementitious composites.

5.2.2.1 Carbon fibers (CFs)

First developed in the 1960s, CFs are fibers comprised of primarily carbon atoms. CFs range in diameter from 5 to 10 micrometers and can come in a number of lengths ranging from micrometers to millimeters. Much research has been done in the field of applying CFs in concrete because they are recognized as the strongest and stiffest material in existence (Cantwell and Morton 1991). CFs exhibit a remarkable strength at a very low self-weight. In CF industry, two major forms of fibers are produced: one form that "contains at least 90% carbon" is called Carbon Fiber; and another one is called Graphite Fiber which "is used for the fibers that have carbon in excess of 99%". An illustration of CFs is shown in Figure 5-1.

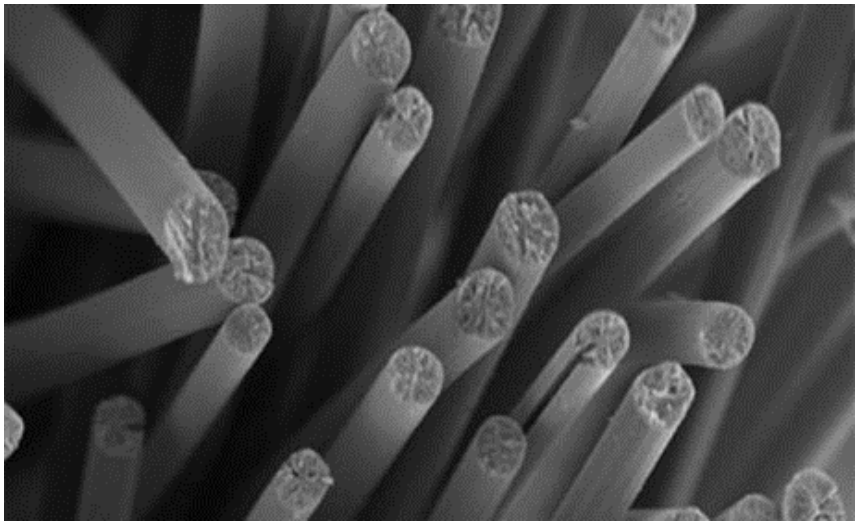

Figure 5-1 Carbon fiber cross section

CF is the first and one of the most commonly used conductive materials to fabricate self-sensing concrete. The addition of CFs leads to a good relationship between the FCR of concrete and the applied load (Chen and Chung 1993). In addition to self-sensing ability provided by CFs,

it also has been recognized that cement-matrix composites containing CFs show attractive improvements in various mechanical properties, including compressive strength, tensile and flexural properties, toughness, low drying shrinkage, high corrosion resistance, and low crack development (Azhari and Banthia 2012; Chung 2000b; Huang 2012). Carbon fibers were used as conductive admixtures in this experiment

5.2.2.2 Carbon black

Carbon black is another commonly used conductive admixture, since it has good electrical conductivity, low price and its being in the form of porous agglomerates of nanoparticles. Carbon black particles are ball-shaped, and the typical diameter is 30~120 nm. Compared to carbon fibers or nanofibers, carbon black exhibits good spreadability which helps the electrical connectivity and leads to very low resistance of the compact of carbon black and manganese dioxide (Wen and Chung 2007b). When carbon black is used with other fiber materials, it is noticed that carbon black can fill the microscopic space between adjacent fibers due to its small size.(Wen and Chung 2007b).

Previous research (Wen and Chung 2007b)shows that CFs have better strain sensing capability than carbon black. Partial (i.e., 50%) replacement of CFs by carbon black not only reduces the cost, and improves the workability, but also the electrical conductivity and the electromagnetic interference shielding property are maintained at the same time. However, the partial replacement weakens the effectiveness of strain sensing. However, another study (Han and Ou 2007) provides quite different results: cementitious materials containing both CFs and carbon black shows more stable self-sensing ability and better repeatability and sensitivity than materials only containing CFs.

Besides, total replacement of CFs by carbon black decreases the ability of conductivity and the shielding properties of the material. It has no effect on the compressive strength, but results in

the reduction of effectiveness of strain sensing and compressive modulus as well as the increase of the compressive strain at failure(Wen and Chung 2007b). Compared to replacement, adding an extra amount of CFs to carbon black reinforced cement reduces the compressive strength, strain at failure.

5.2.2.3 Carbon nanotubes (CNTs)

CNTs were first found by Sumio Iijima in 1991. It is one of the most important materials in nanotechnology with size ranging from 0.4 to 100 nm in diameter and from nanometers up to millimeters in length. The nanostructure of CNTs is rolled graphene sheets that can be either in the form of a single-walled nanotube (SWCNT) or a nanotube of multiple walls (MWCNT). Figure 5-2 shows the structure of both SWCNTs and MWCNTs.

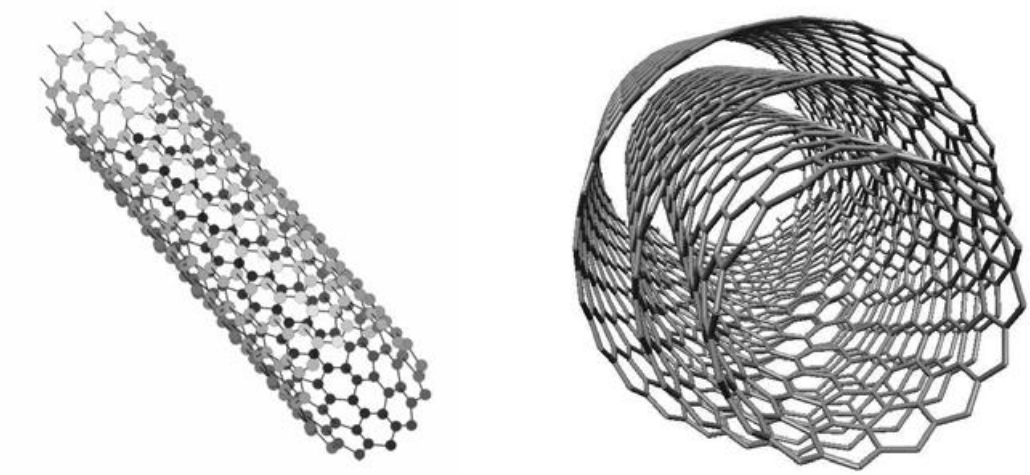

(a) (b)

Figure 5-2 (a) Single-walled carbon nanotube; (b) multi-walled carbon nanotube (Azhari 2008)

CNTs have extraordinary mechanical and electrical properties, such as large elastic modulus, high strength and great electrical conductivity (Li et al. 2007). However, the good piezoresistive property is the most important feature for the material's application in health monitoring of concrete structures (Azhari 2008; Li et al. 2007). Moreover, the combination of

CFs and CNTs exhibits better signal, reliability, and sensitivity than sensors containing CF alone (Azhari and Banthia 2012).

5.2.2.4 Graphite nanoplatelets (GNPs)

GNP is another form of carbon-based nano-particles made from graphite. Natural graphite is a layered compound comprising a series of stacked parallel two-dimensional graphene layers (Pierson 2012). The cost of GNPs is much lower compared with other nano-materials such as CNTs.

GNP is a 2D platelet consisting of a few to several graphene layers that are 1 to 15 nanometers thick and the particle diameter ranging from submicron up to 100μm. They can make the composites reach certain mechanically reinforcement and conductivity level with low content due to their high surface-area-to-volume ratio and aspect ratio. GNP preserves the anisotropic feature as graphite and has excellent mechanical and electrical properties along the basal plane (Huang 2012).

Previous studies (Pang et al. 2014) have shown that GNP reinforced concrete has good electrical conductivity, in addition to its benefits on improving the durability of concrete. Moreover, GNP reinforced composite exhibits a great piezoresistivity behavior when subjected to cyclic compressive and tensile loadings and has a reliable damage-sensing ability which is demonstrated by comparing the electric potential change and the change in elastic compliance(Le et al. 2014; Pang et al. 2014).

5.2.2.5 Graphene

First produced in the lab in 2004, graphene is carbon-based one atom thick material. It has many excellent features, including extremely high strength-to-weight ratio, great thermal and

electrical conductivity effectiveness, high surface area, high modulus of elasticity and ampi-polar electric field effect (Sedaghat et al. 2014).

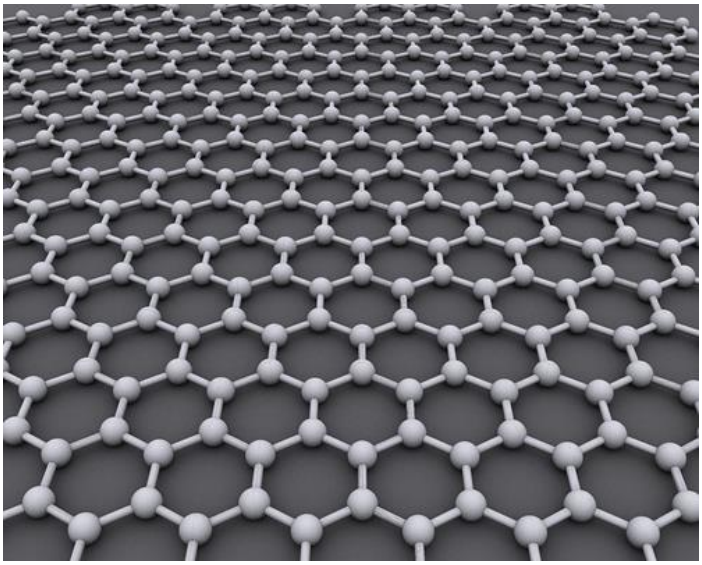

Figure 5-3 Graphene

Graphene is a new material and only a few studies for its application in Cementitious Composites are available. The results of one research (Sedaghat et al. 2014) indicated that the graphene reinforcement in cementitious materials improves the thermal and electrical properties of the hydrated cement which means thermal cracking in early age may be reduced and the durability of the concrete is improved. Another study (Gong et al. 2014) showed that many properties could be changed by the addition of graphene, including reduction of the workability, enhancement of the degree of hydration, refinement of pore structure, and improvement of compressive strength and tensile strength.

5.2.3 Self-sensing capability

5.2.3.1 Compressive loading

A number of experiments (Azhari and Banthia 2012; Chen and Chung 1996; Chung 2000b; Du et al. 2013; Fu and Chung 1998; Han et al. 2008; Pang et al. 2014; Wen and Chung 2007a; b; Yang et al. 2012) have been conducted to study the self-sensing ability of concrete under compressive loading. The reliability of measurement, such as reversibility and repeatability of resistivity measurements subjected to cyclic loading was also investigated. All findings indicated that the FCR is always reduced with the increase of loading level. The self- sensing patterns for different admixtures are very similar and are shown in Figure 5-4.

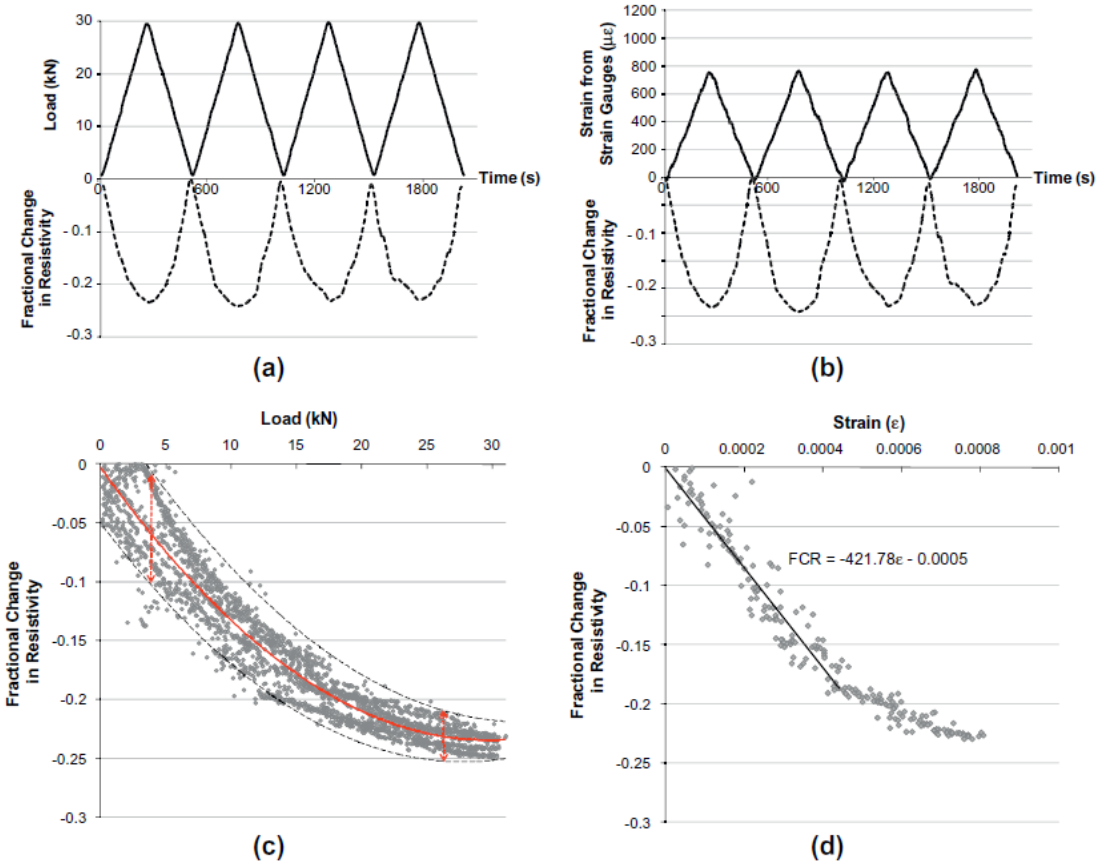

Figure 5-4 Cyclic compression response of self-sensing concrete, (a) FCR vs. load; (b) FCR vs. traditional strain; (c) FCR – load correlation; and (d) FCR – strain correlation.(Azhari and Banthia 2012)

The reversible behavior of the change in piezoresistivity is a key factor in the argument that smart concrete can be a viable self-sensing cementitious composite. The gage factor which

indicated a direct relationship between the applied strain and the measured FCR is different for different conductive mixtures and is not always a constant. With reliable FCR, the smart concrete member can be applied in a structure to monitor the deformation state of the structure. However, there are several issues that need to be resolved. The first one is that the gage factor is a rate dependent parameter instead of a constant and it could be very small under low loading rate. The second one is poor accuracy and repeatability.

5.2.3.2 Tensile loading

As indicated in Figure 5-5, there is also a direct relationship between the applied strain/stress and the FCR. However, unlike compressive loading, the FCR always increase with the increase of tensile loading level.

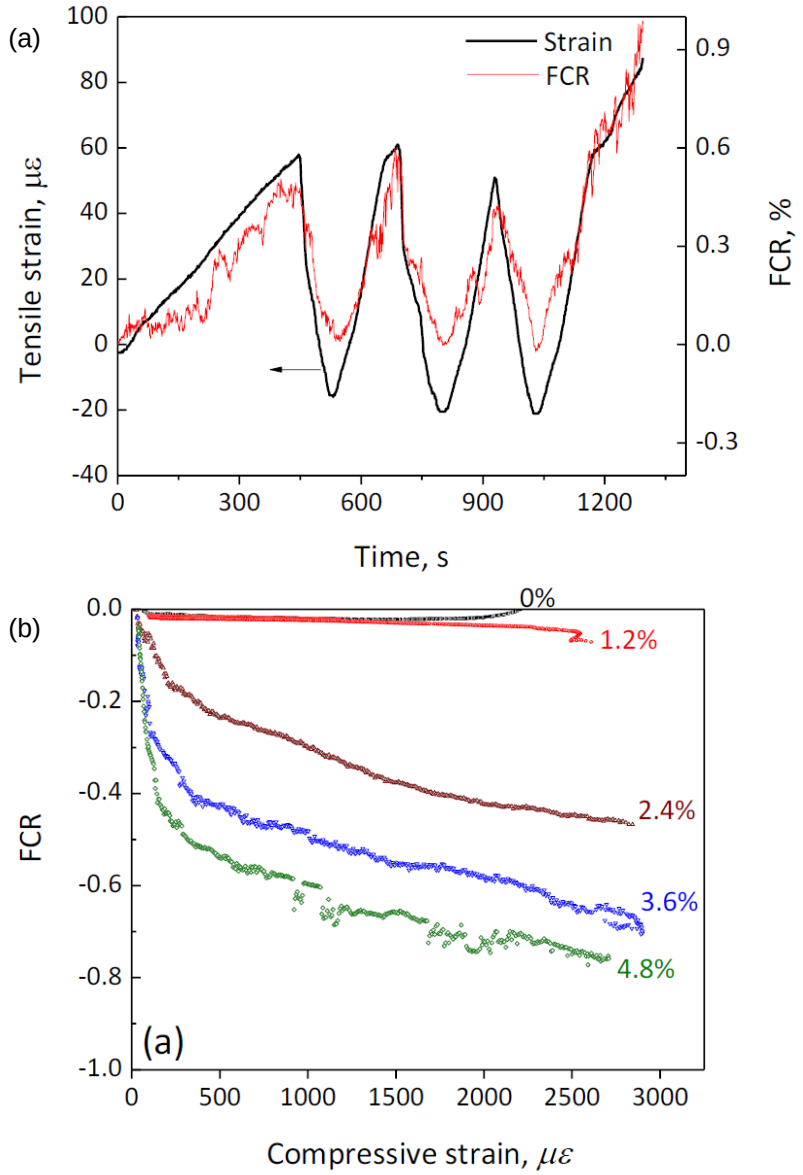

Figure 5-5 Cyclic tension response of self-sensing concrete, (a) FCR vs. traditional strain; (b) FCR – strain correlation. (Pang et al. 2014)

5.2.3.3 Damage sensing

By continuously measuring electrical resistance and the deformation of the specimens, the extent of damage can be figured out by observing the shape of the curve shown in Figure 5-6. The curve can be divided into three successive segments: no damage, minor damage and onset of failure. At a low loading level, the decrease of electrical resistance is mainly owing to the assumed "push-

in" effect, tunneling effect with smaller space between the fibers and higher opportunity for CFs to contact each other. Then, minor damage develops, and a relatively stable electrical resistance is reached. At a high loading level, extensive development of damage leads to the rising of the curve and failure of the material. The damage is reflected as the development of cracks and voids in the concrete, and the cracks and voids are considered as not conductive.

Some studies (Le et al. 2014; Pang et al. 2014) focused on the damage sensing ability of self-sensing cementitious composite by using the electric potential method and notched prisms. Good agreement was reached by comparing between results of the experiment and finite element simulations.

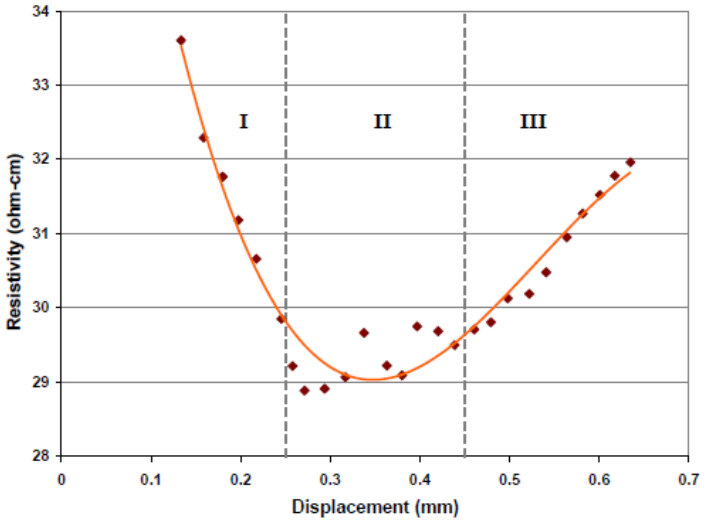

Figure 5-6 Response of self-sensing concrete to vertical displacement under flexure (Azhari 2008)

Moreover, the damage-induced fractional change in electric potential is equivalent to the fractional change in elastic compliance. This feature is very useful for the evaluation of structural health. Figure 5-7 shows one of the experimental results.

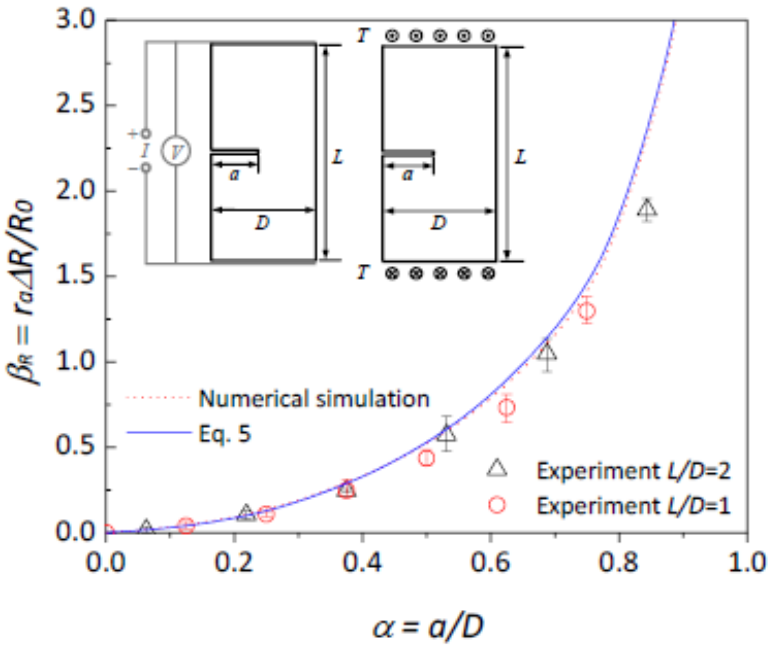

Figure 5-7 Comparison of experimental, numerical and analytical results of damage sensing for GNP reinforced cement mortar (Pang et al. 2014).

However, in order to discover any unexpected structure issues, the real-time structure monitoring system must run continuously which results in an increase in the costs and thus very limited usage of such monitoring techniques. Hence, a monitoring technique with the damage-memorizing ability is very useful, which means that a previously occurred damage can be still detectable even when the applied loading causing the damage is removed (Huang 2012).

Comparing with CF reinforced cementitious composite, CNT, and carbon black reinforced cementitious composite can sense internal damage at a much smaller scale, and hence have higher gage factors. Particularly, the conductive system in the cement-based strain sensor composed by carbon black particles was found to be very sensitive to damage in concrete (Xiao and Li 2006).

5.2.3.4 Fundamental mechanisms and theoretical modeling

Many researchers have tried to explain the self-sensing mechanism of carbon fiber cementitious composite theoretically. So far, there are two major theories.

(1) The research of Professor Chung D.D.L. (Chung 2003) provided an explanation that under loading or unloading, CF is “push-in” the cement matrix or is “pull-out” which results in the variation of the contact resistance between CF and the matrix. Based on the concept the slight pull-out of the so-called “crack-bridging fibers” during loading and the increase of the contact electrical resistivity of the fiber–cement matrix interface lead to the piezoresistivity behavior of smart concrete, a theoretical model (Wen and Chung 2006; Zhu and Chung 2007) was proposed to calculate the self-sensing cementitious composite piezoresistivity behavior. The comparison between theoretical and experimental results obtained under tension, compression, and flexure showed a good agreement as illustrated in Figure 5-8.

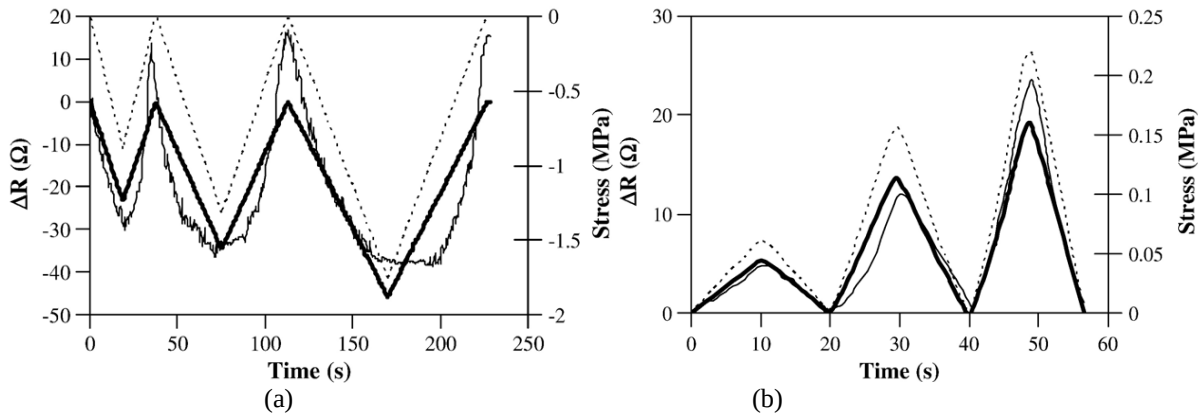

Figure 5-8 Comparing the measured and theoretical values of FCR under (a) uniaxial compression, and (b) uniaxial tension (Wen and Chung 2006)

(2) Some other studies (Hussain et al. 2001) explained the self-sensing mechanism with a quantum mechanical phenomenon called “tunneling effect”. The basic idea is that under compressive loading, the distance between conductive admixtures reduces, which leads to the decrease of the tunnel width and increase of the tunnel current, resulting in a decrease

of electrical resistance of cementitious composite at the macro scale. Besides, the electrical resistance of cementitious composite increases under unloading process.

Although the two theories discussed above explained the self-sensing mechanisms from different perspectives, they share the same fundamental point: electrical resistance of cementitious composite decreases under compressive loading, and increases during the unloading process. There are serval theoretical models (Xiao et al. 2010; Xu et al. 2010) developed based on this fundamental point to predict the piezoresistivity behavior of smart concrete under different loading and environmental conditions.

For CNT reinforced cementitious composite, the self-sensing mechanism is similar to that of CF cementitious composite, except that the proposed mechanisms such as "push-in" and "pull-out" effect, tunneling effect, and the degradation of conductive network due to damage occur at the nano-scale. Furthermore, since the nanostructure of carbon black is ball-shaped, the first theory is not valid for carbon black reinforced cementitious composite. There was a simpler self-sensing mechanism that was related to the compressive stress level and the change of electrical resistance for carbon black reinforced cementitious composite. While the relationships between compress stress level and the change of electrical resistance are non-linear for CF or CNT reinforced cementitious composite, the relationship is almost linear for the cementitious composites reinforced with carbon black (Xiao and Li 2006).

5.2.4 Influential factors

The effectiveness of self-sensing ability of smart concrete can be influenced by a wide range of factors, including not only the internal factors but also environment and testing techniques.

5.2.4.1 Conductive admixture Content

As stated earlier, cementitious composites become conductive due to the addition of conductive admixtures. It was generally accepted that the electrical conductivity could be further improved by increasing conductive admixtures content in the composites. However, many studies (Azhari 2008; Chung 2000a; Du et al. 2013; Le et al. 2014; Pang et al. 2014; Yang et al. 2012) have found that once the volume fractions of the admixtures reached a certain threshold value, the addition of conductive admixtures cannot further effectively improve electrical conductivity and enhance self-sensing ability anymore. Experimental results showed that the relationship between conductivity/resistivity and fraction of conductive admixtures is nonlinear, as illustrated in Figure 5-9. Since the improvement in electrical properties of the composite is related to the formation of a network formed by the admixture, the critical volume fractions can be considered to be linked to the connectivity limit or percolation limit of the network.

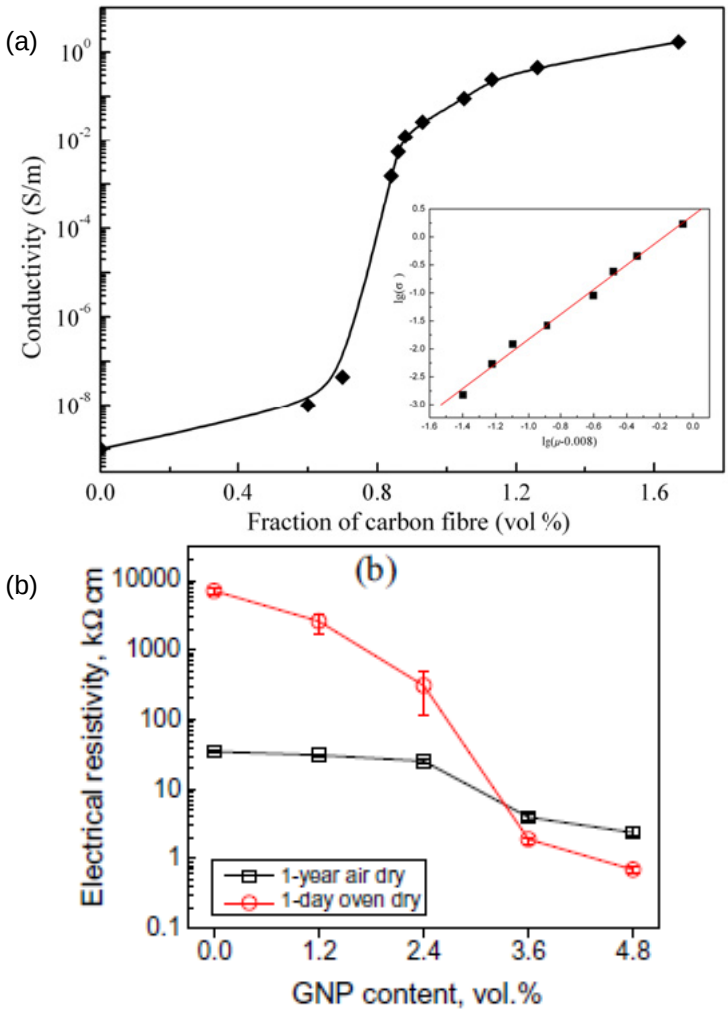

Figure 5-9 Percolation phenomena (a) CF reinforced materials (Yang et al. 2012), and (b) GNP reinforced materials (Le et al. 2014)

Xie et al. (Xie et al. 1996) described percolation phenomena using the concepts of threshold and post-threshold. The conductivity boosts by several orders of magnitude until the volume fraction of conductive admixtures reaches or goes beyond a critical value which is called the percolation threshold. When the volume fraction passes this critical value, the electrical conductivity of the composite will only increase slightly with the addition of conductive admixtures, which means the specimen is in the post-threshold region. Most percolation threshold values are located between 1% vol. to 4% vol.

In addition, as shown in Figure 5-9 (b), when the conductive admixture content goes beyond a percolation threshold, moisture content shows less influence on the electrical resistivity of the self-sensing concrete, which means the damage-sensing ability is more reliable for practical applications (Le et al. 2014).

It is also noted that size and shape of conductive admixtures can influent the percolation threshold as well. For example, the longer the fibers (to a certain extent), the lower the percolation threshold (Chiarello and Zinno 2005).

5.2.4.2 Curing time

During the process of cement hydration, the microstructure of the cement paste changes, resulting in the increase of resistivity for cementitious composite over time. Some researchers (Azhari 2008)investigated the impact of curing time on resistivity, and the findings showed that the electrical resistivity of all CF reinforced specimens increased with curing time first, then, became nearly constant after a certain amount of time depending on the admixture content. This increase is more significant in specimens with smaller amounts of admixture.

One study (Galao et al. 2014) showed that strain-sensing behavior is not noticeable in any of the samples for curing ages up to 14 days, independent from the current intensity applied. However, a relationship between the stress level and electrical response is clear for samples of a curing period of 28 days. Figure 5-10 shows some results of this study about the influence of curing time upon strain-sensing ability.

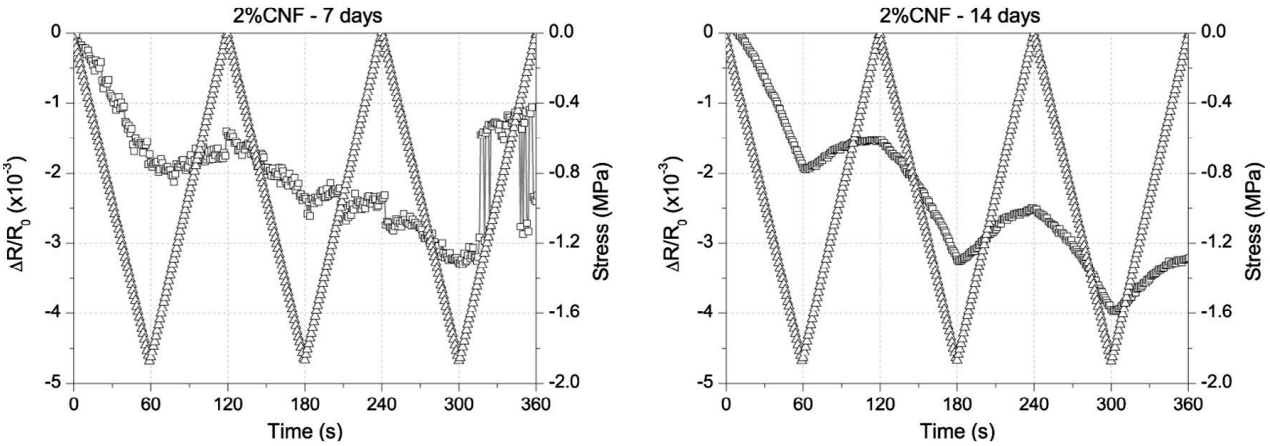

Figure 5-10 Strain-sensing tests for at different curing ages (Galao et al. 2014)

Another study (Chung 2000b) indicated that greater reversibility under cyclic loading and less noise in the resistivity variation at 28 days were observed than that at 7 days for the self-sensing cementitious composite. In practice, concrete is usually fully cured (i.e., more than 28 days of curing). Therefore, the behavior at 28 days is much more important.

5.2.4.3 Loading level and rate

The loading level is very critical to the self-sensing behavior of cementitious composites, since microstructure of the composite is changed during the loading process. It was observed that when the compressive loading amplitude passes a certain value, for example, more than 40% of the ultimate strength, the deformation exceeds the elastic region, and the response of the electrical resistance of samples to plastic deformation is irreversible (Han and Ou 2007). Moreover, loading level also has an impact on the sensitivity of self-sensing behavior of cementitious composites. Results of previous studies (Galao et al. 2014) indicate that gage factor increases with the increasing compressive loading level.

The research conducted by Chung (Chung 2000b) showed that the greater the loading amplitude, the larger and the less reversible is the damage-induced resistance increase. If the

loading amplitude has been reached before, the resistance induced by damage increase is small, unless the level of damage is large. When the damage is extensive, the increase of resistance induced by damage occurs in every loading cycle, even at decreased loading amplitudes, and it can overshadow the strain-induced resistance decrease. Hence, the increase of resistance induced by damage occurs mainly during loading (even within the elastic regime), particularly at a loading level higher than that in prior cycles, unless the loading amplitude is high and/or damage is extensive.

Another important parameter is loading rate. During the static compressive process, FCR decreases with the increase of loading rate (Chung 2003). It was demonstrated that the loading rate could not affect the calculated gage factor (Galao et al. 2014). This is important for traffic monitoring applications. The reason is that if the self-sensing behavior of materials is absolutely independent of the loading rate, it will also be independent of the driving velocity of vehicles.

5.2.4.4 Current and Electrode

The simplest way to measure resistivity is to apply direct current (DC) during the test. However, it has been demonstrated that the DC measurement of electrical resistivity is not straightforward due to the significant polarization phenomenon which results in an exponential rise in the measured value of resistivity (Hou and Lynch 2005). In order to diminish the polarization phenomenon under DC measurement of electrical resistivity, two methods are usually used in practice. One method is to measure the changing values of electrical resistivity of the actual sample under loading and a control sample at the same time and then subtract the latter values from the former values. Another way is to apply a DC signal prior to loading the specimen in order for the electrical resistivity to reach a plateau due to complete polarization as illustrated in Figure 5-12 (d). Besides, since sample geometry can affect its polarization behavior, a large sample takes

more time to fully polarize (Hou and Lynch 2005). Another option is to use Alternating Current (AC) instead of DC. If AC is used, high frequency is recommended to minimize the polarization phenomenon (Azhari 2008).

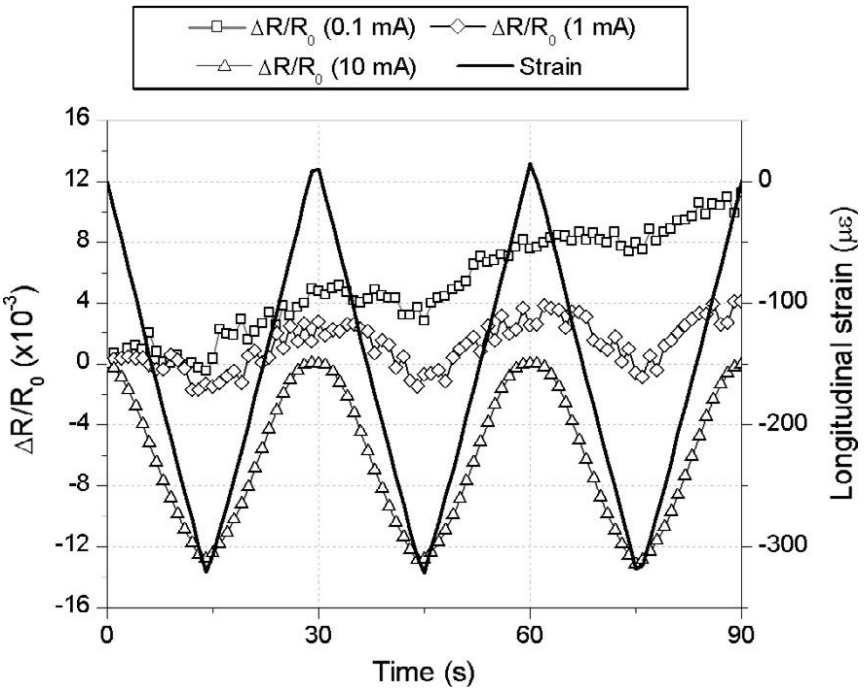

Figure 5-11 FCR and longitudinal strain, versus time, for cement pastes strain-sensing tests, for different current intensities. (Galao et al. 2014)

For DC measurement, a certain current density level is needed to make the behavior of the specimens reversible. Figure 5-11 shows the FCR and strain change over time at three different electrical current densities (0.1 mA, 1 mA, and 10 mA). 10 mA results in the best reversibility on the measures and the clearest and reliable correlation between FCR and compressive strain (Galao et al. 2014).

Electrode materials also have an influence on the measurement. A study (Azhari 2008) indicated that embedded copper mesh exhibited a better performance as an electrode material for self-sensing cementitious composite. However, for compression test using the cylindrical specimen, copper wire and silver paste were the only choice for the setup.

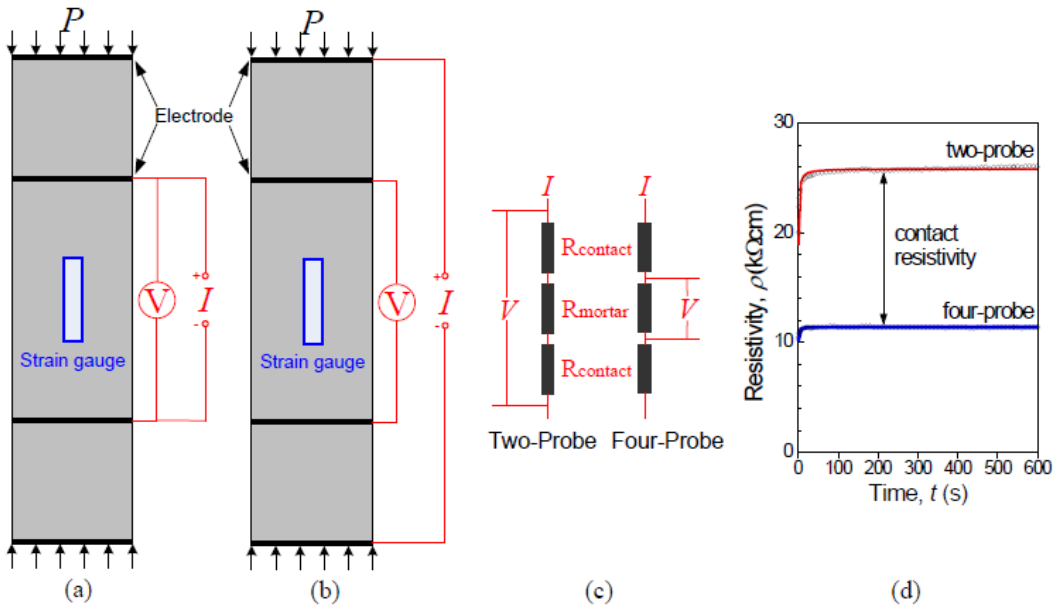

Figure 5-12 Electrical resistance measurement (a) two-probe set-up; (b) four-probe set-up; (c) equivalent circuit representation; and (d) typical test results. (Du et al. 2013)

In addition to the currents and the electrode materials, the number of probes is also very important for the measurement of electrical resistance. There are two basic methods to measure the electrical resistance: two-probe and four-probe methods. It was proven (Du et al. 2013) that the former method creates much higher contact resistance than latter method. Therefore, the four-probe method is more appropriate for electrical resistivity measurements of cement-based sensors. As shown in Figure 5-12 (d), the four-probe method can reduce the polarization effect.

In addition, for cement-based strain sensor made by CF reinforced cement under compression, in the elastic regime, the four-probe method is more effective than the two-probe method for electrical resistance measurement because the four-probe method offers higher gauge factor and less sensitivity to the applied strain amplitude (Wen and Chung 2007a). Therefore, the four-probe method will be used in this experimental study.

5.2.4.5 Environmental variables

It has already been observed that the electrical resistivity decreased upon heating and increased upon cooling at a certain range of temperature (Azhari 2008; Chung 2003, 2000b). This can be used to correct the measurement of the cement-based sensor when the environment temperature is not stable. While the temperature is above zero degree Celsius (i.e., without freezing and thawing), the electrical resistivity variation is reversible during the heating-cooling process, although there is only a slight increase after each cycle (Chung 2003, 2000b). However, the electrical resistivity of the sample varies irreversibly during freeze-thaw cycling, and the hysteresis becomes more significant cycle by cycle (Chung 2003). The test results show that both upper envelope and lower envelope of the loop upshift upon freezing-thaw cycling, but the former one upshifts more which means there is more serious damage during the freezing process than the thawing process. The phase transformation of water at zero degree Celsius results in a slight shift of the resistivity. The findings of a study (Xiao et al. 2010) also indicated that the temperature has a small influence on the gauge factor.

Moisture and chloride concentration were found to have considerable influences on the electrical resistivity of self-sensing cementitious composites (Azhari 2008). Shrinkage induced by the loss of moisture can also lead to the resistivity increase in the strain direction(Chung 2003).

Similar to the stain sensing capability of smart concrete, the impacts of those environmental variables on the electrical resistivity of smart concrete could be considered as the environmental sensing capabilities. Therefore, the smart concrete can also be used as temperature and humidity sensor. There are limited studies on the effect of a single environmental variable, such as temperature or moisture. There has been no study for the coupled effect among the environmental variables, which represents more realistically the service condition of structures.

5.3 Experimental program

5.3.1 Materials

Sensor: carbon fibers were used as conductive admixtures in this experiment. They are ¼" ZOLTEK PX35 unsized chopped fibers (Type-01). Their specifications are listed in Table 5-1. A photo of the carbon fiber is shown in Figure 5-13. The carbon fibers were first air-dried then exposed to ozone at 160°C for surface treatment.

Figure 5-13 Carbon fibers used in the experiment

Table 5-1 Properties of carbon fibers

Tensile Strength	Tensile Modulus	Electrical Conductivity	Density	Fiber Diameter
6.0×10^5 psi	3.5×10^7 psi	0.00061ohm-in	0.065 lb/in^3	$0.283E10^{-3}$ in

Cement: Portland cement Type I/II was used. The specific gravity of the cement is 3.15.

Water: distilled water was used. The mix designs for the six groups will be discussed later. The higher w/c was used for samples with higher CF content because the workability of concrete is getting worse with the increase of CF content.

Silica Fume: Sikacrete 950DP was used as a densifier and dispersant in the amount of 15% by weight of cement.

Superplasticizer: in order to enhance the workability of the fresh concrete matrix, the high-range water-reducer used in the mix was Sika viscocrete 2110 in the amount of 1.2% by weight of cement.

Methylcellulose: Methocel A15 LV from Sigma-Aldrich was used to help disperse CFs in the amount of 0.4% by weight of cement and silica fume.

Defoamer: defoamer from 3M was used whenever methylcellulose is used in the amount of 0.13 vol. %.

Metal Mesh: a piece of metal mesh was cut into proper pieces and used as electrodes.

5.3.2 Mixing proportions

In addition to one control group (Group 0), ten groups of cement paste specimens were made with varying CFs volume fractions. Mix proportions for these experiments are presented in Table 5-2. The amount of CF was increased gradually from zero to 4%. Group 1 is the control group without CFs. As the content of carbon fiber increases, mixing became much more difficult. Even when the water-cement ratio was increased from 0.4 to 0.5, the workability is still not very good as shown in Figure 5-14.

Table 5-2 Mix proportions

Group I.D.	CFs (Vol. %)	No. of specimen	w/c
1	0.1	3	0.4
2	0.2	3	0.4
3	0.3	3	0.4
4	0.5	3	0.4
5	0.7	3	0.4
6	1	3	0.4
7	1.5	3	0.5
8	2	3	0.5
9	3	3	0.5
10	4	3	0.5

Figure 5-14 Bad workabilities during the fabrication of samples with 1.5% CF content

5.3.3 Mixing procedure

(1) Prepare the solution of methylcellulose.

a. Mix methylcellulose with water for about 2 min.

b. Add deformer

c. Keep mixing until the solution becomes thick and clear (takes about 10 min.)

(2) Add CFs to the solution and stirred by hand for about 2 min.

(3) Mix silica fume and cement.

(4) Add superplasticizer and the solution to the mixture and keep mixing until the mixture to form a consistent paste.

5.3.4 Specimen fabrication

The specimens were prepared in a rectangular shape. The mold dimension is 2” × 2” × 11 3/8”. After de-mold, the original samples were cut into smaller ones shown in Figure 5-15.

The fresh mixture was poured into previously surface oiled molds, and metal meshes were installed at the desired positions shown in Figure 5-15. Specimens were de-molded after 24 hours and allowed to cure for 28 days under 100% in humidity and 20 °C. Strain gages were installed after the molds were removed.

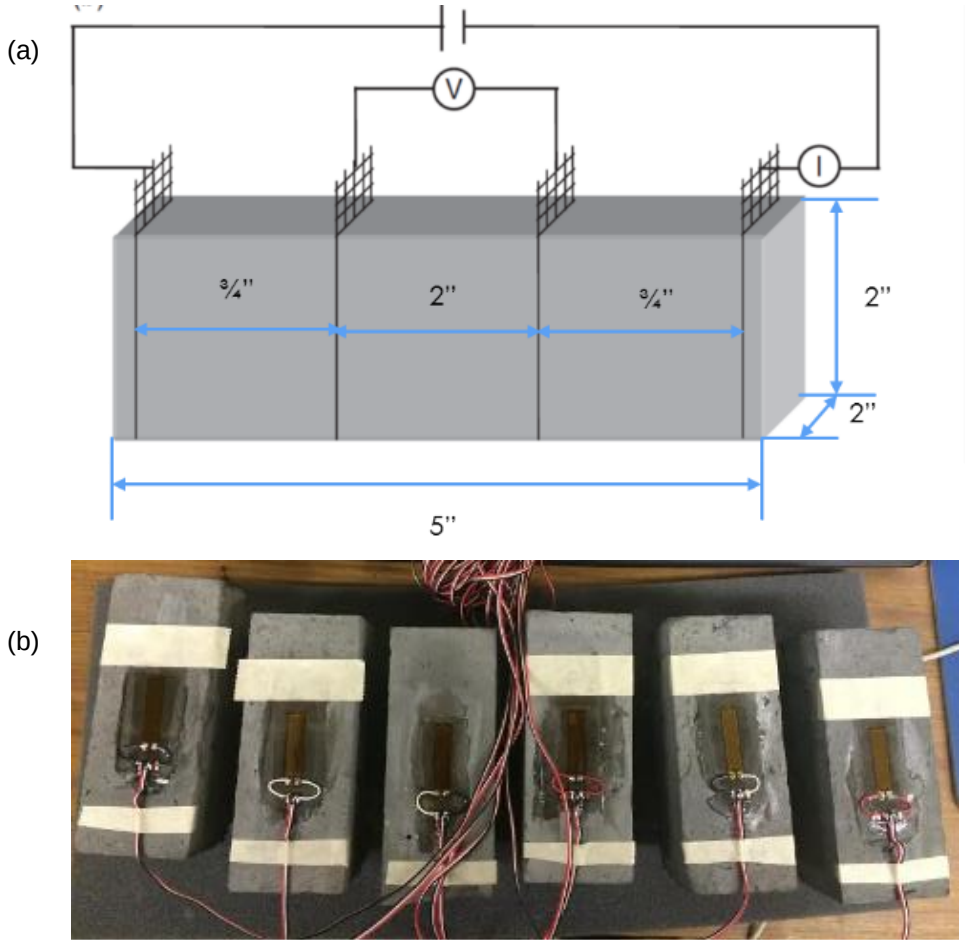

Figure 5-15 (a) Dimensions of specimens and arrangement of electrodes; and (b) Installation of strain gages

5.3.5 Experimental setup and measurements

As illustrated in Figure 5-16, the test will be conducted in an environmental chamber coupled with an MTS load frame. The chamber can produce precisely controlled conditions of temperature and humidity. Both of temperature and humidity can be set to a static value or a profile.

Figure 5-17 shows the setup of the signal measurement circuit. The strains of the sample were measured during loading with conventional strain gages, which were bonded to the middle section between the two inner electrodes on specimens. The resistance was measured using the

direct-current four-electrode method. The resistance was calculated by measuring voltage and current. The test data of strains and resistances should be concurrent.

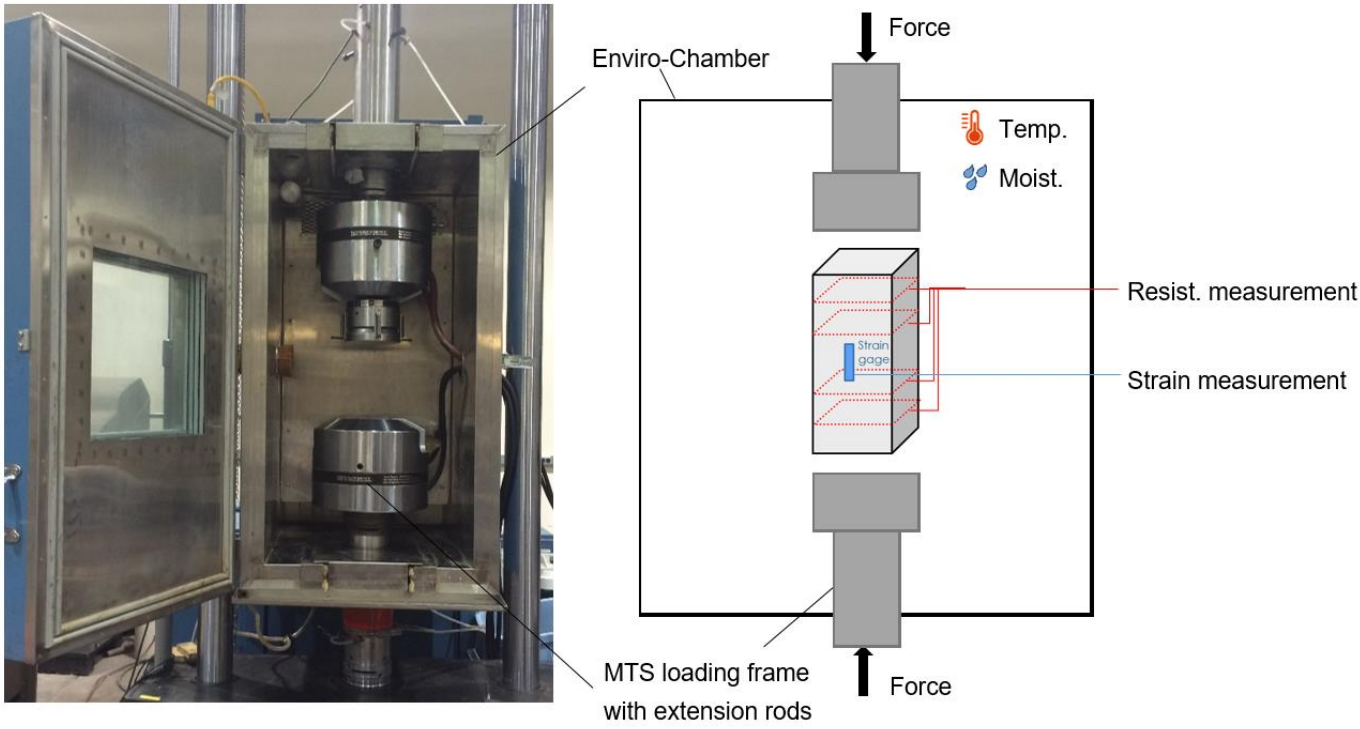

Figure 5-16 Experimental setups for studying the behavior of smart concrete

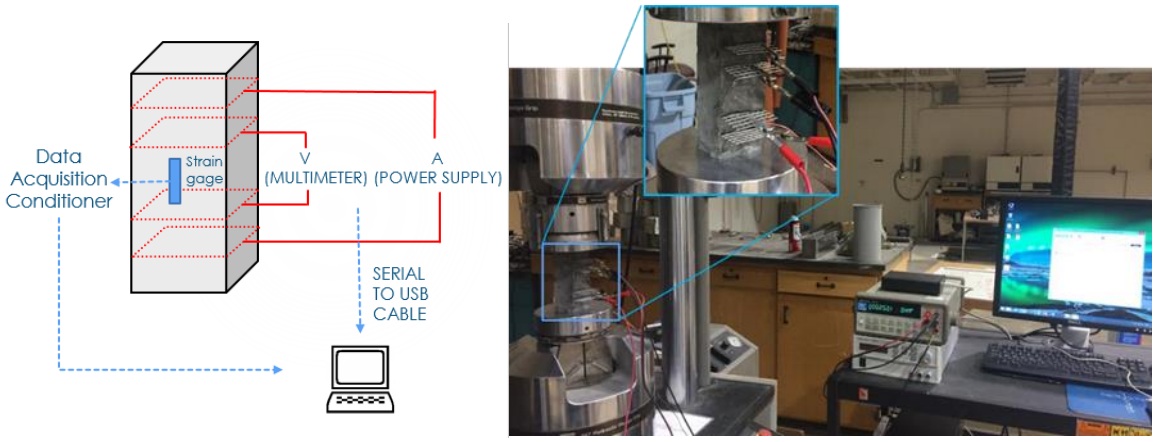

Figure 5-17 Setup of signal measurement circuit and arrangement of sensors and equipment

The equipment used in the main set of tests is as follows:

- Dual-channel RUSSELLS environmental chamber (Model RD-5-1)
- MTS load units
- Micro-Measurements EA-06-10CBE-120/E strain gages
- Micro-Measurements Model D4 Data Acquisition Conditioner
- R232 to USB cable
- HP 34401A Multimeter with test leads
- Agilent U8001A Single Output DC Power Supplies with test leads
- PC with Multi P3-D4 application software and TWedge

5.3.6 Testing configurations

First, the relationship between electrical resistivity and strain under constant temperature and relative humidity were studied. The displacement-controlled compressive loading profile is shown in Figure 5-18.

As what had been summarized in the literature review, the resistivity value of carbon fiber reinforced concrete increases with a decrease in temperature and decreases with an increase in temperature. Therefore, in order to investigate the true strain conditions within the concrete, appropriate measures need to be taken to diminish the temperature effect on the sensing ability of the sensors. As shown in Figure 5-19, a temperature profile cycling between 20 to 60 °C at a rate of 0.5 °C /min will be applied to study the temperature dependence of resistivity. The purpose of using such a low rate is to reduce the temperature gradients in specimens although it is not avoidable as shown in Figure 5-19. The temperature is controlled at the temperature range of concrete structure in an operating NPP. The responses of the specimens to the temperature will be measured. These are important tests in that the results will give us the temperature sensibilities of the material.

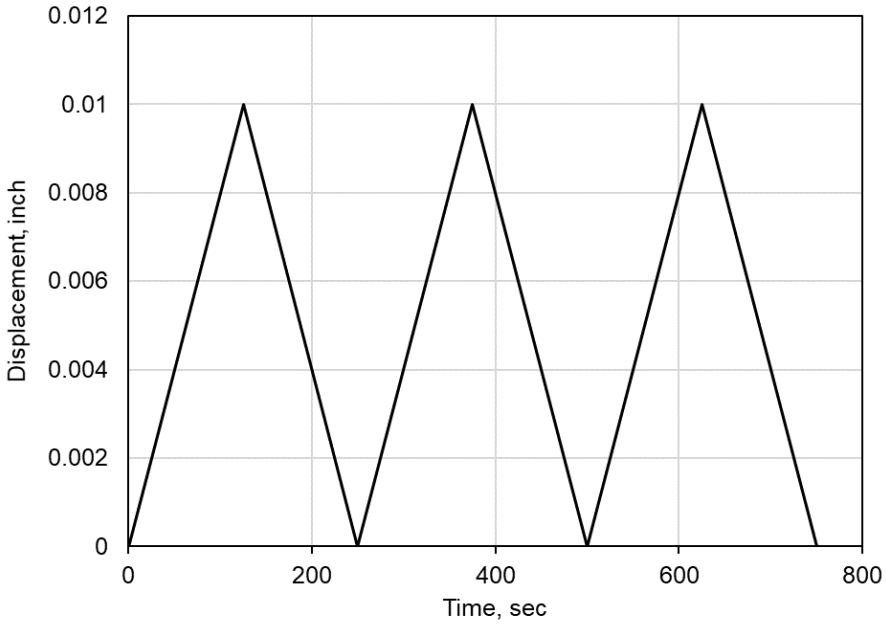

Figure 5-18 Compressive loading profile

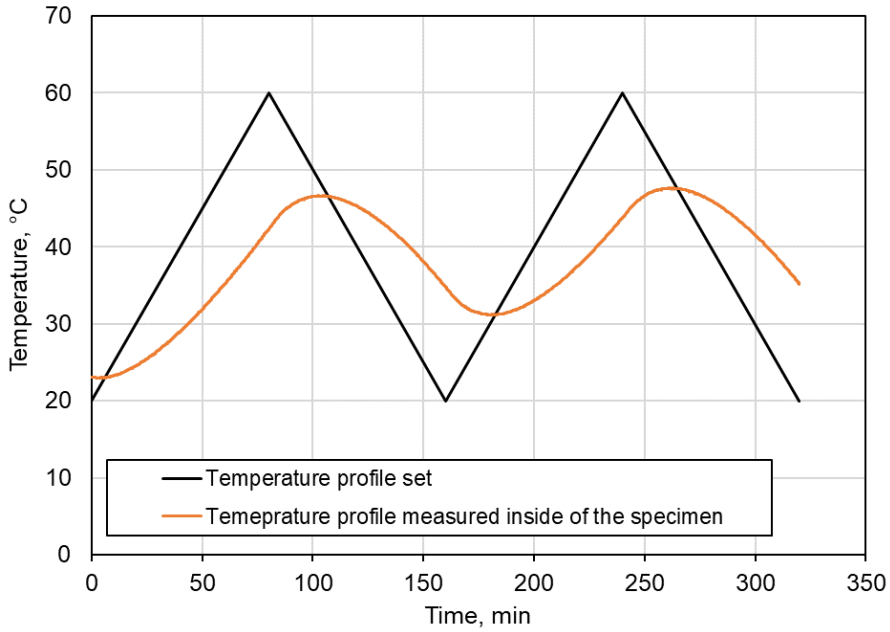

Figure 5-19 Temperature variation profiles

The specimens were air-dried for 1 year before the test. The constant current density applied to the specimens is 10 mA.

5.4 Results

5.4.1 Percolation threshold

As shown in Figure 5-20, the resistance of the specimens drops quickly with the increase of carbon fibers content. Based on these results and the workability of the concrete during the mixing process, the carbon fiber content should be no more than 1 vol. %.

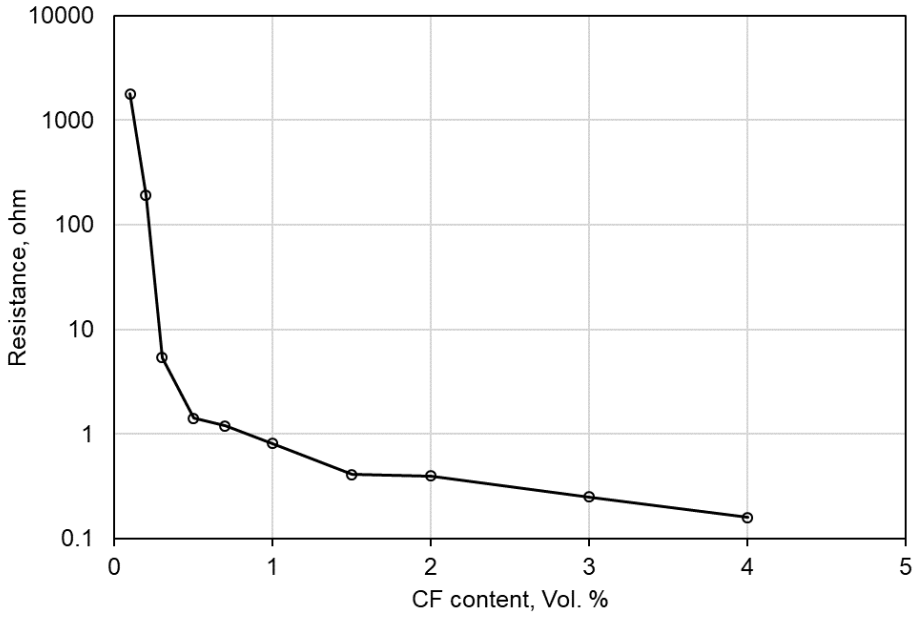

Figure 5-20 Resistance of samples v.s. carbon fiber content

5.4.2 Polarization phenomenon under DC

As mentioned earlier, although direct current (DC) is the simplest way to measure resistivity, significant polarization phenomenon during the test could occur which results in an exponential rise in the measured value of resistivity. However, in our test, the measured resistivity values for all samples decrease with time. The phenomenon for samples with 1 and 0.3 Vol. % CF content is shown in Figure 5-21 as an example. Obviously, this still will lead to a difficult

resistivity measurement procedure. A DC signal was applied well ahead of loading in order to have the electrical resistivity reaching a plateau. This procedure takes about 10-20 min.

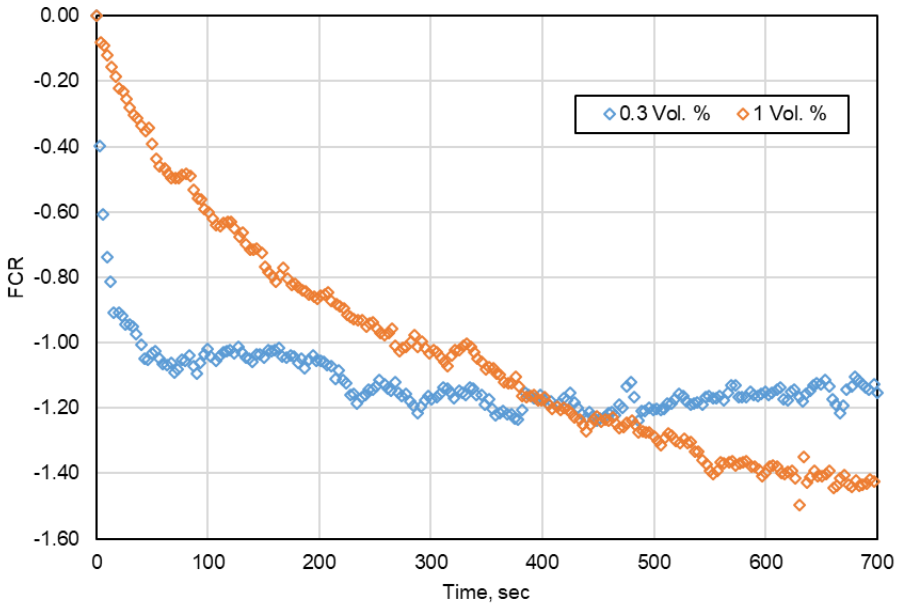

Figure 5-21 Variation of the measured resistivity with time for cement paste with 1 and 0.3 Vol. % CF content under DC

5.4.3 Piezoresistive property

Due to the workability issue of the concrete during the mixing process, the quality of concrete specimens in Group 7 to Group 10 (CF content from 1.5% to 4%) is bad. The results from these specimens are not reliable. Besides, due to its high electrical resistance, the specimens in Group 1 cannot reach 10mA current density during the test. Thus, only results of Group 2-6 are shown and discussed. Our results indicated that the FCR was reduced with increasing compressive loading level. The reversible behavior of the change in piezoresistivity was observed from samples with fiber content ranging from 0.2 vol. % to 1 vol. % as shown in Figure 5-22. The relationship between the FCR and applied strain for specimens containing different carbon fiber contents is shown in Figure 5-23. The slope for each group represents its gage factor. As one can see, the gage

factor decreases with carbon fiber content until 0.7% CF is reached then increases with carbon fiber content. The specimen with 0.2 vol. % CF has largest gage factor which means the best sensitivity. The results also show good reversibility of the strain sensing ability of the samples.

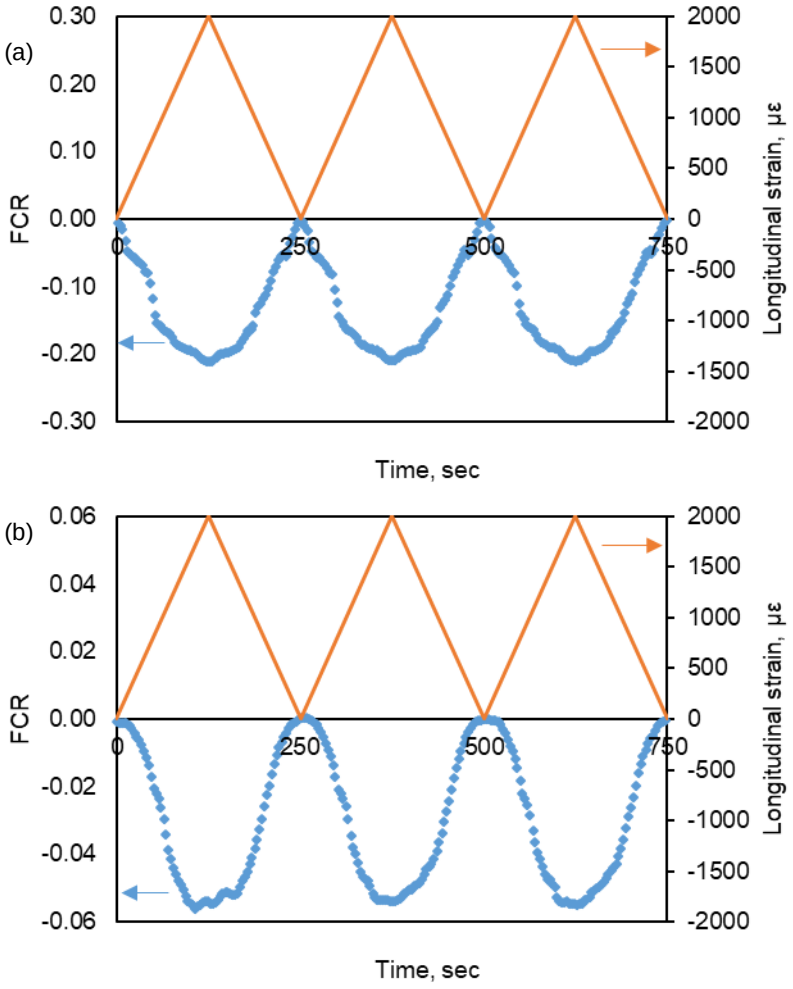

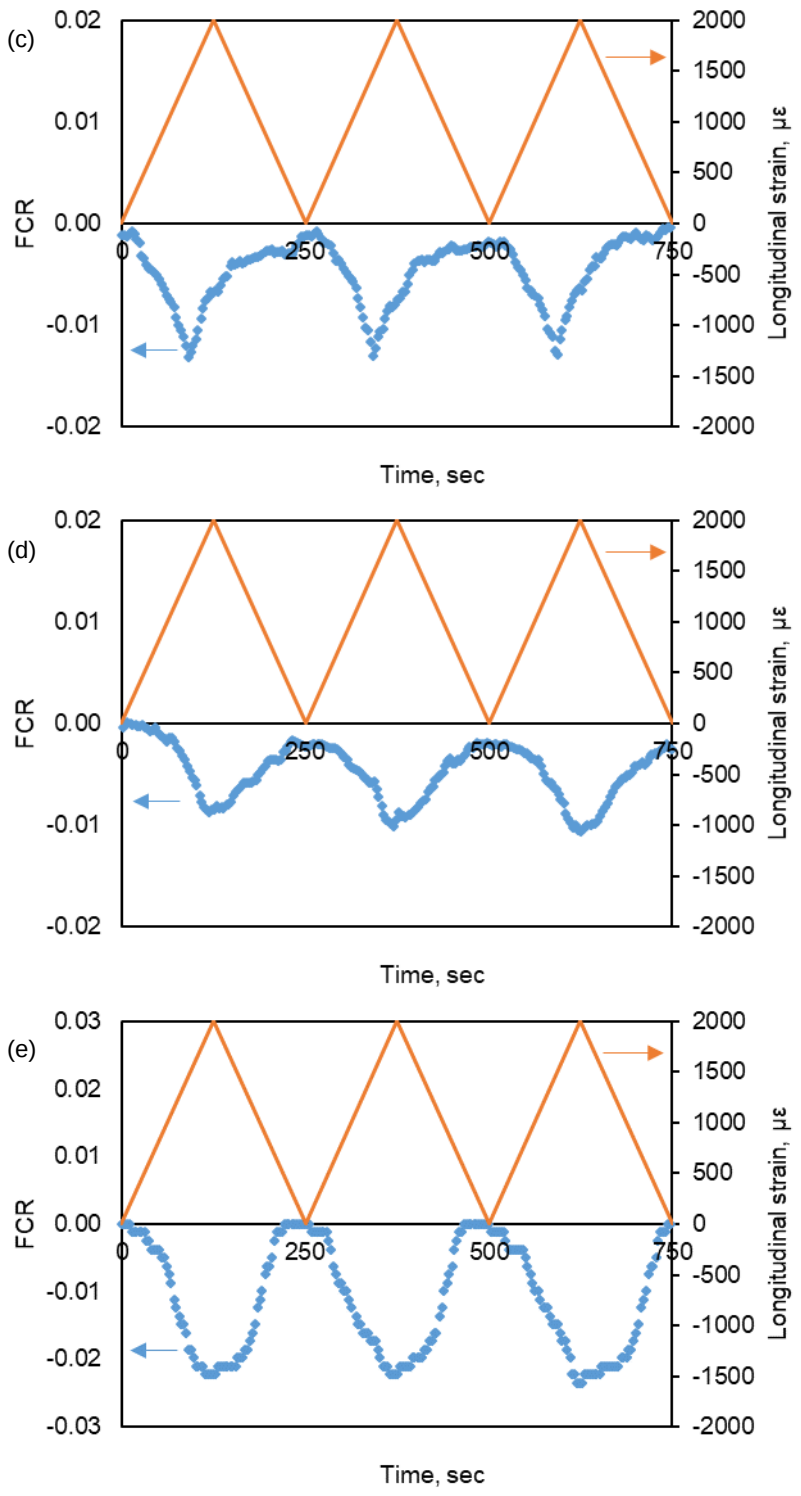

Figure 5-22 Reversible behavior of the change in piezoresistivity under external strain (a) 0.2 vol % CF; (b) 0.3 vol % CF; (c) 0.5 vol % CF; (d) 0.7 vol % CF; (e) 1 vol % CF

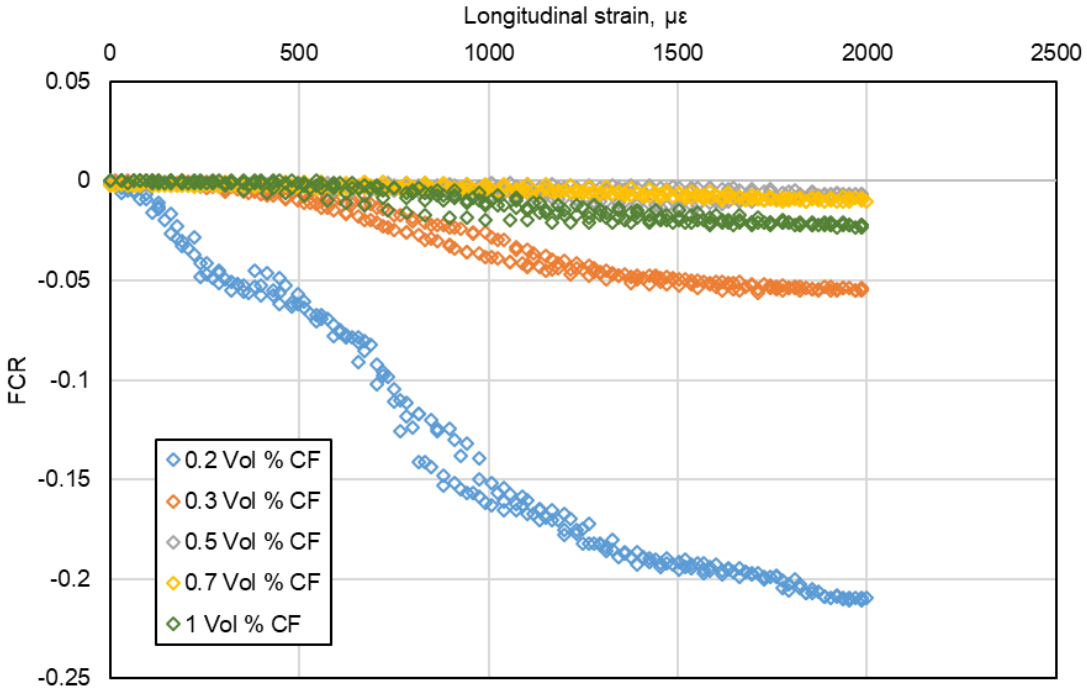

Figure 5-23 FCR as a function of strain at different carbon contents

5.4.4 Temperature effect

As one can see in Figure 5-24, the environmental temperature has a relatively strong effect on the electrical resistance of the samples. From the five figures in Figure 5-24, we can see that the electrical resistance decreases when the temperature increases, and goes up when the temperature goes down. This trend may be called negative correlation. Similar trends were also observed in other studies. The behavior is different for different CF content. The results show bad reversibility of the temperature sensing ability of the samples with 0.2 vol.%, 0.3 vol.% and 1 vol.% CF.

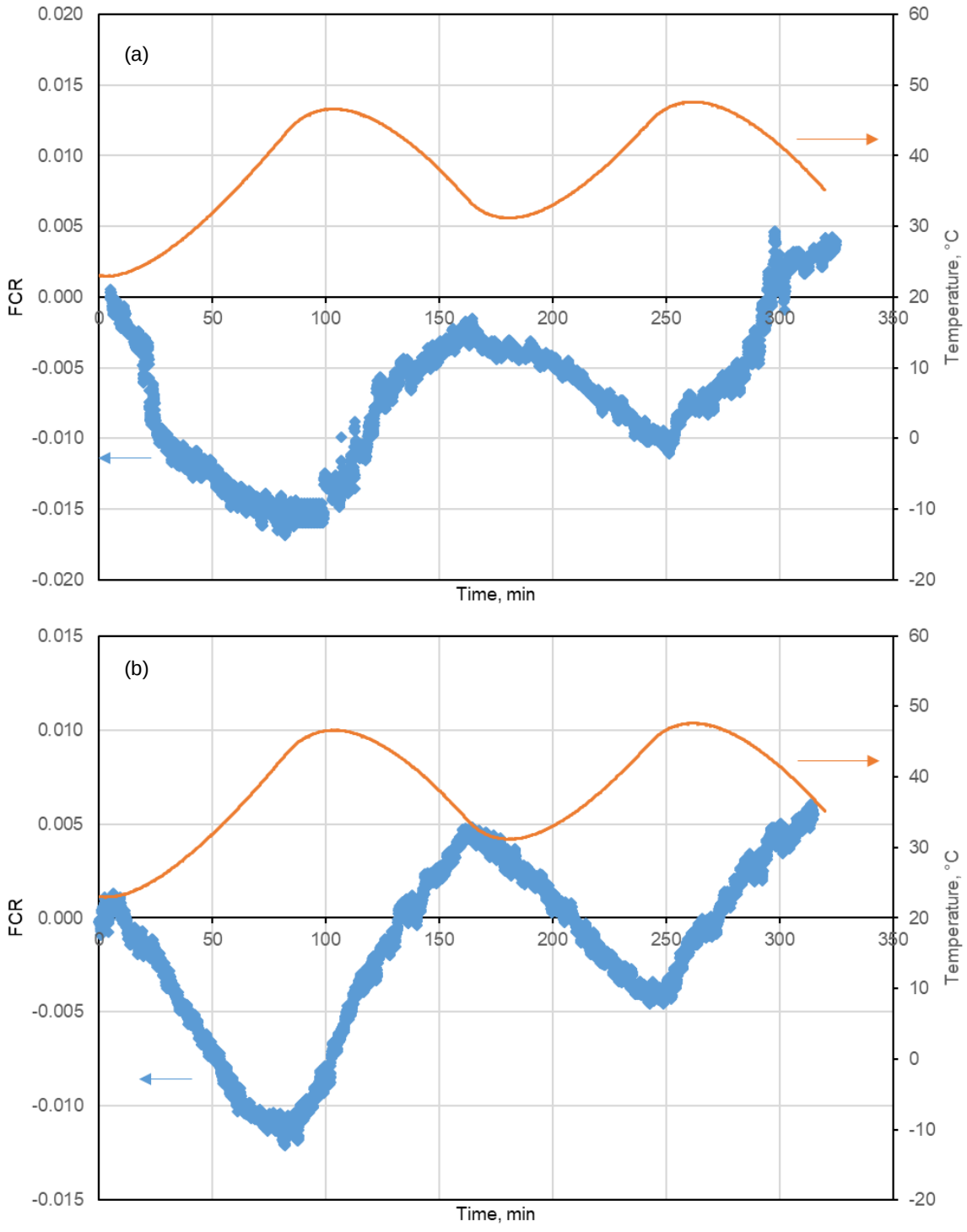
(a)
FCR
Temperature, °C
Time, min
0.020
0.015
0.010
0.005
0.000
-0.005
-0.010
-0.015
-0.020
60
50
40
30
20
10
0
-10
-20
0
50
100
150
200
250
300
350
(b)
FCR
Temperature, °C
Time, min
0.015
0.010
0.005
0.000
-0.005
-0.010
-0.015
60
50
40
30
20
10
0
-10
-20
0
50
100
150
200
250
300
350

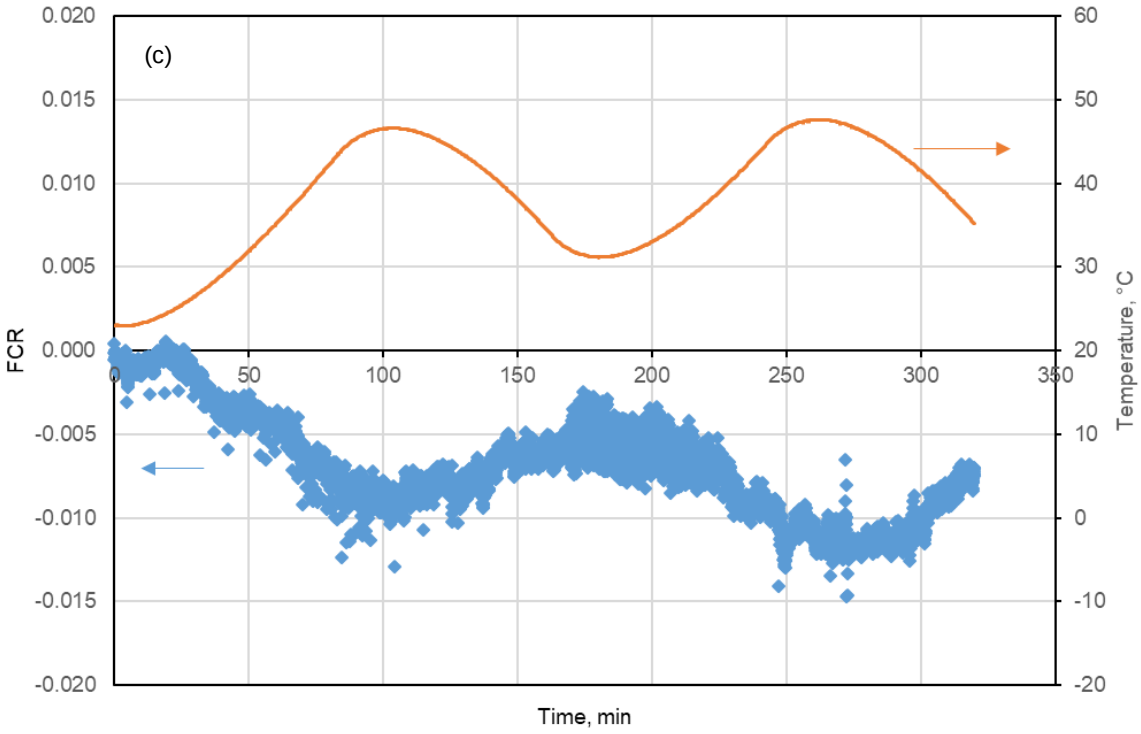
(c)
FCR
Temperature, °C
Time, min
0.020
0.015
0.010
0.005
0.000
-0.005
-0.010
-0.015
-0.020
60
50
40
30
20
10
0
-10
-20
0
50
100
150
200
250
300
350

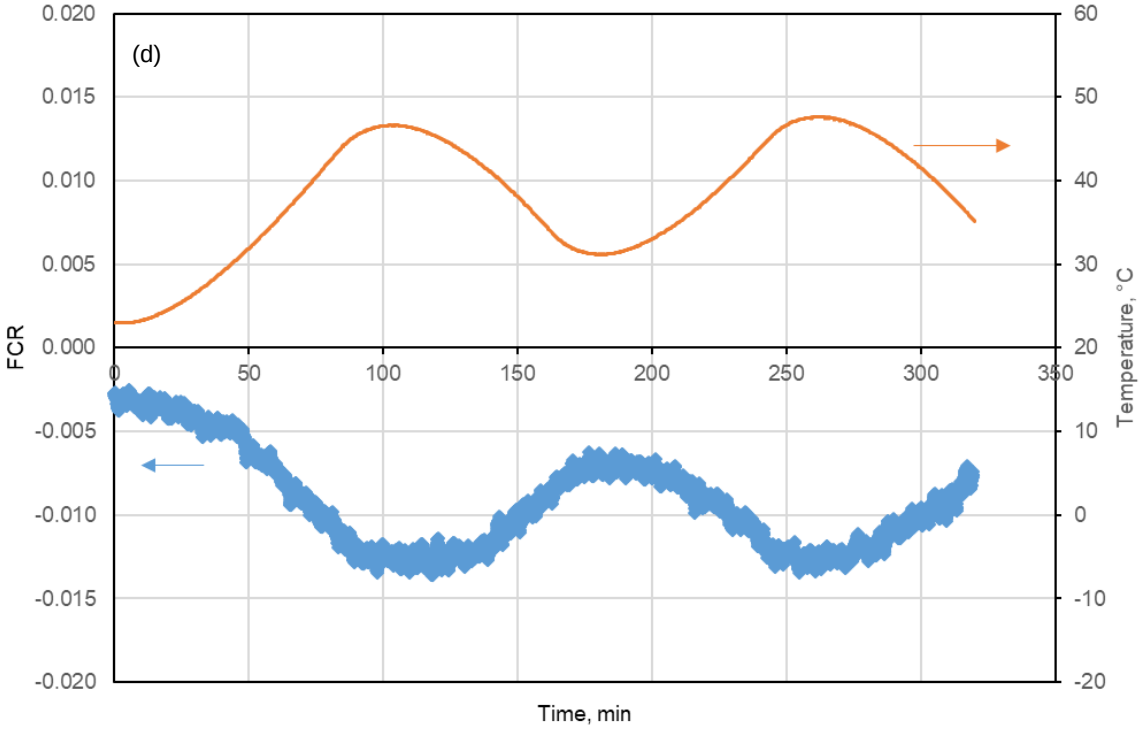
(d)
FCR
Temperature, °C
Time, min
0.020
0.015
0.010
0.005
0.000
-0.005
-0.010
-0.015
-0.020
60
50
40
30
20
10
0
-10
-20
0
50
100
150
200
250
300
350

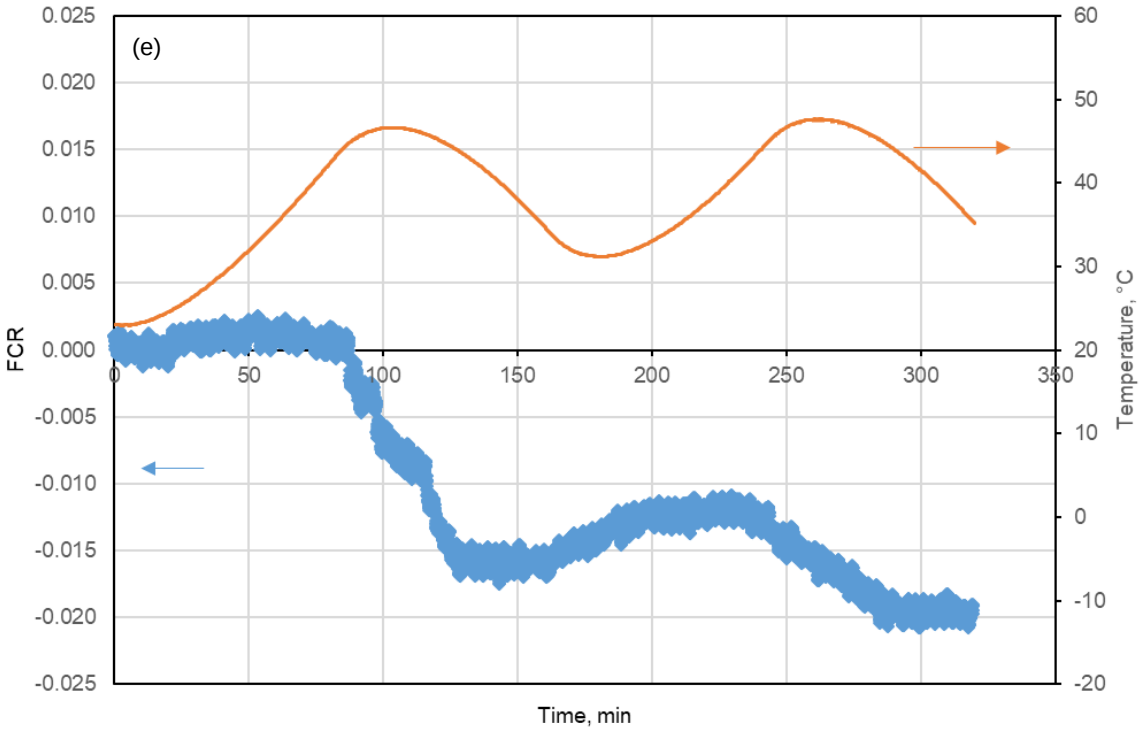

Figure 5-24 The effect of temperature variation on the electrical resistance(a) 0.2 vol % CF; (b) 0.3 vol % CF; (c) 0.5 vol % CF; (d) 0.7 vol % CF; (e) 1 vol % CF

CHAPTER 6

SUMMARY AND CONCLUSIONS

6.1 Summary and conclusions

The studies performed in this thesis mainly focus on the behavior of concrete structures and their components under the long-term neutron radiation. A model was developed first to provide a general framework that can estimate the degradation of elastic properties and volume change of concrete under neutron radiation and radiation heating and can be further improved when new experimental results become available. The second study is the first attempt to deal with the degradation of neutron and heat transport properties of concrete and its effect on neutron fluence distribution in concrete, and provides a possible way to determine the long-term neutron and thermal fields in concrete biological shielding walls. Third, a collection of articles on neutron and gamma-ray radiation damage to concrete and/or its components was acquired, and a comprehensive database including all information on testing conditions and concrete performance was built. Data analysis of the effect of neutrons, water-cement ratio, aggregate fraction, and temperature of the cementitious material was presented. Finally, investigation on the self-sensing capability of carbon fiber reinforced cementitious composites under mechanical loading and elevated temperature was conducted. Its potential to become a sensor was examined.

In Chapter 2, a theoretical model was developed to predict the deterioration of modulus of elasticity and volume change of neutron irradiated concrete. The heterogeneous internal structure of concrete was considered at five different scale levels with different constituent phases, and the

volume fractions for each constituent phase were determined based on hydration reactions of Portland cement.

During the service life of a concrete structure in a nuclear power plant, both neutron radiation and radiation induced heating have considerable effects on mechanical properties and deformation of concrete. The degradation of modulus of elasticity of a neutron irradiated concrete was used as a numerical example to verify the model prediction, and the results of model prediction agreed with the test data quite well. Based on available test data, it was concluded that neutron radiation can directly lead to degradation of elastic modulus of aggregates but has less effect on the elastic properties of hardened cement paste. On the other hand, the elevated temperature has a more significant effect on hardened cement paste than on aggregates.

There are three different types of volumetric strains in concrete under neutron irradiation: the expansion of aggregates, the shrinkage of cement paste and the thermal expansions of the two phases under the heat of neutron irradiation. It was shown that the volume change of concrete is dominated by the expanding characteristic of aggregates. A model was introduced to characterize the volume change of aggregates directly induced by neutron irradiation. For now, the shrinkage of cement paste under neutron radiation was considered only due to the loss of moisture during the heating process of radiation. The thermal strain due to radiation heating was also included in the proposed model.

The model can be used for two different scenarios. One is that the knowledge on irradiation effects of cement paste and aggregates are available, in this case, the model can be used to predict the degradation of the specific concrete based on the knowledge of the two components. The other one is that the knowledge on irradiation effect of the cement paste and aggregates are not available, in this case, the model can be used to estimate the degradation of the concrete based on its mix

design parameters and environmental conditions. An example was provided to show the applications of the model for the two scenarios.

Chapter 3 presents the prediction models for long-term neutron radiation levels in distressed concrete biological shielding walls. One-dimensional and one-speed neutron diffusion equation and the heat conduction equation were used as governing equations for prediction of neutron radiation and thermal field in concrete, respectively. The cross-property correlation theory was used together with a composite damage theory and neutron irradiation test data on the modulus of elasticity of concrete to estimate the change of neutron diffusion coefficient due to neutron radiation and thermal effects. This work is the first attempt to deal with the degradation of neutron and heat transport properties of concrete biological shielding walls and provides a possible way to determine the long-term neutron and thermal fields in concrete biological shielding walls. An ordinary concrete wall was analyzed up to 80 years of operation as a simplified example of a typical concrete biological shield in NPPs. Some preliminary findings were obtained.

Elevated temperature has considerable effects on the damage parameter of concrete. The effect of elevated temperature on distressed concrete under nuclear radiation must be considered, especially for concrete with large depth from the radiation source. The thermal conductivity of concrete under neutron radiation gradually decreases with time, and the damage and radiation heating lead to minor changes of the temperature profile in the concrete. Actually, the damage induced by neutron radiation and elevated temperature neutralizes some of the temperature increase in the concrete caused by radiation heating.

The neutron diffusion coefficient of neutron irradiated concrete gradually increases with time. Neutron radiation and elevated temperature can result in considerable increases of neutron flux in the concrete. The neutron flux increases with time quite a lot, especially for the concrete near the radiation source. Similarly, considerable increases of neutron fluence are observed.

Evidently, the damage of concrete induced by neutron radiation and elevated temperature can effectively accelerate the penetration of neutron radiation into the concrete. For a reliable evaluation of the long-term performance of concrete biological shields in NPPs, effects of neutron radiation and elevated temperature on the neutron and thermal fields must be taken into consideration.

Two-group neutron diffusion model was introduced to treat the neutron energy dependence more realistically. The fast and thermal neutron fields as well as the thermal field in concrete were. Heat generated during the radiation should only result from thermal neutron radiation. When evaluating the neutron radiation induced degradation, only the fast neutron effect is considered, and the thermal neutron damage is ignored. The same concrete wall was analyzed up to 80 years of operation. Some findings were obtained.

The rise of temperature in the concrete increases compared to the results using one-speed diffusion equation. The profiles of thermal neutron flux/fluence are very different from the profiles of fast neutron flux/fluence and peaks near the inner surface of the wall are observed. Besides, the reductions of thermal neutron flux/fluence in the concrete near the inner surface are observed, and the reductions increase with time. In order to predict long-term neutron radiation level in concrete biological shields accurately, a proper treatment of the neutron energy dependence is needed.

In Chapter 4, 59 articles which almost include all experimental data about radiation damage to concrete and/or its components (i.e., rocks) so far was acquired. Information including the material used, material composition, mix design, physical properties, mechanical properties, testing conditions and concrete performance under nuclear radiation was extracted from the collected literature. A database storing all the information collected was developed based on Microsoft Access. The effects of neutron radiation on the cementitious material were analyzed based on the collected data.

Concrete expands with increasing fast neutron radiation. Whereas the cement paste in concrete contracts, the increase in volume for concrete is driven by aggregate expansion. A noticeable increase in volume can be observed at a neutron fluence of 1×10^{19} n/cm^2 or higher for concrete and aggregates. The volume expansion of concrete is very likely to be induced mainly by the expansion of aggregates under neutron irradiation. There is no clear trend for the effect of neutron radiation on weight loss of concrete.

A significant reduction of the compressive strength of concrete and mortar by neutron irradiation and potential thermal effects was observed. On the other hand, there are no general trends for significant reductions of compressive strength of cement paste and aggregate. The results suggest that the strength reduction of concrete is not due to the strength degradation of its components but due to the increased volumetric mismatches in the two constituent phases during the long-term neutron irradiation.

The tensile strength of concrete and mortar is reduced a lot by neutron irradiation. Different from the compressive strength, there are very clear trends for significant reduction of tensile strength of both cement paste and aggregate. The results suggest that the tensile strength reduction of concrete is mainly due to the strength degradation of its components. The volumetric mismatches between the two constituent phases during the long-term neutron irradiation are additional factors. This effect is totally different from the strength reduction in compressive strength.

The general trends shown by the test data about elastic modulus are that there is a significant reduction of the elastic modulus of concrete and mortar as well as aggregate by neutron irradiation and there is a less significant reduction of the elastic modulus of cement paste by neutron irradiation. Therefore, the reduction of the stiffness of concrete as indicated by the reduction of E is mainly due to the reduction of E of the aggregate. However, the reduction in E

may also be due to some contribution from high temperature which has already been confirmed in Chapter 2.

Very clear relationship between temperature and the mechanical properties of concrete and mortar, including compressive strength, tensile strength, and elasticity, can be observed. High environmental temperature can result in significant reductions of mechanical properties at a high neutron irradiation level. It should be mentioned that the reductions are due to the combined effect of neutron radiation and elevated temperature. It is difficult to distinguish between the two effects because many experimental radiation studies in the literature did not have a control group for the temperature effect.

In addition, nuclear radiation can affect the ASR, carbonation and creep in concrete by several different mechanisms.

Chapter 5 presents the experimental study of the self-sensing capability of carbon fiber reinforced cementitious material under mechanical loadings and elevated temperature. Our results indicate that the FCR reduces with increasing compressive loading level. The specimen with 0.2 vol. % CF has largest gage factor which means the best sensitivity. The results also show good reversibility of the strain sensing ability of the samples. The temperature test shows that the electrical resistance decreases when the temperature increases, and goes up when the temperature goes down. The behavior is different for different CF content. The results show good reversibility of the temperature sensing ability of the samples with 0.5 vol.% and 0.7 vol.% CF.

6.2 Future work

The data collection about radiation damage to concrete and/or its components has been completed, and the preliminary analysis of the effect of the water-cement ratio, aggregate fraction, and temperature on concrete subjected to neutron irradiation has been done. Some of the properties

(e.g., modulus of elasticity) of the distressed concrete can be evaluated by the material model based on a given neutron level in concrete. Fast neutron radiation levels at the biological shielding wall could be estimated using the one-speed neutron diffusion model, and fast and thermal neutron radiation levels can be estimated by the two-group neutron diffusion model. The effect of neutron-induced damage on transport properties of concrete was considered. However, in order to examine the structural integrity of a specific structure in a NPP after long-term nuclear radiation exposure, more studies are needed.

The proposed model in Chapter 2 provided a general framework that can estimate the deterioration and deformation of nuclear irradiated concrete. It should be noted that the model introduced assumes that the composite material and all its constituents deformed within elastic range. Various effects outside of the elastic range are not considered in the present study. For instances, the contact pressure generated by the aggregate expansion and cement paste shrinkage could be beyond the elastic range causing damage; since the contact pressure due to the aggregate expansion is a long-term effect, the creep of the cement paste may occur at the interface which can be affected by the moisture change and temperature variation. More sophisticated models need to be developed to analyze the damage and creep at the interface between aggregates and cement paste.

Based on the collected data in Chapter 4, material models need to be developed to predict the mechanical properties of concrete with a given set of concrete design parameters. This is very necessary because the concrete used in a specific NPP may not have the same design parameters as those used in the literature. So, the long-term performance of the concrete in the NPP must be estimated based on available test data obtained from the concretes with different design parameters. For example, the water-cement ratio of the concrete in the NPP is 0.4, and the water-cement ratio of the concrete in the literature is 0.45, then the possible variation of the concrete in

the NPP must be estimated based on the test data. The reliable way for the estimation is to use material models developed based on all test data collected from literature. So, the models can be used to determine the properties of any specific concrete in any specific NPP under different neutron and gamma-ray radiation levels

More experimental studies are also needed in the area of micro-/meso-scale level behaviors of concrete, hardened cement paste, and aggregates under high-level radiation environment. Specifically, comprehensive tests are needed to understand the coupling effects among irradiations, heat, and moisture on cement paste, neutron radiation effects on the crystalline phases of hydration products in hardened cement paste, the behavior of different categories of rocks with different mineral compositions under nuclear irradiations, and shrinkage of hardened cement paste due to moisture loss by gamma-ray radiolysis.

In reality, more energy levels may need to be considered for the neutron diffusion. The framework developed in Chapter 3 can be used as a starting point for further study. The present study focused on the behavior of concrete under neutron irradiation, the effect of gamma rays ought to be considered. Different models and techniques should be used instead of diffusion approximation to describe gamma-ray/photon transportation in the concrete. Secondary gamma-ray from inelastic scattering of neutrons should also be considered.

Finally, a mechanical model for the distressed concrete needs to be developed in order to determine coupled Radio-Thermo-Mechanical field in a specific concrete structure in close proximity to the RPVs. The stress-strain diagrams of the concrete at different locations in concrete structure can be obtained by the models which can be used for analyzing the performance of the distressed concrete, such as ultimate strength capacity and ductility. Strain and stress profiles at a certain time point (e.g., 80 years) under design loadings can then be obtained. These are important for license renew of the NPPs.

REFERENCES

Alexander, M., and Mindess, S. (2005). *Aggregates in Concrete*. CRC Press, Boca Raton, FL.

Alexander, S. C. (1963). "Effects of irradiation on concrete. Final results." *Atomic Energy Research Establishment, Harwell, U.K.*, 34.

ASME. (2015). *BPVC Section III-Rules for Construction of Nuclear Facility Components-Division 2-Code for Concrete Containments*. ASME, New York.

ASTM. (2016). *ASTM C597-16, Standard Test Method for Pulse Velocity Through Concrete*. ASTM International, West Conshohocken, PA.

Azhari, F. (2008). "Cement-based sensors for structural health monitoring." M.S. Thesis, University of British Columbia.

Azhari, F., and Banthia, N. (2012). "Cement-based sensors with carbon fibers and carbon nanotubes for piezoresistive sensing." *Cement and Concrete Composites*, 34(7), 866–873.

Bahr, O., Schaumann, P., Bollen, B., and Bracke, J. (2013). "Young's modulus and Poisson's ratio of concrete at high temperatures: Experimental investigations." *Materials & Design*, 45, 421–429.

Bamonte, P., and Gambarova, P. G. (2016). "High-Temperature Behavior of SCC in Compression: Comparative Study on Recent Experimental Campaigns." *Journal of Materials in Civil Engineering*, 28(3), 04015141.

Bar-Nes, G., Katz, A., Peled, Y., and Zeiri, Y. (2008). "The combined effect of radiation and carbonation on the immobilization of Sr and Cs ions in cementitious pastes." *Materials and Structures*, 41(9), 1563–1570.

Bažant, Z. P., and Kaplan, M. F. (1996). *Concrete at high temperatures: material properties and mathematical models*. Longman, Harlow.

Bonnet, J. P., Vacher, R., Pelous, J., and Laermans, C. (1992). "Effects of anharmonicity and of thermally activated structural relaxation in irradiated quartz." *Physical Review B*, 45(2), 557.

Cantwell, W. J., and Morton, J. (1991). "The impact resistance of composite materials — a review." *Composites*, 22(5), 347–362.

Chen, P.-W., and Chung, D. D. L. (1993). "Concrete reinforced with up to 0.2 vol% of short carbon fibres." *Composites*, 24(1), 33–52.

Chen, P.-W., and Chung, D. D. L. (1996). “Concrete as a new strain/stress sensor.” *Composites Part B: Engineering*, 27(1), 11–23.

Chiarello, M., and Zinno, R. (2005). “Electrical conductivity of self-monitoring CFRC.” *Cement and Concrete Composites*, 27(4), 463–469.

Christensen, R. M. (1979). *Mechanics of composite materials*. Wiley, New York.

Chung, D. (2003). “Damage in cement-based materials, studied by electrical resistance measurement.” *Materials Science and Engineering: R: Reports*, 42(1), 1–40.

Chung, D. D. L. (2000a). “Cement-matrix composites for smart structures.” *Smart materials and structures*, 9(4), 389.

Chung, D. D. L. (2000b). “Cement reinforced with short carbon fibers: a multifunctional material.” *Composites Part B: Engineering*, 31(6–7), 511–526.

Clinard Jr., F. W., Hurley, G. F., and Hobbs, L. W. (1982). “Neutron irradiation damage in MgO, Al2O3 and MgAl2O4 ceramics.” *Journal of Nuclear Materials*, 108–109, 655–670.

Constantinides, G., and Ulm, F.-J. (2004). “The effect of two types of CSH on the elasticity of cement-based materials: Results from nanoindentation and micromechanical modeling.” *Cement and concrete research*, 34(1), 67–80.

Cristiani, G., Granata, S., and Montagnini, A. (1972). “Behaviour of plastic mortar samples under temperature and radiation conditions.” *Proceedings of an Information Exchange Meeting on “Results of Concrete Irradiation Programmes,”* Commission of the European Communities, Luxembourg, 41–53.

DOE Fundamentals Handbook. (1993). *Nuclear Physics and Reactor Theory*. U.S. Department of Energy, Washington, D.C.

Du, H., Quek, S. T., and Pang, S. D. (2013). “Smart multifunctional cement mortar containing graphite nanoplatelet.” J. P. Lynch, C.-B. Yun, and K.-W. Wang, eds., 869238.

Dubrovskii, V. B., Ibragimov, S. S., Kulakovskii, M. Y., Ladygin, A. Y., and Pergamenshchik, B. K. (1967). “Radiation damage in ordinary concrete.” *Soviet Atomic Energy*, 23(4), 1053–1058.

Dubrovskii, V. B., Ibragimov, S. S., Ladygin, A. Y., Kulakovskii, M. Y., and Pergamenshchik, B. K. (1968). “Radiation stability of serpentine concrete.” *Soviet Atomic Energy*, 25(6), 1345–1346.

Dubrovskii, V. B., Ibragimov, S. S., Ladygin, A. Y., and Pergamenshchik, B. K. (1966). “Effect of neutron irradiation on some properties of heat-resistant concretes.” *Soviet Atomic Energy*, 21(2), 740–744.

Duderstadt, J. J., and Hamilton, L. J. (1976). *Nuclear reactor analysis*. Wiley, New York.

Elleuch, L. F., Dubois, F., and Rappeneau, J. (1972). “Effects of neutron radiation on special concretes and their components.” *ACI Special Publication*, 34, 1071–1108.

El-Sayed Abdo, A., and Amin, E. (2001). “Distribution of temperature rise in biological shield due to thermal neutrons.” *Annals of Nuclear Energy*, 28(3), 275–283.

Eskandari-Ghadi, M., Xi, Y., and Sture, S. (2014). “Cross-Property Relations between Mechanical and Transport Properties of Composite Materials.” *Journal of Engineering Mechanics*, 140(7).

Eskandari-Ghadi, M., Zhang, W., Xi, Y., and Sture, S. (2013). “Modeling of Moisture Diffusivity of Concrete at Low Temperatures.” *Journal of Engineering Mechanics*, 139(7), 903–915.

Esselman, T., and Bruck, P. (2013). *Expected Condition of Concrete at Age 80 Years of Reactor Operation. Technical Report, A13276-R-001*. Lucius Pitkin, Inc., Amesbury, MA.

Field, K. G., Remec, I., and Le Pape, Y. (2015). “Radiation effects in concrete for nuclear power plants – Part I: Quantification of radiation exposure and radiation effects.” *Nuclear Engineering and Design*, 282, 126–143.

Fillmore, D. L. (2004). *Literature Review of the Effects of Radiation and Temperature on the Aging of Concrete*. Idaho National Engineering and Environmental Laboratory, Idaho Falls, ID.

Fu, X., and Chung, D. D. (1998). “Strain-sensing concrete improved by carbon fiber surface treatment.” *5th Annual International Symposium on Smart Structures and Materials*, International Society for Optics and Photonics, 53–63.

Fujiwara, K., Ito, M., Sasanuma, M., Tanaka, H., Hirotani, K., Onizawa, K., Suzuki, M., and Amezawa, H. (2009). “Experimental study of the effect of radiation exposure to concrete.” *SMiRT20, Div-I, Paper1981*, Espoo, Finland.

Galao, O., Baeza, F. J., Zornoza, E., and Garcés, P. (2014). “Strain and damage sensing properties on multifunctional cement composites with CNF admixture.” *Cement and Concrete Composites*, 46, 90–98.

Gardner, J. W., and Anderson, A. C. (1981). “Low-temperature specific heat and thermal conductivity of neutron-irradiated crystalline quartz.” *Physical Review B*, 23(2), 474.

Giorla, A. B., Le Pape, Y., and Dunant, C. F. (2017). “Computing creep-damage interactions in irradiated concrete.” *Journal of Nanomechanics and Micromechanics*, 7(2), 04017001.

Gong, K., Pan, Z., Korayem, A. H., Qiu, L., Li, D., Collins, F., Wang, C. M., and Duan, W. H. (2014). “Reinforcing effects of graphene oxide on portland cement paste.” *Journal of Materials in Civil Engineering*, 27(2), A4014010.

Grasse, D., Kocar, O., Peisl, H., Moss, S. C., and Golding, B. (1981). “Diffuse x-ray scattering and phonon echoes from neutron-irradiated crystalline quartz.” *Physical Review Letters*, 46(4), 261.

Graves, H., Le Pape, Y., Naus, D., Rashid, J., Saouma, V., Sheikh, A., and Wall, J. (2014). "Expanded material degradation assessment (EMDA), volume 4: Aging of concrete." *Technical Rep. NUREG/CR-7153, ORNL/TM-2011/545, United State Nuclear Regulatory Commission, Rockville, MD*.

Gray, B. S. (1972). "Effects of Reactor Radiation on Cements and Concrete." *Proceedings of an Information Exchange Meeting on "Results of Concrete Irradiation Programmes,"* Commission of the European Communities, Luxembourg.

Haecker, C.-J., Garboczi, E. J., Bullard, J. W., Bohn, R. B., Sun, Z., Shah, S. P., and Voigt, T. (2005). "Modeling the linear elastic properties of Portland cement paste." *Cement and Concrete Research*, 35(10), 1948–1960.

Han, B. G., Yu, Y., Han, B. Z., and Ou, J. P. (2008). "Development of a wireless stress/strain measurement system integrated with pressure-sensitive nickel powder-filled cement-based sensors." *Sensors and Actuators A: Physical*, 147(2), 536–543.

Han, B., and Ou, J. (2007). "Embedded piezoresistive cement-based stress/strain sensor." *Sensors and Actuators A: Physical*, 138(2), 294–298.

Heuze, F. E. (1983). "High-temperature mechanical, physical and Thermal properties of granitic rocks— A review." *International Journal of Rock Mechanics and Mining Sciences & Geomechanics Abstracts*, 20(1), 3–10.

Hilsdorf, H., Kropp, J., and Koch, H. (1978). "The effects of nuclear radiation on the mechanical properties of concrete." *ACI Special Publication*, 55, 223–254.

Hou, T.-C., and Lynch, J. P. (2005). "Conductivity-based strain monitoring and damage characterization of fiber reinforced cementitious structural components." M. Tomizuka, ed., 419–429.

Houben, J. (1969). "De Bestraling van Mortelproefstukken." Commission of the European Communities, Brussel, 170–178.

Huang, S. (2012). "Multifunctional Graphite Nanoplatelets (GNP) Reinforced Cementitious Composites." M.E. Thesis, National University of Singapore.

Hussain, M., Choa, Y.-H., and Niihara, K. (2001). "Fabrication process and electrical behavior of novel pressure-sensitive composites." *Composites Part A: Applied Science and Manufacturing*, 32(12), 1689–1696.

Ichikawa, T., and Kimura, T. (2007). "Effect of Nuclear Radiation on Alkali-Silica Reaction of Concrete." *Journal of Nuclear Science and Technology*, 44(10), 1281–1284.

Ichikawa, T., and Koizumi, H. (2002). "Possibility of Radiation-Induced Degradation of Concrete by Alkali-Silica Reaction of Aggregates." *Journal of Nuclear Science and Technology*, 39(8), 880–884.

Idei, Y., Kamata, H., Akutsu, Y., Onizawa, K., Nakajima, N., Sukegawa, T., and Kakizaki, M. (1990). *Mechanical properties of JPDR biological shield concrete*. Japan Atomic Energy Research Inst.

Jennings, H. M., and Tennis, P. D. (1994). "Model for the developing microstructure in Portland cement pastes." *Journal of the American Ceramic Society*, 77(12), 3161–3172.

Kelly, B. T., Brocklehurst, J. E., Mottershead, D., McNearney, S., and Davidson, I. (1969). "Effects of Reactor Radiation on Concrete." Commision of the European Communities, Brussels, 237–265.

Kodur, V. (2014). "Properties of Concrete at Elevated Temperatures." *ISRN Civil Engineering*, 2014, 1–15.

Kodur V. K. R., and Sultan M. A. (2003). "Effect of Temperature on Thermal Properties of High-Strength Concrete." *Journal of Materials in Civil Engineering*, 15(2), 101–107.

Kontani, O., Ichikawa, Y., Ishizawa, A., Takizawa, M., and Sato, O. (2014). "Irradiation Effects on Concrete Structures." *Infrastructure Systems for Nuclear Energy*, T. T. C. Hsu, C.-L. Wu, and J.-L. Li, eds., John Wiley & Sons, Ltd, Chichester, UK, 459–473.

Kontani, O., Sawada, S., Maruyama, I., Takizawa, M., and Sato, O. (2013). "Evaluation of Irradiation Effects on Concrete Structure: Gamma-Ray Irradiation Tests on Cement Paste." *ASME 2013 Power Conference*, Boston, Massachusetts, USA.

Le, J.-L., Du, H., and Pang, S. D. (2014). "Use of 2D Graphene Nanoplatelets (GNP) in cement composites for structural health evaluation." *Composites Part B: Engineering*, 67, 555–563.

Le Pape, Y. (2015). "Structural effects of radiation-induced volumetric expansion on unreinforced concrete biological shields." *Nuclear Engineering and Design*, 295, 534–548.

Le Pape, Y., Field, K. G., and Remec, I. (2015). "Radiation effects in concrete for nuclear power plants, Part II: Perspective from micromechanical modeling." *Nuclear Engineering and Design*, 282, 144–157.

Lee, J. (2006). "Experimental studies and theoretical modeling of concrete subjected to high temperatures." Ph.D. Thesis, University of Colorado at Boulder, Boulder, CO.

Lee, J., Xi, Y., Willam, K., and Jung, Y. (2009). "A multiscale model for modulus of elasticity of concrete at high temperatures." *Cement and Concrete Research*, 39(9), 754–762.

Li, G. Y., Wang, P. M., and Zhao, X. (2007). "Pressure-sensitive properties and microstructure of carbon nanotube reinforced cement composites." *Cement and Concrete Composites*, 29(5), 377–382.

Lin, F., and Meyer, C. (2008). "Modeling shrinkage of portland cement paste." *ACI Materials Journal*, 105(3).

Lowinska-Kluge, A., and Piszora, P. (2008). "Effect of gamma irradiation on cement composites observed with XRD and SEM methods in the range of radiation dose 0-1409 MGy." *Acta Physica Polonica-Series A General Physics*, 114(2), 399.

Marechal, J. C. (1972). "Variations in the Modulus of Elasticity and Poisson's Ratio with Temperature." *Special Publication*, 34, 495–504.

Maruyama, I., Haba, K., Sato, O., Ishikawa, S., Kontani, O., and Takizawa, M. (2016). "A Numerical Model for Concrete Strength Change under Neutron and Gamma-ray Irradiation." *Journal of Advanced Concrete Technology*, 14(4), 144–162.

Maruyama, I., Kontani, O., Sawada, S., Sato, O., Igarashi, G., and Takizawa, M. (2013). "Evaluation of Irradiation Effects on Concrete Structure: Background and Preparation of Neutron Irradiation Test." *ASME 2013 Power Conference*, Boston, Massachusetts, USA.

Maruyama, I., Kontani, O., Takizawa, M., Sawada, S., Ishikawao, S., Yasukouchi, J., Sato, O., Etoh, J., and Igari, T. (2017). "Development of Soundness Assessment Procedure for Concrete Members Affected by Neutron and Gamma-Ray Irradiation." *Journal of Advanced Concrete Technology*, 15(9), 440–523.

MATLAB [Computer software]. The MathWorks, Inc. Natick, MA

McDowall, D. C. (1972). "The effect of gamma irradiation on the creep properties of concrete." *Proceedings of an Information Exchange Meeting on "Results of Concrete Irradiation Programmes,"* Commission of the European Communities, Luxembourg.

Meshgin, P., and Xi, Y. (2013). "Multi-scale composite models for the effective thermal conductivity of PCM-concrete." *Construction and Building Materials*, 48, 371–378.

Microsoft Access [Computer software]. Microsoft, Redmond, WA

Naus, D. (2010). *A Compilation of Elevated Temperature Concrete Material Property Data and Information for Use in Assessments of Nuclear Power Plant Reinforced Concrete Structures: Prepared by DJ Naus*. US Nuclear Regulatory Commission, Office of Nuclear Regulatory Research.

Naus, D. J. (2006). *The Effect of Elevated Temperature on Concrete Materials and Structures - a Literature Review*. Oak Ridge National Laboratory, Oak Ridge, TN.

Naus, D. J. (2009). *Inspection of Nuclear Power Plant Structures - Overview of Methods and Related Applications*. Oak Ridge National Laboratory, Oak Ridge, TN.

Neubauer, C. M., Bergstrom, T. B., Sujata, K., Xi, Y., Garboczi, E. J., and Jennings, H. M. (1997). "Drying shrinkage of cement paste as measured in an environmental scanning electron microscope and comparison with microstructural models." *Journal of Materials Science*, 32(24), 6415–6427.

Neubauer, C. M., Jennings, H. M., and Garboczi, E. J. (1996). "A three-phase model of the elastic and shrinkage properties of mortar." *Advanced Cement Based Materials*, 4(1), 6–20.

Pan, J., Zou, R., and Jin, F. (2016). “Experimental Study on Specific Heat of Concrete at High Temperatures and Its Influence on Thermal Energy Storage.” *Energies*, 10(1), 33.

Pang, S. D., Gao, H. J., Xu, C., Quek, S. T., and Du, H. (2014). “Strain and damage self-sensing cement composites with conductive graphene nanoplatelet.” J. P. Lynch, K.-W. Wang, and H. Sohn, eds., 906126.

Pape, Y. L., Giorla, A., and Sanahuja, J. (2016). “Combined Effects of Temperature and Irradiation on Concrete Damage.” *Journal of Advanced Concrete Technology*, 14(3), 70–86.

Pedersen, A. (1972). “Radiation Damage in Concrete: Measurements on Miniature Specimens of Cement Mortar.” *Proceedings of an Information Exchange Meeting on “Results of Concrete Irradiation Programmes,”* Commission of the European Communities, Luxembourg, 5–16.

Pierson, H. O. (2012). *Handbook of Carbon, Graphite, Diamonds and Fullerenes: Processing, Properties and Applications*. William Andrew.

Pignatelli, I., Kumar, A., Field, K. G., Wang, B., Yu, Y., Pape, Y. L., Bauchy, M., and Sant, G. (2016). “Direct Experimental Evidence for Differing Reactivity Alterations of Minerals following Irradiation: The Case of Calcite and Quartz.” *Scientific Reports*, 6, 20155.

Pomaro, B. (2016). “A Review on Radiation Damage in Concrete for Nuclear Facilities: From Experiments to Modeling.” *Modelling and Simulation in Engineering*, 2016, 1–10.

Pomaro, B., Salomoni, V. A., Gramegna, F., Prete, G., and Majorana, C. E. (2011a). “Radiation damage evaluation on concrete within a facility for Selective Production of Exotic Species (SPES Project), Italy.” *Journal of Hazardous Materials*, 194, 169–177.

Pomaro, B., Salomoni, V. A., Gramegna, F., Prete, G., and Majorana, C. E. (2011b). “Radiation damage evaluation on concrete shielding for nuclear physics experiments.” *Annals of Solid and Structural Mechanics*, 2(2–4), 123–142.

Price, B. T., Horton, C. C., and Spinney, K. T. (1957). *Radiation shielding*. Pergamon Press, London.

Primak, W. (1958). “Fast-neutron-induced changes in quartz and vitreous silica.” *Physical Review*, 110(6), 1240.

Rappeneau, J., Lagorio, M., Gilbert, J., and Piron, P. (1966). “Irradiation tests of concretes.” *Bull. Inf. Sci. Tech.*, 110, 31–48.

REACTOR PHYSICS CONSTANTS. (1963). Argonne National Laboratory, IL.

Remec, I., Rosseel, T. M., Field, K. G., and Pape, Y. L. (2016). “Characterization of Radiation Fields in Biological Shields of Nuclear Power Plants for Assessing Concrete Degradation.” *EPJ Web of Conferences*, 106.

Rosen, B. W., and Hashin, Z. (1970). “Effective thermal expansion coefficients and specific heats of composite materials.” *International Journal of Engineering Science*, 8(2), 157–173.

Rosseel, T. M., Maruyama, I., Pape, Y. L., Kontani, O., Giorla, A. B., Remec, I., Wall, J. J., Sircar, M., Andrade, C., and Ordonez, M. (2016). “Review of the Current State of Knowledge on the Effects of Radiation on Concrete.” *Journal of Advanced Concrete Technology*, 14(7), 368–383.

Salomoni, V. A., Majorana, C. E., Pomaro, B., Xotta, G., and Gramegna, F. (2014). “Macroscale and mesoscale analysis of concrete as a multiphase material for biological shields against nuclear radiation.” *International Journal for Numerical and Analytical Methods in Geomechanics*, 38(5), 518–535.

Sancak, E., Dursun Sari, Y., and Simsek, O. (2008). “Effects of elevated temperature on compressive strength and weight loss of the light-weight concrete with silica fume and superplasticizer.” *Cement and Concrete Composites*, 30(8), 715–721.

Sedaghat, A., Ram, M. K., Zayed, A., Kamal, R., and Shanahan, N. (2014). “Investigation of Physical Properties of Graphene-Cement Composite for Structural Applications.” *Open Journal of Composite Materials*, 04(01), 12–21.

Seeberger, J., and Hilsdorf, H. (1982). “Einfluss von radioactiver Strahlung auf die Festogkeit and Struktur von beton.” *Technical Rep. NR2505, Institüt fur Massiubau und Baustofftechnologie, Arbeitlung Baustofftechnologie, Universität Karlsruhe, Karlsruhe, Germany (in German).*

Seshadri, B. S., Venkatesan, R., and Sundararaman, V. (1988). “Fast Neutron Streaming through Duct in Concrete Shields.” *Journal of Nuclear Science and Technology*, 25(9), 682–689.

Shin, K. (1989). “Evaluation Formula for Radiation Duct Streaming.” *Journal of Nuclear Science and Technology*, 26(12), 1067–1080.

Shultis, J. K., and Faw, R. E. (1996). *Radiation shielding*. Prentice Hall PTR, Upper Saddle River, NJ.

Tarkov, A. P., and Vavakin, V. V. (1982). “Poisson’s ratio behaviour in various crystalline rocks: application to the study of the Earth’s interior.” *Physics of the Earth and Planetary Interiors*, Special Issue Properties of Materials at High Pressures and High Temperatures, 29(1), 24–29.

Taylor, H. F. W. (1987). “A method for predicting alkazi ion concentrations in cement pore solutions.” *Advances in Cement Research*, 1(1), 5–17.

Ursu, I. (1985). *Physics and Technology of Nuclear Materials*. Pergamon Press, Oxford, UK.

Vanelstraete, A., and Laermans, C. (1990). “Tunneling states in neutron-irradiated quartz: measurements of the ultrasonic attenuation and velocity change.” *Physical Review B*, 42(9), 5842.

Vanelstraete, A., Laermans, C., and Cornelis, J. (1987). “Low temperature ultrasonic attenuation in neutron-irradiated quartz versus the induced mass-density changes.” *Journal de Physique Colloques*, 48(C8), C8-531-C8-537.

Vodák, F., Trtík, K., Sopko, V., Kapičková, O., and Demo, P. (2005). “Effect of γ-irradiation on strength of concrete for nuclear-safety structures.” *Cement and Concrete Research*, 35(7), 1447–1451.

Vodák, F., Vydra, V., Trtík, K., and Kapičková, O. (2011). “Effect of gamma irradiation on properties of hardened cement paste.” *Materials and Structures*, 44(1), 101–107.

Wang, S. X., Wang, L. M., and Ewing, R. C. (2000). “Irradiation-induced amorphization: Effects of temperature, ion mass, cascade size, and dose rate.” *Physical Review B*, 63(2).

Weber, W. J., Ewing, R. C., Catlow, C. R. A., De La Rubia, T. D., Hobbs, L. W., Kinoshita, C., Matzke, H., Motta, A. T., Nastasi, M., Salje, E. K. H., and others. (1998). “Radiation effects in crystalline ceramics for the immobilization of high-level nuclear waste and plutonium.” *Journal of Materials Research*, 13(06), 1434–1484.

Weber, W. J., Ewing, R. C., and Wang, L.-M. (1994). “The radiation-induced crystalline-to-amorphous transition in zircon.” *Journal of Materials Research*, 9(03), 688–698.

Weissmann, S., and Nakajima, K. (1963). “Defect Structure and Density Decrease in Neutron-Irradiated Quartz.” *Journal of Applied Physics*, 34(3), 611–618.

Wen, S., and Chung, D. D. L. (2006). “Model of piezoresistivity in carbon fiber cement.” *Cement and Concrete Research*, 36(10), 1879–1885.

Wen, S., and Chung, D. D. L. (2007a). “Piezoresistivity-based strain sensing in carbon fiber-reinforced cement.” *ACI materials journal*, 104(2).

Wen, S., and Chung, D. D. L. (2007b). “Partial replacement of carbon fiber by carbon black in multifunctional cement–matrix composites.” *Carbon*, 45(3), 505–513.

Wilks, R. S. (1968). “Neutron-induced damage in BeO, Al2O3 and MgO — a review.” *Journal of Nuclear Materials*, 26(2), 137–173.

William, K., Xi, Y., and Naus, D. (2013). *A review of the effects of radiation on microstructure and properties of concretes used in nuclear power plants (NUREG/CR-7171)*. Office of Nuclear Regulatory Research, U.S. Nuclear Regulatory Commission, Washington, DC.

Wittels, M., and Sherrill, F. A. (1954). “Radiation Damage in SiO2 Structures.” *Physical Review*, 93(5), 1117.

Wittmann, F. H., Roelfstra, P. E., Mihashi, H., Huang, Y.-Y., Zhang, X.-H., and Nomura, N. (1987). “Influence of age of loading, water-cement ratio and rate of loading on fracture energy of concrete.” *Materials and Structures*, 20(2), 103–110.

Xi, Y., Eskandari-Ghadi, M., Suwito, and Sture, S. (2006). “Damage theory based on composite mechanics.” *Journal of engineering mechanics*, 132(11), 1195–1204.

Xi, Y., and Jennings, H. M. (1997). “Shrinkage of cement paste and concrete modelled by a multiscale effective homogeneous theory.” *Materials and Structures*, 30(6), 329–339.

Xiao, H., and Li, H. (2006). “A study on the application of CB-filled cement-based composite as a strain sensor for concrete structures.” 61742T-61742T–8.

Xiao, H., Li, H., and Ou, J. (2010). “Modeling of piezoresistivity of carbon black filled cement-based composites under multi-axial strain.” *Sensors and Actuators A: Physical*, 160(1–2), 87–93.

Xie, P., Gu, P., and Beaudoin, J. J. (1996). “Electrical percolation phenomena in cement composites containing conductive fibres.” *Journal of Materials Science*, 31(15), 4093–4097.

Xu, J., Zhong, W., and Yao, W. (2010). “Modeling of conductivity in carbon fiber-reinforced cement-based composite.” *Journal of Materials Science*, 45(13), 3538–3546.

Yang, L., Ge, Y., Zhu, Q., Zhang, C., Wang, Z., and Liu, P. (2012). “Experimental and numerical studies on the sensitivity of carbon fibre/silicone rubber composite sensors.” *Smart Materials and Structures*, 21(3), 035011.

Yevick, J. G. (1966). *Fast Reactor Technology: Plant Design*. M.I.T. Press, Cambridge.

Zhu, S., and Chung, D. D. L. (2007). “Theory of piezoresistivity for strain sensing in carbon fiber reinforced cement under flexure.” *Journal of Materials Science*, 42(15), 6222–6233.

APPENDIX: BIBLIOGRAPHY OF CONCRETE IRRADIATION DATABASE

Alexander, S. C. (1963). “Effects of irradiation on concrete. Final results.” Atomic Energy Research Establishment, Harwell, U.K., 34.

Blosser, T. V., Bond, G. W., Lee, L. A., Morgan, D. T., Nichols, J. F., Reid, R. C., Reynolds, A. B., Speidel, T. O. P., Vroom, D. W., and Welt, M. A. (1958). A Study of the Nuclear and Physical Properties of the Ornl Graphite Reactor Shield. Oak Ridge National Lab., Tenn.

Bonnet, J. P., Vacher, R., Pelous, J., and Laermans, C. (1992). “Effects of anharmonicity and of thermally activated structural relaxation in irradiated quartz.” Physical Review B, 45(2), 557.

Bouniol, P., and Aspart, A. (1998). “Disappearance of oxygen in concrete under irradiation: the role of peroxides in radiolysis.” Cement and Concrete Research, 28(11), 1669–1681.

Bouniol, P., Muzeau, B., and Dauvois, V. (2013). “Experimental evidence of the influence of iron on pore water radiolysis in cement-based materials.” Journal of Nuclear Materials, 437(1–3), 208–215.

Bykov, V. N., Denisov, A. V., Dubrovskii, V. B., Korenevskii, V. V., Krivokoneva, G. K., and Muzalevskii, L. P. (1981). “Effect of irradiation temperature on the radiation expansion of quartz.” Atomic Energy, 51(3), 593–595.

Chisholm-Batten, A. W. (1960). Effect of Irradiation on the Strength of Concrete. Research Reactors Division, Atomic Energy Research Establishment, Harwell, Berkshire, U.K.

Crispino, E., Fizzotti, C., and Gasparini, R. (1971). “Irradiation Effects on Reactor Structural Materials.” United Nations and International Atomic Energy Agency, Geneva, Switzerland.

Cristiani, G., Granata, S., and Montagnini, A. (1972). “Behaviour of plastic mortar samples under temperature and radiation conditions.” Proceedings of an Information Exchange Meeting on “Results of Concrete Irradiation Programmes,” Commission of the European Communities, Luxembourg, 41–53.

Dickeman, R. (1951). Technical Activities Report – Pile Physics. Technical Report HW-22132.

Dubrovskii, V. B., Ibragimov, S. S., Korenevskii, V. V., Ladygin, A. Y., Pergamenshchik, V. K., and Perevalov, V. S. (1970). “Hematite concrete for shielding against high neutron fluxes.” Soviet Atomic Energy, 28(3), 336–338.

Dubrovskii, V. B., Ibragimov, S. S., Kulakovskii, M. Y., Ladygin, A. Y., and Pergamenshchik, B. K. (1967). “Radiation damage in ordinary concrete.” Soviet Atomic Energy, 23(4), 1053–1058.

Dubrovskii, V. B., Ibragimov, S. S., Ladygin, A. Y., Kulakovskii, M. Y., and Pergamenshchik, B. K. (1968). “Radiation stability of serpentine concrete.” Soviet Atomic Energy, 25(6), 1345–1346.

Dubrovskii, V. B., Ibragimov, S. S., Ladygin, A. Y., and Pergamenshchik, B. K. (1966). “Effect of neutron irradiation on some properties of heat-resistant concretes.” Soviet Atomic Energy, 21(2), 740–744.

Elleuch, L. F., Dubois, F., and Rappeneau, J. (1972). “Effects of neutron radiation on special concretes and their components.” ACI Special Publication, 34, 1071–1108.

Fujiwara, K., Ito, M., Sasanuma, M., Tanaka, H., Hirotani, K., Onizawa, K., Suzuki, M., and Amezawa, H. (2009). “Experimental study of the effect of radiation exposure to concrete.” SMiRT20, Div-I, Paper1981, Espoo, Finland.

Gardner, J. W., and Anderson, A. C. (1981). “Low-temperature specific heat and thermal conductivity of neutron-irradiated crystalline quartz.” Physical Review B, 23(2), 474.

Granata, S., and Montagnini, A. (1972). Studies on behavior of concretes under irradiation. AGIP Nucleare SpA, Milan.

Grantham, W. J. (1960). A Study of Concrete Samples Taken from The Top Shield of the ORNL Graphite Reactor, Neutron Division Annual Progress Report for Period Ending September 1, 1960. Oak Ridge National Lab., Tenn.

Grasse, D., Kocar, O., Peisl, H., Moss, S. C., and Golding, B. (1981). “Diffuse x-ray scattering and phonon echoes from neutron-irradiated crystalline quartz.” Physical Review Letters, 46(4), 261.

Gray, B. S. (1972). “Effects of Reactor Radiation on Cements and Concrete.” Proceedings of an Information Exchange Meeting on “Results of Concrete Irradiation Programmes,” Commission of the European Communities, Luxembourg.

Houben, J. (1969). “De Bestraling van Mortelproefstukken.” Commission of the European Communities, Brussel, 170–178.

Kelly, B. T., Brocklehurst, J. E., Mottershead, D., McNearney, S., and Davidson, I. (1969). “Effects of Reactor Radiation on Concrete.” Commision of the European Communities, Brussels, 237–265.

Kontani, O., Ichikawa, Y., Ishizawa, A., Takizawa, M., and Sato, O. (2011). “Irradiation effects on concrete durability of nuclear power plants.” Proceedings of ICAPP 2011.

Kontani, O., Ichikawa, Y., Ishizawa, A., Takizawa, M., and Sato, O. (2014). "Irradiation Effects on Concrete Structures." Infrastructure Systems for Nuclear Energy, T. T. C. Hsu, C.-L. Wu, and J.-L. Li, eds., John Wiley & Sons, Ltd, Chichester, UK, 459–473.

Kontani, O., Sawada, S., Maruyama, I., Takizawa, M., and Sato, O. (2013). "Evaluation of Irradiation Effects on Concrete Structure: Gamma-Ray Irradiation Tests on Cement Paste." ASME 2013 Power Conference, Boston, Massachusetts, USA.

Lowinska-Kluge, A., and Piszora, P. (2008). "Effect of gamma irradiation on cement composites observed with XRD and SEM methods in the range of radiation dose 0-1409 MGy." Acta Physica Polonica-Series A General Physics, 114(2), 399.

Lukesh, J. S. (1955). "Neutron damage to the structure of vitreous silica." Physical Review, 97(2), 345.

Lyon, R. N. ed. (1950a). General Reactor-Engineering Research Quarterly Progress Report for Period Ending November 20, 1950. Oak Ridge National Lab., Tenn.

Lyon, R. N. ed. (1950b). General Reactor-Engineering Research Quarterly Progress Report for Period Ending August 31, 1950. Oak Ridge National Lab., Tenn.

Maruyama, I., Kontani, O., Takizawa, M., Sawada, S., Ishikawao, S., Yasukouchi, J., Sato, O., Etoh, J., and Igari, T. (2017). "Development of Soundness Assessment Procedure for Concrete Members Affected by Neutron and Gamma-Ray Irradiation." Journal of Advanced Concrete Technology, 15(9), 440–523.

McDowall, D. C. (1972). "The effect of gamma irradiation on the creep properties of concrete." Proceedings of an Information Exchange Meeting on "Results of Concrete Irradiation Programmes," Commission of the European Communities, Luxembourg.

Pedersen, A. (1972). "Radiation Damage in Concrete: Measurements on Miniature Specimens of Cement Mortar." Proceedings of an Information Exchange Meeting on "Results of Concrete Irradiation Programmes," Commission of the European Communities, Luxembourg, 5–16.

Price, B. T., Horton, C. C., and Spinney, K. T. (1957). Radiation shielding. Pergamon Press, London.

Primak, W. (1955). "Experimental evidence for thermal spikes in radiation damage." Physical Review, 98(6), 1854.

Primak, W. (1957). "Fast Neutron Damaging in Nuclear Reactors. II. The Radiation Damage Function of Graphite." Nuclear Science and Engineering, 2(2), 117–125.

Primak, W. (1958). "Fast-neutron-induced changes in quartz and vitreous silica." Physical Review, 110(6), 1240.

Primak, W. (1975). The compacted states of vitreous silica. Studies in radiation effects in solids, Gordon and Breach Science Publishers, New York.

Primak, W., and Edwards, E. (1962). “Radiation-induced dilatations in vitreous silica.” Physical Review, 128(6), 2580.

Primak, W., Fuchs, L. H., and Day, P. (1953). “Radiation damage in insulators.” Physical Review, 92(4), 1064.

Primak, W., and Kampwirth, R. (1968). “The Radiation Compaction of Vitreous Silica.” Journal of Applied Physics, 39(12), 5651–5658.

Rockwell, T. I. ed. (1948). Physical Tests of Core Drilling from the ORNL Graphite Reactor Shield. Technical Report ORNL-248. OAK RIDGE NATIONAL LABORATORY.

Simon, I. (1956). “Structure of neutron-disordered silica.” Physical Review, 103(5), 1587.

Simon, I. (1957). “Structure of Neutron-Irradiated Quartz and Vitreous Silica.” Journal of the American Ceramic Society, 40(5), 150–153.

Sommers, J. F. (1969). “Gamma radiation damage of structural concrete immersed in water.” Health physics, 16(4), 503–508.

Soo, P., and Milian, L. M. (2001). “The effect of gamma radiation on the strength of Portland cement mortars.” Journal of materials science letters, 20(14), 1345–1348.

Soo, P., and Milian, L. W. (1989). Sulfate-Attack Resistance and Gamma-Irradiation Resistance of Some Portland Cement Based Mortars. Nuclear Regulatory Commission, Washington, DC (USA). Div. of Engineering; Brookhaven National Lab., Upton, NY (USA).

Sopko, V., Trtík, K., and Vodák, F. (2004). “Influence of Irradiation on Concrete Strength.” Acta Polytechnica, 44(1).

Stoces, B., Otopal, P., Juricka, V., and Gabriel, J. (1970). Radiation Effects on Mechanical Properties of Concrete. Ceskoslovesnka Akademie Ved, Rez. Ustav Jaderneho Vyzkumu.

Van der Schaaf, C. F. (1969). “Invloed van Bestraling en Verhitting op de Sterkte van Mortels en Beton.” Commission of the European Communities, Brussel, 179–183.

Van der Schaaf, C. F. (1970). Effect of Heating and Radiation on Some Properties of Mortar and Concrete Specimens with Different Compositions. Bredero N.V., Utrecht (Netherlands).

Vanelstraete, A., and Laermans, C. (1990). “Tunneling states in neutron-irradiated quartz: measurements of the ultrasonic attenuation and velocity change.” Physical Review B, 42(9), 5842.

Vanelstraete, A., Laermans, C., and Cornelis, J. (1987). “Low temperature ultrasonic attenuation in neutron-irradiated quartz versus the induced mass-density changes.” Journal de Physique Colloques, 48(C8), C8-531-C8-537.

Vodák, F., Trtík, K., Sopko, V., Kapičková, O., and Demo, P. (2005). “Effect of γ-irradiation on strength of concrete for nuclear-safety structures.” Cement and Concrete Research, 35(7), 1447–1451.

Vodák, F., Vydra, V., Trtík, K., and Kapičková, O. (2011). “Effect of gamma irradiation on properties of hardened cement paste.” Materials and Structures, 44(1), 101–107.

Weissmann, S., and Nakajima, K. (1963). “Defect Structure and Density Decrease in Neutron‐Irradiated Quartz.” Journal of Applied Physics, 34(3), 611–618.

Wittels, M. (1953). “The Lattice Expansion of Quartz Due to Fast Neutron Bombardment.” Physical Review, 89(3), 656–657.

Wittels, M. C. (1957). “Structural behaviou of neutron irradiated quartz.” Philosophical Magazine, 2(24), 1445–1461.

Wittels, M., and Sherrill, F. A. (1954). “Radiation Damage in SiO2 Structures.” Physical Review, 93(5), 1117.